Universitatea *Transilvania* din Braşov

HABILITATION THESIS

Contributions to the mechanics of polymer matrix composite materials

Domain: Mechanical Engineering

Author: Assoc.Prof. Horatiu TEODORESCU-DRAGHICESCU

University: Transilvania University of Brasov

BRASOV, 2015

CONTENT

Abstract

In this paper I have presented briefly some theoretical and experimental scientific contributions in the fascinating field of mechanics of polymer matrix composites. These contributions have been finalized after conferring the PhD title, distinction „*Cum Laudae*" in the field of Mechanical Engineering for the PhD thesis entitled "*Contributions to the increase of loading capability of fibers-reinforced polymer matrix composite tubes by introducing supplementary internal stresses*", titled conferred according to the Order of Minister of National Education no. 4202 from 27th July 2001.

In first chapter I have presented some major contributions materialized in computing the tensile strength of a multiphase Sheet Molding Compound (SMC) composite material taking into consideration the notion of substitute matrix formed by combination of resin and filler. I have computed the substitute matrix' Young's modulus as the harmonic mean between the elastic properties of the isotropic compounds. I have determined the upper and lower limits of the homogenized coefficients of a SMC composite material with 27% fibers volume fraction. I have used three averaging methods of the elastic properties of this material. The experimental results revealed close values to the arithmetic mean of the elastic properties of the isotropic compounds.

In the second chapter I have carried out simulations of the elastic properties of some fibers-reinforced composite laminates subjected to off-axis loading system. I have computed the matrix strain increase factor in case of transverse lamina's loading for a hexagonal arrangement of fibers in matrix. The comparison of this factor to that of a square arrangement of fibers in matrix indicates an advantage of hexagonal arrangement, this being closer to reality.

In chapter three I have performed simulations regarding the thermo-mechanical behavior of different unidirectional reinforced laminae with various fibers, subjected to some sequential and combined temperature and humidity

variations. I have computed the coefficients of thermal and humidity expansions of these laminae. I have simulated the axial and transverse thermal conductivities of different unidirectional carbon fibers-reinforced thermo-conductive resins, with possible applications in heating radiant systems. I have presented the thermal response of a sandwich structure with nonwoven polyester mat as core and dissimilar skins.

In chapter four I have carried out a damping analysis of a twill weave carbon fabric. I have computed the fabric's dampings, rigidities and compliances using an equivalent model of it.

In chapter five I have presented the behavior of a three-phase composite material subjected to static tensile-compression cyclic loadings. I have accomplished experimental tests with different test speeds, load limits and number of cycles. The difference between the extension at first and last cycle put into evidence a maximum hysteresis effect at 10 mm/min test speed.

In chapter six I have experimentally determined the most important mechanical characteristics of seven types of composite laminates subjected to tensile as well as three and four-point bending loadings.

In the last chapter I have presented the most important mechanical properties of both a twill weave carbon fabric subjected to tensile and of a sandwich structure with expanded polystyrene core and skins from the same type of fabric, structure subjected to some three-point bend loadings. Loding-unloading flexural tests have been accomplished highlighting an outstanding stiffness of this structure.

Rezumat

În lucrarea de faţă am prezentat sub formă succintă câteva contribuţii ştiinţifice, teoretice şi experimentale, în domeniul fascinant al mecanicii materialelor compozite cu matrice polimerică. Aceste contribuţii s-au definitivat după conferirea titlului de doctor, distincţia "*Cum Laudae*", în domeniul Inginerie Mecanică pentru teza de doctorat intitulată "*Contribuţii la creşterea capacităţii de încărcare a tuburilor din materiale compozite plastice armate cu fibre prin introducerea de tensiuni interne suplimentare*", titlu conferit în baza Ordinului Ministrului Educaţiei Naţionale Nr. 4202 din 27 iulie 2001.

În primul capitol am prezentat câteva contribuţii majore materializate în calculul rezistenţei la tracţiune a unui material compozit multifazic de tip Sheet Molding Compound (SMC) luându-se în considerare noţiunea de matrice substitut formată din combinaţia răşinii cu materialul de umplere. Am calculat modulul lui Young al matricei substitut ca medie armonică între proprietăţile elastice ale componentelor izotrope. Am determinat limitele superioară şi inferioară ale coeficienţilor omogenizaţi ai unui material compozit de tip SMC cu 27% fracţiune volumică a fibrelor. Am folosit trei metode de mediere a proprietăţilor elastice ale acestui material. Rezultatele experimentale au scos în evidenţă valori apropiate de media aritmetică a proprietăţilor elastice ale componentelor izotrope.

În al doilea capitol am realizat simulări ale proprietăţilor elastice ale câtorva stratificate compozite armate cu fibre, supuse unui sistem de sarcini în afara axelor globale de coordonate ale compozitului. Am calculat factorul de mărire al alungirii matricei în cazul solicitării perpendicular pe fibre a laminei, pentru o dispunere hexagonală a fibrelor în matrice. Comparaţia acestui factor cu cel al unei dispuneri pătrate a fibrelor în matrice indică un avantaj al dispunerii hexagonale, aceasta fiind mai aproape de realitate.

În capitolul trei am efectuat simulări referitoare la comportarea termomecanică a diferitelor lamine armate unidirecţional cu diverse fibre, supuse unor variaţii secvenţiale şi combinate de temperatură şi umiditate. Am calculat coeficienţii de dilatare termică şi datorită umidităţii a acestor lamine. Am simulat

conductivităţile termice pe direcţiile axială şi transversală ale diferitelor răşini termoconductive armate cu fibre unidirecţionale de carbon, cu posibile aplicaţii în sisteme radiante de încălzire. Am prezentat răspunsul termic al unei structuri sandwich cu miez din împâslitură neţesută din poliester şi învelişuri asimetrice.

În capitolul patru am realizat o analiză a amortizării unei ţesături cu legătură diagonală, din fibre de carbon. Am calculat amortizările, rigidităţile şi complianţele acestei ţesături utilizând un model echivalent al acesteia.

În capitolul cinci am prezentat comportarea unui material compozit trifazic supus la sarcini statice de tracţiune-compresiune ciclică. Am realizat teste experimentale cu viteze de încercare, limite de sarcină şi număr de cicluri diferite. Diferenţa dintre deformaţia la primul şi ultimul ciclu a scos în evidenţă un efect maxim de histerezis la o viteză de încercare de 10 mm/min.

În capitolul şase am determinat experimental cele mai importante caracteristici mecanice a şapte tipuri de stratificate compozite supuse la sarcini de tracţiune şi încovoiere în trei şi patru puncte.

În ultimul capitol am prezentat cele mai importante proprietăţi mecanice atât ale unei ţesături din fibre de carbon, cu legătură diagonală, supusă la tracţiune, cât şi a unei structuri sandwich cu miez din polistiren expandat şi învelişuri din acest tip de ţesătură, structură supusă unor sarcini de încovoiere în trei puncte. S-au realizat teste de încovoiere de încărcare-descărcare evidenţiindu-se o rigiditate excepţională a acestei structuri.

PART (B-i)

Scientific, Professional and Academic Achievements

Chapter 1

Contributions to the tensile behavior and prediction of elastic properties of pre-impregnated composite materials

1.1. Introduction

One of my important contribution in the field of mechanics of polymer matrix composite materials has been published in *Computational Materials Science* in 2011 [45]. My previous developments have been published in various proceedings [49], [51], [52], [55], [59], [60], [62], [67], [69], [70], [71], the last one being published in 2013 [43].

An original approach to compute the longitudinal tensile break stress of multiphase composite materials with short fibers reinforcement is presented. The most obvious mechanical model which reflects a multiphase composite material is a pre-impregnated material, known as prepreg. In the class of prepregs the most known are Sheet and Bulk Molding Compounds (SMCs and BMCs). The model is seen as consisting of three phase compounds: resin, filler and fibers, model that is reduced to two phase compounds: replacement matrix and fibers.

The Sheet Molding Compounds reinforced with discontinuous and almost parallel fibers, subjected to longitudinal tensile loads, presents a specific note by the existence of a shear mechanism between fibers and matrix. This shear mechanism transfers the tensile load through the fibers. Young's moduli for the replacement matrix and for the entire composite are computed and a comparison between theoretical approach and the experimental data is carried out.

This chapter presents also a homogenization method and some original averaging methods to predict the elastic properties of these materials. The upper and lower limits of the homogenized coefficients for a 27% fibers volume fraction

SMC are computed. It is presented a comparison between the upper and lower limits of the homogenized elastic coefficients of a SMC material and the experimental data. The estimation model used as a homogenization method of these heterogeneous composite materials, gave emphasis to a good agreement between this theoretical approach and experimental data.

1.2. Tensile behavior of a parallel discontinuous fibers-reinforced lamina. Scientific context

A lamina reinforced with discontinuous almost parallel fibers, subjected to longitudinal tensile loads, presents a particularity by the existence of a shear mechanism between fibers and matrix, mechanism that transfer the tensile load to the fibers. Due to a difference between the matrix longitudinal strain and the fibers strain, a shear stress along the fiber-matrix interface occurs.

The normal stress distribution in a discontinuous fiber can be computed, considering an infinitely small portion *dx* at the distance *x* from one fiber end (fig. 1.1) [21]:

$$\left(\frac{\pi}{4}\cdot d_F^2\right)\cdot\left(\sigma_F+d\sigma_F\right)-\left(\frac{\pi}{4}\cdot d_F^2\cdot\sigma_F\right)-\pi\cdot d_F\cdot dx\cdot\tau_i=0 \qquad (1.1)$$

or:

$$\frac{d\sigma_F}{dx}=\frac{4\tau_i}{d_F}, \qquad (1.2)$$

where: σ_F is the fiber longitudinal stress at the distance x from one of its end, d_F is the fiber diameter and τ_i represents the shear stress at the fiber-matrix interface.

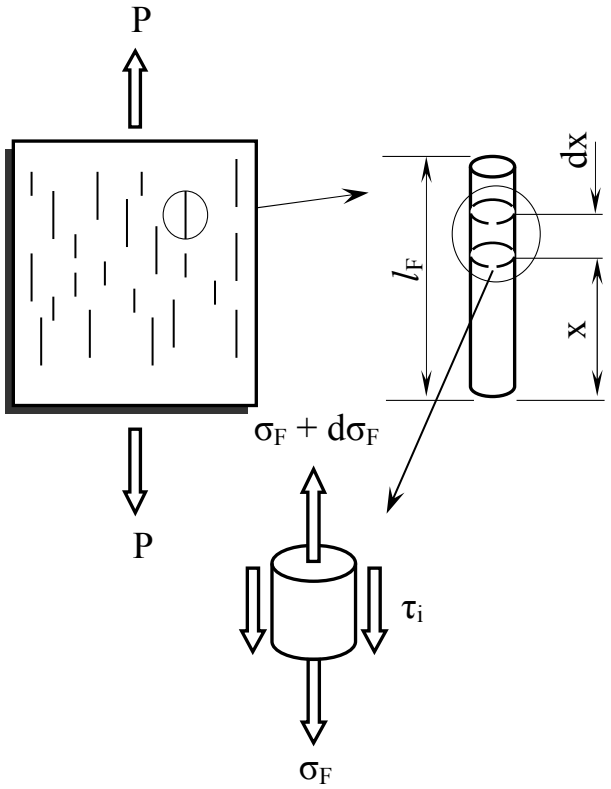

Fig. 1.1. Stresses distribution in a fiber of a parallel discontinuous fibers-reinforced lamina subjected to tensile loads [21]

Assuming τ_i constant, $\sigma_F = 0$ at the distance x being equal to zero and integrating (1.2), we get [21]:

$$\sigma_F = \frac{4}{d_F} \cdot \int_0^x \tau_i \cdot dx = \frac{4\tau_i}{d_F} \cdot x. \tag{1.3}$$

The maximum fiber stress can be reached at a distance $x = \frac{l_T}{2}$ from both fiber ends, l_T being the load transfer length and represents the fiber minimum length in which fiber maximum stress is reached [21]:

$$\sigma_{max\,F} = 2\tau_i \cdot \frac{l_T}{d_F}. \tag{1.4}$$

From (1.4), a critical fiber length for given d_F and τ_i may be computed [21]:

$$l_{critical} = \frac{\sigma_{bF}}{2\tau_i} \cdot d_F. \tag{1.5}$$

Taking into account the normal stress distributions also near the fiber ends (for $x < \frac{l_T}{2}$) then a fiber medium stress can be computed [21]:

$$\underline{\sigma}_F = \frac{1}{l_F} \cdot \int_0^{l_F} \sigma_F \cdot dx, \tag{1.6}$$

or:

$$\underline{\sigma}_F = \sigma_{max\,F}\left(1 - \frac{l_T}{2l_F}\right). \tag{1.7}$$

1.3. Contributions regarding the tensile behavior of pre-impregnated composite materials

In general, a composite material can be regarded as a system of at least two components: resin (or matrix) and reinforcement material (usually fibers). Multiphase composites may present at least three compounds: resin, filler and reinforcement, these materials are known as pre-impregnated materials. I have considered the resin–filler system as a distinct phase compound called replacement matrix, so a multiphase composite can be seen as a two phase compound material (fig. 1.2).

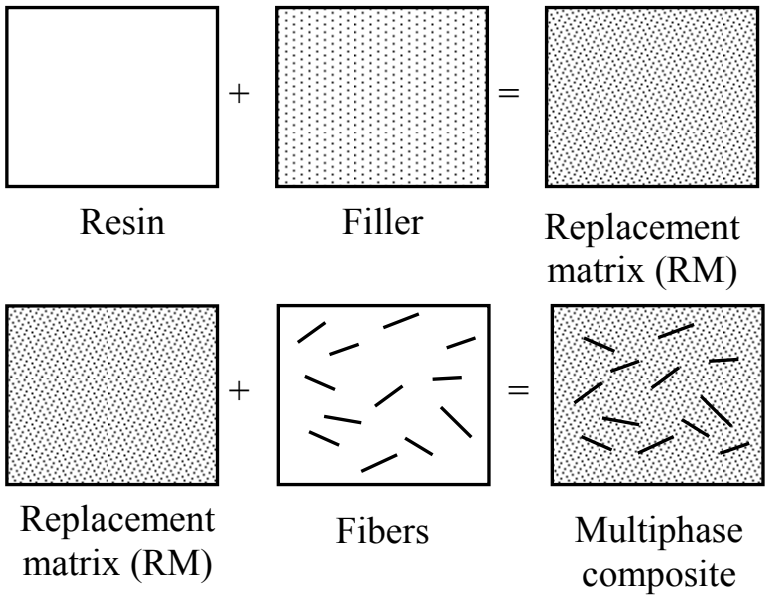

Fig. 1.2. Schematic representation of a multiphase composite

This replacement matrix presents the virtual volume fractions $V_r^{'}$ for resin and $V_f^{'}$ for filler. These virtual volume fractions are connected to the real volume fractions V_r and V_f, through the relations:

$$V_r' = \frac{V_r}{V_r + V_f}; \quad V_f' = \frac{V_f}{V_r + V_f}, \tag{1.8}$$

so:

$$V_r' + V_f' = 1. \tag{1.9}$$

It is known that during the manufacturing process of a SMC, there is dependence between the production line speed and the fibers plane orientation on its advance direction. So, this material can be assumed to have the fibers oriented almost parallel to the production line of the SMC. Due to the longitudinal tensile loading, the SMC strain (ε_C) is identical with the replacement matrix strain (ε_{RM}) and fibers strain (ε_F), see Figs. 1.3 – 1.4.

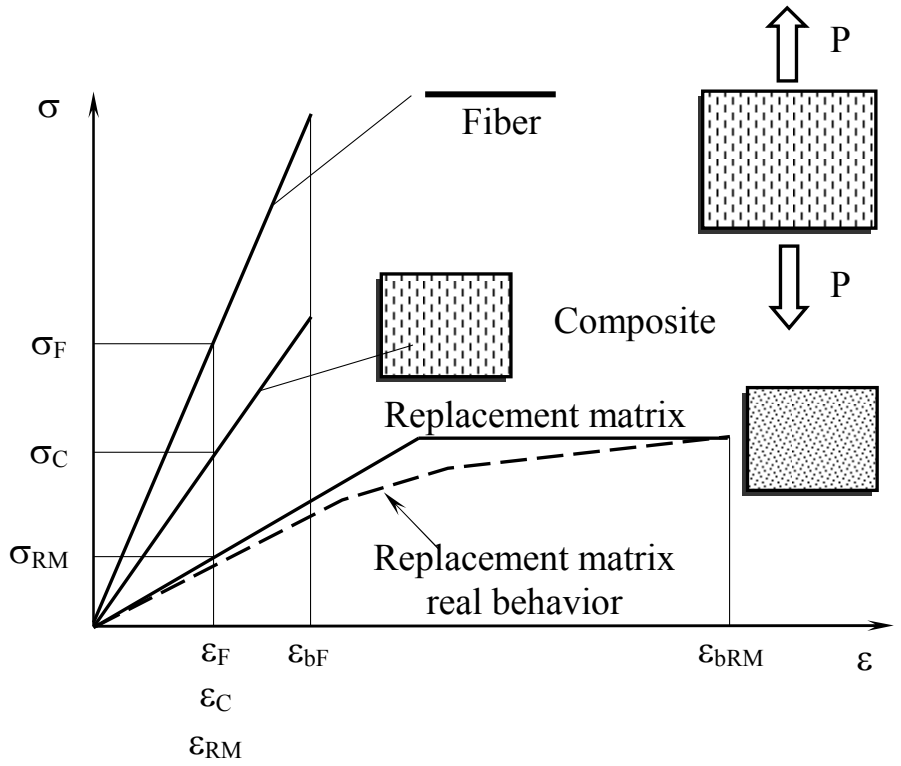

Fig. 1.3. Stress-strain schematic behavior of a pre-impregnated composite material

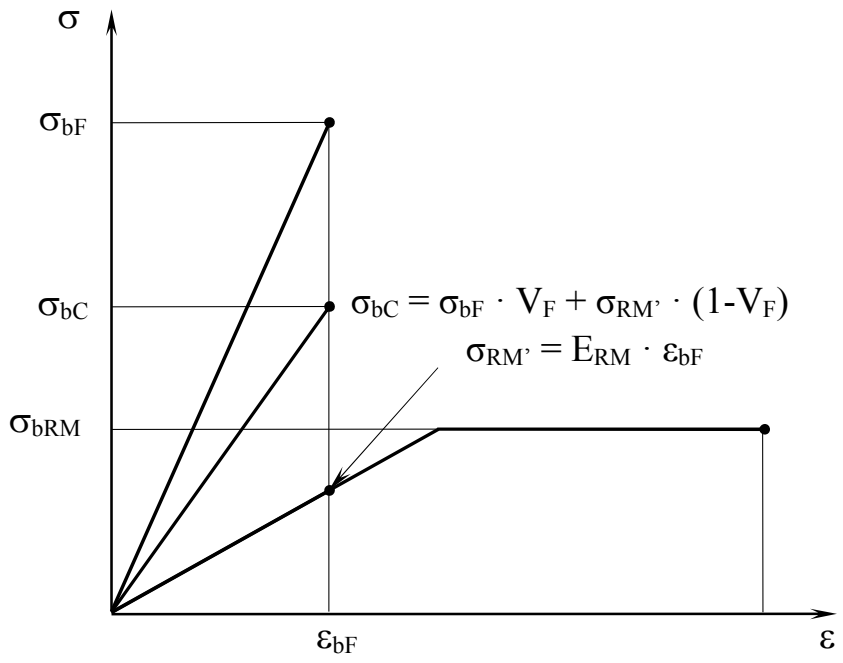

Fig. 1.4. Important points in stress-strain behavior of a pre-impregnated composite material

Assuming the fact that both fibers and replacement matrix present an elastic linear behavior, the respective longitudinal stresses are:

$$\sigma_F = E_F \cdot \varepsilon_F = E_F \cdot \varepsilon_C, \tag{1.10}$$

$$\sigma_{RM} = E_{RM} \cdot \varepsilon_{RM} = E_{RM} \cdot \varepsilon_C. \tag{1.11}$$

The tensile force applied to the entire composite is taken over by both fibers and replacement matrix:

$$P = P_F + P_{RM} \tag{1.12}$$

or:

$$\sigma_C \cdot A_C = \sigma_F \cdot A_F + \sigma_{SM} \cdot A_{SM},$$
$$\sigma_C = \sigma_F \cdot \frac{A_F}{A_C} + \sigma_{SM} \cdot \frac{A_{SM}}{A_C}, \quad (1.13)$$

where σ_C represents the medium tensile stress in the composite, A_F is the net area of the fibers transverse surface, A_{RM} represents the net area of the replacement matrix transverse surface and $A_C = A_F + A_{SM}$.

The ratio: $\frac{A_F}{A_C} = V_F$ is the fibers volume fraction and $\frac{A_{RM}}{A_C} = V_{RM} = 1 - V_F$ represents the replacement matrix volume fraction, so that equations (1.13) become:

$$\sigma_C = \sigma_F \cdot V_F + \sigma_{RM} \cdot (1 - V_F). \quad (1.14)$$

Considering the equations (1.10) and (1.11) and dividing both terms of relation (1.14) through ε_C, the longitudinal elasticity modulus for the composite may be computed as following:

$$E_C = E_F \cdot V_F + E_{RM} \cdot (1 - V_F). \quad (1.15)$$

Equation (1.15) shows that the value of the longitudinal elasticity modulus of the composite is situated between the values of the fibers and replacement matrix longitudinal elasticity moduli. In general, the fibers break strain is lower than the matrix break strain, so assuming that all fibers present the same strength, their break lead inevitable to the composite break. According to equation (1.14), the break strength at longitudinal tensile loads of a pre-impregnated composite material, is:

$$\sigma_{bC} = \sigma_{bF} \cdot V_F + \sigma_{RM'} \cdot (1 - V_F), \quad (1.16)$$

where σ_{bF} is the fibers break strength and $\sigma_{RM'}$ represents the replacement matrix stress at the moment when its strain reaches the fibers break strain ($\varepsilon_{RM} = \varepsilon_{bF}$). Assuming the linear stress-strain distribution of the replacement matrix at the fibers break strain, equation (1.16) becomes:

$$\sigma_{bC} = \sigma_{bF} \cdot V_F + E_{RM} \cdot \varepsilon_{bF} \cdot (1 - V_F). \tag{1.17}$$

The estimation of the replacement matrix longitudinal elasticity modulus in case of pre-impregnated composites, obtained by mixing some materials with well-defined properties, depends both on the basic elastic properties of the isotropic compounds and the volume fraction of each compound. If we denote E_r the basic elastic property of the resin, E_f the basic elastic property of the filler, V_r the resin volume fraction and V_f the filler volume fraction, the replacement matrix longitudinal elasticity modulus can be estimated computing the harmonic media of the basic elastic properties of the isotropic compounds, as follows:

$$E_{RM} = \frac{2}{\frac{1}{E_r \cdot V_r} + \frac{1}{E_f \cdot V_f}}. \tag{1.18}$$

If the fiber length is greater than its critical length, replacing $\sigma_{max\ F}$ being equal to σ_{bF} and $l_T = l_{critical}$, the longitudinal break strength of a pre-impregnated composite material can be computed as follows:

$$\sigma_{bC} = \underline{\sigma}_{bF} \cdot V_F + \sigma_{RM'} \cdot (1 - V_F) = \sigma_{bF} \cdot \left(1 - \frac{l_{critical}}{2 l_F}\right) \cdot V_F + \sigma_{RM'} \cdot (1 - V_F). \tag{1.19}$$

According to equations (1.18) and (1.15), the longitudinal elasticity moduli E_{RM} (for the replacement matrix) and E_C (for the entire composite) can be computed. A comparison between these moduli and experimental data is presented

in fig. 1.5, computed for a 27% fibers volume fraction SMC material. In practice, due to technical reasons, the fraction of each isotropic compound is expressed as percent of weight, so that the dependence between volume and weight fraction can be determined:

$$\varphi = \frac{1}{1 + \frac{1-\psi}{\psi} \cdot \frac{\rho_F}{\rho_{RM}}}, \tag{1.20}$$

where φ and ψ are the volume respective the weight fraction, ρ_F as well as ρ_{RM} represent the fibers respective the replacement matrix density.

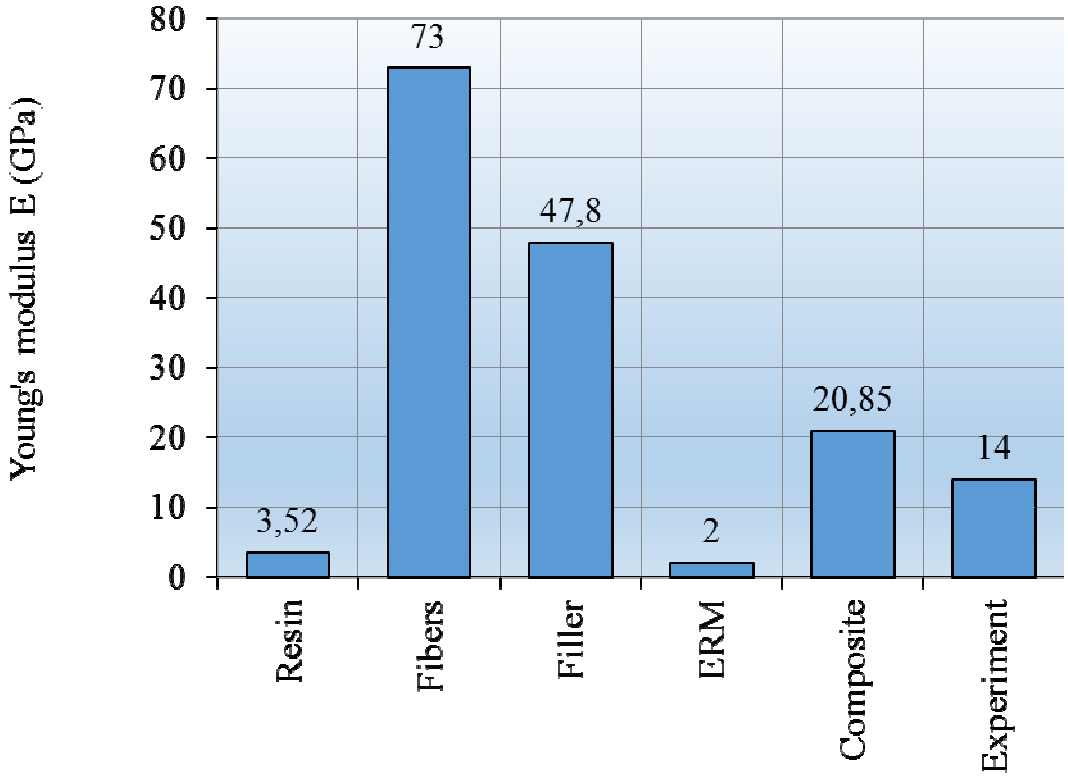

Fig. 1.5. Young's moduli E_{RM} (replacement matrix) and E_C (composite) for a 27% fibers volume fraction SMC material

From fig. 1.5, it can be noticed that the Young's modulus for the entire composite is closer to the experimental value unlike the Young's modulus for the

replacement matrix. This means that the rule of mixture used in equation (1.15) give better results than the inverse rule of mixture presented in equation (1.18), in which the basic elastic property of the filler and the filler volume fraction can be replaced with the fibers Young's modulus and fibers volume fraction, appropriate for a good comparison.

As conclusions, for the same fibers length (e.g. l_F = 4.75 mm) but with a shear stress ten times greater at the fiber-matrix interface, it results an increase with 18% of the longitudinal break strength of the composite. Therefore, improving the bond between fibers and matrix by using a technology that increases the fibers adhesion to matrix, an increase of composite longitudinal break strength will be achieved. In the case of using some fibers with greater lengths (e.g. l_F = 25.4 mm), the ten times increase of the shear stress at the fiber-matrix interface leads to an increase with only 3% of the composite longitudinal break strength. Two SMC composite materials with same shear stress at the fiber-matrix interface (e.g. τ_i = 5 MPa) but with different fibers lengths, present different longitudinal break strength values, the composite with fibers length l_F = 25.4 mm exhibit an increase with about 16% of this strength.

The computing model regarding the longitudinal tensile behavior of multiphase composite materials like SMCs shows that the composite's Young's modulus computed by help of rule of mixture is closer to experimental data than the inverse rule of mixture.

1.4. Prediction of elastic properties of pre-impregnated composite materials. Scientific context

General information regarding this subject can be found in references [1], [2], [4], [6], [12], [16], [18], [19], [22], and [27]. The most obvious mechanical model which features a multiphase composite material is a pre-impregnated material, known as prepreg. In the wide range of prepregs the most common used are Sheet and Bulk Molding Compounds. A Sheet Molding Compound (SMC) is a pre-impregnated material, chemically thickened, manufactured as a continuous mat of chopped glass fibers, resin (known as matrix), filler and additives, from which blanks can be cut and placed into a press for hot press molding. The result of this combination of chemical compounds is a heterogeneous, anisotropic composite material, reinforced with discontinuous reinforcement.

A typical SMC material is composed of the following chemical compounds: calcium carbonate (36.8% weight fraction); chopped glass fibers roving (30% weight fraction); unsaturated polyester resin (18.4% weight fraction); low-shrink additive (7.9% weight fraction); styrene (1.5% weight fraction); different additives (1.3% weight fraction); pigmented paste (1.3% weight fraction); release agent (1.2% weight fraction); magnesium oxide paste (1.1% weight fraction); organic peroxide (0.4% weight fraction); inhibitors (0.1% weight fraction) [40].

The matrix (resin) system play a significant role within a SMC, acting as compounds binder and being “embedded material” for the reinforcement. To decrease the shrinkage during the cure of a SMC prepreg, filler (calcium carbonate) have to be added in order to improve the flow capabilities and the uniform fibers transport in the mold.

For the materials that contain many compounds, an authentic, general method of dimensioning is hard to find. In a succession of hypotheses, some authors tried to describe the elastic properties of SMCs based on ply models and on

material compounds. Glass fibers represent the basic element of SMC prepreg reinforcement. Quantity and rovings' orientation determine, in a decisive manner, the subsequent profile of the SMC structure's properties. There are different grades of SMC prepregs: R-SMC (with randomly oriented reinforcement), D-SMC (with unidirectional orientation of the chopped fibers), C-SMC (with unidirectional oriented continuous fibers) and a combination between R-SMC and C-SMC, known as C/R-SMC [40].

Following information are essential for the development of any model to describe the composite materials behavior: the thermo-elastic properties of every single compound and the volume fraction concentration of each compound. Theoretical researches regarding the behavior of heterogeneous materials lead to the elaboration of some homogenization methods that try to replace a heterogeneous material with a homogeneous one [4], [12], [16], [18], [22], [27]. The aim is to obtain a computing model which takes into account the microstructure or the local heterogeneity of a material.

The homogenization theory is a computing method to study the differential operators' convergence with periodic coefficients. This method is indicated in the study of media with periodic structure like SMCs and BMCs. The matrix and fillers elastic coefficients are very different but periodical in spatial variables. This periodicity or frequency is suitable to apply the homogenization theory to the study of heterogeneous materials.

A homogenization method

Ene and Pasa have considered Ω a domain from R^3 space, in coordinates x_i, domain in which the matrix (resin system) is represented by the field Y_1 and the reinforcement occupies the field Y_2 seen as a bundle of glass fibers, (figs. 1.6 – 1.7). They took into consideration the following equation [12]:

$$f(x) = -\frac{\partial}{\partial x_i}\left[a_{ij}(x) \cdot \frac{\partial u}{\partial x_j} \right]; \quad a_{ij} = a_{ji} \tag{1.21}$$

or under the equivalent form [12]:

$$f = -\frac{\partial p_i}{\partial x_i}; \quad p_i = a_{ij} \cdot \frac{\partial u}{\partial x_j}. \tag{1.22}$$

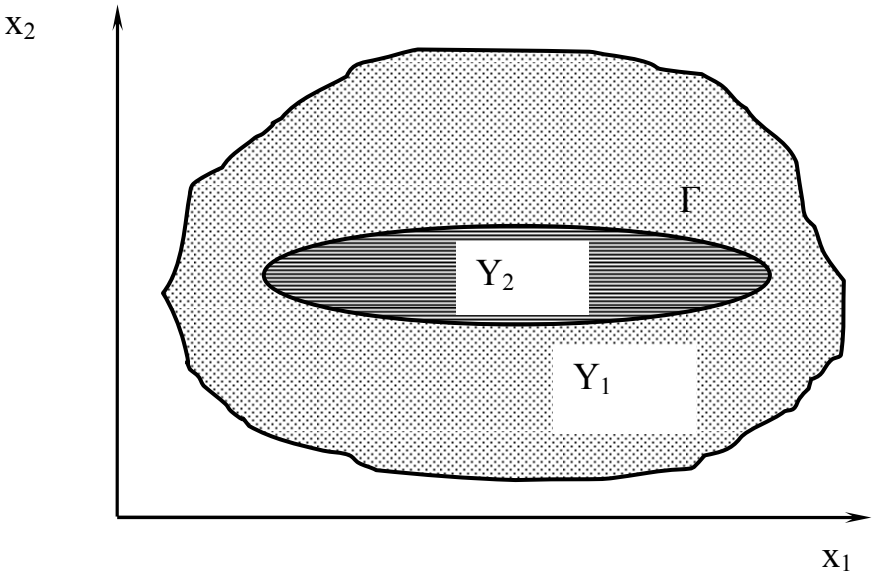

Fig. 1.6. Domains and inclusions of a composite material [12]

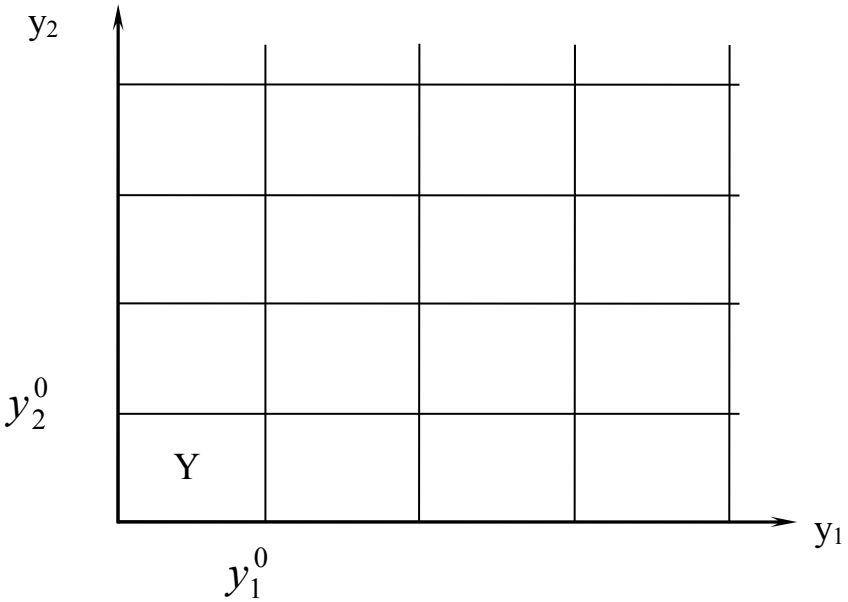

Fig. 1.7. Periodicity definition of a composite material [12]

In the case of composite materials that present a periodic structure containing inclusions, $a_{ij}(x)$ is a function of x. If the period's dimensions are small in comparison with the dimensions of the whole domain then the solution u of the equation (1.21) can be considered equal with the solution suitable for a homogenized material, where the coefficients a_{ij} are constants. In the R^3 space of y_i coordinates, a parallelepiped with y_i^0 sides (fig. 1.7) is considered, as well as parallelepipeds obtained by translation $n_i y_i^0$ (n_i integer) in axes directions. The functions [12]:

$$a_{ij}^{\eta}(x) = a_{ij}\left(\frac{x}{\eta}\right), \tag{1.23}$$

can be defined, where η is a real, positive parameter. The functions $a_{ij}(x)$ are ηY-periodical in variable x (ηY being the parallelepiped with ηy_i^0 sides).

If the function $f(x)$ is in Ω defined, the problem at limit can be considered [12]:

$$f(x) = -\frac{\partial}{\partial x_i}\left[a_{ij}^{\eta}(x)\cdot\frac{\partial u^{\eta}}{\partial x_j}\right], \quad u^{\eta}\big|_{\partial\Omega} = 0. \tag{1.24}$$

Similar with equation (1.22), the vector $\vec{p}^{\,\eta}$ can be defined with the elements [12]:

$$p_i^{\eta}(x) = a_{ij}^{\eta}(x)\cdot\frac{\partial u^{\eta}}{\partial x_j}. \tag{1.25}$$

For the function $u^{\eta}(x)$, an asymptotic development will be looking for, under the form [12]:

$$u^{\eta}(x)=u^{0}(x,y)+\eta^{1}u^{1}(x,y)+\eta^{2}u^{2}(x,y)+\ldots;\quad y=\frac{x}{\eta}, \tag{1.26}$$

where $u^i(x,y)$ are Y-periodical in y variable. The functions $u^i(x,y)$ are defined on Ω x R^3 so that the derivatives behave in the following manner [12]:

$$\frac{d}{dx_i}\rightarrow\frac{\partial}{\partial x_i}+\frac{1}{\eta}\cdot\frac{\partial}{\partial y_i}. \tag{1.27}$$

If the values of $u^i\left(x,\frac{x}{\eta}\right)$ are compared in two homologous points P_1 and P_2, homologous through periodicity in neighbor periods, it can be notice that the dependence in $\frac{x}{\eta}$ is the same and the dependence in x is almost the same since the distance P_1P_2 is small (fig. 1.8).

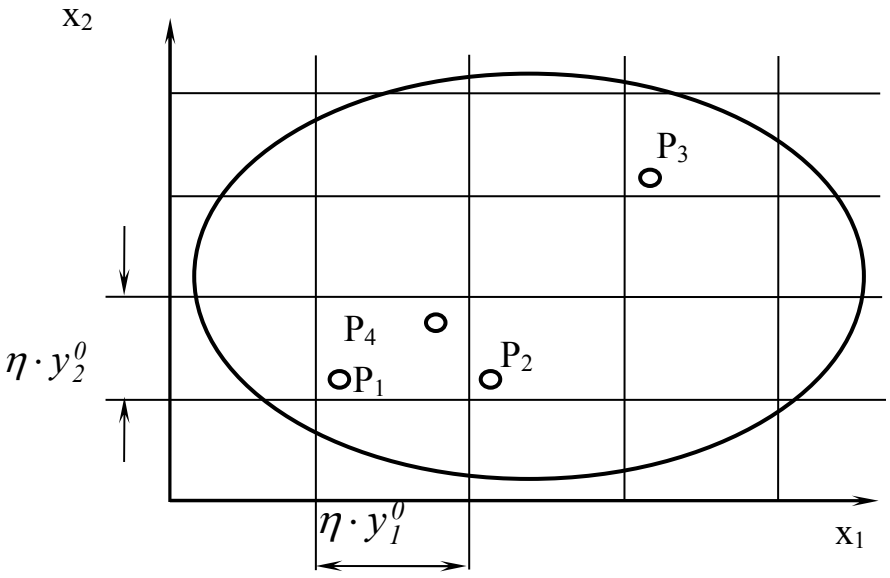

Fig. 1.8. Physical meaning of inclusions' periodicity of a composite [12]

It is considered P_3 a point homologous to P_1 through periodicity, situated far from P_1. The dependence of u^i in y is the same but the dependence in x is very different since P_1 and P_3 are far away. For instance, in the case of two points P_1 and P_4 situated in the same period, the dependence in x is almost the same since P_1 and P_4 are very close, but the dependence in y is very different since P_1 and P_4 are not homologous through periodicity. The function u^η depends on the periodic coefficients a_{ij}, on the function $f(x)$ and on the boundary $\partial\Omega$.

The development (1.26) is valid at the inner of the boundary $\partial\Omega$, where the periodic phenomena are prevalent but near and on the boundary, the non-periodic phenomena prevail. Using the development (1.26), the expressions $\frac{\partial u^\eta}{\partial x_i}$ and p^η can be computed as following [12]:

$$\frac{\partial u^\eta}{\partial x_i}=\left(\frac{\partial}{\partial x_i}+\frac{1}{\eta}\cdot\frac{\partial}{\partial y_i}\right)\cdot\left(u^0+\eta\cdot u^1+\ldots\right)=$$

$$=\frac{\partial u^0}{\partial x_i}+\frac{\partial u^1}{\partial y_i}+\eta\cdot\left(\frac{\partial u^1}{\partial x_i}+\frac{\partial u^2}{\partial y_i}\right)+\ldots, \tag{1.28}$$

$$p_i^\eta(x)=p_i^0(x,y)+\eta\cdot p_i^1(x,y)+\eta\cdot p_i^2(x,y)+\ldots, \tag{1.29}$$

where [12]:

$$\begin{aligned} p_i^0(x,y)&=a_{ij}(y)\cdot\left(\frac{\partial u^0}{\partial x_j}+\frac{\partial u^1}{\partial y_j}\right),\\ p_i^1(x,y)&=a_{ij}(y)\cdot\left(\frac{\partial u^1}{\partial x_j}+\frac{\partial u^2}{\partial y_j}\right),\ldots \end{aligned} \tag{1.30}$$

The function *f(x)* presented in equation (1.24) can be written in the following manner [12]:

$$f(x)=\left(-\frac{\partial}{\partial x_i}-\frac{1}{\eta}\cdot\frac{\partial}{\partial y_i}\right)\cdot\left(p_i^0+\eta\cdot p_i^1+...\right). \tag{1.31}$$

The terms η^{-1} and η^0 will be [12]:

$$\frac{\partial p_i^0}{\partial y_i}=0, \tag{1.32}$$

$$f(x)=-\frac{\partial p_i^0}{\partial x_i}-\frac{\partial p_i^1}{\partial y_i}. \tag{1.33}$$

Equation (1.33) leads to the homogenized or macroscopic equation. For this, the medium operator is introduced, defined for any function Ψ(y), Y-periodical [12]:

$$\langle\Psi\rangle=\frac{1}{|Y|}\int_Y\Psi(y)dy, \tag{1.34}$$

where $|Y|$ represents the periodicity cell volume. To obtain the homogenized equation, the operator (1.34) is applied to equation (1.33) [12]:

$$f(x)=-\frac{\partial\langle P_1^0\rangle}{\partial x_i}-\left\langle\frac{\partial p_i^1}{\partial y_i}\right\rangle. \tag{1.35}$$

According to the operator (1.34), the second term of the left side of the equation (1.35) becomes [12]:

$$\left\langle \frac{\partial p_i^1}{\partial y_i} \right\rangle = \frac{1}{|Y|}\int_Y \frac{\partial p_i^1}{\partial y_i} dy = \frac{1}{|Y|}\int_{\partial Y} p_i^1 n_i ds = 0. \tag{1.36}$$

Due to *Y*-periodicity of p_i^1 and the fact that $\vec{n}$ is the normal vector at the boundary of *Y*, the relation (1.36) is equal with zero. So, the equation (1.35) will be [12]:

$$f(x) = -\frac{\partial \left\langle P_I^0 \right\rangle}{\partial x_i}. \tag{1.37}$$

With help of relation (1.30), the equation (1.32) can be written as follows [12]:

$$\frac{\partial}{\partial y_i}\left[a_{ij}(y) \cdot \left(\frac{\partial u^0}{\partial x_j} + \frac{\partial u^1}{\partial y_j} \right) \right] = 0, \tag{1.38}$$

therefore [12]:

$$-\frac{\partial}{\partial y_i}\left[a_{ij}(y) \cdot \frac{\partial u^1}{\partial y_j} \right] = \frac{\partial u^0}{\partial y_j} \cdot \frac{\partial a_{ij}}{\partial y_j}. \tag{1.39}$$

The solution $u^1(y)$ of equation (1.39) is Y-periodical and to determine it is necessary to introduce the space $U_y(Y) = \{u \in H^1(Y), uY - periodical\}$. The equation (1.39) is equivalent with the problem to find a solution $u^1 \in U_y$ that verifies [12]:

$$\int_Y a_{ij}(y) \frac{\partial u^1}{\partial y_j} \cdot \frac{\partial v}{\partial y_i} dy = \frac{\partial u^0}{\partial x_j} \int_Y \frac{\partial a_{ij}}{\partial y_i} v dy, \tag{1.40}$$

for $\forall v \in U_y$.

If $\chi^k \in U_y$ is introduced, with $\langle \chi^k \rangle = 0$, that satisfy [12]:

$$\int_Y a_{ij}(y) \frac{\partial \chi^k}{\partial y_j} \cdot \frac{\partial v}{\partial y_i} dy = \int \frac{\partial a_{ik}}{\partial y_i} v dy, \tag{1.41}$$

for $\forall v \in U_y$, then from the problem's linearity (1.40), its solution can be written under the form [12]:

$$u^1(x,y) = \frac{\partial u^0}{\partial x_k} \chi^k(y) + c(x), \tag{1.42}$$

where *c(x)* is a constant as a function of *x*.

Knowing the expression of u^1 as a function of u^0, from the expressions (1.30) with (1.42), the following homogenized coefficients can be computed [12]:

$$\begin{aligned} p_i^0(x,y) &= a_{ij}(y)\left(\frac{\partial u^0}{\partial x_j} + \frac{\partial u^1}{\partial y_j}\right) = a_{ij}(y)\left(\frac{\partial u^0}{\partial x_j} + \frac{\partial u^0}{\partial x_k} \cdot \frac{\partial \chi^k}{\partial y_j}\right) = \\ &= \left[a_{ij}(y) + a_{ij}(y) \cdot \frac{\partial \chi^k}{\partial y_j}\right] \frac{\partial u^0}{\partial x_k}. \end{aligned} \tag{1.43}$$

Applying the medium operator (1.34), the relation (1.43) can be written [12]:

$$p_i^0(x) = a_{ik}^0 \frac{\partial u^0}{\partial x_k}, \tag{1.44}$$

$$a_{ik}^{0} = \left\langle a_{ik}(y) + a_{ij}(y)\frac{\partial \chi^{k}}{\partial y_j} \right\rangle = \left\langle a_{ij}(y) \cdot \left(\delta_{jk} + \frac{\partial \chi^{k}}{\partial y_j} \right) \right\rangle =$$

$$= \langle a_{ik} \rangle + \left\langle a_{ij} \frac{\partial \chi^{k}}{\partial y_j} \right\rangle. \qquad (1.45)$$

Therefore, the relation (1.35) becomes an equation in u^0 with constant coefficients [12]:

$$f = -\frac{\partial}{\partial x_i}\left(a_{ik}^{0} \frac{\partial u^{0}}{\partial x_k} \right). \qquad (1.46)$$

For a composite material in which the matrix occupies the domain Y_1 and presents the coefficient a_{ij}^{1} and the inclusion occupies the domain Y_2 with the coefficient a_{ij}^{2} separated by a surface Γ, the equation (1.23) must be seen as a distribution.

1.5. Contributions regarding the prediction of elastic properties of pre-impregnated composite materials

In the case of a pre-impregnated composite material like SMC which behaves macroscopically as a homogeneous elastic environment, is important the knowledge of the elastic coefficients. Unfortunately, a precise calculus of the homogenized coefficients can be achieved only in two cases: the one-dimensional case and the case in which the matrix and inclusion coefficients are functions of only one variable. For a SMC composite material is preferable to estimate these homogenized coefficients between an upper and a lower limit.

Since the fibers volume fraction of common SMCs is 27%, to lighten the calculus, I have considered an ellipsoidal inclusion of area 0.27 situated in a square of side 1. The plane problem will be considered and the homogenized coefficients will be 1 in matrix and 10 in the ellipsoidal inclusion. In fig. 1.9, the structure's periodicity cell of a SMC composite material is presented, where the fibers bundle is seen as an ellipsoidal inclusion.

Let us consider the function $f(x_1, x_2) = 10$ in inclusion and 1 in matrix. To determine the upper and the lower limit of the homogenized coefficients, first the arithmetic mean as a function of x_2-axis followed by the harmonic mean as a function of x_1-axis must be computed.

The lower limit is obtained computing first the harmonic mean as a function of x_1-axis and then the arithmetic mean as a function of x_2-axis. If we denote with $\varphi(x_1)$ the arithmetic mean against x_2-axis of the function $f(x_1, x_2)$, it follows:

$$\varphi(x_1) = \int_{-0,5}^{0,5} f(x_1, x_2)\,dx_2 = 1,$$
$$for \quad x_1 \in (-0,5;\ -0,45) \cup (0,45;\ 0,5), \tag{1.47}$$

$$\varphi(x_1) = \int_{-0,5}^{0,5} f(x_1, x_2)dx_2 = 1 + 9{,}45\sqrt{0{,}2025 - x_1^2},$$
$$for \quad x_1 \in (-0{,}45;\ \ 0{,}45). \tag{1.48}$$

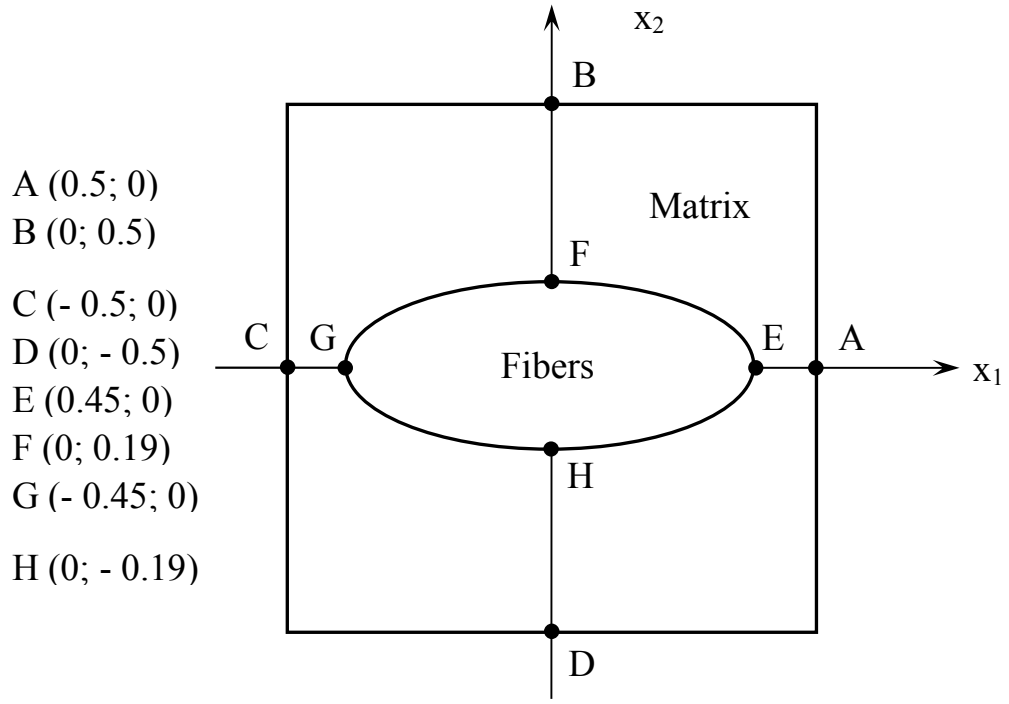

Fig. 1.9. Structure's periodicity cell of a SMC composite material with 27% fibers volume fraction. The points A to H are given with their coordinates

The upper limit is obtained computing the harmonic mean of the function $\varphi(x_1)$:

$$a^+ = \frac{1}{\int_{-0,5}^{0,5} \frac{1}{\varphi(x_1)} dx_1} =$$
$$= \frac{1}{\int_{-0,5}^{-0,45} dx_1 + \int_{-0,45}^{0,45} \frac{dx_1}{1 + 9{,}45\sqrt{0{,}2025 - x_1^2}} + \int_{0,45}^{0,5} dx_1}. \tag{1.49}$$

To compute the lower limit, I have considered $\psi(x_2)$ the harmonic mean of the function $f(x_1, x_2)$ against x_1:

$$\psi(x_2) = \frac{1}{\int_{-0,5}^{0,5} \frac{1}{f(x_1, x_2)} dx_1} = 1,$$
$$for \quad x_2 \in (-0,5;\ -0,19) \cup (0,19;\ 0,5), \tag{1.50}$$

$$\psi(x_2) = \frac{1}{\int_{-0,5}^{0,5} \frac{1}{f(x_1, x_2)} dx_1} = \frac{1}{1 - 3,42\sqrt{0,0361 - x_2^2}},$$
$$for \quad x_2 \in (-0,19;\ 0,19). \tag{1.51}$$

The lower limit will be given by the arithmetic mean of the function $\psi(x_2)$:

$$a_- = \int_{-0,5}^{0,5} \psi(x_2) dx_2 = \int_{-0,5}^{-0,19} dx_2 +$$
$$+ \int_{-0,19}^{0,19} \frac{dx_2}{1 - 3,42\sqrt{0,0361 - x_2^2}} + \int_{0,19}^{0,5} dx_2. \tag{1.52}$$

Since the ellipsoidal inclusion of the SMC structure may vary angular against the axes' center, the upper and lower limits of the homogenized coefficients will vary as a function of the intersection points coordinates of the ellipses, with the axes x_1 and x_2 of the periodicity cell (fig. 1.10).

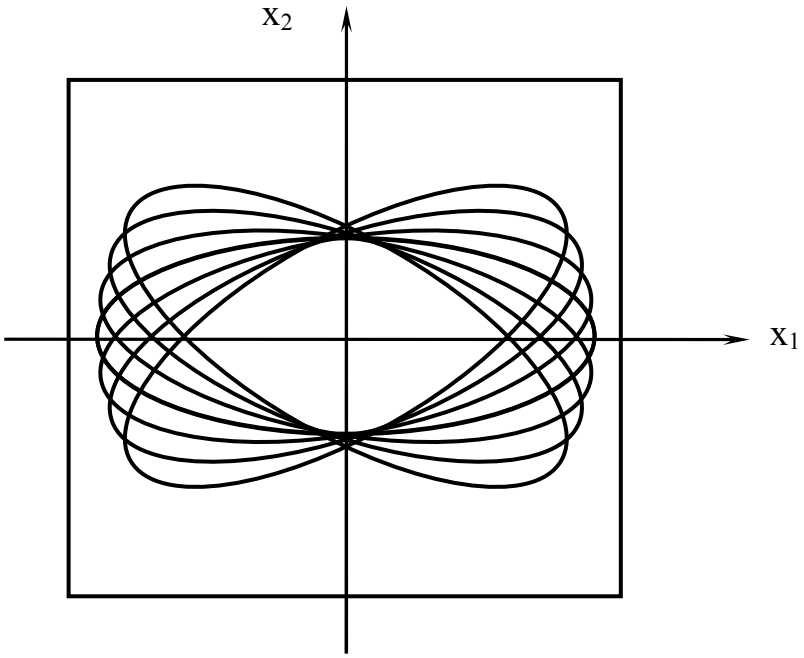

Fig. 1.10. ± 30° angular variation of the ellipsoidal inclusion of a SMC composite material

The following micrographs (figs. 1.11 – 1.12) make obvious this angular variation of the fibers' bundles and the extreme heterogeneity and the layered structure of SMC composite materials as well as the glass fibers and fillers distribution. The micrographs show that there are areas between 100 – 200 μm in which the glass fibers are missing and areas where the fibers distribution is very high.

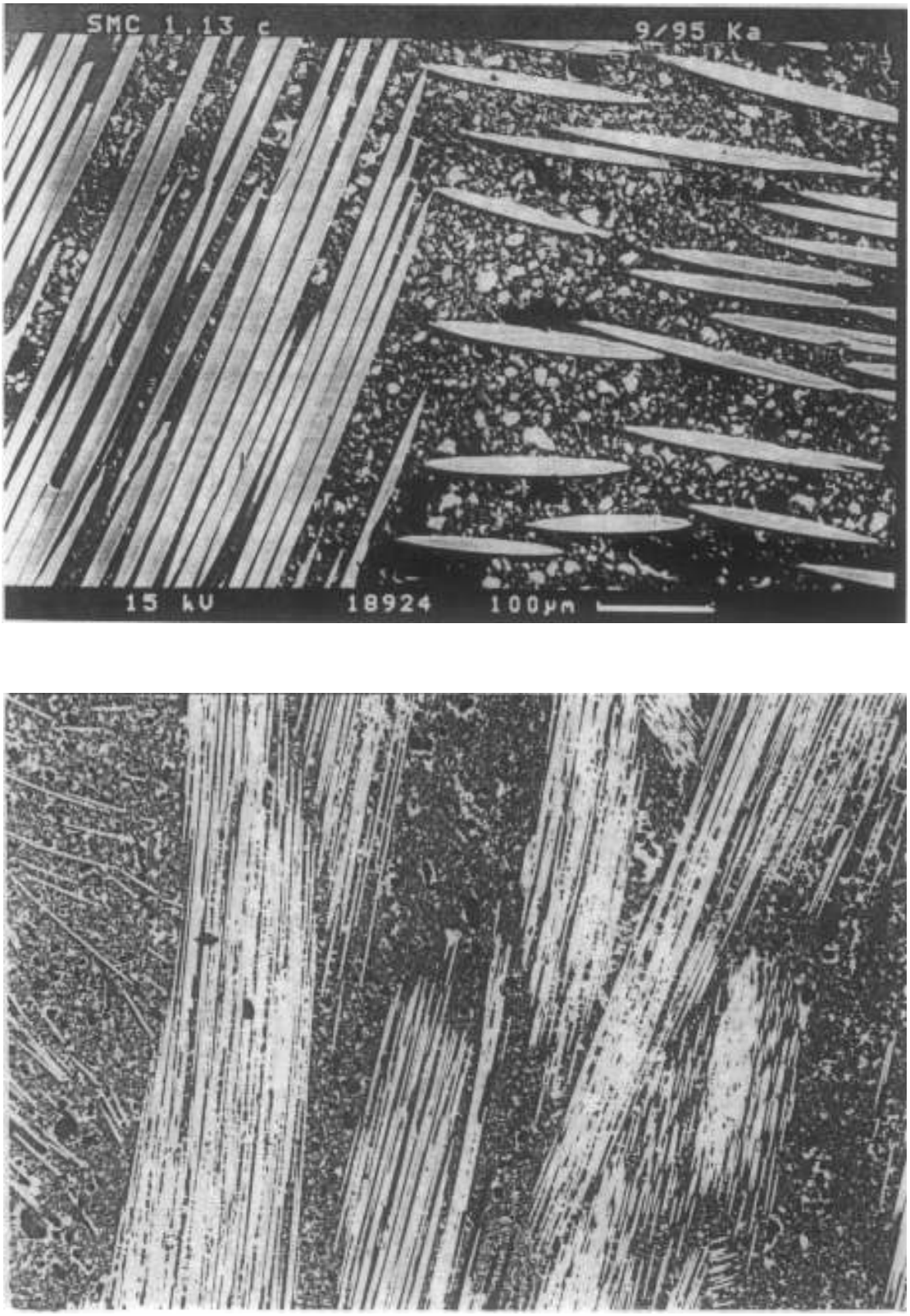

Fig. 1.11. Micrographs of various SMC composite materials with various magnitudes taken in-plane [40]

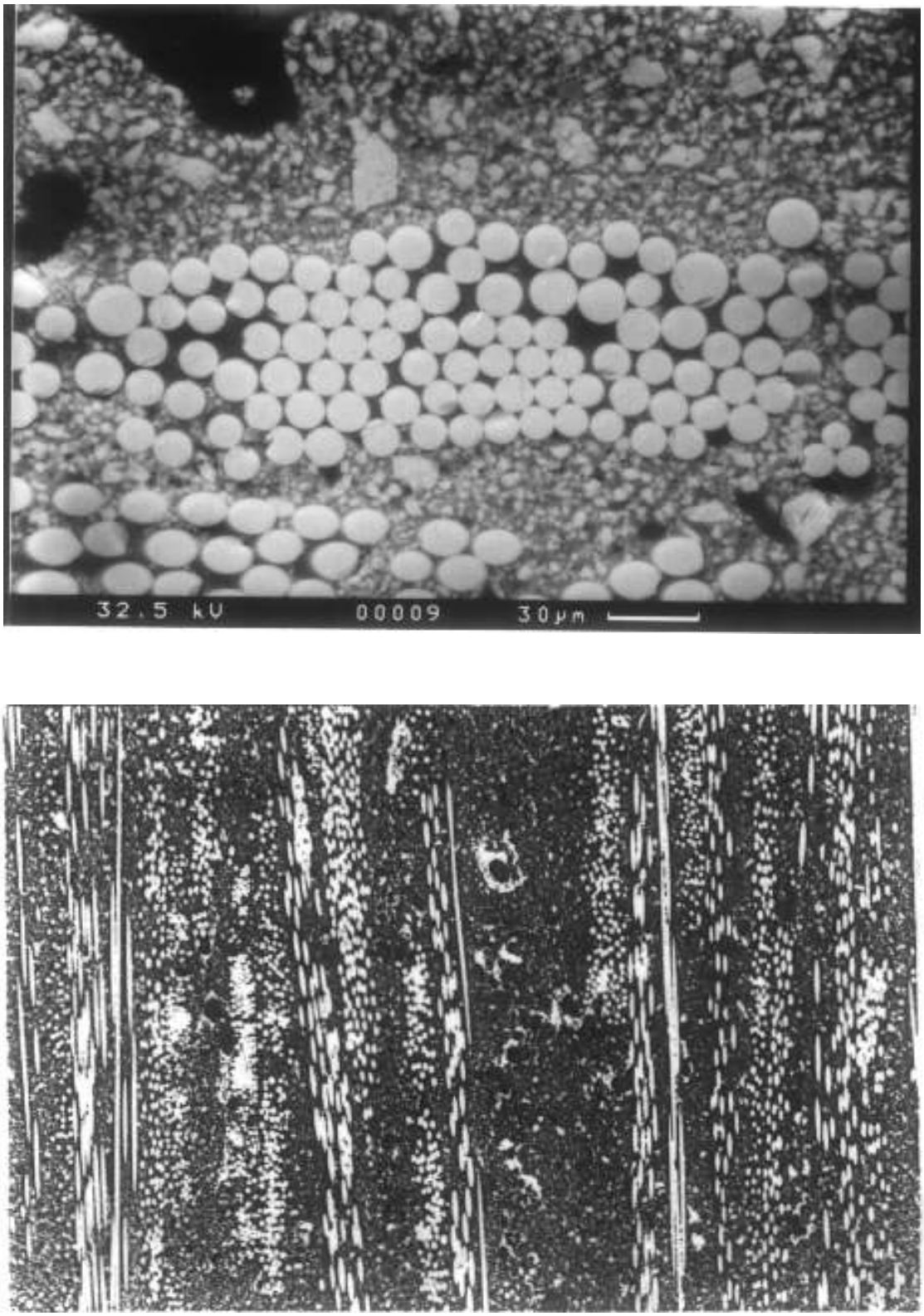

Fig. 1.12. Micrographs of various SMC composite materials with various magnitudes taken perpendicular to their thickness [40]

Results

To predict the elastic properties of pre-impregnated composite materials, as an example to compute these properties, structural features of a 27% fibers volume fraction SMC composite material are presented in table 1. According to equations (1.49) and (1.52), the upper and lower limits of the homogenized coefficients for a 27% fibers volume fraction SMC composite material are computed and shown in table 2.

Table 1. Typical elasticity properties of the SMC isotropic compounds and composite structural features

Property	UP resin	Fiber (E-glass)	Filler ($CaCO_3$)
Young's modulus E (GPa)	3.52	73	47.8
Shear modulus G (GPa)	1.38	27.8	18.1
Volume fraction (%)	30	27	43

Table 2. Upper and lower limits of the homogenized coefficients for a 27% fibers volume fraction SMC composite material

Angular variation of the ellipsoidal inclusion	Upper limit a^+	Lower limit a_
0°	2.52	0.83
± 15°	2.37	0.851
± 30°	2.17	0.886

The results presented in table 2, show that the upper limit of the homogenized coefficients decreases with the increase of angular variation of the ellipsoidal inclusion unlike the lower limit which increases with the increase of this angular variation.

The material's coefficients estimation depends both on the basic elasticity properties of the isotropic compounds and the volume fraction of each compound. If we write P_M, the basic elasticity property of the matrix, P_F and P_f the basic elasticity property of the fibers respective of the filler, φ_M the matrix volume fraction, φ_F and φ_f the fibers- respective the filler volume fraction, then the upper limit of the homogenized coefficients can be estimated computing the arithmetic mean of these basic elasticity properties taking into account the volume fractions of the compounds:

$$A_a = \frac{P_M \cdot \varphi_M + P_F \cdot \varphi_F + P_f \cdot \varphi_f}{3}. \tag{1.53}$$

The lower limit of the homogenized elastic coefficients can be estimated computing the harmonic mean of the basic elasticity properties of the isotropic compounds:

$$A_h = \frac{3}{\frac{1}{P_M \cdot \varphi_M} + \frac{1}{P_F \cdot \varphi_F} + \frac{1}{P_f \cdot \varphi_f}}, \tag{1.54}$$

An intermediate limit between the arithmetic and harmonic mean is given by the geometric mean written below:

$$A_g = \sqrt[3]{P_M \cdot \varphi_M \cdot P_F \cdot \varphi_F \cdot P_f \cdot \varphi_f}, \tag{1.55}$$

where P and A can be the Young's modulus respective the shear modulus.

Fig. 1.13 shows the Young's moduli and fig. 1.14 presents the shear moduli of the isotropic SMC compounds as well as the upper and lower limits of the homogenized elastic coefficients.

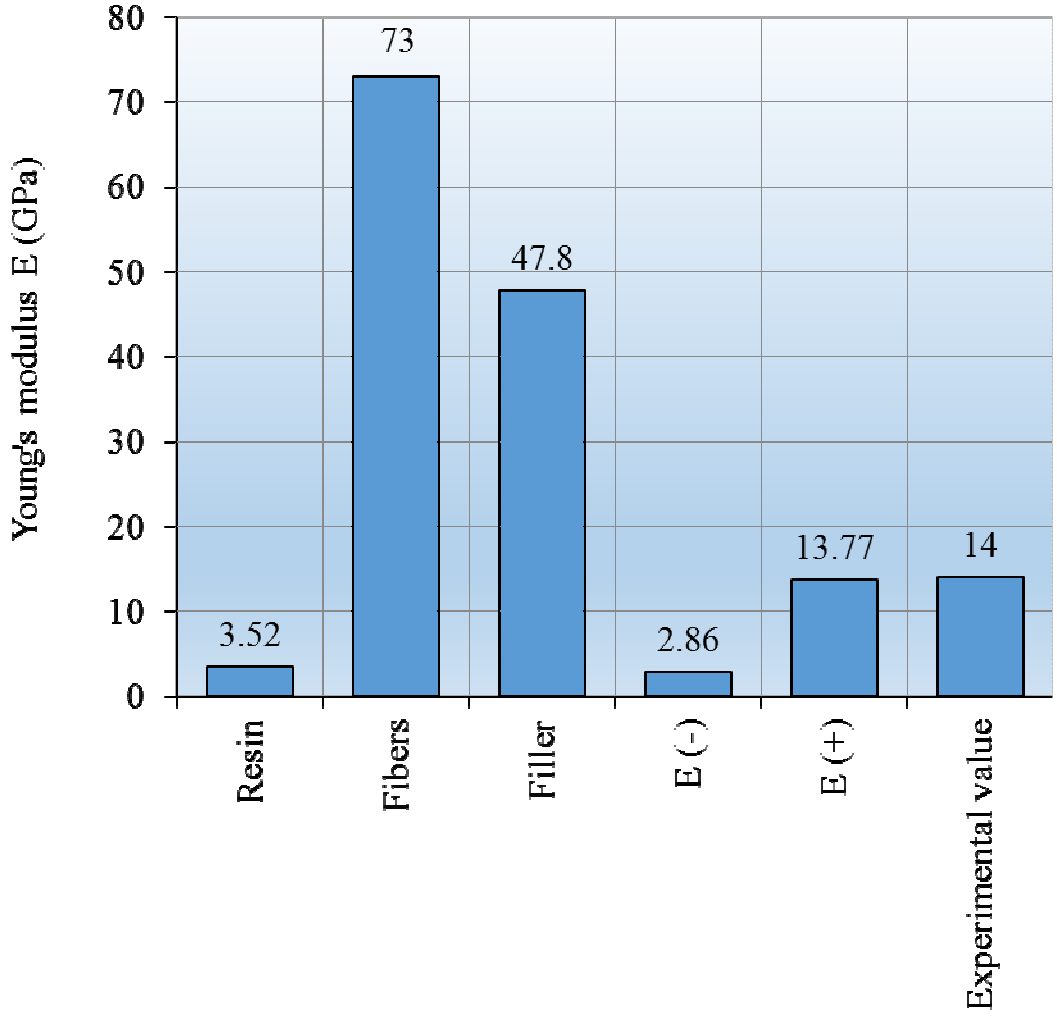

Fig. 1.13. Young's moduli of the isotropic SMC compounds, the upper (E+) and lower limits (E-) of the homogenized elastic coefficients

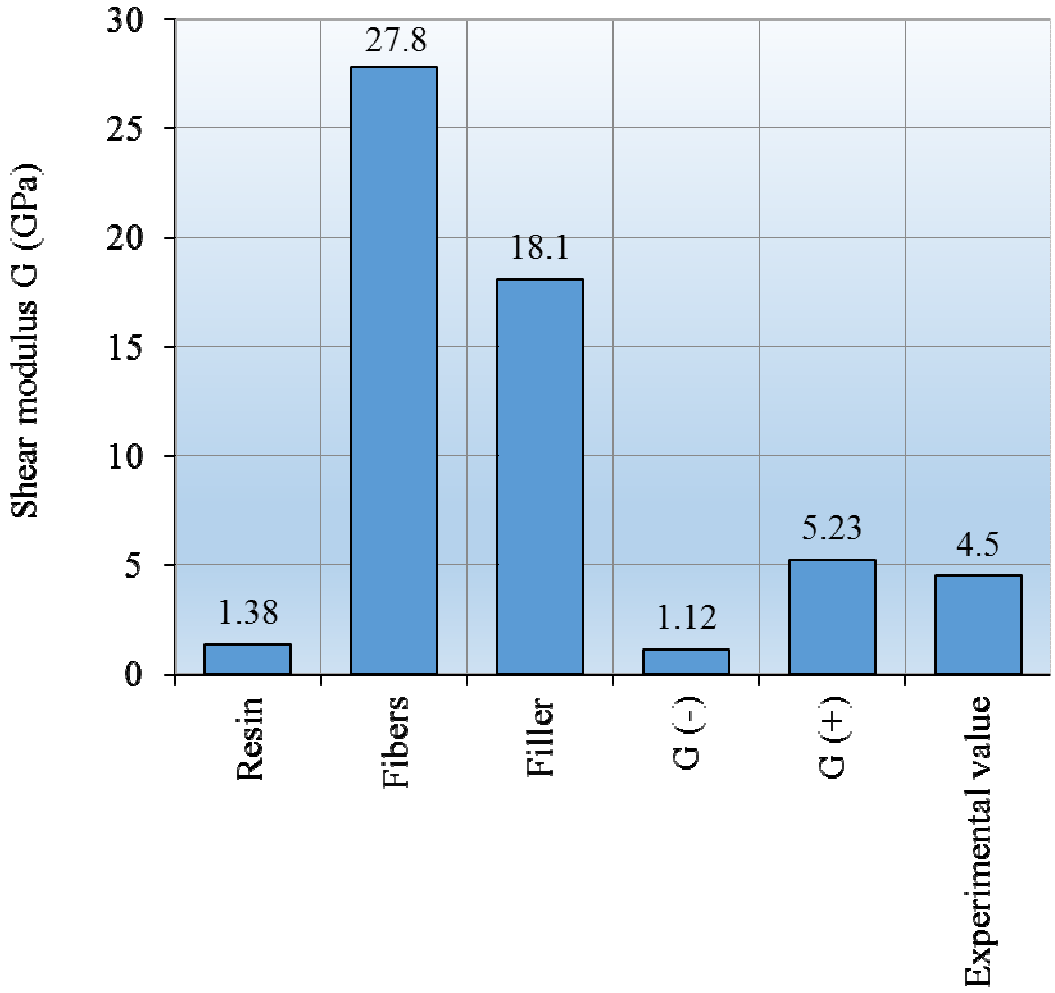

Fig. 1.14. Shear moduli of the isotropic SMC compounds, the upper (G+) and lower limits (G-) of the homogenized elastic coefficients

According to equations (1.53) – (1.55), the averaging methods of Young's and shear moduli of various SMCs with different fibers volume fractions present following distributions shown in figs. 1.15 and 1.16. By increasing the fibers volume fraction, the difference has been equally divided between matrix and filler volume fraction. The averaging methods to compute the Young's and shear moduli of various SMCs with different fibers volume fractions show that for a 27% fibers volume fraction SMC, the arithmetic means between matrix, fibers and filler Young's moduli respective shear moduli give close values to those determined experimentally.

The presented results suggest that the environmental geometry given through the angular variation of the ellipsoidal domains can leads to different results for same fibers volume fraction. This fact is due to the extreme heterogeneity and anisotropy of these materials. The upper limits of the homogenized elastic coefficients are very close to experimental data, showing that the proposed homogenization method give better results than the computed composite's Young modulus determined by help of rule of mixture.

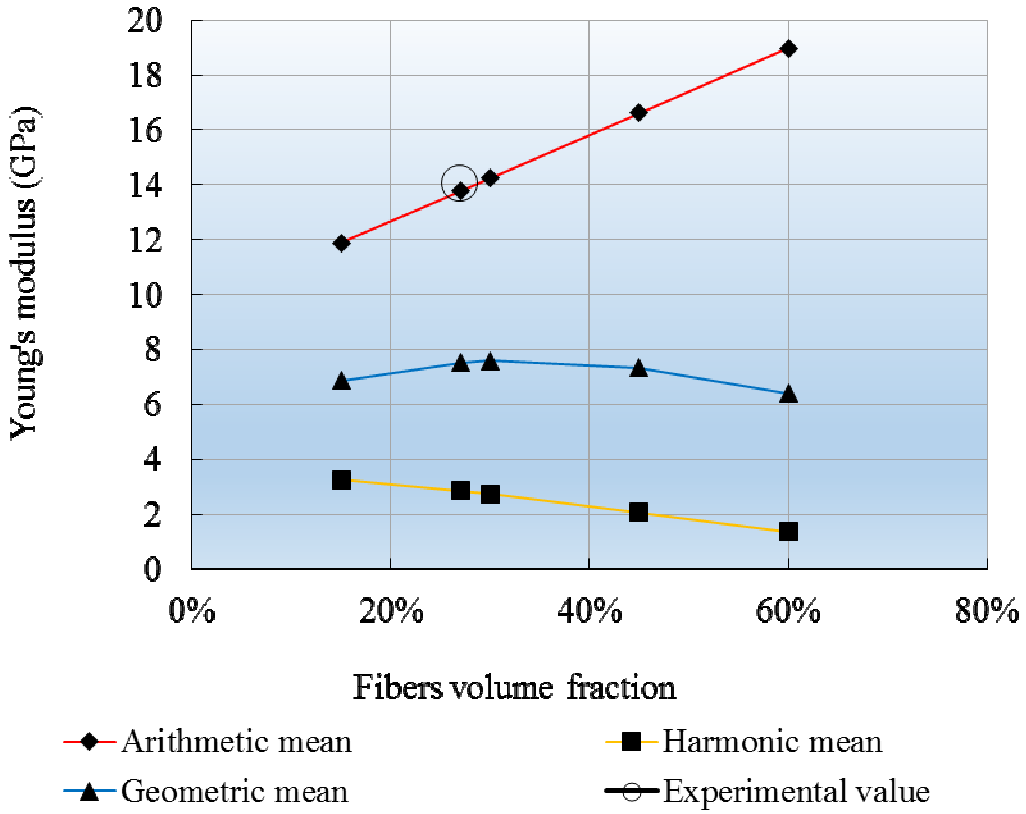

Fig. 1.15. Arithmetic, geometric and harmonic averaging methods to compute the Young's moduli of various SMCs with different fibers volume fractions

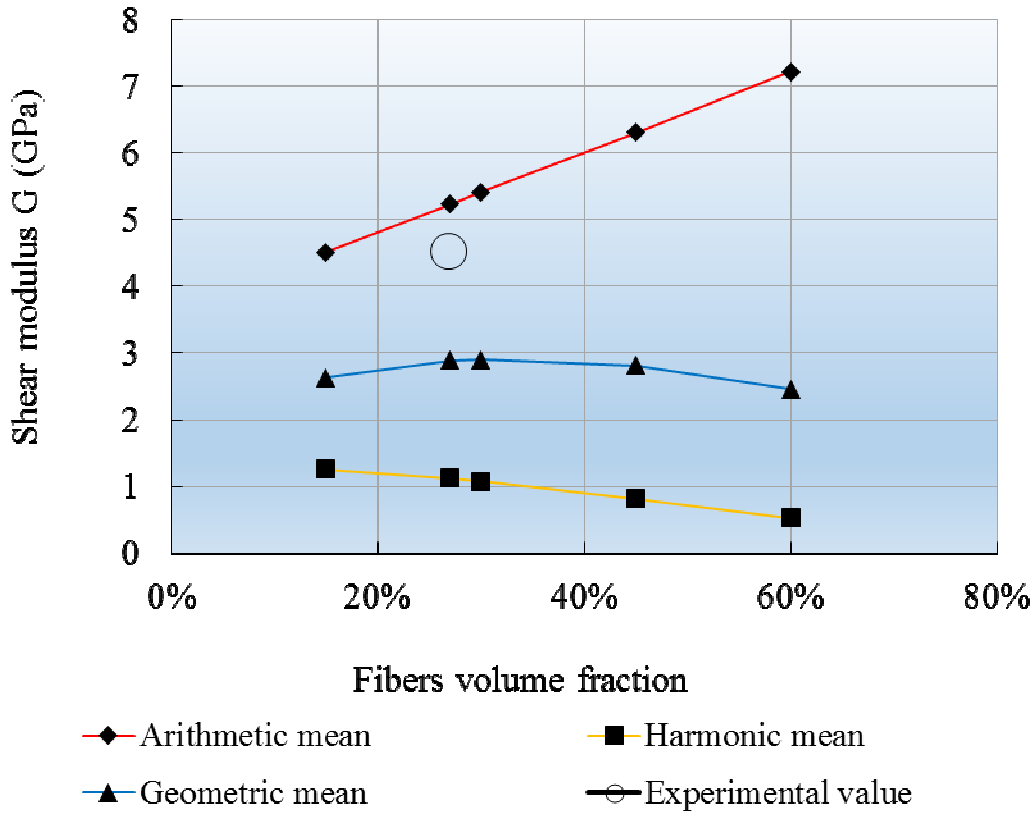

Fig. 1.16. Arithmetic, geometric and harmonic averaging methods to compute the shear moduli of various SMCs with different fibers volume fractions

The proposed estimation of the homogenized elastic coefficients of pre-impregnated composite materials can be extended to determine elastic properties of any multiphase, heterogeneous and anisotropic composite material. Future researches will be carried out taking into account the filler's particles size upon the homogenized elastic coefficients of these materials.

Chapter 2

Contributions to the simulations of elastic properties of fibers-reinforced laminates under off-axis loading system

2.1. Introduction

Personal simulations of elastic properties of some fibers-reinforced composite laminates under off-axis loading system, as well as the behavior of different polymer matrix composite laminates subjected to three and four-point bending using the finite element method have been published in two issues of *Optoelectronics and Advanced Materials – Rapid Communications (OPTOELECTRON ADV MAT)* in 2011 [46], [83]. I have been taken into consideration various composite laminates to simulate their elastic properties using MAP_COMP_LAMSTR and MAP_COMP_LAMSTI programs developed by Hull and Clyne [17]. These simulations have been published in different proceedings [29], [48], [54], [56], [57], [58], [64], [65], the last one being published in 2013 [44]. General information regarding this subject are presented in the general references [23], [33], [42], [66], [86], [88].

Distributions of Young's moduli determined on two orthogonal directions, shear modulus as well as Poisson ratio of various composite laminates based especially on epoxy resin reinforced with different types of fibers, subjected to off-axis loading system are presented. Stresses in various composite laminates subjected to a general set of in-plane loads are also computed.

2.2. The laminate theory. Scientific context

Elasticity laws of a unidirectional fibers-reinforced lamina

Fibers-reinforced polymer matrix composites belong to the class of heterogeneous and anisotropic materials, so their mechanics is much more complex than that of conventional materials. The basic element of a layered composite structure is represented by an individual layer called lamina reinforced with continuous unidirectional fibers inserted into a resin system called matrix.

Basic assumptions in the description of the interaction between fibers and matrix in a lamina subjected to tensile loads, are [33]:

- Both fibers and matrix behave as linear elastic materials;
- Initially, the lamina does not present residual stresses;
- The loads are applied parallel or perpendicular to the fibers direction;
- The matrix does not present voids and failures;
- The bond between fibers and matrix is perfect;
- The fibers are uniform distributed in matrix.

In a general case, the plane loading of a lamina is formed by three components that have been connected to the main directions in material (fig. 2.1) [33]:

- The longitudinal loading, in which normal stress $\sigma_{\parallel}$ is parallel to fibers direction;
- The transverse loading, in which normal stress $\sigma_{\perp}$ acts perpendicular to fibers direction;
- The shear loading, determined by shear stresses $\tau_{\#}$ that act both parallel and perpendicular to fibers direction.

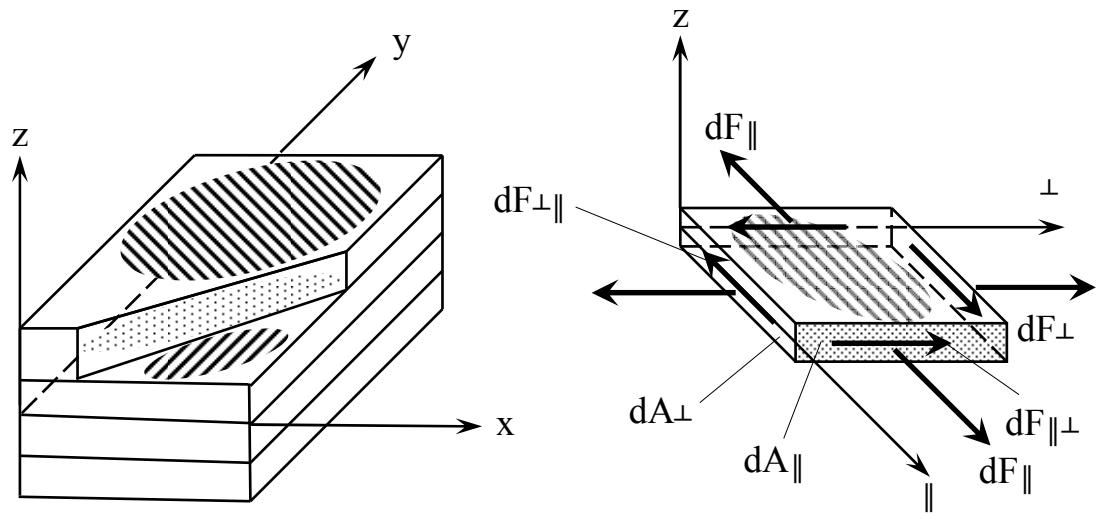

Fig. 2.1. Composite laminate and loadings of a lamina's representative volume element [33]

Three loadings can be defined on a representative volume element of the lamina. From a macroscopic point of view a lamina can be imagined as a continuous anisotropic homogeneous element in which the infinitely long fibers are inserted into the matrix. The lamina's cross section is not homogeneous, so the computational approach is carried out with medium stresses defined below. The stress along fibers direction will be [33]:

$$\sigma_{II} = \frac{dF_{II}}{dA_{II}} = \frac{1}{A_{II}} \int_{A_{II}} \sigma \, dA \,. \tag{2.1}$$

The stress transverse to fibers direction can be defined in the following way [33]:

$$\sigma_{\perp} = \frac{dF_{\perp}}{dA_{\perp}} = \frac{1}{A_{\perp}} \int_{A_{\perp}} \sigma \, dA \,, \tag{2.2}$$

and the shear stress $\tau_{\parallel\perp}$ is [33]:

$$\tau_{\#} = \frac{dF_{II\perp}}{dA_{II}} = \frac{dF_{\perp II}}{dA_{\perp}} = \frac{1}{A_{II}} \int_{A_{II}} \tau \, dA = \frac{1}{A_{\perp}} \int_{A_{\perp}} \tau \, dA \,, \qquad (2.3)$$

where σ and τ represent the normal and shear stresses that act on an infinitesimal area element dA belonging to the matrix or fiber.

Since on lamina acts a single longitudinal loading, $\sigma_{\parallel}$, then it causes the following strains [33]:

- Parallel on fibers direction: $\frac{\sigma_{II}}{E_{II}}$;
- Transverse to fibers direction: $-\upsilon_{\perp II} \frac{\sigma_{II}}{E_{II}}$.

Since on lamina acts a single longitudinal loading, $\sigma_{\perp}$, then it causes the following strains [33]:

- Transverse to fibers direction: $\frac{\sigma_{\perp}}{E_{\perp}}$;
- Parallel on fibers direction: $-\upsilon_{II\perp} \frac{\sigma_{\perp}}{E_{\perp}}$.

Regarding the Poisson's ratio, the first index represents the shrinkage direction and the second defines the loading direction that produce this shrinkage. Normal stresses $\sigma_{\parallel}$ and $\sigma_{\perp}$ cause the strains $\varepsilon_{\parallel}$ and $\varepsilon_{\perp}$ on the respective loading directions. In the same time, normal stresses $\sigma_{\parallel}$ and $\sigma_{\perp}$ cause also a shrinkage on the lamina's thickness direction, shrinkage that is often irrelevant in case of thin-walled structural elements. Positive/negative strains $\varepsilon_{\parallel}$ and $\varepsilon_{\perp}$ lead to lamina's lengthening/shortening on $\parallel$ respective $\perp$ direction (fig. 2.2). A positive/negative strain $\gamma_{\#}$ is caused by a positive/negative shear stress $\tau_{\#}$.

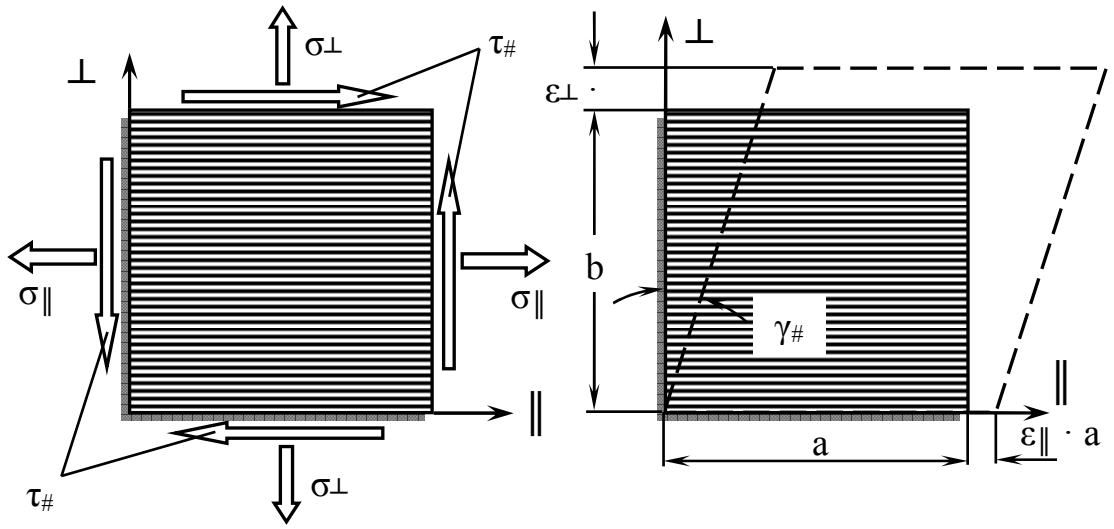

Fig. 2.2. Lamina's strains in the plane loading state [33]

The transverse tensile loading

On fibers subjected to transverse tensile loading act different influences affecting the lamina's mechanical behavior [11]:

- Stresses due to the loadings action;
- Interference stresses;
- Possible internal stresses;
- Additional stresses that cause an increase in the matrix strain.

Since an element from the composite laminate having parallel disposed fibers is deformed under a transverse tensile stress, the external measurable deformations should also take place within the material (see fig. 2.3). Due to its high Young's modulus, the fiber lengthens slightly, so that almost all transverse strain is taken up by matrix. This matrix transverse strain is greater than the strain noticed outside the lamina [11].

The equilibrium equation can be determined from fig. 2.3 [11]:

$$P = P_F = P_M, \quad \sigma = \sigma_F = \sigma_M. \tag{2.4}$$

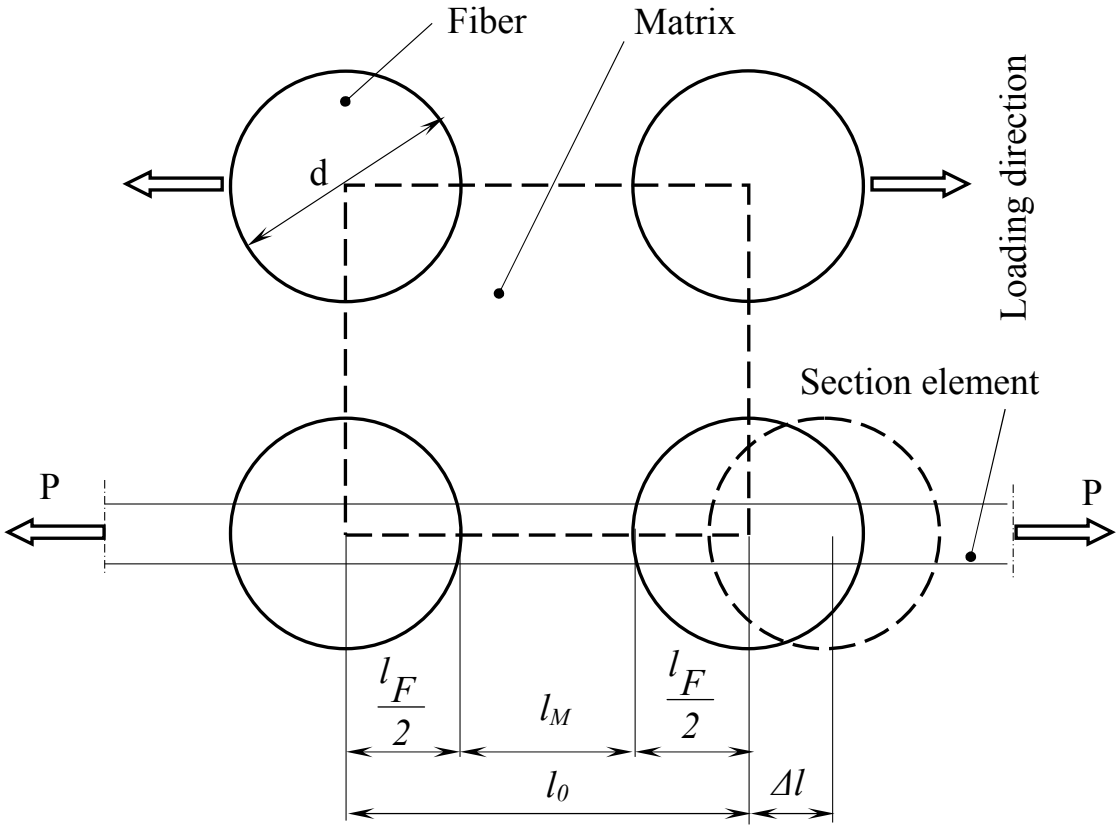

Fig. 2.3. Parallel "square shape" disposed fibers in a composite lamina subjected to transverse tensile loading [11]

The geometric conditions are [11]:

$$\frac{\Delta l}{l_0} = \varepsilon_{\perp}, \quad \Delta l = \Delta l_M + \Delta l_F . \tag{2.5}$$

Taking into consideration that [11]:

$$\frac{\Delta l_M}{l_M} = \varepsilon_M ; \frac{\Delta l_F}{l_F} = \varepsilon_F \text{ and } l_F = l_0 - l_M, \tag{2.6}$$

it follows [11]:

$$\varepsilon_{\perp} \cdot l_0 = \varepsilon_M \cdot l_M + \varepsilon_F \cdot l_F, \tag{2.7}$$

$$\varepsilon_{\perp} = \varepsilon_M \cdot \frac{l_M}{l_0} + \varepsilon_F \left(1 - \frac{l_M}{l_0} \right). \tag{2.8}$$

From the uniaxial material law [11]:

$$\varepsilon_F = \frac{\sigma_F}{E_F}; \quad \varepsilon_M = \frac{\sigma_M}{E_M}, \tag{2.9}$$

and taking onto consideration that $\sigma = \sigma_M = \sigma_F$, it follows [11]:

$$\varepsilon_{\perp} = \varepsilon_M \left[\frac{l_M}{l_0} + \frac{E_M}{E_F} \left(1 - \frac{l_M}{l_0} \right) \right] \tag{2.10}$$

as well as the matrix strain increase factor [11]:

$$f_{\varepsilon} = \frac{\varepsilon_M}{\varepsilon_{\perp}} = \frac{1}{\frac{l_M}{l_0} + \frac{E_M}{E_F} \left(1 - \frac{l_M}{l_0} \right)} > 1. \tag{2.11}$$

The geometric relations are [11]:

$$l_M = l_0 - d, \quad \frac{l_M}{l_0} = 1 - \frac{d}{l_0}, \tag{2.12}$$

and according to fig. 2.3, the fibers volume fraction can be expressed under following form [11]:

$$\frac{\pi \cdot d^2}{4 \cdot l_0^2} = \varphi, \tag{2.13}$$

from which it follows [11]:

$$\frac{d}{l_0} = \frac{2}{\sqrt{\pi}} \cdot \sqrt{\varphi}. \tag{2.14}$$

$$\frac{l_M}{l_0} = 1 - \frac{2}{\sqrt{\pi}} \cdot \sqrt{\varphi}. \tag{2.15}$$

For "square shape" disposed fibers, it follows the matrix strain increase factor [11]:

$$f_\varepsilon = \frac{1}{\left(1 - \frac{2}{\sqrt{\pi}} \cdot \sqrt{\varphi}\right) \cdot \left(1 - \frac{E_M}{E_F}\right) + \frac{E_M}{E_F}}. \tag{2.16}$$

<u>Elasticity laws of a continuous parallel fibers-reinforced lamina</u>

A continuous, parallel fibers-reinforced lamina is considered with fibers inserted in matrix (fig. 2.4). To describe the composite lamina's elastic features, two systems of coordinate axes have been defined [33]:

- *The x-y-z system*, called also the global coordinate system, in which the *x* and *y*-axes represent the resultant loadings' directions and *z*-axis takes place transverse to the plane formed by the *x-y* axes;
- *The* ∥ - ⊥ *– z system*, or (1)-(2)-(3), called also the local coordinate system, that determines the material's main directions, in which the ∥-axis takes

place along fibers and represents the lamina's longitudinal direction. The sense of ⊥-axis is transverse to fibers direction and determines the lamina's transverse direction.

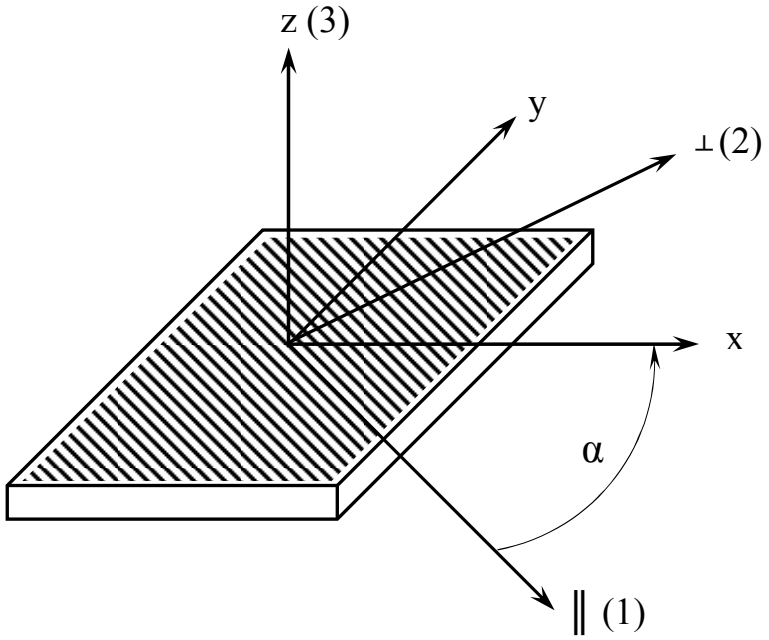

Fig. 2.4. Coordinate axes of a fibers-reinforced composite lamina [33]

The α angle between the positive x-axis direction and the positive ∥-axis direction is called fibers orientation angle and is positive when is measured in counter-clockwise sense by overlapping the positive ∥-axis direction over the positive x-axis direction.

The lamina's elastic properties such as longitudinal Young's modulus, E, Poisson ratio, υ and shear modulus, G, are defined using two indices. The first index represents the direction of the loading's action and the second represents the measuring direction of respective property.

For instance, $G_{\parallel\perp}$ (denoted also $G_{\#}$) is the shear modulus measured on ⊥ direction due to the loading action on ∥ direction.

Stresses and strains are also represented by two indices. The first index represents the direction transverse to the plane in which act the stress component and the second represents the action direction of the stress component. For instance, the first index of shear stress τ_{xy} represents the transverse direction to the

y-z plane and the *y*-index is the direction of the stress component. Stresses σ_{xx}, σ_{yy} and $\tau_{xy} = \tau_{yx}$ are also called in-plane intralaminar stresses, while σ_{zz}, τ_{xz} and τ_{yz} are called interlaminar stresses.

In case of the plane stress state by overlapping the action of three loadings, $\sigma_{\parallel}$, $\sigma_{\perp}$ and $\tau_{\#}$ (fig. 2.2), it follows the elasticity law [33]:

$$\begin{bmatrix} \varepsilon_{II} \\ \varepsilon_{\perp} \\ \gamma_{\#} \end{bmatrix} = \begin{bmatrix} \frac{1}{E_{II}} & -\frac{\upsilon_{II\perp}}{E_{\perp}} & 0 \\ -\frac{\upsilon_{\perp II}}{E_{II}} & \frac{1}{E_{\perp}} & 0 \\ 0 & 0 & \frac{1}{G_{\#}} \end{bmatrix} \cdot \begin{bmatrix} \sigma_{II} \\ \sigma_{\perp} \\ \tau_{\#} \end{bmatrix}, \tag{2.17}$$

or the matrix expression (2.17) may be written as follows [33]:

$$\begin{bmatrix} \varepsilon_{II} \\ \varepsilon_{\perp} \\ \gamma_{\#} \end{bmatrix} = \begin{bmatrix} c_{II} & c_{II\perp} & 0 \\ c_{\perp II} & c_{\perp} & 0 \\ 0 & 0 & c_{\#} \end{bmatrix} \cdot \begin{bmatrix} \sigma_{II} \\ \sigma_{\perp} \\ \tau_{\#} \end{bmatrix}, \tag{2.18}$$

where [33]:

$$[C] = \begin{bmatrix} c_{II} & c_{II\perp} & 0 \\ c_{\perp II} & c_{\perp} & 0 \\ 0 & 0 & c_{\#} \end{bmatrix}, \tag{2.19}$$

is called also the compliances matrix or flexibility matrix.

The transverse Poisson ratios $\upsilon_{\parallel\perp}$ and $\upsilon_{\perp\parallel}$ are not independent of each other. If the existence of small deformations as well as linear elastic behavior of the composite material is assumed then there is following expression between transverse Poisson ratios and the Young's moduli [33]:

$$\frac{\upsilon_{\perp II}}{E_{II}} = \frac{\upsilon_{II\perp}}{E_{\perp}}. \tag{2.20}$$

Relation (2.20) is called also the Maxwell-Betti law. Therefore, the unidirectional reinforced lamina can be described by four basic elasticity constants: $E_{\parallel}$, $E_{\perp}$, $\upsilon_{\perp\parallel}$ and $G_{\#}$. When the expression of stresses versus strains is required then relation (2.17) becomes [33]:

$$\begin{bmatrix} \sigma_{II} \\ \sigma_{\perp} \\ \tau_{\#} \end{bmatrix} = \begin{bmatrix} \frac{E_{II}}{1-\upsilon_{\perp II}\cdot\upsilon_{II\perp}} & \frac{\upsilon_{II\perp}\cdot E_{\perp}}{1-\upsilon_{\perp II}\cdot\upsilon_{II\perp}} & 0 \\ \frac{\upsilon_{\perp II}\cdot E_{II}}{1-\upsilon_{\perp II}\cdot\upsilon_{II\perp}} & \frac{E_{\perp}}{1-\upsilon_{\perp II}\cdot\upsilon_{II\perp}} & 0 \\ 0 & 0 & G_{\#} \end{bmatrix} \cdot \begin{bmatrix} \varepsilon_{II} \\ \varepsilon_{\perp} \\ \gamma_{\#} \end{bmatrix}, \tag{2.21}$$

or the equation (2.21) can be expressed as [33]:

$$\begin{bmatrix} \sigma_{II} \\ \sigma_{\perp} \\ \tau_{\#} \end{bmatrix} = \begin{bmatrix} r_{II} & r_{II\perp} & 0 \\ r_{\perp II} & r_{\perp} & 0 \\ 0 & 0 & r_{\#} \end{bmatrix} \cdot \begin{bmatrix} \varepsilon_{II} \\ \varepsilon_{\perp} \\ \gamma_{\#} \end{bmatrix}, \tag{2.22}$$

where [33]:

$$[R] = \begin{bmatrix} r_{II} & r_{II\perp} & 0 \\ r_{\perp II} & r_{\perp} & 0 \\ 0 & 0 & r_{\#} \end{bmatrix}, \tag{2.23}$$

represents the stiffness matrix.

The expression of strains versus stresses has the advantage to compute the compliances according to lamina's elasticity constants, also known as technical

constants. These constants can be determined from the lamina's micromechanics, as follows [33]:

$$E_{II} = E_F \cdot \varphi + E_M \cdot (1 - \varphi), \tag{2.24}$$

$$\upsilon_{\perp II} = \varphi \cdot \upsilon_F + (1 - \varphi) \cdot \upsilon_M \ , \tag{2.25}$$

$$E_{\perp} = \frac{E_M}{1 - \upsilon_M^2} \cdot \frac{1 + 0{,}85 \cdot \varphi^2}{(1 - \varphi)^{1{,}25} + \frac{\varphi \cdot E_M}{(1 - \upsilon_M^2) \cdot E_F}}, \tag{2.26}$$

$$\upsilon_{II\perp} = \upsilon_{\perp II} \cdot \frac{E_{\perp}}{E_{II}}, \tag{2.27}$$

$$G_{\#} = G_M \cdot \frac{1 + 0{,}6 \cdot \varphi^{0{,}5}}{(1 - \varphi)^{1{,}25} + \varphi \cdot \frac{G_M}{G_F}}. \tag{2.28}$$

The index M refers to matrix and index F is used for fibers.

In many cases, the directions of external loadings σ_{xx}, σ_{yy}, τ_{xy} do not coincide with the main directions in material (the local coordinate system $\parallel$ - $\perp$ – z) which means that the global coordinate system x-y-z of external loadings is not identical with the lamina's local coordinate system. In order to be able to transform stresses and strains from one coordinate system to another, simple transformation formulae have been used. A lamina has been considered in which stresses act in-plane, which means that $\sigma_{zz} = \tau_{xz} = \tau_{yz} = 0$ (fig. 2.5).

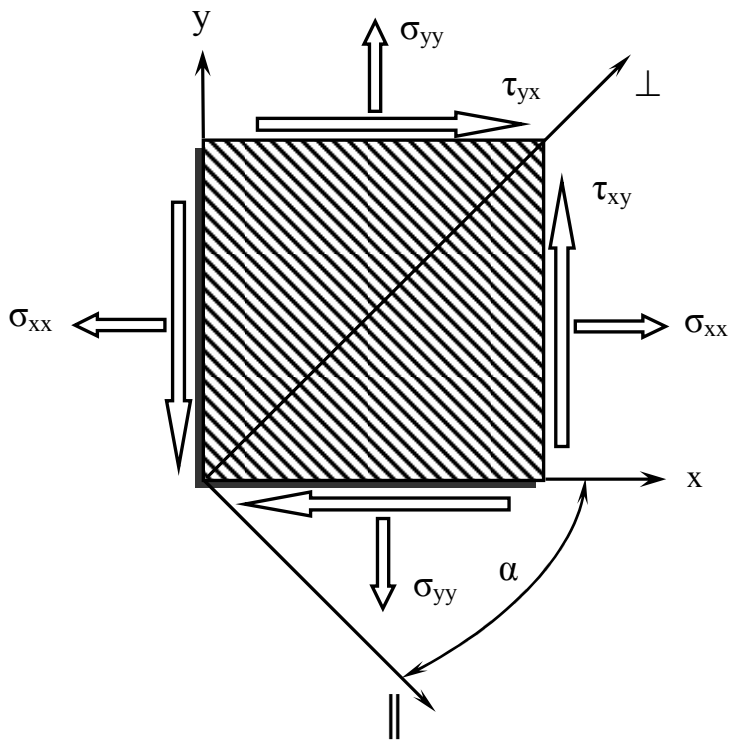

Fig. 2.5. Stresses in a lamina in case of stress plane state [33]

The transformed stresses and strains from the global to local coordinate system and vice-versa, are [26]:

$$\begin{bmatrix} \sigma_{xx} \\ \sigma_{yy} \\ \tau_{xy} \end{bmatrix} = \begin{bmatrix} \cos^2\alpha & \sin^2\alpha & -2\sin\alpha\cos\alpha \\ \sin^2\alpha & \cos^2\alpha & 2\sin\alpha\cos\alpha \\ \sin\alpha\cos\alpha & -\sin\alpha\cos\alpha & \left(\cos^2\alpha - \sin^2\alpha\right) \end{bmatrix} \cdot \begin{bmatrix} \sigma_{II} \\ \sigma_{\perp} \\ \tau_{\#} \end{bmatrix}. \quad (2.29)$$

$$\begin{bmatrix} \sigma_{II} \\ \sigma_{\perp} \\ \tau_{\#} \end{bmatrix} = \begin{bmatrix} \cos^2\alpha & \sin^2\alpha & 2\sin\alpha\cos\alpha \\ \sin^2\alpha & \cos^2\alpha & -2\sin\alpha\cos\alpha \\ -\sin\alpha\cos\alpha & \sin\alpha\cos\alpha & \left(\cos^2\alpha - \sin^2\alpha\right) \end{bmatrix} \cdot \begin{bmatrix} \sigma_{xx} \\ \sigma_{yy} \\ \tau_{xy} \end{bmatrix}. \quad (2.30)$$

$$\begin{bmatrix} \varepsilon_{xx} \\ \varepsilon_{yy} \\ \gamma_{xy} \end{bmatrix} = \begin{bmatrix} \cos^2\alpha & \sin^2\alpha & -\sin\alpha\cos\alpha \\ \sin^2\alpha & \cos^2\alpha & \sin\alpha\cos\alpha \\ 2\sin\alpha\cos\alpha & -2\sin\alpha\cos\alpha & \left(\cos^2\alpha - \sin^2\alpha\right) \end{bmatrix} \cdot \begin{bmatrix} \varepsilon_{II} \\ \varepsilon_{\perp} \\ \gamma_{\#} \end{bmatrix}. \qquad (2.31)$$

$$\begin{bmatrix} \varepsilon_{II} \\ \varepsilon_{\perp} \\ \gamma_{\#} \end{bmatrix} = \begin{bmatrix} \cos^2\alpha & \sin^2\alpha & \sin\alpha\cos\alpha \\ \sin^2\alpha & \cos^2\alpha & -\sin\alpha\cos\alpha \\ -2\sin\alpha\cos\alpha & 2\sin\alpha\cos\alpha & \left(\cos^2\alpha - \sin^2\alpha\right) \end{bmatrix} \cdot \begin{bmatrix} \varepsilon_{xx} \\ \varepsilon_{yy} \\ \gamma_{xy} \end{bmatrix}. \qquad (2.32)$$

Regarding the lamina being in the plane stress state (see fig. 2.5), its strains can be expressed according to stresses by means of the transformed components of the compliances' matrix [33]:

$$\begin{bmatrix} \varepsilon_{xx} \\ \varepsilon_{yy} \\ \gamma_{xy} \end{bmatrix} = \begin{bmatrix} c_{11} & c_{12} & c_{13} \\ c_{12} & c_{22} & c_{23} \\ c_{13} & c_{23} & c_{33} \end{bmatrix} \cdot \begin{bmatrix} \sigma_{xx} \\ \sigma_{yy} \\ \tau_{xy} \end{bmatrix}. \qquad (2.33)$$

These transformed compliances, c_{ij}, can be computed according to the basic elasticity constants of the unidirectional reinforced lamina, $E_{\parallel}$, $E_{\perp}$, $\upsilon_{\perp\parallel}$, $G_{\#}$ as well as according to the fibers disposal angle, α [33]:

$$c_{11} = \frac{\cos^4\alpha}{E_{II}} + \frac{\sin^4\alpha}{E_{\perp}} + \frac{1}{4}\cdot\left(\frac{1}{G_{\#}} - \frac{2\cdot\upsilon_{\perp II}}{E_{II}}\right)\cdot\sin^2 2\alpha, \qquad (2.34)$$

$$c_{22} = \frac{\sin^4\alpha}{E_{II}} + \frac{\cos^4\alpha}{E_{\perp}} + \frac{1}{4}\cdot\left(\frac{1}{G_{\#}} - \frac{2\cdot\upsilon_{\perp II}}{E_{II}}\right)\cdot\sin^2 2\alpha, \qquad (2.35)$$

$$c_{33} = \frac{\cos^2 2\alpha}{G_{\#}} + \left(\frac{1}{E_{II}} + \frac{1}{E_{\perp}} + \frac{2\cdot\upsilon_{\perp II}}{E_{II}}\right)\cdot\sin^2 2\alpha, \qquad (2.36)$$

$$c_{12}=\frac{1}{4}\cdot\left(\frac{1}{E_{II}}+\frac{1}{E_{\perp}}-\frac{1}{G_{\#}}\right)\cdot sin^2 2\alpha-\frac{\upsilon_{\perp II}}{E_{II}}\cdot\left(sin^4\alpha+cos^4\alpha\right),\quad(2.37)$$

$$c_{13}=\left(\frac{2}{E_{\perp}}+\frac{2\cdot\upsilon_{\perp II}}{E_{II}}-\frac{1}{G_{\#}}\right)\cdot sin^3\alpha\cdot cos\alpha-$$

$$-\left(\frac{2}{E_{II}}+\frac{2\cdot\upsilon_{\perp II}}{E_{II}}-\frac{1}{G_{\#}}\right)\cdot cos^3\alpha\cdot sin\alpha,\quad(2.38)$$

$$c_{23}=\left(\frac{2}{E_{\perp}}+\frac{2\cdot\upsilon_{\perp II}}{E_{II}}-\frac{1}{G_{\#}}\right)\cdot cos^3\alpha\cdot sin\alpha-$$

$$-\left(\frac{2}{E_{II}}+\frac{2\cdot\upsilon_{\perp II}}{E_{II}}-\frac{1}{G_{\#}}\right)\cdot sin^3\alpha\cdot cos\alpha.\quad(2.39)$$

If the composite laminate's stresses are expressed according to the strains [33]:

$$\begin{bmatrix}\sigma_{xx}\\ \sigma_{yy}\\ \tau_{xy}\end{bmatrix}=\begin{bmatrix}r_{11} & r_{12} & r_{13}\\ r_{12} & r_{22} & r_{23}\\ r_{13} & r_{23} & r_{33}\end{bmatrix}\cdot\begin{bmatrix}\varepsilon_{xx}\\ \varepsilon_{yy}\\ \gamma_{xy}\end{bmatrix},\quad(2.40)$$

then r_{ij} represent the transformed components of the stiffness matrix that can be computed according to the lamina's basic elasticity constants, $E_{\parallel}$, $E_{\perp}$, $\upsilon_{\perp\parallel}$, $G_{\#}$ as well as according to the fibers disposal angle, α [33]:

$$r_{11}=\frac{E_{II}\cdot cos^4\alpha}{1-\upsilon_{\perp II}\cdot\upsilon_{II\perp}}+\frac{E_{\perp}\cdot sin^4\alpha}{1-\upsilon_{\perp II}\cdot\upsilon_{II\perp}}+\frac{1}{2}\cdot\left(\frac{\upsilon_{\perp II}\cdot E_{\perp}}{1-\upsilon_{\perp II}\cdot\upsilon_{II\perp}}+2\cdot G_{\#}\right)\cdot sin^2 2\alpha, \quad (2.41)$$

$$r_{22}=\frac{E_{II}\cdot sin^4\alpha}{1-\upsilon_{\perp II}\cdot\upsilon_{II\perp}}+\frac{E_{\perp}\cdot cos^4\alpha}{1-\upsilon_{\perp II}\cdot\upsilon_{II\perp}}+$$

$$+\frac{1}{2}\cdot\left(\frac{\upsilon_{\perp II}\cdot E_{\perp}}{1-\upsilon_{\perp II}\cdot\upsilon_{II\perp}}+2\cdot G_{\#}\right)\cdot sin^2 2\alpha, \quad (2.42)$$

$$r_{33}=G_{II\perp}+\frac{1}{4}\cdot\left(\frac{E_{II}}{1-\upsilon_{\perp II}\cdot\upsilon_{II\perp}}+\frac{E_{\perp}}{1-\upsilon_{\perp II}\cdot\upsilon_{II\perp}}-\right.$$

$$\left.-\frac{2\cdot\upsilon_{\perp II}\cdot E_{\perp}}{1-\upsilon_{\perp II}\cdot\upsilon_{II\perp}}-4\cdot G_{\#}\right)\cdot sin^2 2\alpha, \quad (2.43)$$

$$r_{12}=\frac{\upsilon_{\perp II}\cdot E_{\perp}}{1-\upsilon_{\perp II}\cdot\upsilon_{II\perp}}+\frac{1}{4}\cdot\left(\frac{E_{II}}{1-\upsilon_{\perp II}\cdot\upsilon_{II\perp}}+\frac{E_{\perp}}{1-\upsilon_{\perp II}\cdot\upsilon_{II\perp}}-\right.$$

$$\left.-\frac{2\cdot\upsilon_{\perp II}\cdot E_{\perp}}{1-\upsilon_{\perp II}\cdot\upsilon_{II\perp}}-4\cdot G_{\#}\right)\cdot sin^2 2\alpha, \quad (2.44)$$

$$r_{13}=\frac{1}{2}\cdot\left[\left(\frac{E_{II}}{1-\upsilon_{\perp II}\cdot\upsilon_{II\perp}}+\frac{E_{\perp}}{1-\upsilon_{\perp II}\cdot\upsilon_{II\perp}}-\frac{2\cdot\upsilon_{\perp II}\cdot E_{\perp}}{1-\upsilon_{\perp II}\cdot\upsilon_{II\perp}}-4\cdot G_{\#}\right)\cdot sin^2\alpha-\right.$$

$$\left.-\left(\frac{E_{II}}{1-\upsilon_{\perp II}\cdot\upsilon_{II\perp}}-\frac{\upsilon_{\perp II}\cdot E_{\perp}}{1-\upsilon_{\perp II}\cdot\upsilon_{II\perp}}-2\cdot G_{\#}\right)\right]\cdot sin 2\alpha, \quad (2.45)$$

$$r_{23}=\frac{1}{2}\cdot\left[\left(\frac{E_{\perp}}{1-\upsilon_{\perp II}\cdot\upsilon_{II\perp}}-\frac{\upsilon_{\perp II}\cdot E_{\perp}}{1-\upsilon_{\perp II}\cdot\upsilon_{II\perp}}-2\cdot G_{\#}\right)-\left(\frac{E_{II}}{1-\upsilon_{\perp II}\cdot\upsilon_{II\perp}}+\right.\right.$$

$$\left.\left.+\frac{E_{\perp}}{1-\upsilon_{\perp II}\cdot\upsilon_{II\perp}}-\frac{2\cdot\upsilon_{\perp II}\cdot E_{\perp}}{1-\upsilon_{\perp II}\cdot\upsilon_{II\perp}}-4\cdot G_{\#}\right)\cdot sin^{2}\alpha\right]\cdot sin 2\alpha. \quad (2.46)$$

Dimensioning of a composite laminate structure

A composite laminate structure can be manufactured by stacking many unidirectional reinforced laminae one above the other on their thickness (fig. 2.6). It is assumed that the laminate is thin with perfect bond between laminae, the strains distribution on the direction of laminate thickness is linear and all laminae are homogeneous and behave linear elastic. The assumptions are always satisfied in case of symmetrical arrangement of laminae against the laminate median surface. The loading scheme of a composite laminate is presented in fig. 2.7.

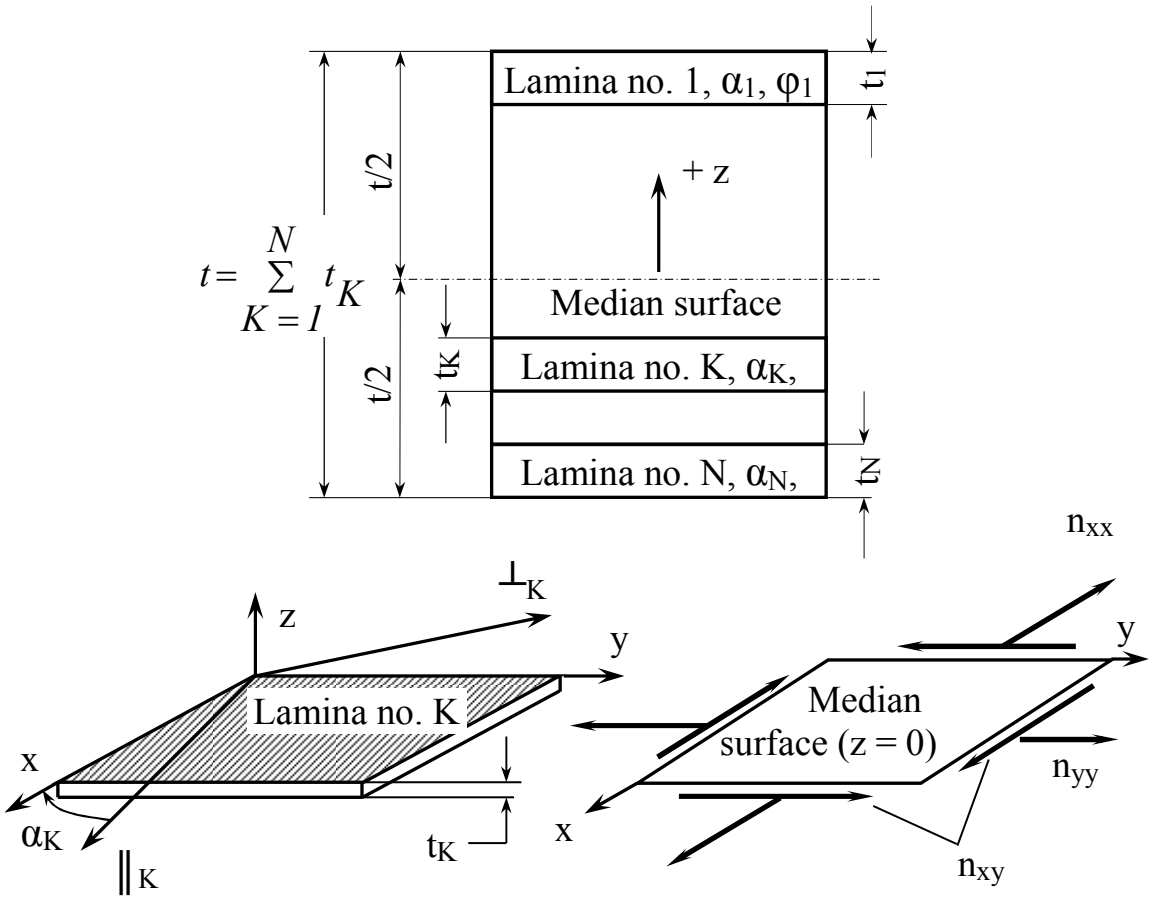

Fig. 2.6. Constructive scheme of a fibers-reinforced composite laminate [33]

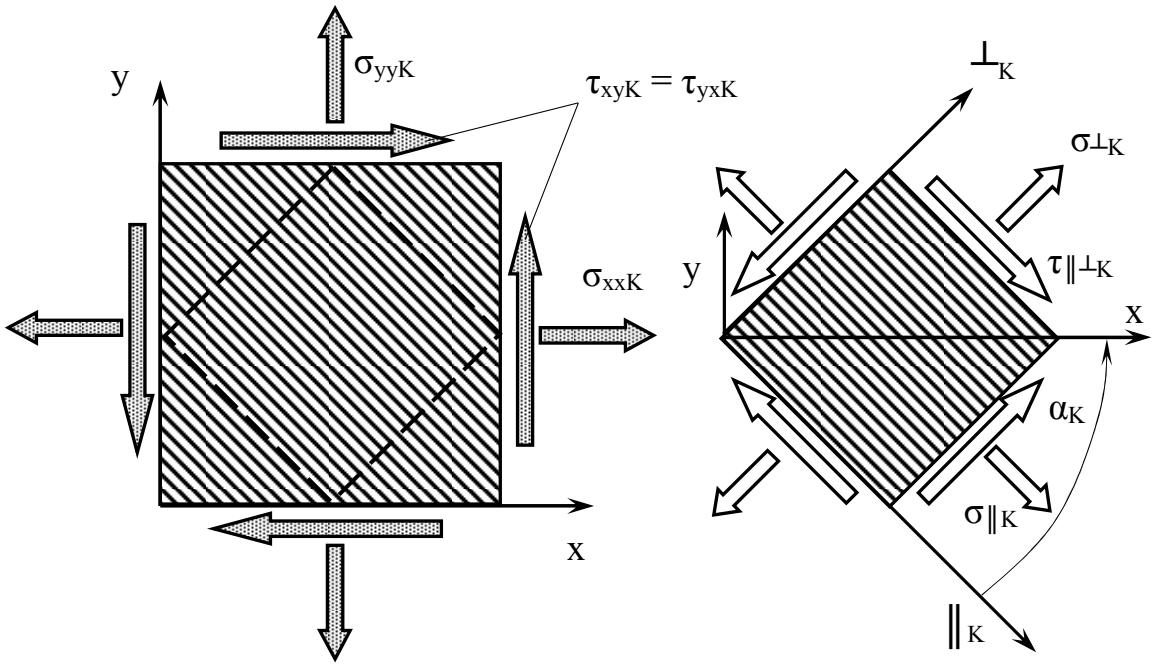

Fig. 2.7. Loading scheme of a composite laminate [33]

The elasticity law of *K* unidirectional lamina is [33]:

$$\begin{bmatrix} \sigma_{xx\,K} \\ \sigma_{yy\,K} \\ \tau_{xy\,K} \end{bmatrix} = \begin{bmatrix} r_{11\,K} & r_{12\,K} & r_{13\,K} \\ r_{12\,K} & r_{22\,K} & r_{23\,K} \\ r_{13\,K} & r_{23\,K} & r_{33\,K} \end{bmatrix} \cdot \begin{bmatrix} \varepsilon_{xx\,K} \\ \varepsilon_{yy\,K} \\ \gamma_{xy\,K} \end{bmatrix}, \tag{2.47}$$

where r_{ijK} represent the transformed stiffness in relations (2.41) – (2.46).

The equilibrium equations of the laminate structure, are [33]:

$$n_{xx} = \underline{\sigma}_{xx} \cdot t = \sum_{K=1}^{N} \left(\sigma_{xxK} \cdot t_K \right) = \sum_{K=1}^{N} n_{xxK}, \tag{2.48}$$

$$n_{yy} = \underline{\sigma}_{yy} \cdot t = \sum_{K=1}^{N} \left(\sigma_{yyK} \cdot t_K \right) = \sum_{K=1}^{N} n_{yyK}, \tag{2.49}$$

$$n_{xy} = \underline{\tau}_{xy} \cdot t = \sum_{K=1}^{N} \left(\tau_{xyK} \cdot t_K \right) = \sum_{K=1}^{N} n_{xyK}, \tag{2.50}$$

where n_{xx} and n_{yy} represent the normal forces and n_{xy} is the shear force. The stresses $\underline{\sigma}_{xx}$, $\underline{\sigma}_{yy}$ and $\underline{\tau}_{xy}$ are according to the *x*-*y* coordinate system.

The geometrical conditions are [33]:

$$\begin{aligned} \varepsilon_{xxK} &= \varepsilon_{xx}, \\ \varepsilon_{yyK} &= \varepsilon_{yy}, \\ \gamma_{xyK} &= \gamma_{xy}, \end{aligned} \tag{2.51}$$

for all *K* laminae.

With relations (2.47) – (2.51), following elasticity law can be obtained [33]:

$$\begin{bmatrix} \underline{\sigma}_{xx} \\ \underline{\sigma}_{yy} \\ \underline{\tau}_{xy} \end{bmatrix} = \begin{bmatrix} \sum_{K=1}^{N}\left(r_{11\,K}\cdot\frac{t_K}{t}\right) & \sum_{K=1}^{N}\left(r_{12\,K}\cdot\frac{t_K}{t}\right) & \sum_{K=1}^{N}\left(r_{13\,K}\cdot\frac{t_K}{t}\right) \\ \sum_{K=1}^{N}\left(r_{12\,K}\cdot\frac{t_K}{t}\right) & \sum_{K=1}^{N}\left(r_{22\,K}\cdot\frac{t_K}{t}\right) & \sum_{K=1}^{N}\left(r_{23\,K}\cdot\frac{t_K}{t}\right) \\ \sum_{K=1}^{N}\left(r_{13\,K}\cdot\frac{t_K}{t}\right) & \sum_{K=1}^{N}\left(r_{23\,K}\cdot\frac{t_K}{t}\right) & \sum_{K=1}^{N}\left(r_{33\,K}\cdot\frac{t_K}{t}\right) \end{bmatrix} \cdot \begin{bmatrix} \varepsilon_{xx} \\ \varepsilon_{yy} \\ \gamma_{xy} \end{bmatrix}, \quad (2.52)$$

with the stiffness of the composite laminate [33]:

$$\underline{r}_{ij} = \sum_{K=1}^{N}\left(r_{ijK}\cdot\frac{t_K}{t}\right). \quad (2.53)$$

So, the elasticity law of a composite laminate becomes [33]:

$$\begin{bmatrix} \underline{\sigma}_{xx} \\ \underline{\sigma}_{yy} \\ \underline{\tau}_{xy} \end{bmatrix} = \begin{bmatrix} \underline{r}_{11} & \underline{r}_{12} & \underline{r}_{13} \\ \underline{r}_{12} & \underline{r}_{22} & \underline{r}_{23} \\ \underline{r}_{13} & \underline{r}_{23} & \underline{r}_{33} \end{bmatrix} \cdot \begin{bmatrix} \varepsilon_{xx} \\ \varepsilon_{yy} \\ \gamma_{xy} \end{bmatrix}, \quad (2.54)$$

The strains of individual laminae follows by transformation [33]:

$$\begin{bmatrix} \varepsilon_{II\,K} \\ \varepsilon_{\perp K} \\ \gamma_{\#K} \end{bmatrix} = \begin{bmatrix} cos^2\alpha_K & sin^2\alpha_K & sin\alpha_K cos\alpha_K \\ sin^2\alpha_K & cos^2\alpha_K & -sin\alpha_K cos\alpha_K \\ -2sin\alpha_K cos\alpha_K & 2sin\alpha_K cos\alpha_K & \left(cos^2\alpha_K - sin^2\alpha_K\right) \end{bmatrix} \cdot \begin{bmatrix} \varepsilon_{xx\,K} \\ \varepsilon_{yy\,K} \\ \gamma_{xy} \end{bmatrix}. \quad (2.55)$$

Finally, the stresses in every lamina can be computed [33]:

$$\sigma_{II\,K} = \frac{E_{II\,K}}{1-\upsilon_{\perp II\,K}\cdot\upsilon_{II\perp K}}\cdot\varepsilon_{II\,K} + \frac{\upsilon_{\perp II\,K}\cdot E_{\perp K}}{1-\upsilon_{\perp II\,K}\cdot\upsilon_{II\perp K}}\cdot\varepsilon_{\perp K}, \quad (2.56)$$

$$\sigma_{\perp K}=\frac{\upsilon_{\perp II K}\cdot E_{\perp K}}{1-\upsilon_{\perp II K}\cdot\upsilon_{II\perp K}}\cdot\varepsilon_{II K}+\frac{E_{\perp K}}{1-\upsilon_{\perp II K}\cdot\upsilon_{II\perp K}}\cdot\varepsilon_{\perp K}, \qquad (2.57)$$

$$\tau_{\#K}=G_{\#}\cdot\gamma_{\#}. \qquad (2.58)$$

To make a prediction of break danger in individual laminae, a break criterion is usually used.

2.3. Contributions to compute the matrix strain increase factor

In case of transverse tensile loading of a unidirectional fibers-reinforced lamina, the matrix strain increase factor for “square shape” disposal of fibers is given in relation (2.16).

To compute the matrix strain increase factor in case of parallel “hexagonal shape” disposed fibers in a unidirectional fibers-reinforced lamina, I have developed a scheme presented in fig. 2.8.

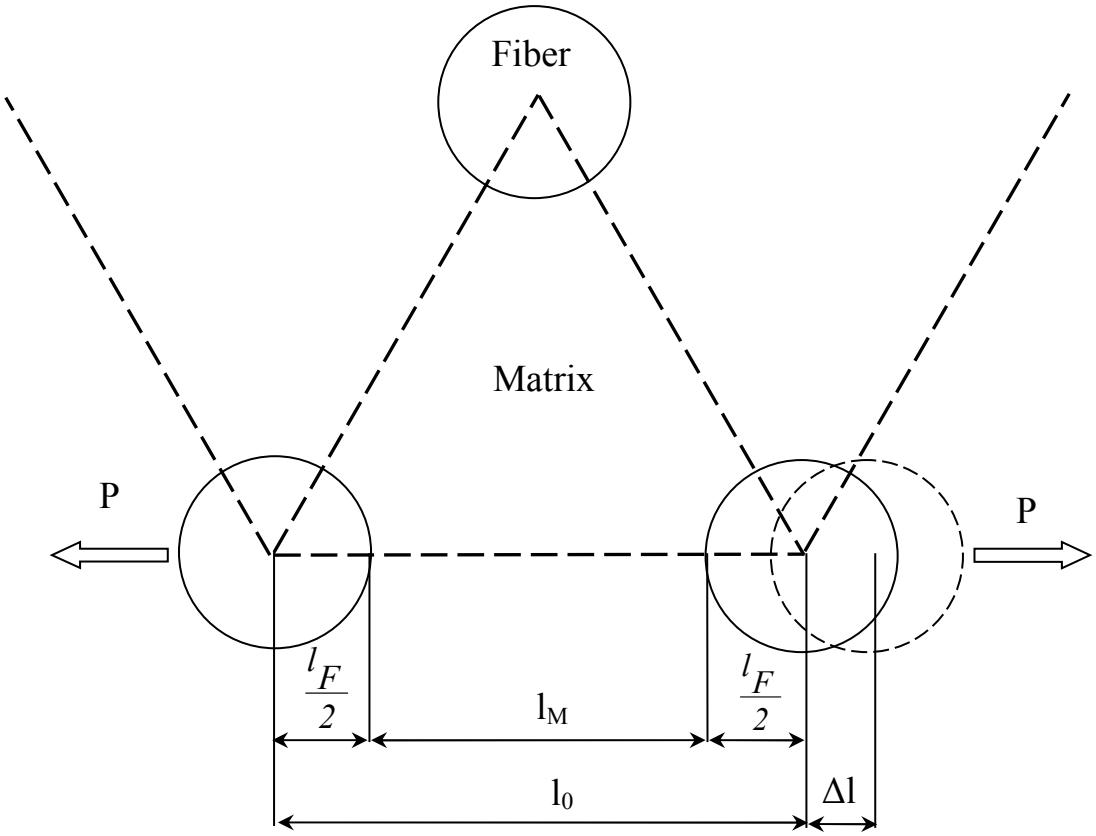

Fig. 2.8. Parallel "hexagonal shape" disposed fibers in a composite lamina subjected to transverse tensile loads

The maximum fibers volume fraction in this case can be computed using the scheme shown in fig. 2.9.

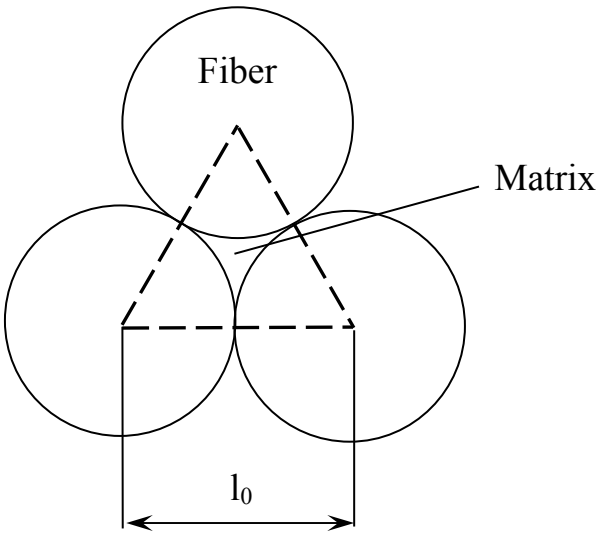

Fig. 2.9. Maximum fibers volume fraction in case of parallel "hexagonal shape" disposed fibers

I have started from the fact that:

$$\frac{\pi d^2}{8} = \varphi \cdot \frac{l_0^2 \cdot \sqrt{3}}{4}. \tag{2.59}$$

So, the maximum fibers volume fraction in case of parallel "hexagonal shape" disposed fibers in a unidirectional fibers-reinforced lamina subjected to transverse tensile loads can be computed as follows:

$$\varphi = \frac{\pi d^2}{2 l_0^2 \cdot \sqrt{3}}. \tag{2.60}$$

From relation (2.60), following important ratio can be determined:

$$\frac{d}{l_0} = \sqrt{\frac{2\varphi\sqrt{3}}{\pi}}. \tag{2.61}$$

Relation (2.61) gives the theoretical maximum fibers volume fraction in case of "hexagonal shape" disposed fibers in a unidirectional fibers-reinforced lamina in which the ratio $\frac{d}{l_0} = 1$:

$$\varphi_{max\ theoretic} = \frac{\pi}{2\sqrt{3}} = 0.906 \tag{2.62}$$

The ratio between matrix length and the length between fibers can be computed using following relation:

$$\frac{l_M}{l_0}=1-\frac{d}{l_0}=1-\sqrt{\frac{2\varphi\sqrt{3}}{\pi}}. \tag{2.63}$$

So, in this case, the matrix strain increase factor will be:

$$f_\varepsilon=\frac{\varepsilon_M}{\varepsilon_\perp}=\frac{1}{\frac{l_M}{l_0}+\frac{E_M}{E_F}\left(1-\frac{l_M}{l_0}\right)}=\frac{1}{\frac{l_M}{l_0}\left(1-\frac{E_M}{E_F}\right)+\frac{E_M}{E_F}}= \tag{2.64}$$
$$=\frac{1}{\left(1-\sqrt{\frac{2\varphi\sqrt{3}}{\pi}}\right)\left(1-\frac{E_M}{E_F}\right)+\frac{E_M}{E_F}}.$$

A comparison between the matrix strain increase factor in case of "square shape" and "hexagonal shape" disposed fibers for a unidirectional glass fibers-reinforced epoxy resin lamina subjected to transverse tensile loads is presented in table 2.1 and shown in fig. 2.10. Input data for Young's moduli of epoxy resin and glass fibers, are:

- For epoxy resin: $E_M = 3$ GPa;
- For E-glass fibers: $E_F = 73$ GPa.

Table 2.1. Matrix strain increase factors for two shapes of disposed fibers in a unidirectional glass fibers-reinforced epoxy resin lamina

φ (%)	0	10	20	30	40	50	60	70
$f_{\varepsilon\ hexagon}$	1	1.46	1.81	2.22	2.75	3.47	4.54	6.34
$f_{\varepsilon\ square}$	1	1.52	1.93	2.45	3.16	4.25	6.17	10.55

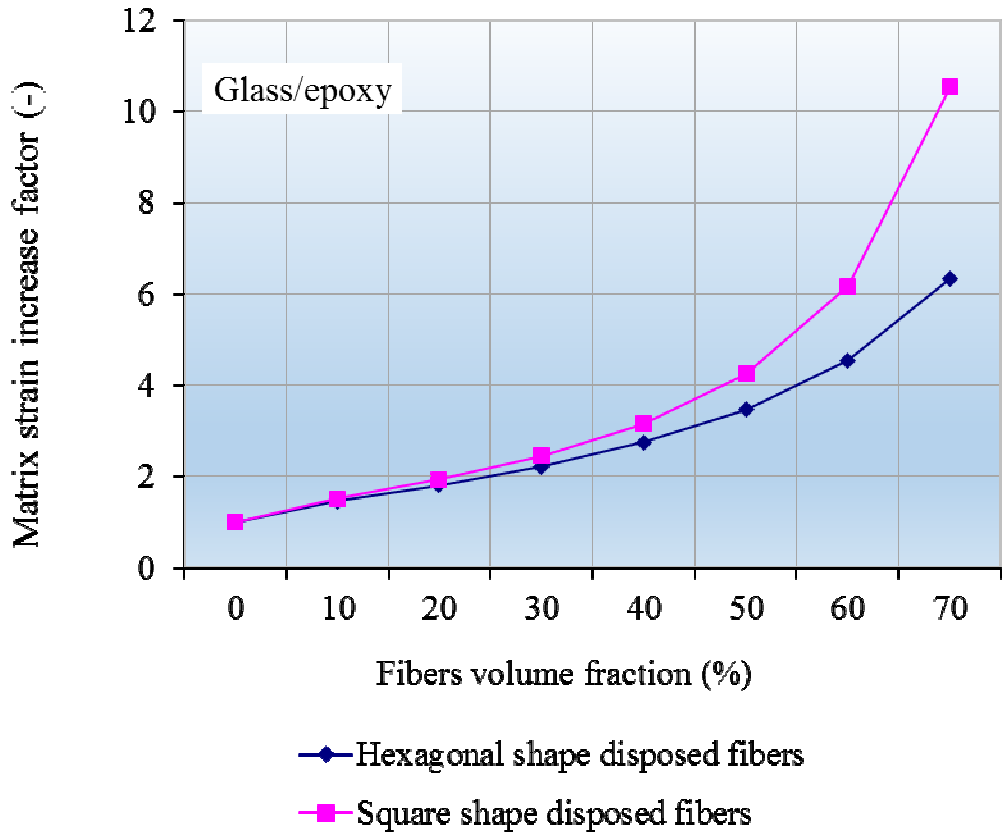

Fig. 2.10. Matrix strain increase factors for hexagonal and square shape disposed fibers in a glass fibers-reinforced epoxy resin lamina

In case of HM carbon fibers-reinforced epoxy resin lamina, due to strong anisotropy of these fibers, the matrix strain increase factors for both "hexagonal" and "square shape" disposed fibers, will be:

$$f_{\varepsilon\, hex.}=\frac{\varepsilon_M}{\varepsilon_\perp}=\frac{1}{\frac{l_M}{l_0}+\frac{E_M}{E_{F\perp}}\left(1-\frac{l_M}{l_0}\right)}=\frac{1}{\frac{l_M}{l_0}\left(1-\frac{E_M}{E_{F\perp}}\right)+\frac{E_M}{E_{F\perp}}}= \\ =\frac{1}{\left(1-\sqrt{\frac{2\varphi\sqrt{3}}{\pi}}\right)\left(1-\frac{E_M}{E_{F\perp}}\right)+\frac{E_M}{E_{F\perp}}}. \qquad (2.65)$$

$$f_{\varepsilon\ square} = \frac{\varepsilon_M}{\varepsilon_\perp} = \frac{1}{\frac{l_M}{l_0} + \frac{E_M}{E_{F\perp}}\left(1 - \frac{l_M}{l_0}\right)} = \frac{1}{\frac{l_M}{l_0}\left(1 - \frac{E_M}{E_{F\perp}}\right) + \frac{E_M}{E_{F\perp}}} = \\ = \frac{1}{\left(1 - 2\sqrt{\frac{\varphi}{\pi}}\right)\left(1 - \frac{E_M}{E_{F\perp}}\right) + \frac{E_M}{E_{F\perp}}}. \quad (2.66)$$

For this type of lamina, following input data have been used to compute the matrix strain increase factors for both "hexagonal" and "square shape" disposed fibers:

- For epoxy resin: $E_M = 3$ GPa;
- For HM carbon fibers: $E_{F\perp} = 25$ GPa.

A comparison between the matrix strain increase factor in case of "square shape" and "hexagonal shape" disposed fibers for a unidirectional HM carbon fibers-reinforced epoxy resin lamina subjected to transverse tensile loads is presented in table 2.2 and visualized in fig. 2.11. The comparison of both matrix strain increase factors in case of both types of fibers are presented in figs. 2.12 – 2.13.

Table 2.2. Matrix strain increase factors for two shapes of disposed fibers in a unidirectional HM carbon fibers-reinforced epoxy resin lamina

φ (%)	0	10	20	30	40	50	60	70
$f_{\varepsilon\ hexagon}$	1	1.41	1.7	2.02	2.4	2.88	3.51	4.4
$f_{\varepsilon\ square}$	1	1.45	1.79	2.19	2.68	3.35	4.33	5.9

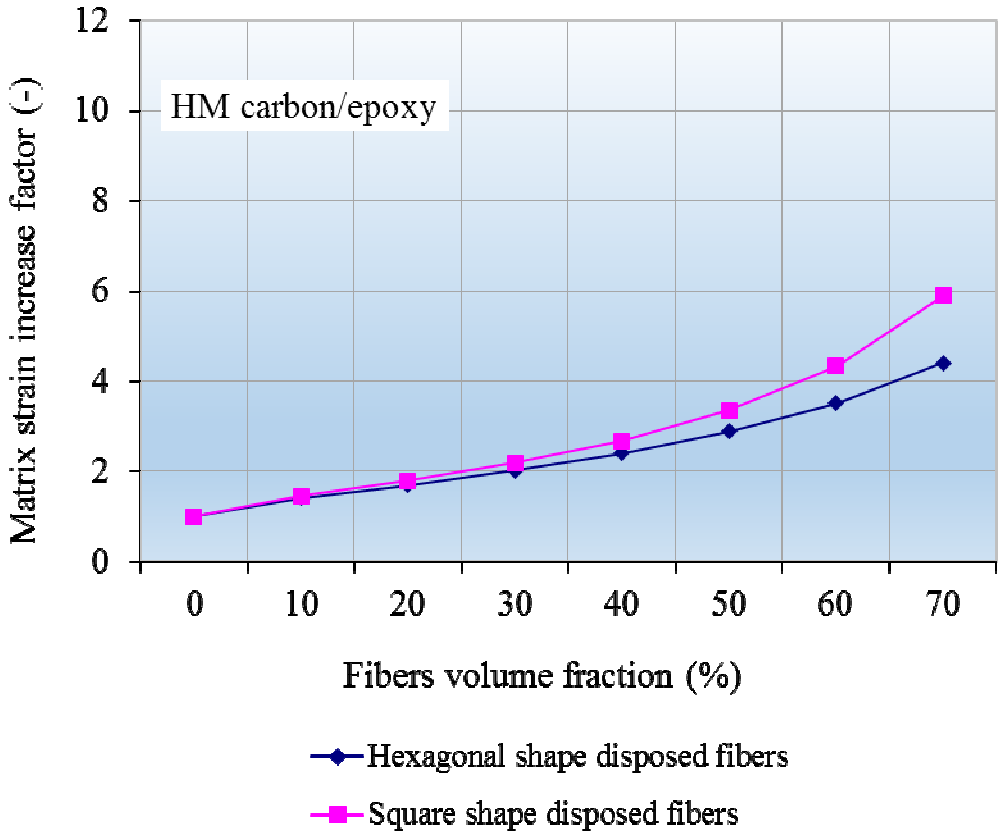

Fig. 2.11. Matrix strain increase factors for "hexagonal" and "square shape" disposed fibers in a HM carbon fibers-reinforced epoxy resin lamina

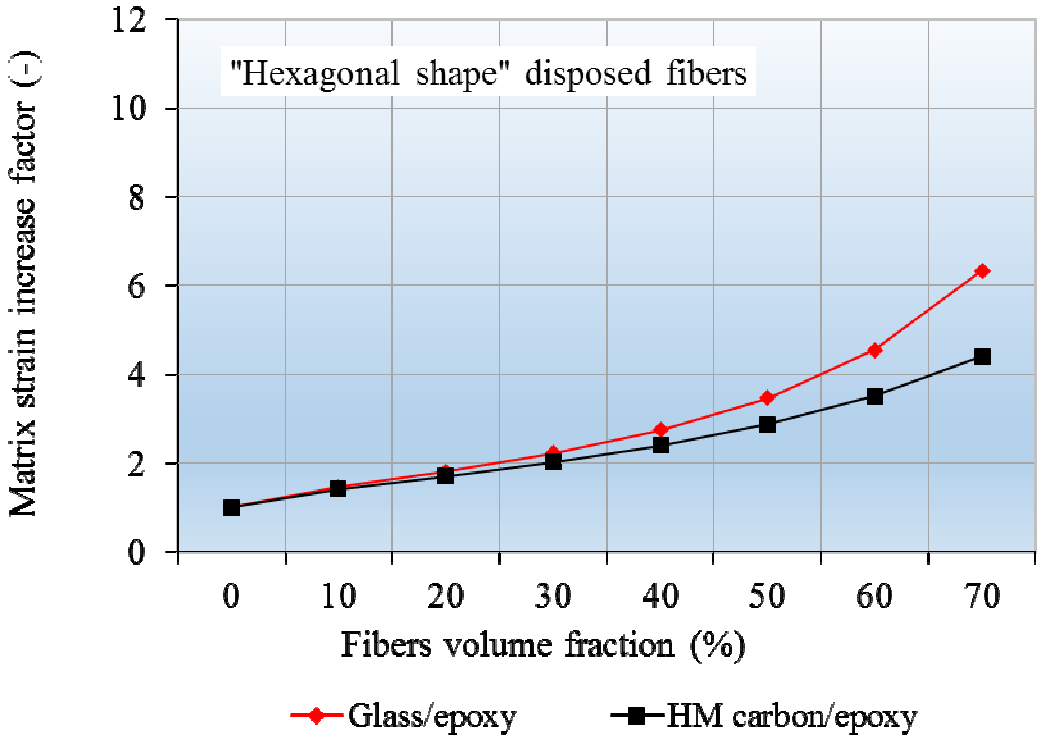

Fig. 2.12. Matrix strain increase factors in HM carbon and glass fibers-reinforced epoxy resin laminae for "hexagonal shape" disposed fibers

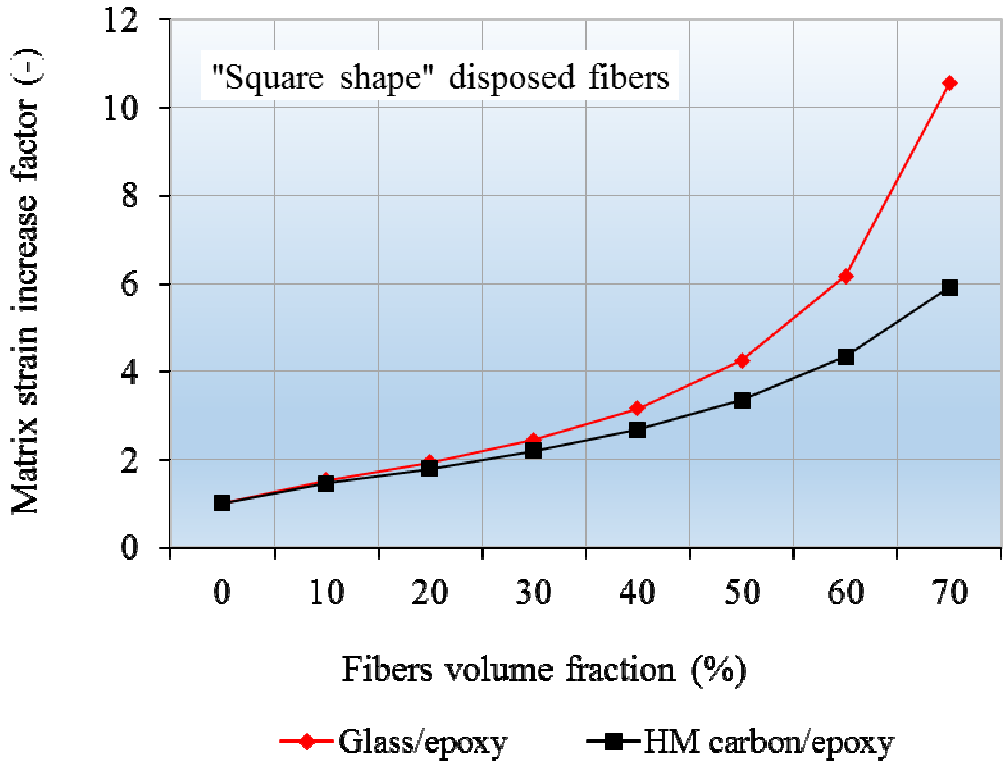

Fig. 2.13. Matrix strain increase factors in HM carbon and glass fibers-reinforced epoxy resin laminae for "square shape" disposed fibers

Conclusions

With the increase of fibers volume fraction in a composite laminate, increases also the matrix strain increase factor. In case of "hexagonal shape" disposed fibers, the matrix strain increase factor presents lower values than the "square shape" disposed fibers, which indicates that the "hexagonal shape" is more advantageous being closer to reality. Moreover, at fibers volume fractions over 40%, the difference between these two factors increases. This is more significant in case of glass fibers-reinforced lamina than the HM-carbon fibers-reinforced lamina, as well as in the case of "square shape" disposed fibers than the "hexagonal shape" disposed fibers.

2.4. Simulations of elasticity laws of unidirectional fibers-reinforced composite laminae

Case of a [45] unidirectional glass fibers-reinforced lamina

A unidirectional [45] glass fibers-reinforced composite lamina being in a stress plane state is considered. The basic elasticity constants of this kind of lamina are: $E_{\parallel} = 47000$ MPa; $E_{\perp} = 14800$ MPa; $\upsilon_{\perp\parallel} = 0.3$; $G_{\parallel\perp} = 5700$ MPa; and $\alpha = 0° – 90°$. It is required to compute the transformed compliances and rigidities versus the variation of fibers' disposal angle.

According to the equations (2.34 – 2.39), following transformed compliances have been computed:

$$c_{11} = \frac{\cos^4 45°}{47000} + \frac{\sin^4 45°}{14800} + \frac{1}{4} \cdot \left(\frac{1}{5700} - \frac{2 \cdot 0,3}{47000} \right) \cdot \sin^2 90° = 62 \cdot 10^{-6}\ MPa^{-1},$$

$$c_{22} = \frac{\sin^4 45°}{47000} + \frac{\cos^4 45°}{14800} + \frac{1}{4} \cdot \left(\frac{1}{5700} - \frac{2 \cdot 0,3}{47000} \right) \cdot \sin^2 90° = 62 \cdot 10^{-6}\ MPa^{-1},$$

$$c_{33} = \frac{\cos^2 90°}{5700} + \left(\frac{1}{47000} + \frac{1}{14800} + \frac{2 \cdot 0,3}{47000} \right) \cdot \sin^2 90° = 101 \cdot 10^{-6}\ MPa^{-1},$$

$$c_{12} = \frac{1}{4} \cdot \left(\frac{1}{47000} + \frac{1}{14800} - \frac{1}{5700} \right) \cdot \sin^2 90° -$$

$$- \frac{0,3}{47000} \cdot \left(\sin^4 45° + \cos^4 45° \right) = -24 \cdot 10^{-6}\ MPa^{-1},$$

$$c_{13} = \left(\frac{2}{14800} + \frac{2 \cdot 0,3}{47000} - \frac{1}{5700} \right) \cdot \sin^3 45° \cdot \cos 45° -$$

$$- \left(\frac{2}{47000} + \frac{2 \cdot 0,3}{47000} - \frac{1}{5700} \right) \cdot \cos^3 45° \cdot \sin 45° = 23 \cdot 10^{-6}\ MPa^{-1},$$

$$c_{23}=\left(\frac{2}{14800}+\frac{2\cdot 0{,}3}{47000}-\frac{1}{5700}\right)\cdot \cos^3 45^\circ\cdot \sin 45^\circ -$$

$$-\left(\frac{2}{47000}+\frac{2\cdot 0{,}3}{47000}-\frac{1}{5700}\right)\cdot \sin^3 45^\circ\cdot \cos 45^\circ = 23\cdot 10^{-6}\ MPa^{-1}.$$

Distributions of the transformed compliances in case of a [45] glass fibers-reinforced composite lamina versus the variation of fibers disposal angle are presented in Figs. 2.14 and 2.15.

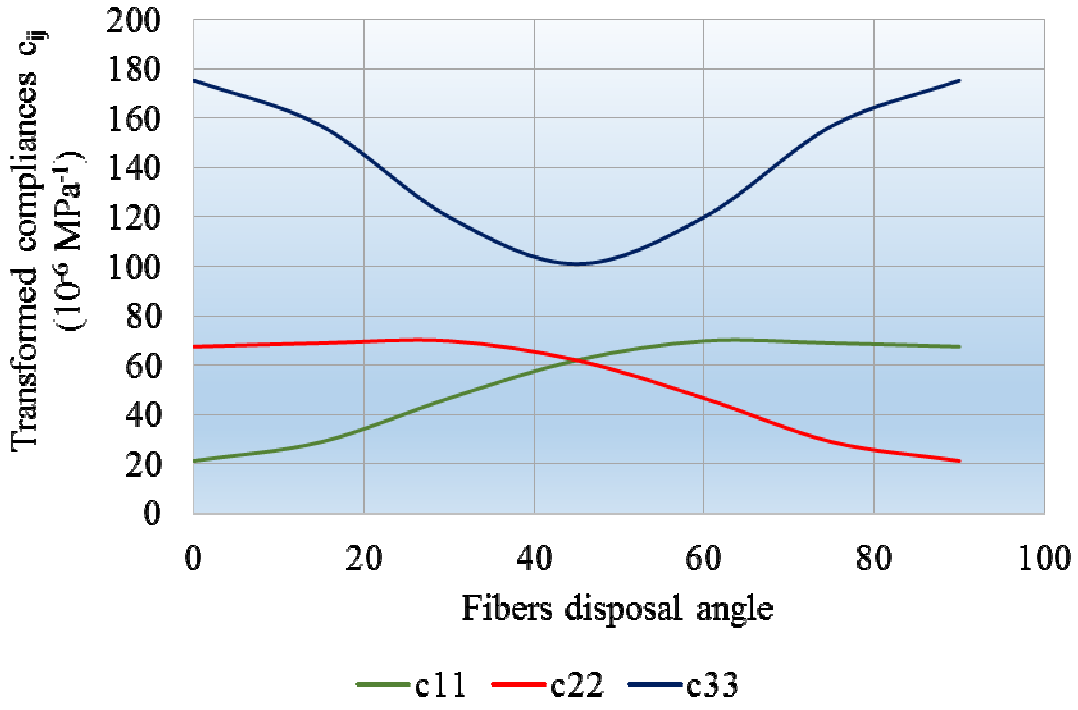

Fig. 2.14. Distributions of transformed compliances c_{11}, c_{22} and c_{33}

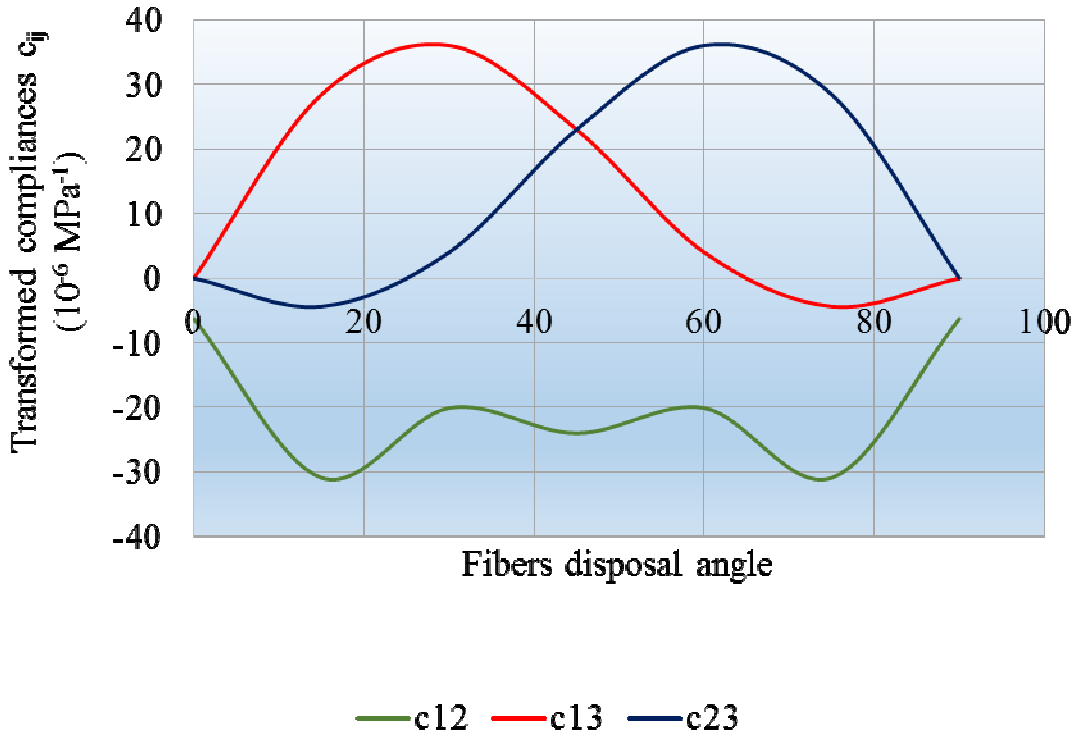

Fig. 2.15. Distributions of transformed compliances c_{12}, c_{13} and c_{23} of [45] unidirectional glass fibers-reinforced lamina

From equation 2.20, the Poisson's ratio $\upsilon_{\parallel\perp}$ can be computed:

$$\upsilon_{II\perp} = \upsilon_{\perp II} \cdot \frac{E_{\perp}}{E_{II}} = 0{,}3 \cdot \frac{14800}{47000} = 0{,}094 .$$

The transformed rigidities in case of 45° glass fibers disposal angle in a unidirectional reinforced lamina can be computed using the relations (2.41) – (2.46):

$$r_{11} = r_{22} = \frac{47000 \cdot \cos^4 45°}{1 - 0{,}3 \cdot 0{,}094} + \frac{14800 \cdot \sin^4 45°}{1 - 0{,}3 \cdot 0{,}094} +$$

$$+ \frac{1}{2} \cdot \left(\frac{0{,}3 \cdot 14800}{1 - 0{,}3 \cdot 0{,}094} + 2 \cdot 5700 \right) \cdot \sin^2 90° = 23 \cdot 10^3 \ MPa ,$$

$$r_{33}=5700+\frac{1}{4}\cdot\left(\frac{47000}{1-0,3\cdot0,094}+\frac{14800}{1-0,3\cdot0,094}-\frac{2\cdot0,3\cdot14800}{1-0,3\cdot0,094}-4\cdot5700\right)\cdot\sin^2 90^\circ=13\cdot10^3\ MPa,$$

$$r_{12}=\frac{0,3\cdot14800}{1-0,3\cdot0,094}+$$

$$+\frac{1}{4}\cdot\left(\frac{47000}{1-0,3\cdot0,094}+\frac{14800}{1-0,3\cdot0,094}-\frac{2\cdot0,3\cdot14800}{1-0,3\cdot0,094}-4\cdot5700\right)\cdot\sin^2 90^\circ=12\cdot10^3\ MPa,$$

$$r_{13}=\frac{1}{2}\cdot\left[\left(\frac{47000}{1-0,3\cdot0,094}+\frac{14800}{1-0,3\cdot0,094}-\frac{2\cdot0,3\cdot14800}{1-0,3\cdot0,094}-4\cdot5700\right)\cdot\sin^2 45^\circ-\right.$$

$$\left.-\left(\frac{47000}{1-0,3\cdot0,094}-\frac{0,3\cdot14800}{1-0,3\cdot0,094}-2\cdot5700\right)\right]\cdot\sin 90^\circ=-8\cdot10^3\ MPa,$$

$$r_{23}=\frac{1}{2}\cdot\left[\left(\frac{14800}{1-0,3\cdot0,094}-\frac{0,3\cdot14800}{1-0,3\cdot0,094}-2\cdot5700\right)-\left(\frac{47000}{1-0,3\cdot0,094}+\frac{14800}{1-0,3\cdot0,094}-\right.\right.$$

$$\left.\left.-\frac{2\cdot0,3\cdot14800}{1-0,3\cdot0,094}-4\cdot5700\right)\cdot\sin^2 90^\circ\right]\cdot\sin 90^\circ=-8\cdot10^3\ MPa.$$

Distributions of the transformed rigidities r_{11}, r_{22}, r_{33}, r_{12}, r_{13} and r_{23} in case of a unidirectional [45] glass fibers-reinforced lamina versus the variation of fibers disposal angle are presented in Figs. 2.16 – 2.17.

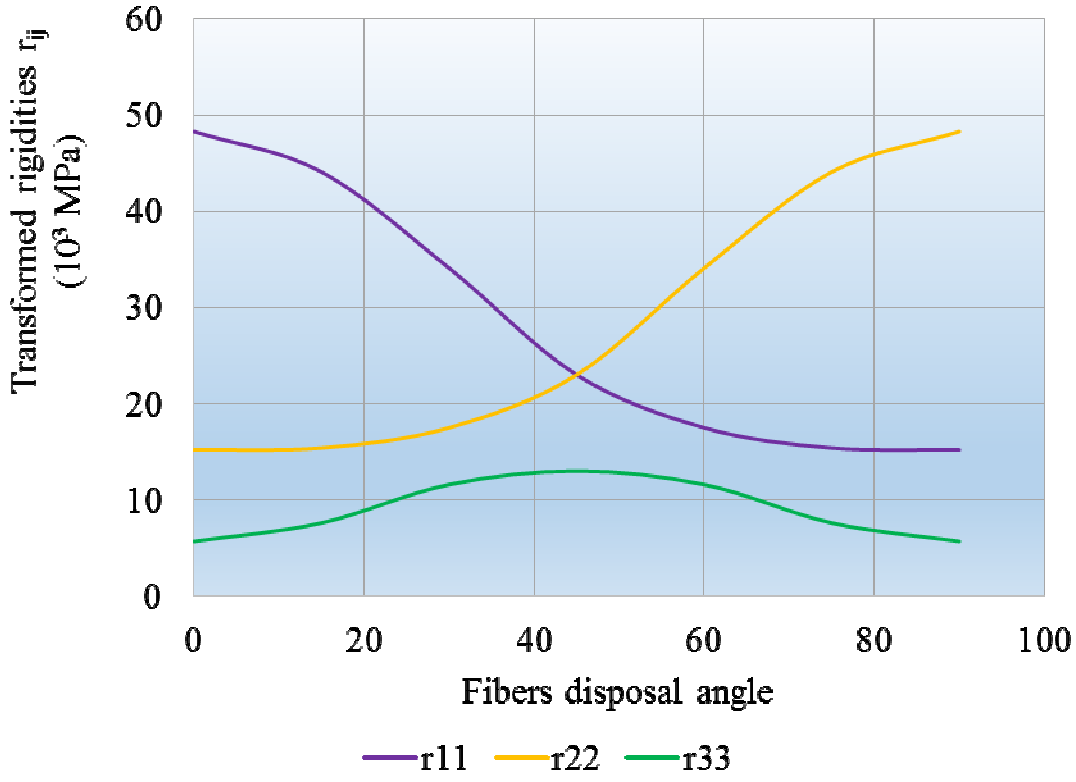

Fig. 2.16. Distributions of transformed rigidities r_{11}, r_{22} and r_{33} of [45] unidirectional glass fibers-reinforced lamina

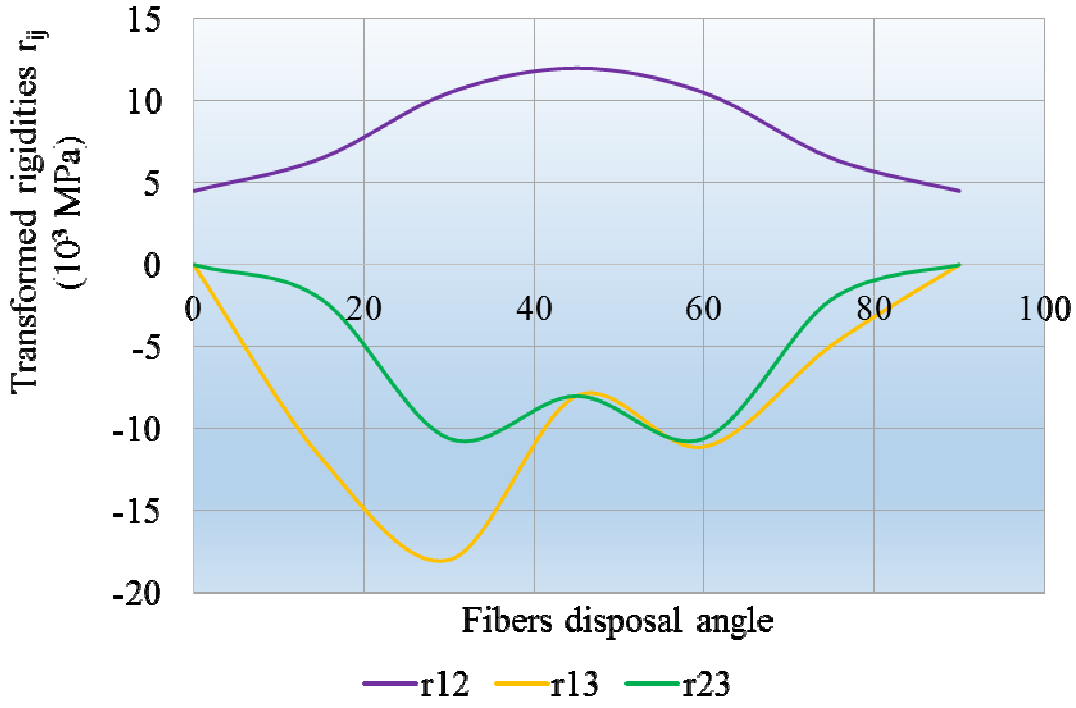

Fig. 2.17. Distributions of transformed rigidities r_{12}, r_{13} and r_{23} of [45] unidirectional glass fibers-reinforced lamina

Case of a 40% glass fibers volume fraction unidirectional reinforced lamina

An epoxy/glass fibers unidirectional reinforced lamina with 40% fibers volume fraction, being in a stress plane state has been considered. The input data regarding fibers and matrix properties are: $E_F = 73$ GPa; $E_M = 3.6$ GPa; $\upsilon_F = 0.25$; $\upsilon_M = 0.35$; the fibers volume fraction varies between 10% and 70%.

To compute the basic elasticity constants of the unidirectional reinforced lamina, first I have determined the fibers and matrix shear moduli:

$$G_M = \frac{E_M}{2(1+\upsilon_M)} = \frac{3,6}{2(1+0,35)} = 1,33\,GPa,$$

$$G_F = \frac{E_F}{2(1+\upsilon_F)} = \frac{73}{2(1+0,25)} = 29,2\ GPa.$$

For instance, for 40% fibers volume fraction, the basic elasticity constants according to the relations (2.24) – (2.28) are:

$$E_{II} = \varphi \cdot E_F + (1-\varphi)E_M = 0,4 \cdot 73 + (1-0,4) \cdot 3,6 = 31,36\,GPa,$$

$$\upsilon_{\perp II} = \varphi \cdot \upsilon_F + (1-\varphi)\upsilon_M = 0,4 \cdot 0,25 + (1-0,4) \cdot 0,35 = 0,31,$$

$$E_{\perp} = \frac{E_M}{1-\upsilon_M^2} \cdot \frac{1+0,85\varphi^2}{(1-\varphi)^{1,25} + \frac{\varphi \cdot E_M}{(1-\upsilon_M^2) \cdot E_F}} =$$

$$= \frac{3,6}{1-0,35^2} \cdot \frac{1+0,85 \cdot 0,4^2}{(1-0,4)^{1,25} + \frac{0,4 \cdot 3,6}{(1-0,35^2) \cdot 73}} = 15,98\,GPa,$$

$$\upsilon_{II\perp}=\upsilon_{\perp II}\cdot\frac{E_{\perp}}{E_{II}}=0{,}31\cdot\frac{15{,}98}{31{,}36}=0{,}157\ ,$$

$$G_{II\perp}=G_M\cdot\frac{1+0{,}6\cdot\varphi^{0{,}5}}{(1-\varphi)^{1{,}25}+\varphi\cdot\frac{G_M}{G_F}}=1{,}33\cdot\frac{1+0{,}6\cdot 0{,}4^{0{,}5}}{(1-0{,}4)^{1{,}25}+0{,}4\cdot\frac{1{,}33}{29{,}2}}=2{,}93\,GPa\,.$$

The distributions of basic elasticity constants versus the fibers volume fraction for a unidirectional glass fibers-epoxy reinforced lamina are presented in Figs. 2.18 – 2.19.

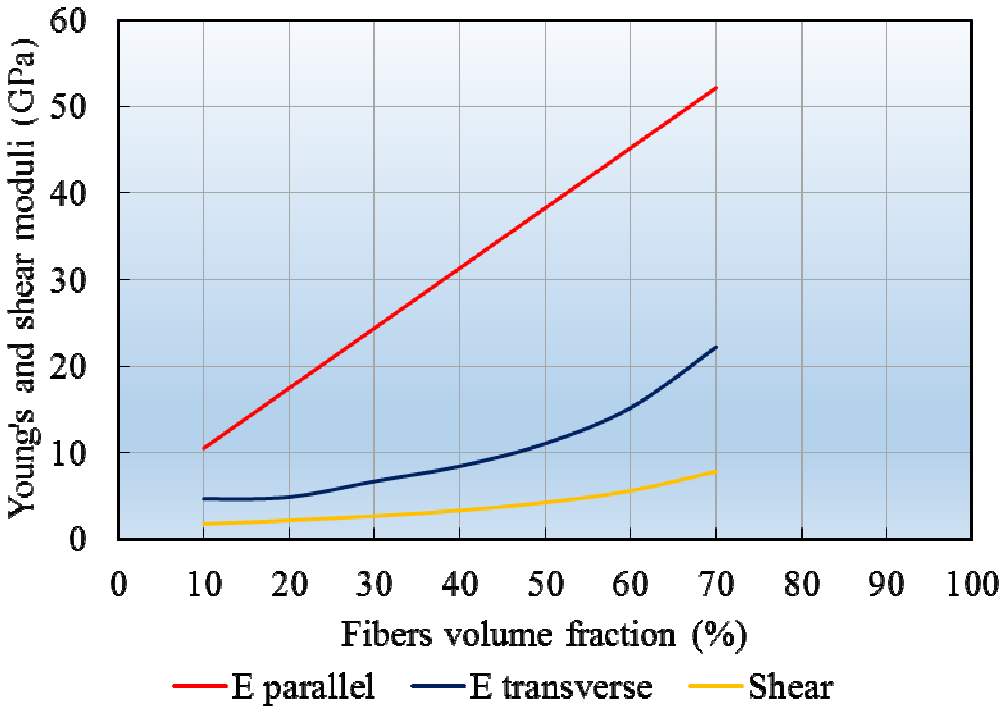

Fig. 2.18. Basic elasticity constants $E_{\parallel}$, $E_{\perp}$ and $G_{\parallel\perp}$ of an epoxy/glass fibers unidirectional reinforced lamina

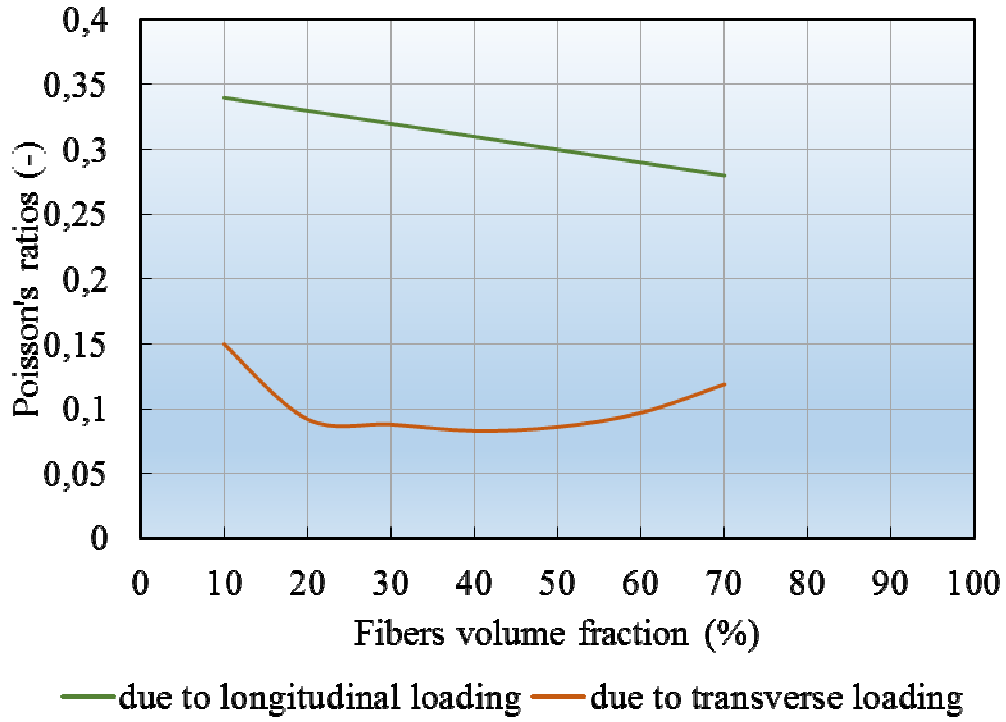

Fig. 2.19. Poisson's ratios $\nu_{\perp\parallel}$ and $\nu_{\parallel\perp}$ of an epoxy/glass fibers unidirectional reinforced lamina

Case of an [0] epoxy/boron unidirectional fibers reinforced lamina subjected to biaxial stresses

An [0] epoxy/boron fibers unidirectional reinforced lamina with 60% fibers volume fraction subjected to biaxial stresses σ_{xx} and σ_{yy} has been considered. The aim is to compute the lamina's strains ε_{xx} and ε_{yy}. Following input data has been used: E_F = 420 GPa; E_M = 3.6 GPa; ν_F = 0.1; ν_M = 0.35; φ = 60%; α = 0°; σ_{xx} = 1 GPa; σ_{yy} = 0.5 GPa.

The fibers and matrix shear moduli can be computed in the following way:

$$G_M = \frac{E_M}{2(1+\upsilon_M)} = \frac{3,6}{2(1+0,35)} = 1,33\ GPa,$$

$$G_F = \frac{E_F}{2(1+\upsilon_F)} = \frac{420}{2(1+0,1)} = 190,9\ GPa.$$

The lamina's basic elasticity constants are:

$$E_{II} = \varphi \cdot E_F + (1-\varphi) E_M = 0,6 \cdot 420 + (1-0,6) \cdot 3,6 = 253,44\, GPa,$$

$$\upsilon_{\perp II} = \varphi \cdot \upsilon_F + (1-\varphi) \upsilon_M = 0,6 \cdot 0,1 + (1-0,6) \cdot 0,35 = 0,2,$$

$$E_{\perp} = \frac{E_M}{1-\upsilon_M^2} \cdot \frac{1+0,85\varphi^2}{(1-\varphi)^{1,25} + \frac{\varphi \cdot E_M}{(1-\upsilon_M^2) \cdot E_F}} =$$

$$= \frac{3,6}{1-0,35^2} \cdot \frac{1+0,85 \cdot 0,6^2}{(1-0,6)^{1,25} + \frac{0,6 \cdot 3,6}{(1-0,35^2) \cdot 420}} = 16,53\, GPa,$$

$$\upsilon_{II\perp} = \upsilon_{\perp II} \cdot \frac{E_{\perp}}{E_{II}} = 0,2 \cdot \frac{16,53}{253,44} = 0,013,$$

$$G_{II\perp} = G_M \cdot \frac{1+0,6 \cdot \varphi^{0,5}}{(1-\varphi)^{1,25} + \varphi \cdot \frac{G_M}{G_F}} = 1,33 \cdot \frac{1+0,6 \cdot 0,6^{0,5}}{(1-0,6)^{1,25} + 0,6 \cdot \frac{1,33}{190,9}} = 6,04\, GPa.$$

To compute the strains ε_{xx} and ε_{yy}, the transformed compliances have to be computed:

$$c_{11} = \frac{\cos^4 0°}{253,44} + \frac{\sin^4 0°}{16,53} + \frac{1}{4} \cdot \left(\frac{1}{6,04} - \frac{2 \cdot 0,2}{253,44} \right) \cdot \sin^2 0° = 3945,7 \cdot 10^{-6}\ GPa^{-1},$$

$$c_{22} = \frac{\sin^4 0°}{253,44} + \frac{\cos^4 0°}{16,53} + \frac{1}{4} \cdot \left(\frac{1}{6,04} - \frac{2 \cdot 0,2}{253,44} \right) \cdot \sin^2 0° = 60496 \cdot 10^{-6}\ GPa^{-1},$$

$$c_{12} = \frac{1}{4}\cdot\left(\frac{1}{253,44}+\frac{1}{16,53}-\frac{1}{6,04}\right)\cdot sin^2\,0° -$$

$$-\frac{0,2}{253,44}\cdot\left(sin^4\,0°+cos^4\,0°\right) = -789,1\cdot10^{-6}\ GPa^{-1}.$$

Keeping in mind that the shear stress $\tau_{xy} = 0$, the strains ε_{xx} and ε_{yy} can be computed using the following relations:

$$\varepsilon_{xx} = c_{11}\cdot\sigma_{xx} + c_{12}\cdot\sigma_{yy} = \left(3945,7\cdot10^{-6}\right)\cdot(1) + \left(-789,1\cdot10^{-6}\right)\cdot(0,5) = 3551\cdot10^{-6},$$

$$\varepsilon_{yy} = c_{12}\cdot\sigma_{xx} + c_{22}\cdot\sigma_{yy} = \left(-789,1\cdot10^{-6}\right)\cdot(1) + \left(60496\cdot10^{-6}\right)\cdot(0,5) = 29458\cdot10^{-6}.$$

It is interesting to notice that although the loading of y-axis direction is half of that on x-axis direction, the ε_{yy} strain is eight times greater than that on x-axis direction which means that the lamina's tensile strength transverse to the fibers direction is very low (Fig. 2.20).

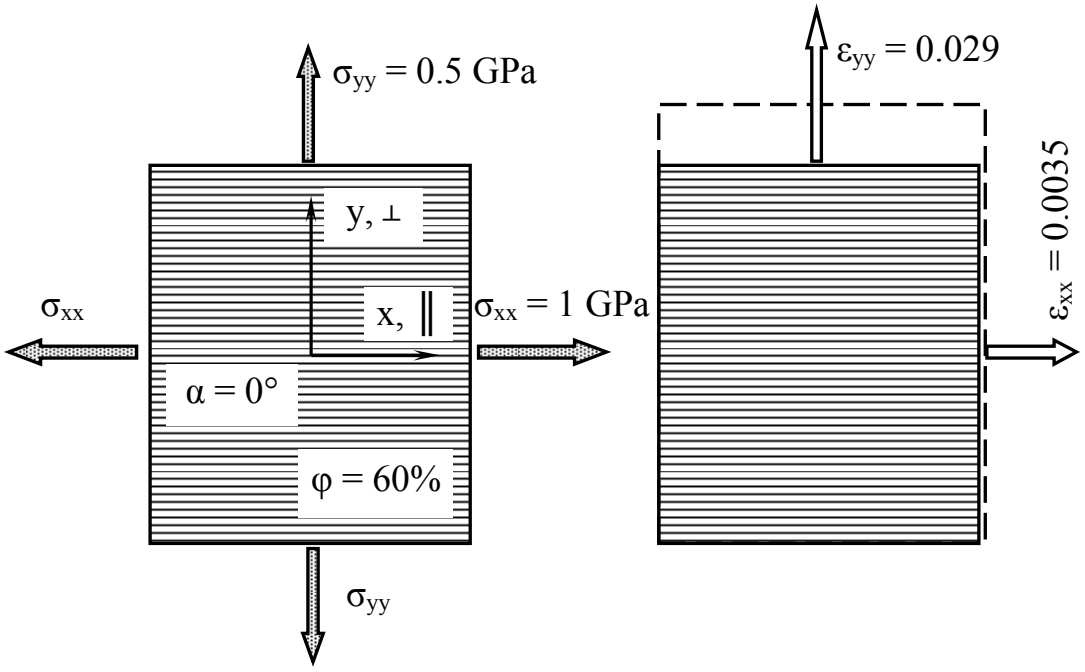

Fig. 2.20. Stresses and strains in an [0] epoxy/boron fibers unidirectional reinforced lamina

Case of an [-45] epoxy/boron unidirectional fibers reinforced lamina subjected to biaxial stresses

An [-45] epoxy/boron fibers unidirectional reinforced lamina with 60% fibers volume fraction subjected to biaxial stresses σ_{xx} and σ_{yy} has been considered. The task is to compute the lamina's strains ε_{xx}, ε_{yy} and γ_{xy}. Following input data has been used: E_F = 420 GPa; E_M = 3.6 GPa; ν_F = 0.1; ν_M = 0.35; φ = 60%; α = -45°; σ_{xx} = 1 GPa; σ_{yy} = 0.5 GPa.

The fibers and matrix shear moduli can be computed in the following way:

$$G_M = \frac{E_M}{2(1+\upsilon_M)} = \frac{3,6}{2(1+0,35)} = 1,33\ GPa,$$

$$G_F = \frac{E_F}{2(1+\upsilon_F)} = \frac{420}{2(1+0,1)} = 190,9\ GPa.$$

The lamina's basic elasticity constants are:

$$E_{II} = \varphi \cdot E_F + (1-\varphi)E_M = 0,6 \cdot 420 + (1-0,6) \cdot 3,6 = 253,44\,GPa,$$

$$\upsilon_{\perp II} = \varphi \cdot \upsilon_F + (1-\varphi)\upsilon_M = 0,6 \cdot 0,1 + (1-0,6) \cdot 0,35 = 0,2,$$

$$E_{\perp} = \frac{E_M}{1-\upsilon_M^2} \cdot \frac{1+0,85\varphi^2}{(1-\varphi)^{1,25} + \frac{\varphi \cdot E_M}{(1-\upsilon_M^2) \cdot E_F}} =$$

$$= \frac{3,6}{1-0,35^2} \cdot \frac{1+0,85 \cdot 0,6^2}{(1-0,6)^{1,25} + \frac{0,6 \cdot 3,6}{(1-0,35^2) \cdot 420}} = 16,53\,GPa,$$

$$\upsilon_{II\perp} = \upsilon_{\perp II} \cdot \frac{E_{\perp}}{E_{II}} = 0,2 \cdot \frac{16,53}{253,44} = 0,013,$$

$$G_{II\perp}=G_M\cdot\frac{1+0,6\cdot\varphi^{0,5}}{(1-\varphi)^{1,25}+\varphi\cdot\frac{G_M}{G_F}}=1,33\cdot\frac{1+0,6\cdot 0,6^{0,5}}{(1-0,6)^{1,25}+0,6\cdot\frac{1,33}{190,9}}=6,04\,GPa.$$

To compute the strains ε_{xx}, ε_{yy} and γ_{xy}, the transformed compliances have to be determined:

$$c_{11}=\frac{\cos^4(-45°)}{253,44}+\frac{\sin^4(-45°)}{16,53}+\frac{1}{4}\cdot\left(\frac{1}{6,04}-\frac{2\cdot 0,2}{253,44}\right)\cdot\sin^2(-90°)=57106,6\cdot 10^{-6}\ GPa^{-1},$$

$$c_{22}=\frac{\sin^4(-45°)}{253,44}+\frac{\cos^4(-45°)}{16,53}+\frac{1}{4}\cdot\left(\frac{1}{6,04}-\frac{2\cdot 0,2}{253,44}\right)\cdot\sin^2(-90°)=57106,6\cdot 10^{-6}\ GPa^{-1},$$

$$c_{12}=\frac{1}{4}\cdot\left(\frac{1}{253,44}+\frac{1}{16,53}-\frac{1}{6,04}\right)\cdot\sin^2(-90°)-$$
$$-\frac{0,2}{253,44}\cdot\left[\sin^4(-45°)+\cos^4(-45°)\right]=-25674,8\cdot 10^{-6}\ GPa^{-1},$$

$$c_{13}=\left(\frac{2}{16,53}+\frac{2\cdot 0,2}{253,44}-\frac{1}{6,04}\right)\cdot\sin^3(-45°)\cdot\cos(-45°)-$$
$$-\left(\frac{2}{253,44}+\frac{2\cdot 0,2}{253,44}-\frac{1}{6,04}\right)\cdot\cos^3(-45°)\cdot\sin(-45°)=-28275,1\cdot 10^{-6}\,GPa^{-1},$$
$$c_{23}=\left(\frac{2}{16,53}+\frac{2\cdot 0,2}{253,44}-\frac{1}{6,04}\right)\cdot\cos^3(-45°)\cdot\sin(-45°)-$$
$$-\left(\frac{2}{253,44}+\frac{2\cdot 0,2}{253,44}-\frac{1}{6,04}\right)\cdot\sin^3(-45°)\cdot\cos(-45°)=-28275,1\cdot 10^{-6}\,GPa^{-1}.$$

The strains ε_{xx}, ε_{yy} and γ_{xy} can be computed using the relations presented below:

$$\varepsilon_{xx} = c_{11} \cdot \sigma_{xx} + c_{12} \cdot \sigma_{yy} = \left(57106{,}6 \cdot 10^{-6}\right) \cdot (1) +$$

$$+ \left(-25674{,}8 \cdot 10^{-6}\right) \cdot (0{,}5) = 44269{,}2 \cdot 10^{-6},$$

$$\varepsilon_{yy} = c_{12} \cdot \sigma_{xx} + c_{22} \cdot \sigma_{yy} = \left(-25674{,}8 \cdot 10^{-6}\right) \cdot (1) +$$

$$+ \left(57106{,}6 \cdot 10^{-6}\right) \cdot (0{,}5) = 2878{,}5 \cdot 10^{-6},$$

$$\gamma_{xy} = c_{13} \cdot \sigma_{xx} + c_{23} \cdot \sigma_{yy} = \left(-28275{,}1 \cdot 10^{-6}\right) \cdot (1) +$$

$$+ \left(-28275{,}1 \cdot 10^{-6}\right) \cdot (0{,}5) = -42412{,}6 \cdot 10^{-6}.$$

It can be notice that fact that although the tangential stress $\tau_{xy} = 0$, the biaxial stress field causes a γ_{xy} strain in case of unidirectional fibers-reinforced laminae with different disposal angles. Fig. 2.21 presents the strains of an [-45] epoxy/boron fibers unidirectional reinforced lamina with 60% fibers volume fraction subjected to biaxial stresses σ_{xx} and σ_{yy}.

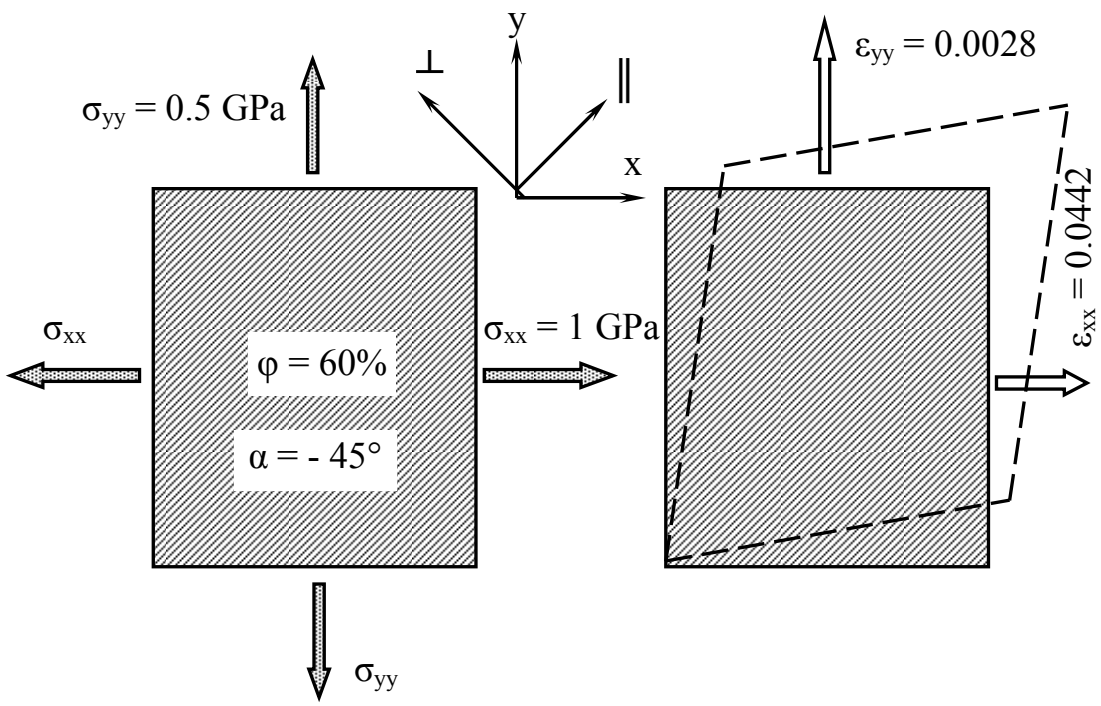

Fig. 2.21. Stresses and strains in an [-45] epoxy/boron fibers unidirectional reinforced lamina

2.5. Simulations to evaluate the elastic properties of fibers-reinforced laminates under off-axis loading system

Case of HM-carbon, HS-carbon and Kevlar49 [0/90/0/90], [0/45/-45/90] and [45/-45/45/-45] laminates

It is well known that composite laminates with aligned reinforcement are very stiff along the fibers direction, but also very weak in the transverse direction. The solution to obtain equal stiffness of laminates subjected in all directions within a plane is by stacking and bonding together plies with different fibers orientations. Generally, for composite laminates it is assumed that all laminae are bonded together and withstand, in a specific point, the same strains as well as for the entire laminate.

The architectures of some advanced composite laminates based on epoxy resin reinforced with HM-carbon, HS-carbon and Kevlar49 fibers are presented in Fig. 2.22, laminates subjected under off-axis loading system and taken into account to evaluate their elastic properties. These laminates present following plies sequence: [0/90/0/90], [0/45/-45/90] and [45/-45/45/-45]. Carbon fibers of type HM (high modulus) present a value of Young's modulus greater than 300 GPa. High strength (HS) carbon fibers represent a general purpose, cost effective carbon fiber, designed for industrial as well as recreational applications and is usually used for non-structural components of aircrafts. Kevlar49 aramid fiber is characterized by low-density and high tensile strength and modulus. A top view of a loading scheme of a composite laminate subjected to off-axis loading system is presented in Fig. 2.23.

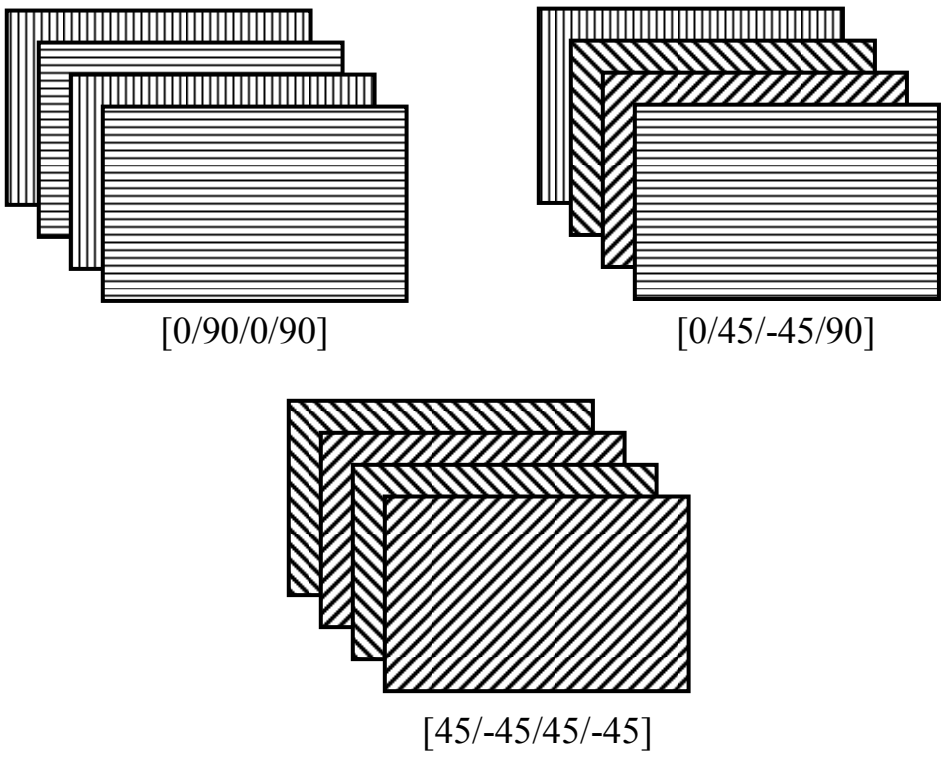

Fig. 2.22. Architectures of some advanced HM-carbon, HS-carbon and Kevlar49 composite laminates

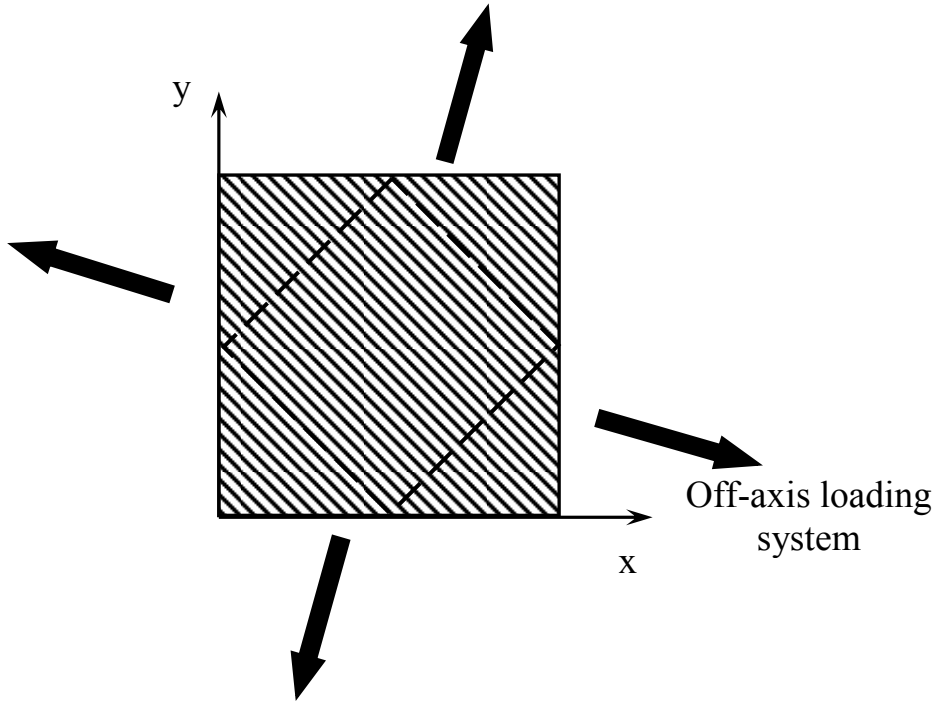

Fig. 2.23. Loading scheme of a composite laminate subjected to off-axis loading system

Results

General input data are: fibers volume fraction φ = 0.5 in all cases, laminates thickness t = 1 mm and off-axis loading systems varies between 0 and 90 degrees. The elastic constants E_{xx}, G_{xy} and υ_{xy} are presented in Figs. 2.24 – 2.32.

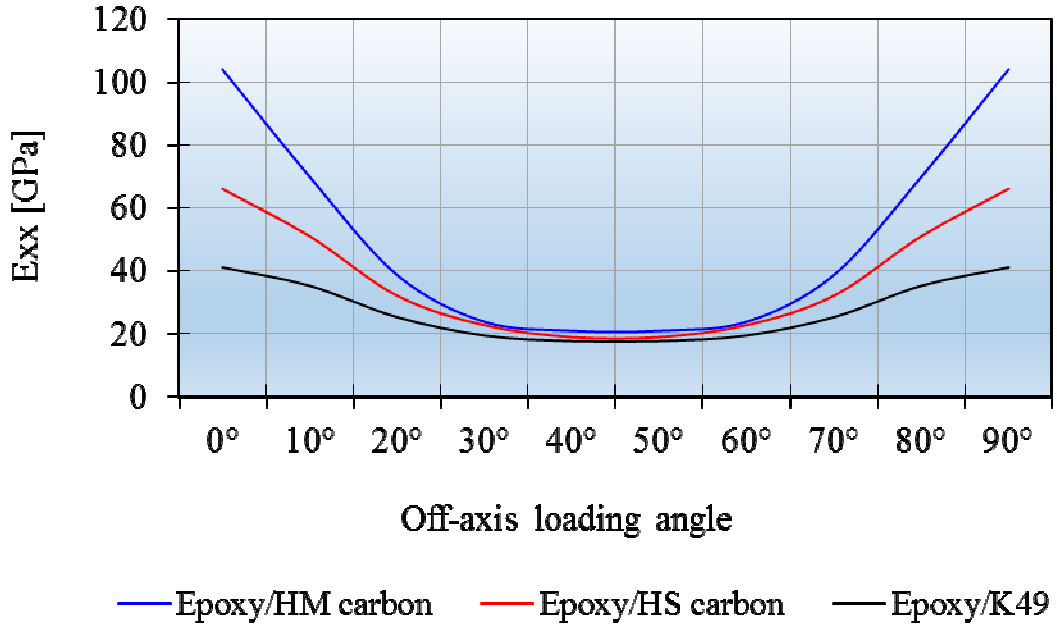

Fig. 2.24. . Young's modulus for [0/90/0/90] epoxy composite laminate

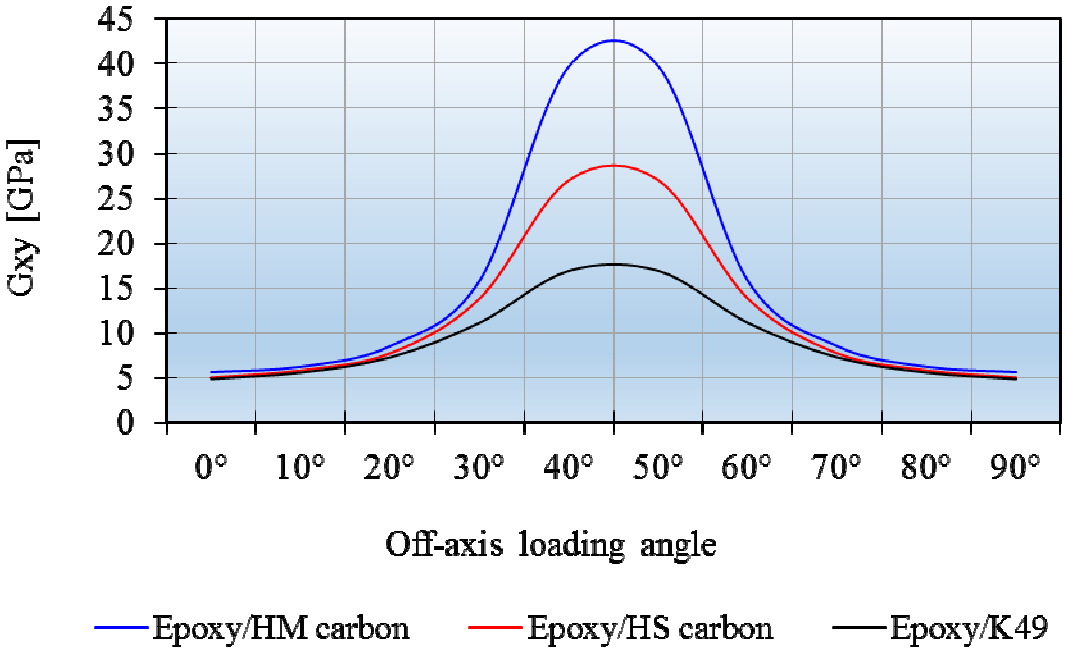

Fig. 2.25. Shear modulus for [0/90/0/90] epoxy composite laminate

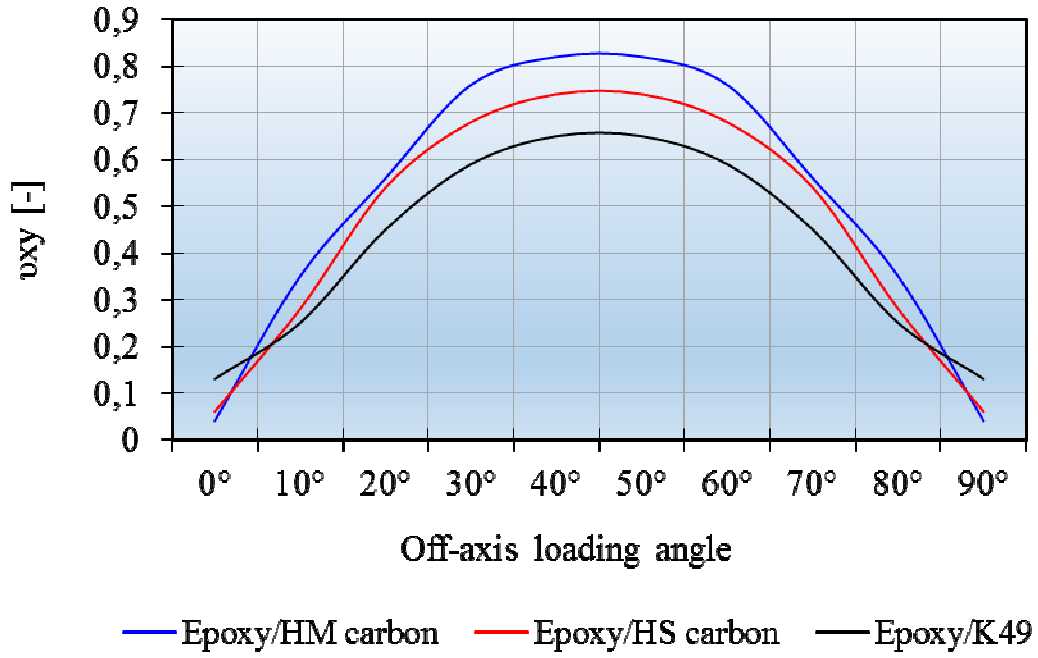

Fig. 2.26. Poisson's ratio for [0/90/0/90] epoxy based composite laminate

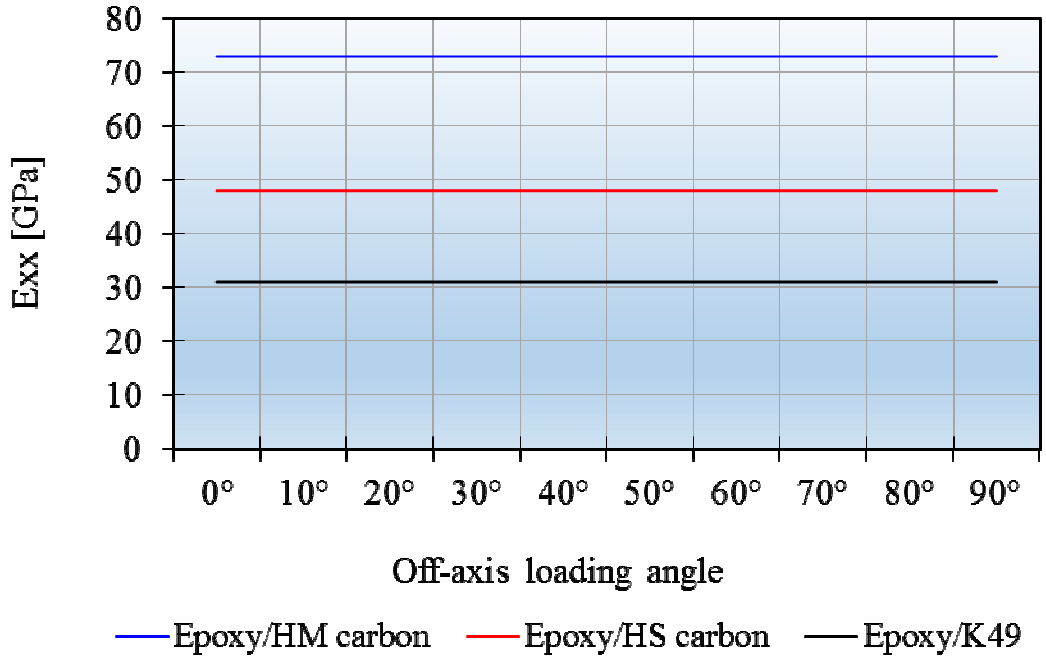

Fig. 2.27. Young's modulus for [0/45/-45/90] epoxy based composite laminate

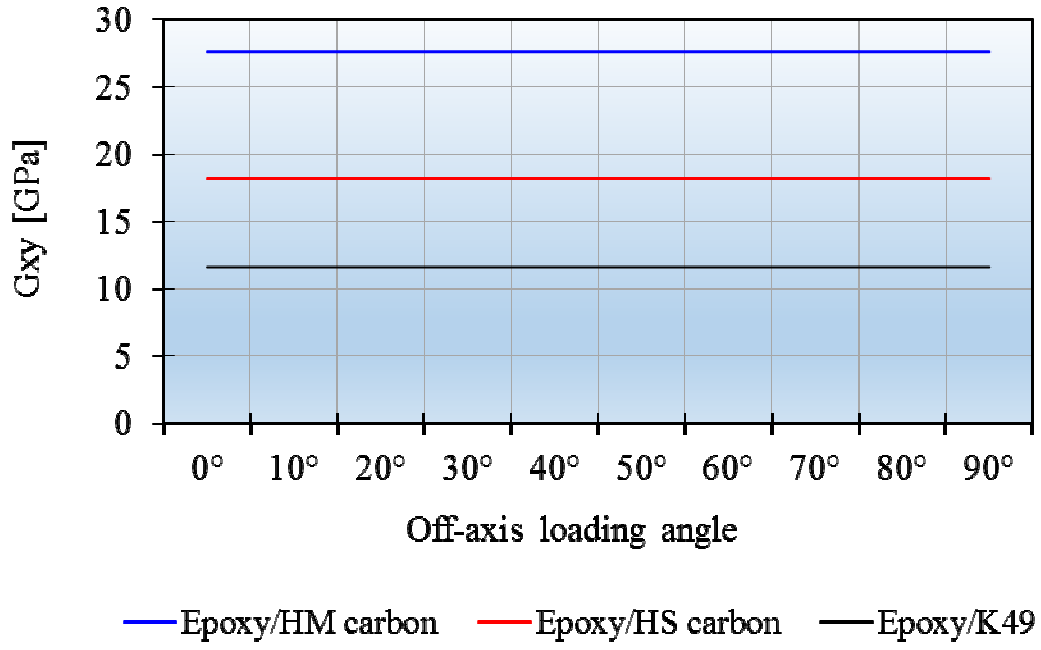

Fig. 2.28. **Shear modulus for [0/45/-45/90] epoxy based composite laminate**

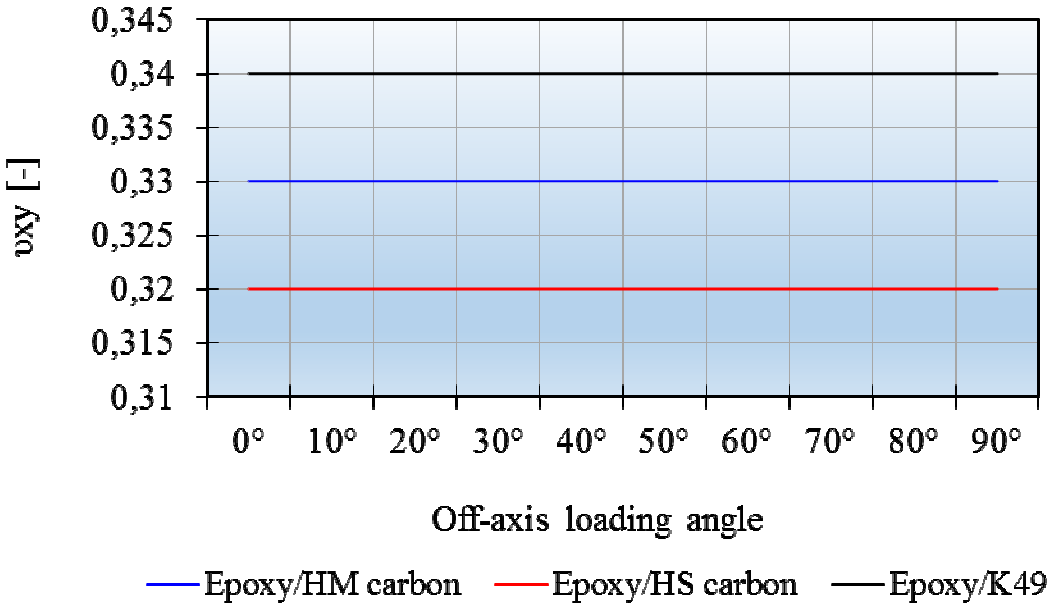

2.29. Poisson's ratio for [0/45/-45/90] epoxy based composite laminate

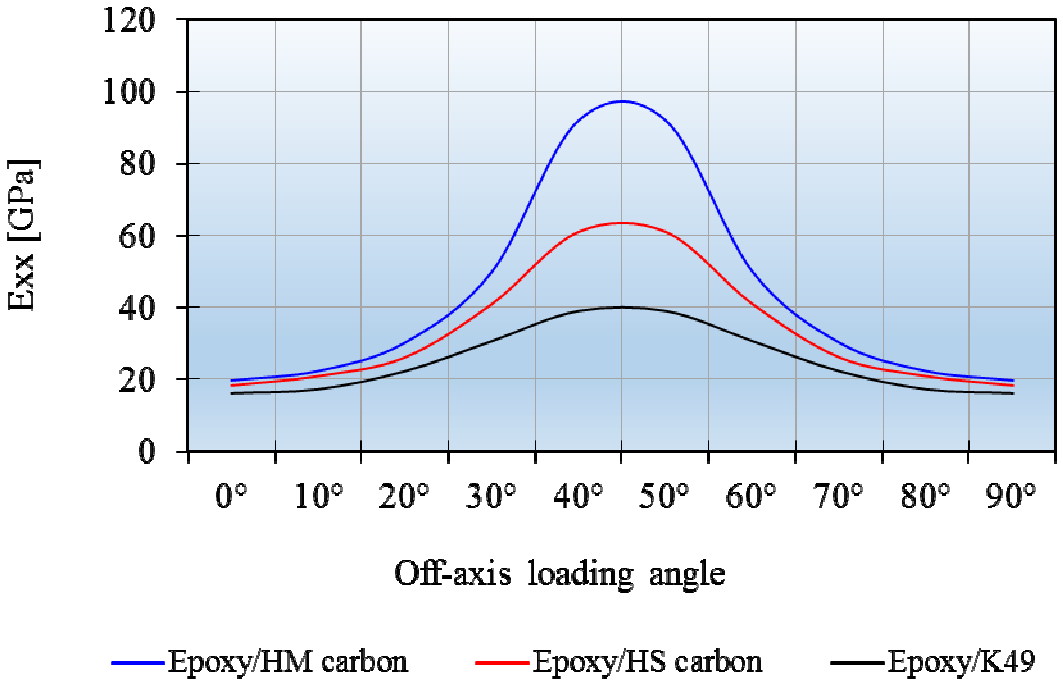

Fig. 2.30. Young's modulus for [45/-45/45/-45] epoxy based composite laminate

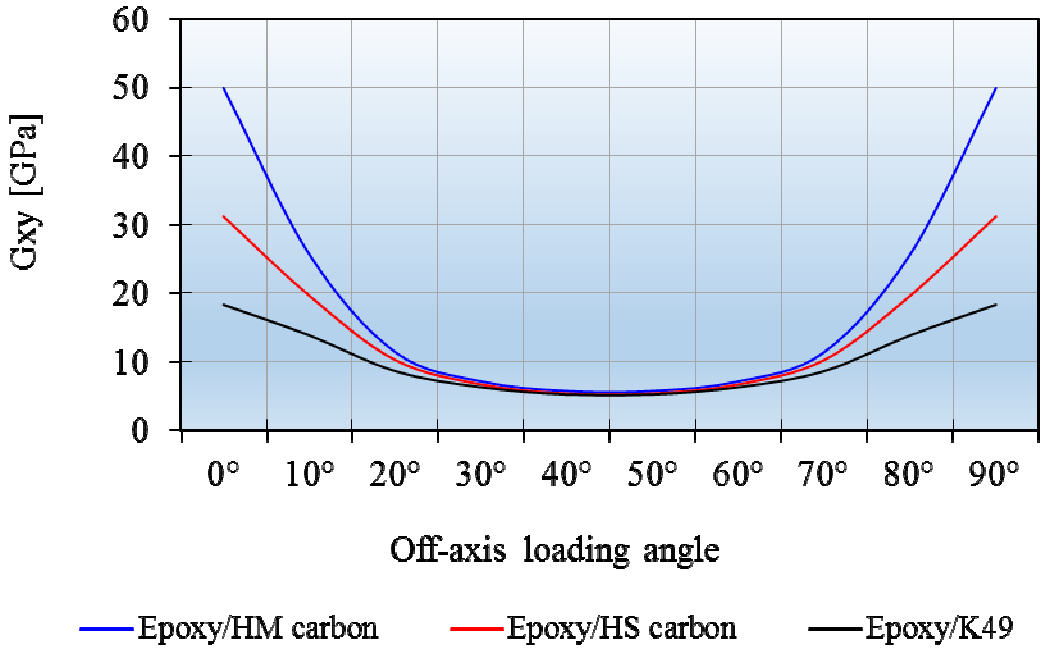

Fig. 2.31. Shear modulus for [45/-45/45/-45] epoxy based composite laminate

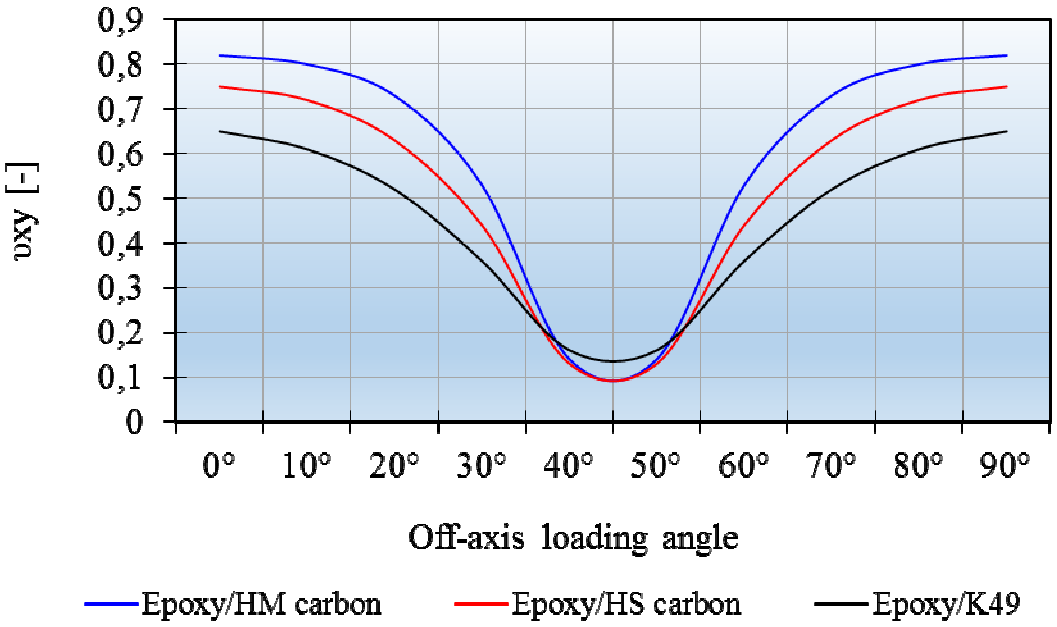

Fig. 2.32. Poisson's ratio for [45/-45/45/-45] epoxy based composite laminate

Conclusions

Tensile-shear interactions lead to distortions and local micro-structural damage and failure, so in order to obtain equal stiffness in all off-axis loading systems, a composite laminate have to present balanced angle plies, for instance [0/45/-45/90]. Under off-axis loading, normal stresses produce shear strains (and of course normal strains) and shear stresses produce normal strains (as well as shear strains). This tensile-shear interaction is also present in laminates but does not occur if the loading system is applied along the main axes of a single lamina or if a laminate is balanced.

Example of tensile-shear interaction in a [0/90/0/90] composite laminate is presented in Fig. 2.33.

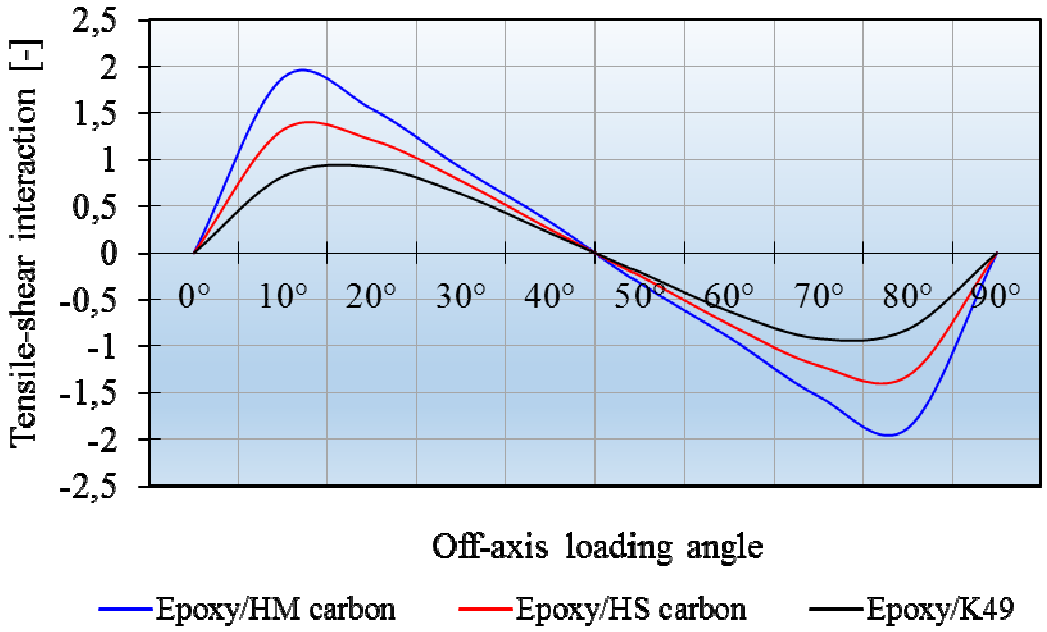

Fig. 2.33. Distribution of tensile-shear interaction in a [0/90/0/90] composite laminate

Case of HM-carbon, HS-carbon and Kevlar49 $[0/30/-30/60]_S$, $[0/45/90]_{2S}$ and $[90/45_2/0]_S$ laminates

The elasticity evaluation of some advanced symmetric composite laminates based on epoxy resin reinforced alternatively with HM-carbon, HS-carbon and Kevlar49 fibers are presented. The laminates taken into account into this evaluation have following plies sequences: $[0/30/-30/60]_S$, $[0/45/90]_{2S}$, $[90/45_2/0]_S$ and are subjected to off-axis loading systems.

General input data are: fibers volume fraction $\varphi = 0.5$ in all cases, laminates thickness t = 1 mm and off-axis loading systems varies between 0° and 90°. For HM-carbon fibers, following data have been used:

- $E_M = 3.9$ GPa;
- $E_{\parallel} > 300$ GPa;
- $E_{\perp} < 100$ GPa;
- $\upsilon_M < 0.5$;
- $\upsilon_F < 0.4$;

- $G_M < 25$ GPa;
- $G_F < 50$ GPa.

For HS-carbon fibers the input data are:

- $E_{\parallel} < 300$ GPa;
- $E_{\perp} < 80$ GPa.

For Kevlar49 Fibers the following data have been used:

- $E_{\parallel} < 200$ GPa;
- $E_{\perp} < 50$ GPa.

The computed elastic constants E_{xx}, E_{yy}, G_{xy} and υ_{xy} are presented in Figs. 2.34 – 2.37.

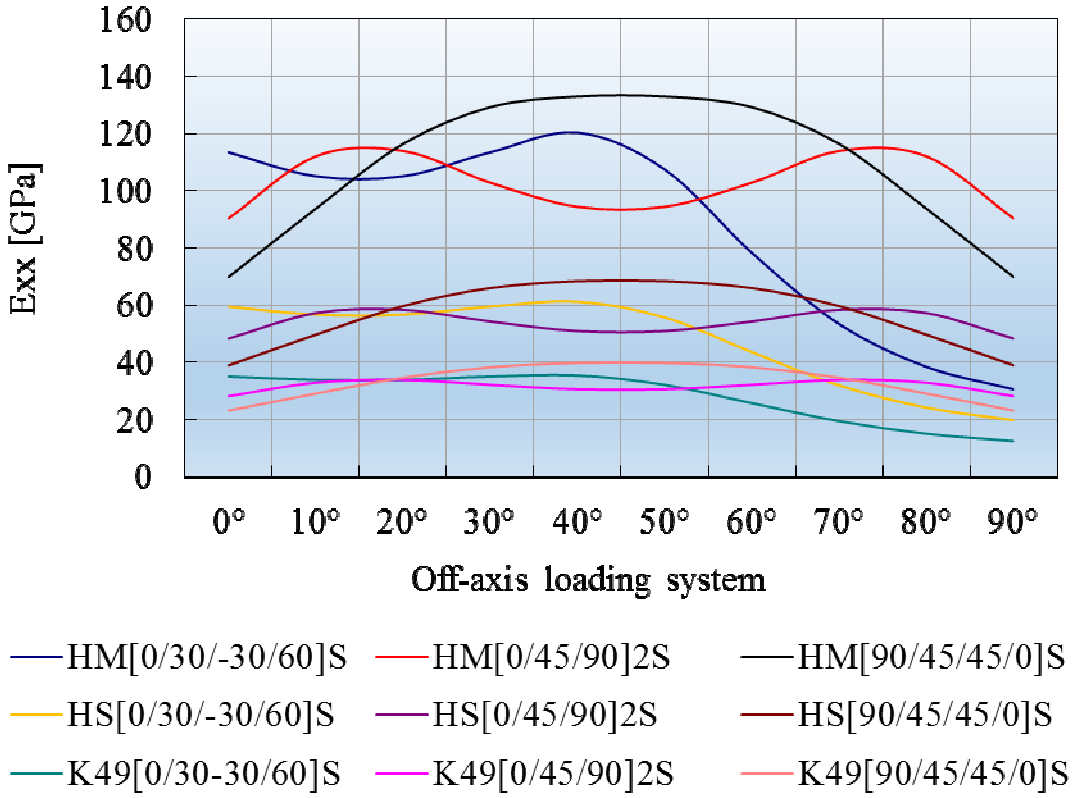

Fig. 2.34. E_{xx} distribution of some carbon and aramid fibers-reinforced epoxy based symmetric laminates

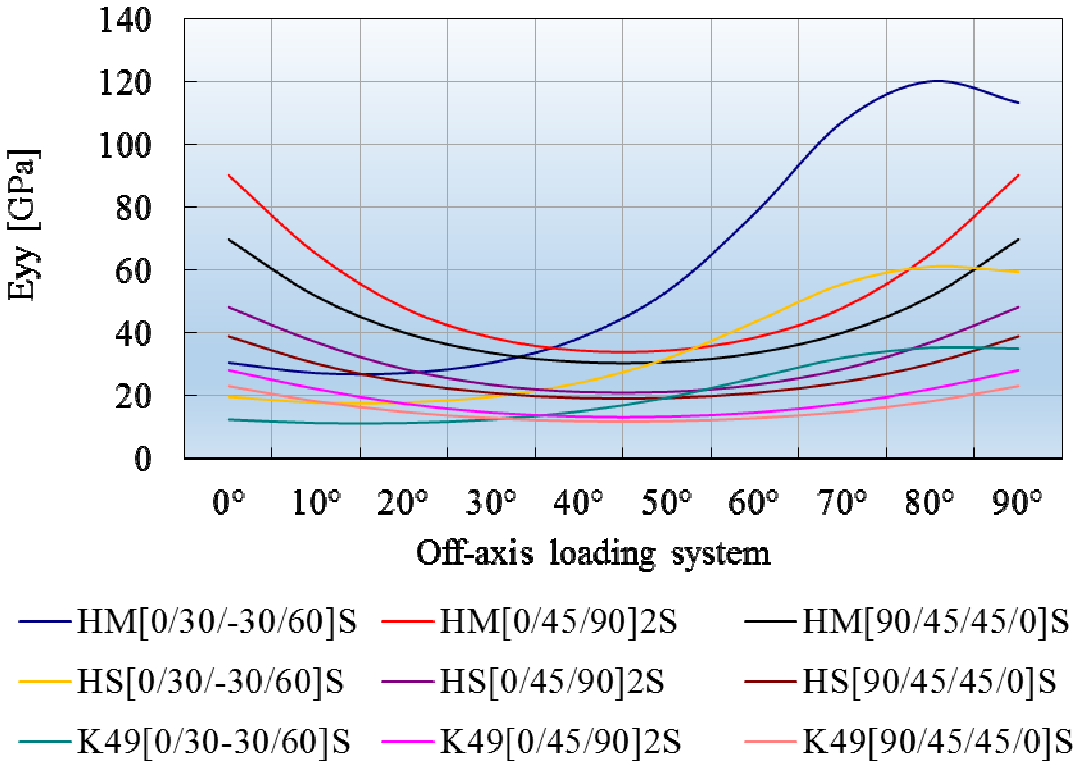

Fig. 2.35. E_{yy} distribution of some carbon and aramid fibers-reinforced epoxy based symmetric laminates

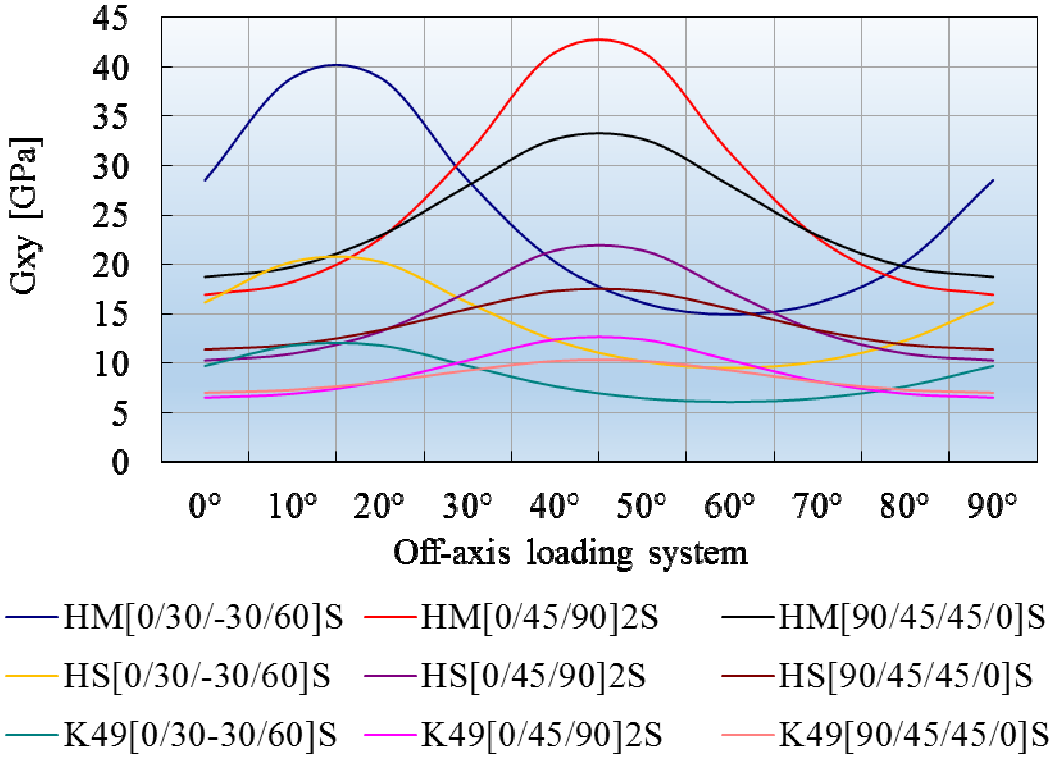

Fig. 2.36. G_{xy} distribution of some carbon and aramid fibers-reinforced epoxy based symmetric laminates

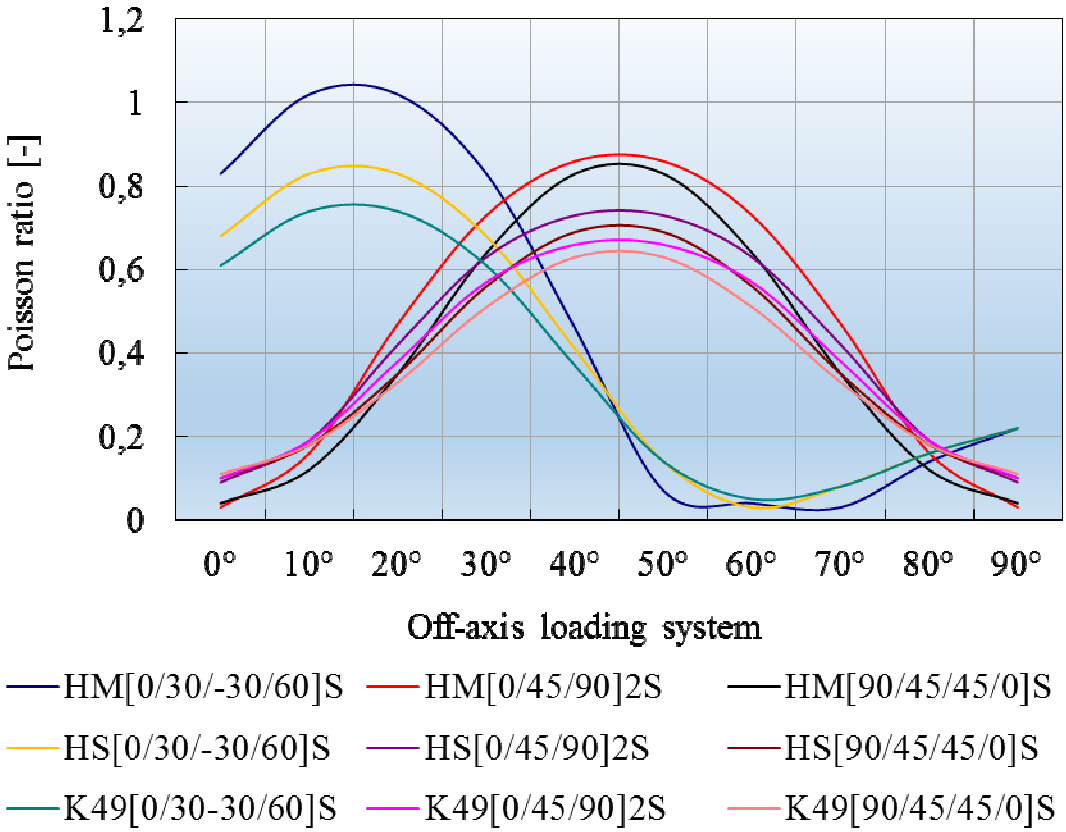

Fig. 2.37. υ_{xy} distribution of some carbon and aramid fibers-reinforced epoxy based symmetric laminates

Case of E-glass fibers-reinforced [16/-81.8], [30/-30/90] and [55/-55] laminates

The E-glass fibers laminates with the above plies sequence are commonly used to withstand the inner pressure of composite tubes and tanks. General input data are: fibers volume fraction $\varphi = 0.5$ in all cases, plies thickness t = 0.125 mm and off-axis loading systems varies between 0 and 90 degrees. For the E-glass fibers-reinforced laminates, following data have been used:

- $E_M = 3.9$ GPa;
- $E_F = 73$ GPa;
- $\upsilon_M = 0.38$; $\upsilon_F = 0.25$; $G_M < 10$ GPa; $G_F < 25$ GPa.

The elastic constants E_{xx}, E_{yy}, G_{xy} and υ_{xy} for the E-glass fibers [16/-81.8], [30/-30/90] and [55/-55] laminates have been presented in Figs. 2.38 – 2.41 as well

as the distribution of $\underline{c}_{33}$ compound of the transformed compliance tensor (Fig. 2.42).

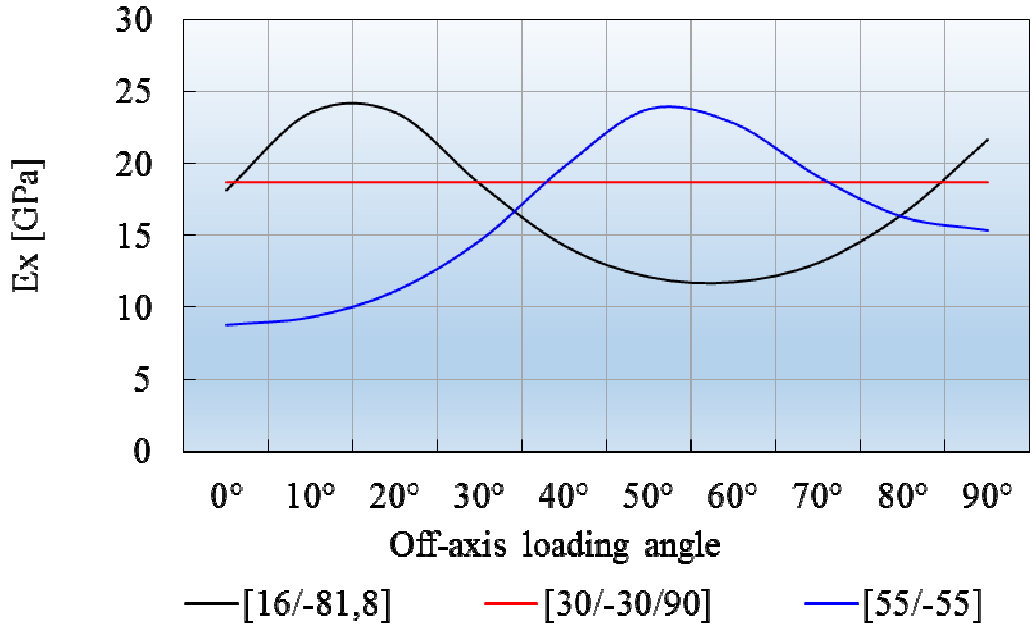

Fig. 2.38. . E_x Young's modulus of three epoxy based E-glass fibers-reinforced composite laminates

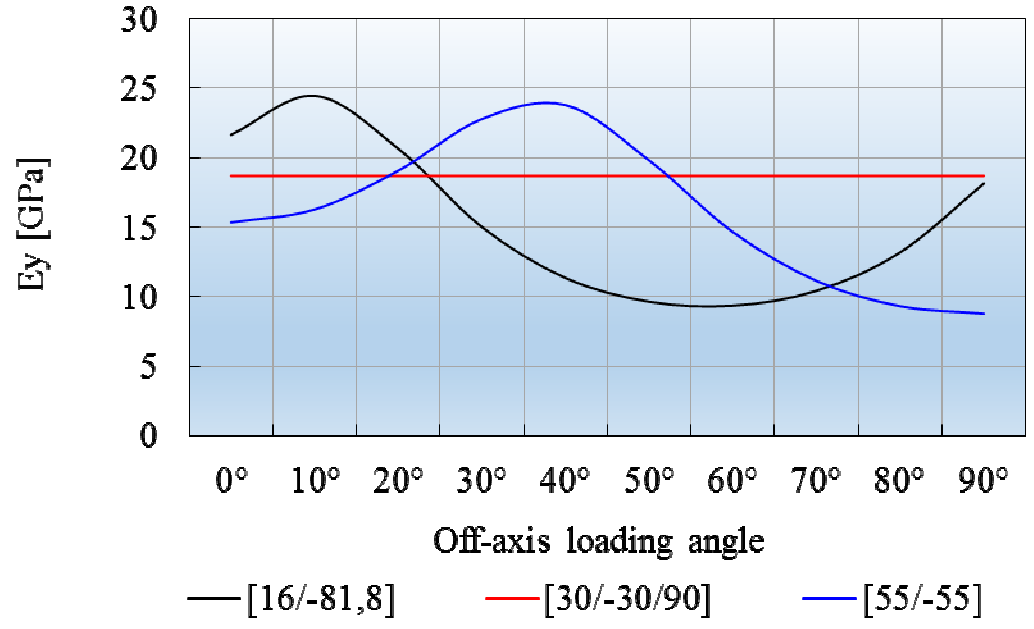

Fig. 2.39. . E_y Young's modulus of three epoxy based E-glass fibers-reinforced composite laminates

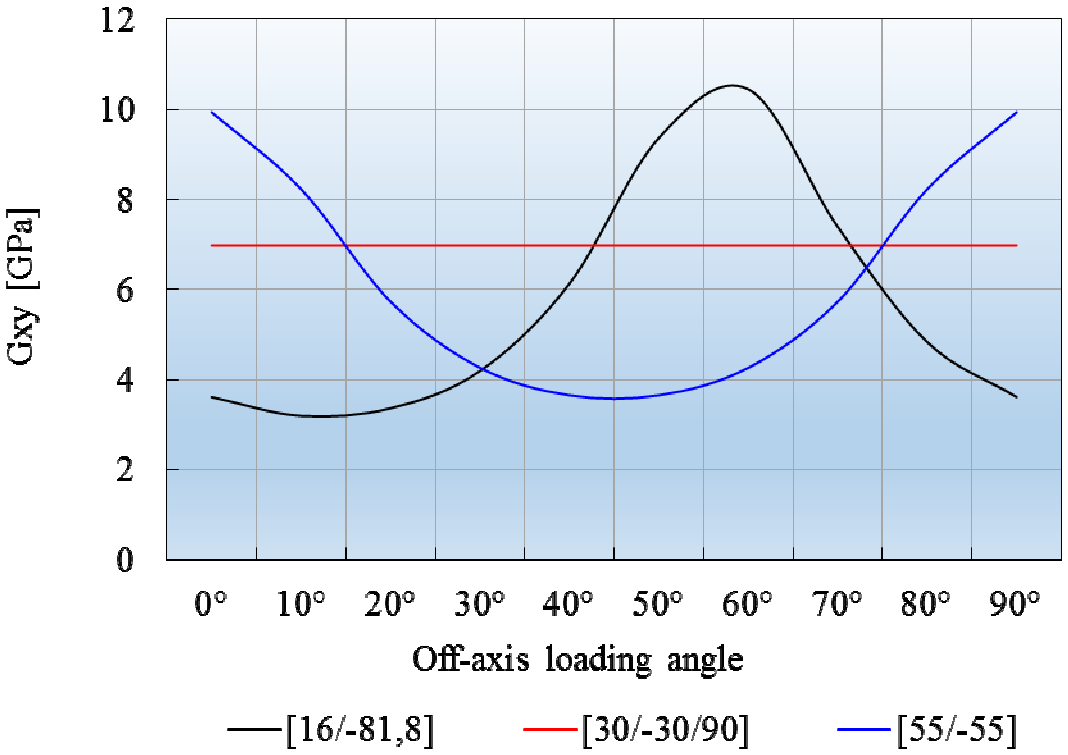

Fig. 2.40. Shear modulus distribution of three epoxy based E-glass fibers-reinforced composite laminates

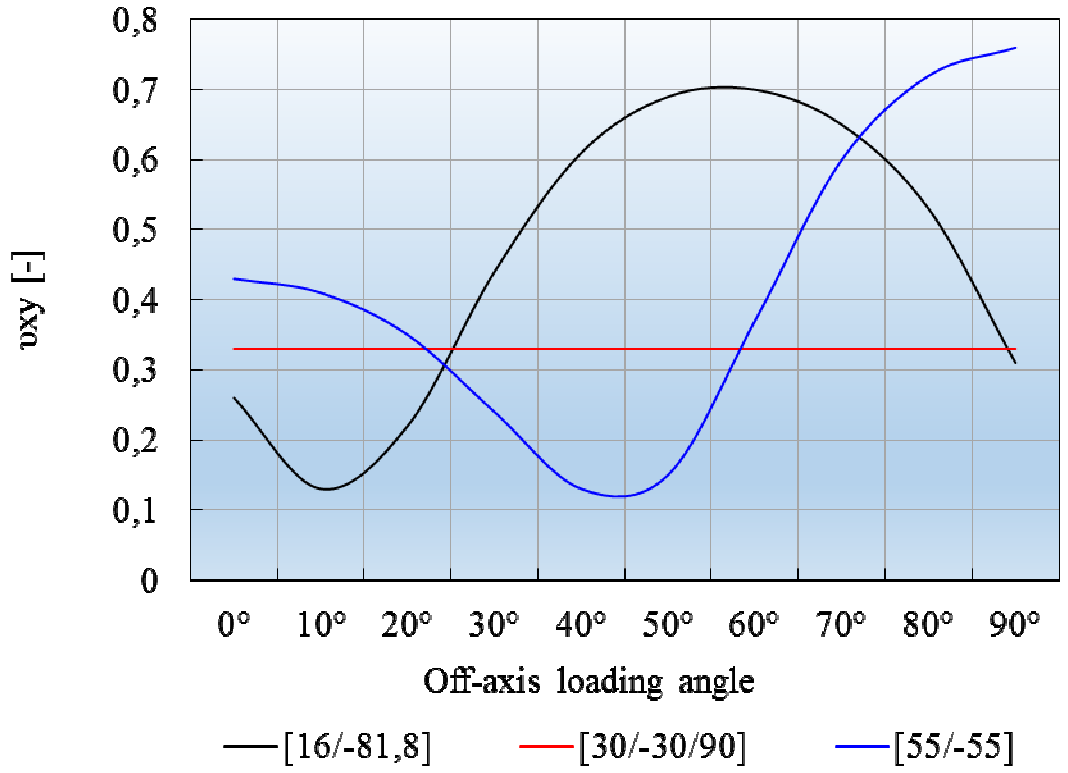

Fig. 2.41. Poisson's ratio distribution of three epoxy based E-glass fibers-reinforced composite laminates

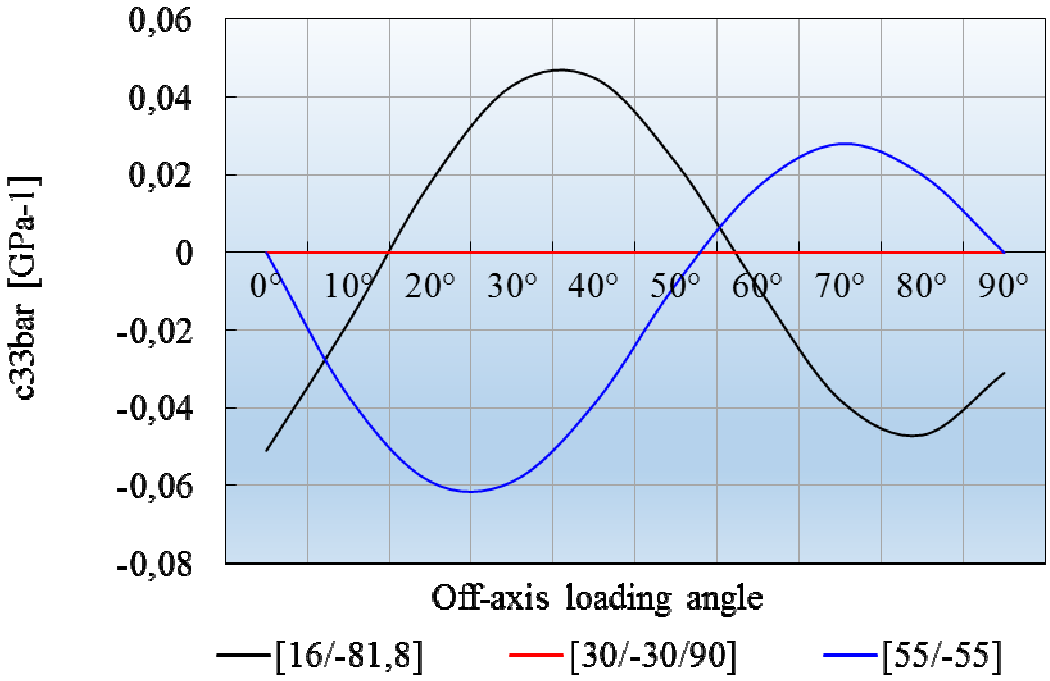

Fig. 2.42. Distribution of $\underline{c}_{33}$ compound of the transformed compliance tensor

Conclusions

Figs. 2.38 – 2.41 show an equal stiffness distribution for the laminate with the plies sequence [30/-30/90], which means that this laminate provides balanced angle plies. This kind of structure is more suitable for tubes manufacturing subjected to internal pressure than the laminates [16/-81.9] and [55/-55]. Under off-axis loading system, normal stresses produce shear strains and of course, normal strains and shear stresses cause normal strains as well as shear strains.

2.6. Stresses evaluation in various composite laminates for general set of applied in-plane loads

In order to compute stresses in each individual lamina of a composite laminate, four examples of laminates have been chosen: anti-symmetric laminate with following plies sequence: [30/0/0/-30]; symmetric cross-ply laminate with plies distribution: [90/0/0/90]; symmetric angle-ply laminate with plies sequence: [30/-30/-30/30]; balanced angle-ply laminate with following plies distribution: [30/30/-30/-30]. For all types of laminates, the Tenax IMS65 carbon fibers have been taken into account as well as Huntsman XB3585 epoxy resin with following input data:

- Matrix axial and transverse Young's modulus: 3.2 GPa;
- Fibers axial Young's modulus: 290 GPa;
- Fibers transverse Young's modulus: 4.8 GPa;
- Matrix axial-transverse Poisson ratio : 0.3 ;
- Fibers axial-transverse Poisson ratio : 0.05 ;
- Matrix axial-transverse shear modulus: 1.15 GPa;
- Fibers axial-transverse shear modulus: 4.2 GPa;
- Fibers volume fraction: 0.51;
- Applied normal stress in x-direction: 2000 MPa;
- Applied normal stress in y-direction: 200 MPa;
- Applied shear stress in x-y plane: 100 MPa;
- Off-axis loading system: between 0° and 90°.

For these types of laminates following stresses in each lamina have been computed. Example of stresses in some plies in case of all considered laminates subjected to a general set of in-plane loads are presented in tables 2.3 – 2.14 and the stresses distributions at 0° off-axis loading angle are visualized in Figs. 2.43 – 2.46. A strong anisotropy at all considered composite laminates can be noticed.

Table 2.3. Example of computational stresses in first ply in case of [30/0/0/-30] anti-symmetric laminate

Off-axis loading system	Normal stress $\sigma_{\parallel}$ [GPa]	Normal stress $\sigma_{\perp}$ [GPa]	Shear stress $\tau_{\#}$ [GPa]
0°	2179.08820396	-0.71697426	-35.75065488
10°	939.39407259	36.90536763	-49.96934150
20°	122.51085318	121.05810845	-26.13182244
30°	-173.03328210	241.59118570	32.88674569
40°	88.40865122	383.96653138	119.96785257
50°	875.30289753	531.01157756	224.60823152
60°	2092.73839739	664.99052153	334.18670852
70°	3593.87446208	769.74352531	435.48650202
80°	5197.65192780	832.63583067	516.28936191
90°	6710.63156295	846.08169739	566.84927077

Table 2.4. Example of computational stresses in first ply in case of [90/0/0/90] symmetric cross-ply laminate

Off-axis loading system	Normal stress $\sigma_{\parallel}$ [GPa]	Normal stress $\sigma_{\perp}$ [GPa]	Shear stress $\tau_{\#}$ [GPa]
0°	373.01363977	103.92906445	-100.00000000
10°	412.30478474	103.07095551	213.84886691
20°	659.32319009	97.67613434	501.90440441
30°	1084.27479052	88.39529598	729.42286341
40°	1635.90415140	76.34784651	868.96215995
50°	2247.67663063	62.98688614	903.69179548
60°	2845.80343841	49.92394388	829.42286342
70°	3358.14165431	38.73460334	655.11329304
80°	3722.89572819	30.76846414	401.78739109
90°	3896.07093555	26.98636024	100.00000002

Table 2.5. Example of computational stresses in first ply in case of [30/-30/-30/30] symmetric angle-ply laminate

Off-axis loading system	Normal stress $\sigma_{\parallel}$ [GPa]	Normal stress $\sigma_{\perp}$ [GPa]	Shear stress $\tau_{\#}$ [GPa]
0°	2644.74794562	-227.66078547	-271.90180554
10°	1933.08992283	-197.32835504	-268.75541845
20°	1198.73745590	-88.30747413	-188.28195259
30°	530.26429024	86.25233006	-40.18769559
40°	8.29815524	305.29656890	157.66499951
50°	-304.20412982	542.40527445	381.41217769
60°	-369.55017733	768.97963747	604.06662711
70°	-179.85828954	957.69144589	798.77293513
80°	241.99189232	1085.77927052	942.04664745
90°	845.11901047	1137.79382935	1016.60683987

Table 2.6. Example of computational stresses in last ply in case of [30/30/-30/-30] balanced angle-ply laminate

Off-axis loading system	Normal stress $\sigma_{\parallel}$ [GPa]	Normal stress $\sigma_{\perp}$ [GPa]	Shear stress $\tau_{\#}$ [GPa]
0°	2200.87965101	-217.96681116	279.10535845
10°	2882.29724146	-218.05880925	253.35070217
20°	3426.53197635	-136.96195813	152.12700324
30°	3767.94111459	15.54226510	-12.35666635
40°	3865.34567546	221.05960040	-220.26114851
50°	3706.99723137	454.80162400	-446.51009437
60°	3311.99494166	688.57559821	-663.81454196
70°	2727.98191207	894.18493159	-845.96436785
80°	2025.39873309	1046.83010407	-970.98961477

Table 2.7. Example of computational stresses in case of [30/0/0/-30] anti-symmetric laminate (plies 2 and 3)

Laminate [30/0/0/-30] – plies no. 2 and 3			
Off-axis loading system	**Normal stress $\sigma_{\parallel}$ [GPa]**	**Normal stress $\sigma_{\perp}$ [GPa]**	**Shear stress $\tau_{\#}$ [GPa]**
0	2637.35409447	-10.72538852	13.43901899
10	2556.01400009	1.59878631	-28.73918983
20	2044.63922564	79.07929789	-67.45102820
30	1164.90911601	212.37085303	-98.02727710
40	22.93210584	385.39652301	-116.77998965
50	-1243.55252364	577.28685845	-121.44731197
60	-2481.78803481	764.89705288	-111.46629608
70	-3542.42495061	925.59854803	-88.04079983
80	-4297.53480566	1040.00837188	-53.99628377
90	-4656.04020720	1094.32701117	-13.43901899

Table 2.8. Example of computational stresses in case of [30/0/0/-30] anti-symmetric laminate (ply 4)

Laminate [30/0/0/-30] – ply no. 4			
Off-axis loading system	**Normal stress $\sigma_{\parallel}$ [GPa]**	**Normal stress $\sigma_{\perp}$ [GPa]**	**Shear stress $\tau_{\#}$ [GPa]**
0	1351.00315911	17.36819930	49.18967386
10	2710.24455809	-1.76957112	21.23015168
20	4278.70616551	30.28782579	-41.31920575
30	5867.20836348	109.67379484	-130.91402279
40	7284.15434313	226.81321655	-236.74784223
50	8358.63950743	367.57734787	-346.05554349
60	8961.06508785	514.98795711	-445.65300460
70	9018.76966854	651.26514923	-523.52730185
80	8524.79322543	759.97188364	-570.28564568
90	7538.71660788	827.99652383	-580.28828975

Table 2.9. Example of computational stresses in case of [90/0/0/90] symmetric cross-ply laminate (plies 1 and 4)

Laminate [90/0/0/90] – plies no. 1 and 4			
Off-axis loading system	**Normal stress $\sigma_{\parallel}$ [GPa]**	**Normal stress $\sigma_{\perp}$ [GPa]**	**Shear stress $\tau_{\#}$ [GPa]**
0	373.01363977	103.92906445	-100.00000000
10	412.30478474	103.07095551	213.84886691
20	659.32319009	97.67613434	501.90440441
30	1084.27479052	88.39529598	729.42286341
40	1635.90415140	76.34784651	868.96215995
50	2247.67663063	62.98688614	903.69179548
60	2845.80343841	49.92394388	829.42286342
70	3358.14165431	38.73460334	655.11329304
80	3722.89572819	30.76846414	401.78739109
90	3896.07093555	26.98636024	100.00000002

Table 2.10. Example of computational stresses in case of [90/0/0/90] symmetric cross-ply laminate (plies 2 and 3)

Laminate [90/0/0/90] – plies no. 2 and 3			
Off-axis loading system	**Normal stress $\sigma_{\parallel}$ [GPa]**	**Normal stress $\sigma_{\perp}$ [GPa]**	**Shear stress $\tau_{\#}$ [GPa]**
0	3896.07093555	26.98636024	100.00000000
10	3856.77979057	27.84446917	-213.84886691
20	3609.76138522	33.23929035	-501.90440441
30	3184.80978479	42.52012871	-729.42286341
40	2633.18042390	54.56757818	-868.96215995
50	2021.40794468	67.92853855	-903.69179548
60	1423.28113690	80.99148082	-829.42286342
70	910.94292100	92.18082135	-655.11329304
80	546.18884712	100.14696054	-401.78739109
90	373.01363977	103.92906445	-100.00000002

Table 2.11. Example of computational stresses in case of [30/-30/-30/30] symmetric angle-ply laminate (plies 1 and 4)

Laminate [30/-30/-30/30] – plies no. 1 and 4			
Off-axis loading system	**Normal stress $\sigma_{\parallel}$ [GPa]**	**Normal stress $\sigma_{\perp}$ [GPa]**	**Shear stress $\tau_{\#}$ [GPa]**
0	2644.74794562	-227.66078547	-271.90180554
10	1933.08992283	-197.32835504	-268.75541845
20	1198.73745590	-88.30747413	-188.28195259
30	530.26429024	86.25233006	-40.18769559
40	8.29815524	305.29656890	157.66499951
50	-304.20412982	542.40527445	381.41217769
60	-369.55017733	768.97963747	604.06662711
70	-179.85828954	957.69144589	798.77293513
80	241.99189232	1085.77927052	942.04664745
90	845.11901047	1137.79382935	1016.60683987

Table 2.12. Example of computational stresses in case of [30/-30/-30/30] symmetric angle-ply laminate (plies 2 and 3)

Laminate [30/-30/-30/30] – plies no. 2 and 3			
Off-axis loading system	**Normal stress $\sigma_{\parallel}$ [GPa]**	**Normal stress $\sigma_{\perp}$ [GPa]**	**Shear stress $\tau_{\#}$ [GPa]**
0	2200.87965101	-217.96681116	279.10535845
10	2882.29724146	-218.05880925	253.35070217
20	3426.53197635	-136.96195813	152.12700324
30	3767.94111459	15.54226510	-12.35666635
40	3865.34567546	221.05960040	-220.26114851
50	3706.99723137	454.80162400	-446.51009437
60	3311.99494166	688.57559821	-663.81454196
70	2727.98191207	894.18493159	-845.96436785
80	2025.39873309	1046.83010407	-970.98961477
90	1288.98730513	1128.09985505	-1023.81039279

Table 2.13. Example of computational stresses in case of [30/30/-30/-30] balanced angle-ply laminate (plies 1 and 2)

Laminate [30/30/-30/-30] – plies no. 1 and 2			
Off-axis loading system	**Normal stress $\sigma_{\parallel}$ [GPa]**	**Normal stress $\sigma_{\perp}$ [GPa]**	**Shear stress $\tau_{\#}$ [GPa]**
0	2644.74794562	-227.66078547	-271.90180554
10	1933.08992283	-197.32835504	-268.75541845
20	1198.73745590	-88.30747413	-188.28195259
30	530.26429024	86.25233006	-40.18769559
40	8.29815524	305.29656890	157.66499951
50	-304.20412982	542.40527445	381.41217769
60	-369.55017733	768.97963747	604.06662711
70	-179.85828954	957.69144589	798.77293513
80	241.99189232	1085.77927052	942.04664745
90	845.11901047	1137.79382935	1016.60683987

Table 2.14. Example of computational stresses in case of [30/30/-30/-30] balanced angle-ply laminate (plies 3 and 4)

Laminate [30/30/-30/-30] – plies no. 3 and 4			
Off-axis loading system	**Normal stress $\sigma_{\parallel}$ [GPa]**	**Normal stress $\sigma_{\perp}$ [GPa]**	**Shear stress $\tau_{\#}$ [GPa]**
0	2200.87965101	-217.96681116	279.10535845
10	2882.29724146	-218.05880925	253.35070217
20	3426.53197635	-136.96195813	152.12700324
30	3767.94111459	15.54226510	-12.35666635
40	3865.34567546	221.05960040	-220.26114851
50	3706.99723137	454.80162400	-446.51009437
60	3311.99494166	688.57559821	-663.81454196
70	2727.98191207	894.18493159	-845.96436785
80	2025.39873309	1046.83010407	-970.98961477
90	1288.98730513	1128.09985505	-1023.81039279

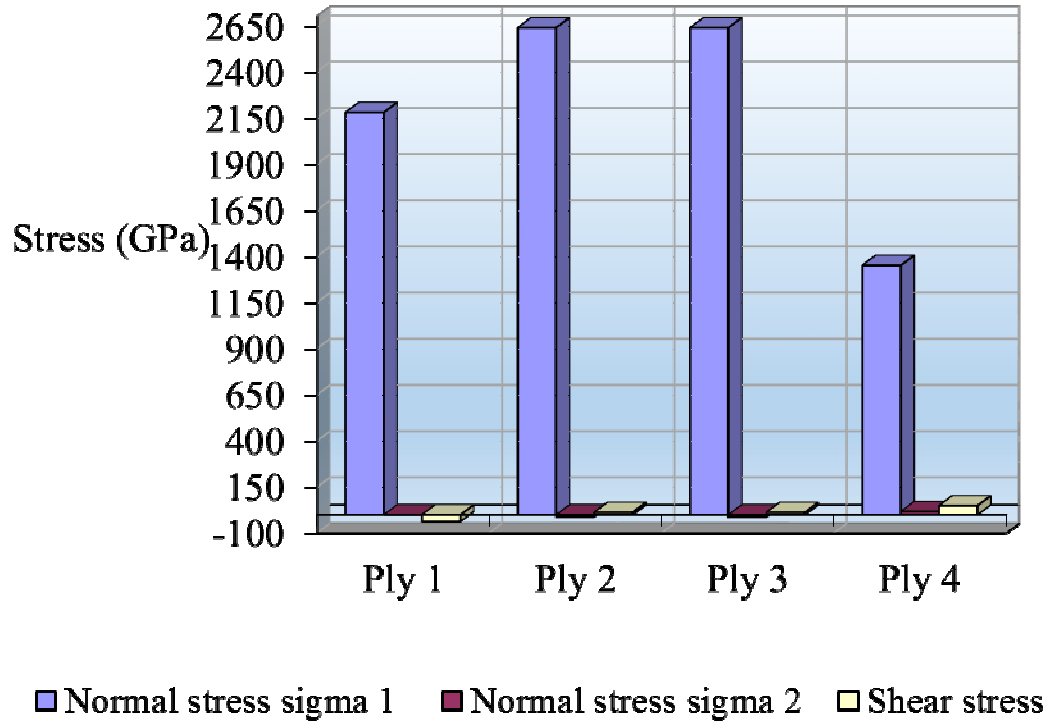

Fig. 2.43. Stresses in anti-symmetric laminate [30/0/0/-30]

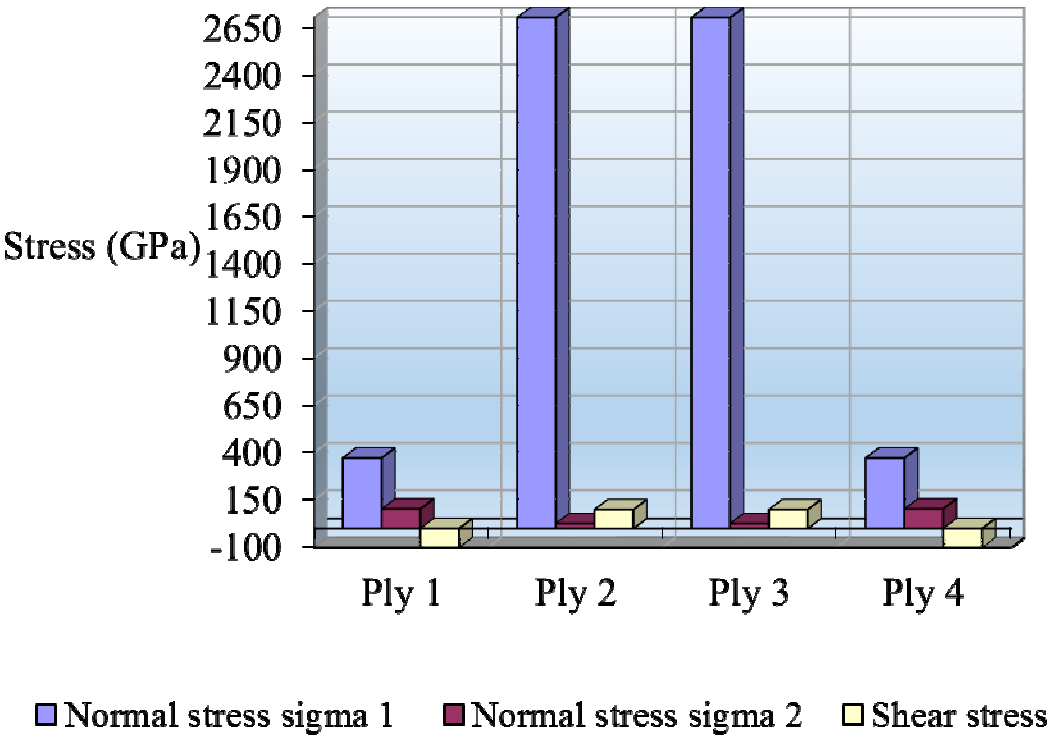

Fig. 2.44. Stresses in symmetric cross-ply laminate [90/0/0/90]

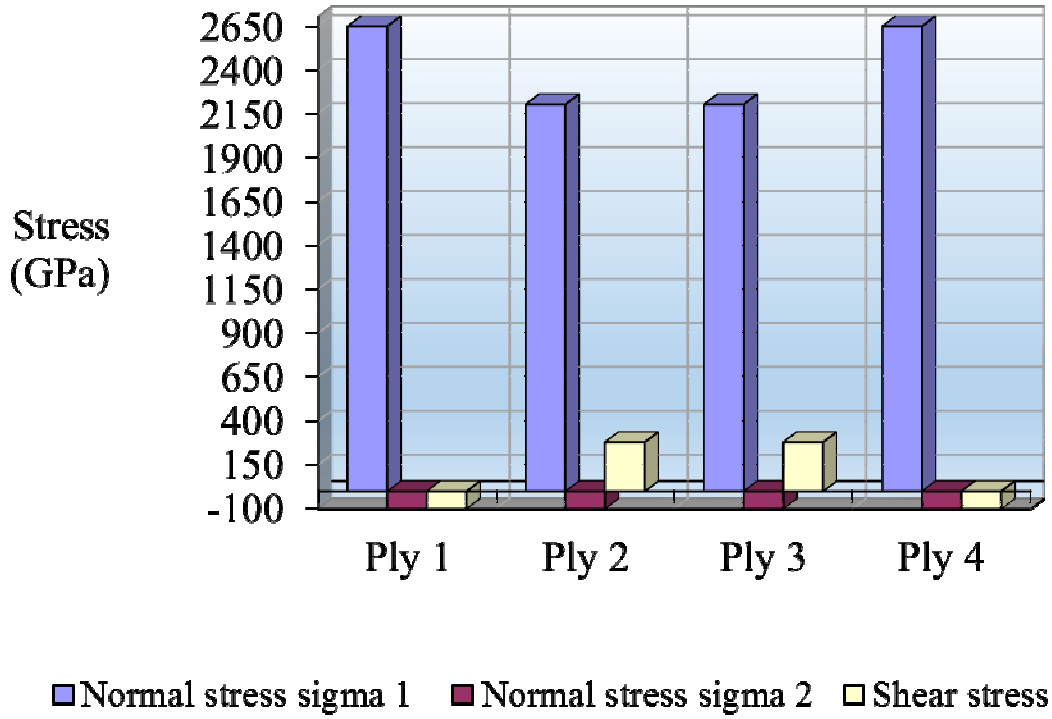

Fig. 2.45. Stresses in symmetric angle-ply laminate [30/-30/-30/30]

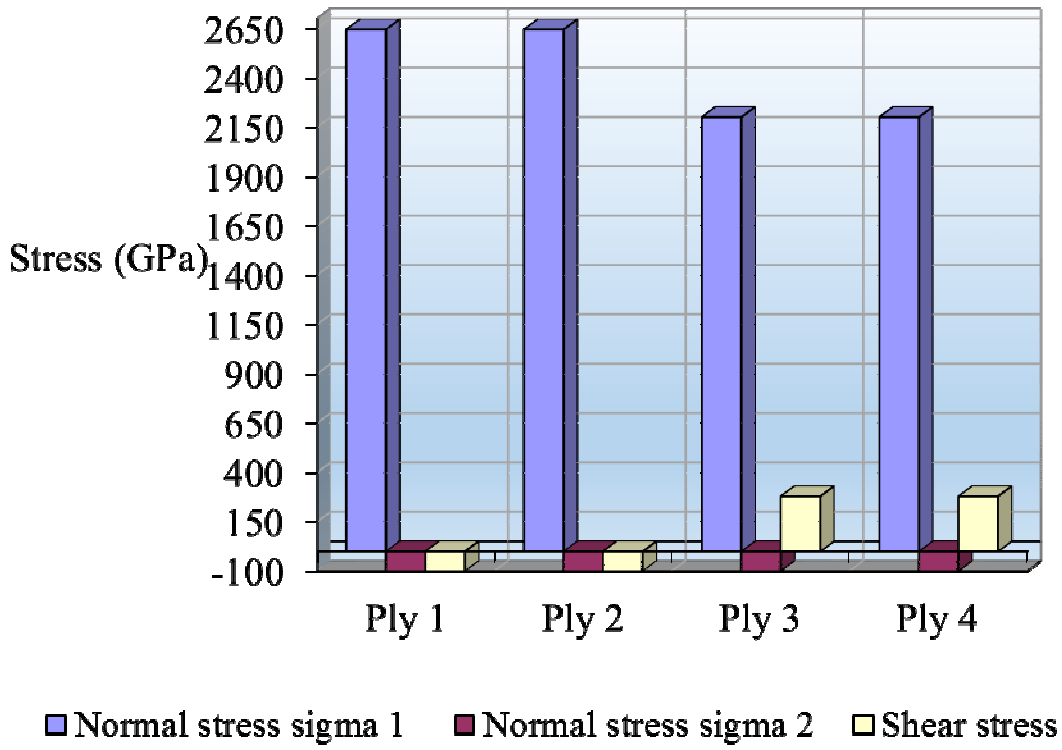

Fig. 2.46. Stresses in balanced angle-ply laminate [30/30/-30/-30]

Case of a [0/90/0/90] glass fibers-reinforced composite laminate subjected to a biaxial field of loads

A unidirectional glass fibers-reinforced composite laminate has been considered with following characteristics:

- Plies sequence [0/90/0/90].
- Number of laminae: 4.
- Fibers volume fraction: 60%.
- Laminate thickness: 2 mm.
- Thickness of each lamina: 0.5 mm.

The laminate is subjected to a biaxial field of normal loads n_{xx}, n_{yy} and a shear load n_{xy}. The aim is to compute the stresses and strains in each lamina. Following input data have been used:

- $\varphi_{1...4} = 60\%$;
- $\alpha_1 = 0°$; $\alpha_2 = 90°$; $\alpha_3 = 0°$; $\alpha_4 = 90°$;
- $t_{1...4} = 0.5$ mm; $t = 2$mm;
- $n_{xx} = 300$ N/mm; $n_{yy} = 150$ N/mm; $n_{xy} = 50$ N/mm;
- $E_F = 73000$ N/mm^2;
- $\upsilon_F = 0.25$;
- $G_F = 29200$ N/mm^2;
- $E_M = 3750$ N/mm^2;
- $\upsilon_M = 0.35$;
- $G_M = 1390$ N/mm^2.

First, I have determined the basic elasticity constants of each lamina using the eqations

$$E_{II1...4} = \varphi_{1...4} \cdot E_F + \left(1 - \varphi_{1...4}\right) E_M = 0.6 \cdot 73000 + (1 - 0.6) \cdot 3750 = 45300 N/mm^2,$$

$$\upsilon_{\perp II1...4} = \varphi_{1...4} \cdot \upsilon_F + \left(1 - \varphi_{1...4}\right) \upsilon_M = 0.6 \cdot 0.25 + (1 - 0.6) \cdot 0.35 = 0.29,$$

$$E_{\perp 1...4} = \frac{3750}{1-0.35^2} \cdot \frac{1+0.85\cdot 0.6^2}{(1-0.6)^{1.25} + \frac{0.6\cdot 3750}{\left(1-0.35^2\right)\cdot 73000}} = 15800\, N/mm^2,$$

$$\upsilon_{II\perp 1...4} = \upsilon_{\perp II 1...4} \cdot \frac{E_{\perp 1...4}}{E_{II 1...4}} = 0.29 \cdot \frac{15800}{45300} = 0.101,$$

$$G_{II\perp 1...4} = 1390 \cdot \frac{1+0.6\cdot 0.6^{0.5}}{(1-0.6)^{1.25} + 0.6\cdot \frac{1390}{29200}} = 5873\, N/mm^2.$$

Second, I have computed the transformed rigidities of each lamina using the relations (2.41) – (2.46):

- <u>For laminae 1 and 3</u>:

$$r_{11\,1,3} = \frac{45300\cdot \cos^4 0°}{1-0.29\cdot 0{,}101} + \frac{15800\cdot \sin^4 0°}{1-0.29\cdot 0.101} +$$

$$+\frac{1}{2}\cdot\left(\frac{0.29\cdot 15800}{1-0.29\cdot 0.101} + 2\cdot 5873\right)\cdot \sin^2 0° = 46666.8\, N/mm^2,$$

$$r_{22\,1,3} = \frac{45300\cdot \sin^4 0°}{1-0.29\cdot 0.101} + \frac{15800\cdot \cos^4 0°}{1-0.29\cdot 0.101} +$$

$$+\frac{1}{2}\cdot\left(\frac{0.29\cdot 15800}{1-0.29\cdot 0.101} + 2\cdot 5873\right)\cdot \sin^2 0° = 16276.7\, N/mm^2,$$

$$r_{33\,1,3} = 5873 + \frac{1}{4}\cdot\left(\frac{45300}{1-0.29\cdot 0.101} + \frac{15800}{1-0.29\cdot 0.101} -\right.$$

$$-\frac{2\cdot 0.29\cdot 15800}{1-0.29\cdot 0.101}-4\cdot 5873\Big)\cdot\sin^2 0°=5873\,N/mm^2,$$

$$r_{12\,1,3}=\frac{0.29\cdot 15800}{1-0.29\cdot 0.101}+\frac{1}{4}\cdot\Big(\frac{45300}{1-0.29\cdot 0.101}+\frac{15800}{1-0.29\cdot 0.101}-$$

$$-\frac{2\cdot 0.29\cdot 15800}{1-0.29\cdot 0.101}-4\cdot 5873\Big)\cdot\sin^2 0°=4720.2\,N/mm^2,$$

$$r_{13\,1,3}=r_{23\,1,3}=0.$$

- For laminae 2 and 4 the transformed rigidities are:

$$r_{11\,2,4}=\frac{45300\cdot\cos^4 90°}{1-0.29\cdot 0.101}+\frac{15800\cdot\sin^4 90°}{1-0.29\cdot 0.101}+$$

$$+\frac{1}{2}\cdot\Big(\frac{0.29\cdot 15800}{1-0.29\cdot 0.101}+2\cdot 5873\Big)\cdot\sin^2 180°=16276.7\,N/mm^2,$$

$$r_{22\,2,4}=\frac{45300\cdot\sin^4 90°}{1-0.29\cdot 0.101}+\frac{15800\cdot\cos^4 90°}{1-0.29\cdot 0.101}+$$

$$+\frac{1}{2}\cdot\Big(\frac{0.29\cdot 15800}{1-0.29\cdot 0.101}+2\cdot 5873\Big)\cdot\sin^2 180°=46666.8\,N/mm^2,$$

$$r_{33\,2,4}=5873+\frac{1}{4}\cdot\Big(\frac{45300}{1-0.29\cdot 0.101}+\frac{15800}{1-0.29\cdot 0.101}-$$

$$-\frac{2\cdot 0.29\cdot 15800}{1-0.29\cdot 0.101}-4\cdot 5873\Big)\cdot\sin^2 180°=5873\,N/mm^2,$$

$$r_{12\,2,4}=\frac{0.29\cdot 15800}{1-0.29\cdot 0.101}+\frac{1}{4}\cdot\left(\frac{45300}{1-0.29\cdot 0.101}+\frac{15800}{1-0.29\cdot 0.101}-\right.$$

$$\left.-\frac{2\cdot 0.29\cdot 15800}{1-0.29\cdot 0.101}-4\cdot 5873\right)\cdot\sin^2 180°=4720.2\,N/mm^2,$$

$$r_{13\,2,4}=r_{23\,2,4}=0.$$

Third, I have determined the laminate's rigidities adding the rigidities of all laminae using the relation (2.53):

$$\underline{r}_{11}=2\cdot\left(46666.8\cdot\frac{0.25}{2}\right)+2\cdot\left(16276.7\cdot\frac{0.25}{2}\right)=15735.8\,N/mm^2,$$

$$\underline{r}_{22}=2\cdot\left(16276.7\cdot\frac{0.25}{2}\right)+2\cdot\left(46666.8\cdot\frac{0.25}{2}\right)=15735.8\,N/mm^2,$$

$$\underline{r}_{33}=2\cdot\left(5873\cdot\frac{0.25}{2}\right)+2\cdot\left(5873\cdot\frac{0.25}{2}\right)=2936.5\,N/mm^2,$$

$$\underline{r}_{12}=2\cdot\left(4720.2\cdot\frac{0.25}{2}\right)+2\cdot\left(4720.2\cdot\frac{0.25}{2}\right)=2360.1\,N/mm^2,$$

$$\underline{r}_{13}=\underline{r}_{23}=0.$$

Fourth, I have computed the transformed compliances of each lamina using the relations (2.34) – (2.39):

- <u>For laminae 1 and 3:</u>

$$c_{11\,1,3}=\frac{\cos^4 0°}{45300}+\frac{\sin^4 0°}{15800}+\frac{1}{4}\cdot\left(\frac{1}{5873}-\frac{2\cdot 0.29}{45300}\right)\cdot\sin^2 0°=22\cdot 10^{-6}\,mm^2/N,$$

$$c_{22\,1,3}=\frac{\sin^4 0°}{45300}+\frac{\cos^4 0°}{15800}+\frac{1}{4}\cdot\left(\frac{1}{5873}-\frac{2\cdot 0.29}{45300}\right)\cdot\sin^2 0°=63.2\cdot 10^{-6}\,mm^2/N,$$

$$c_{33\,1,3}=\frac{\cos^2 0°}{5873}+\left(\frac{1}{45300}+\frac{1}{15800}+\frac{2\cdot 0.29}{45300}\right)\cdot\sin^2 0°=170.2\cdot 10^{-6}\,mm^2/N,$$

$$c_{12\,1,3}=\frac{1}{4}\cdot\left(\frac{1}{45300}+\frac{1}{15800}-\frac{1}{5873}\right)\cdot\sin^2 0°-$$

$$-\frac{0.29}{45300}\cdot\left(\sin^4 0°+\cos^4 0°\right)=-6.4\cdot 10^{-6}\,mm^2/N,$$

$$c_{13\,1,3}=c_{23\,1,3}=0.$$

- <u>For laminae 2 and 4, the transformed compliances are:</u>

$$c_{11\,2,4}=\frac{\cos^4 90°}{45300}+\frac{\sin^4 90°}{15800}+\frac{1}{4}\cdot\left(\frac{1}{5873}-\frac{2\cdot 0.29}{45300}\right)\cdot\sin^2 180°=63.2\cdot 10^{-6}\,mm^2/N,$$

$$c_{22\,2,4}=\frac{\sin^4 90°}{45300}+\frac{\cos^4 90°}{15800}+\frac{1}{4}\cdot\left(\frac{1}{5873}-\frac{2\cdot 0.29}{45300}\right)\cdot\sin^2 180°=22\cdot 10^{-6}\,mm^2/N,$$

$$c_{33\,2,4}=\frac{\cos^2 180°}{5873}+\left(\frac{1}{45300}+\frac{1}{15800}+\frac{2\cdot 0.29}{45300}\right)\cdot\sin^2 180°=170.2\cdot 10^{-6}\,mm^2/N,$$

$$c_{12\,2,4}=\frac{1}{4}\cdot\left(\frac{1}{45300}+\frac{1}{15800}-\frac{1}{5873}\right)\cdot\sin^2 180°-$$

$$-\frac{0.29}{45300}\cdot\left(\sin^4 90°+\cos^4 90°\right)=-6.4\cdot 10^{-6}\,mm^2/N,$$

$$c_{13\,2,4}=c_{23\,2,4}=0.$$

Fifht, I have computed the laminate's compliance adding the compliances of each lamina:

$$\underline{c}_{11}=c_{11\,1}+c_{11\,2}+c_{11\,3}+c_{11\,4}=170.4\cdot10^{-6}\,mm^2/N,$$

$$\underline{c}_{22}=c_{22\,1}+c_{22\,2}+c_{22\,3}+c_{22\,4}=170.4\cdot10^{-6}\,mm^2/N,$$

$$\underline{c}_{33}=c_{33\,1}+c_{33\,2}+c_{33\,3}+c_{33\,4}=680.8\cdot10^{-6}\,mm^2/N,$$

$$\underline{c}_{12}=c_{12\,1}+c_{12\,2}+c_{12\,3}+c_{12\,4}=-25.6\cdot10^{-6}\,mm^2/N,$$

$$\underline{c}_{13}=\underline{c}_{23}=0.$$

Sixth, I have determined the laminate's strains ε_{xx}, ε_{yy} and γ_{xy} under the stresses $\underline{\sigma}_{xx}$, $\underline{\sigma}_{yy}$ and $\underline{\tau}_{xy}$. From the relations (2.54) I have computed the normal stresses on x respective y-axis directions as well as the shear stress according to the x-y coordinate system:

$$\underline{\sigma}_{xx}=\frac{n_{xx}}{t}=\frac{300}{2}=150\,N/mm^2,$$

$$\underline{\sigma}_{yy}=\frac{n_{yy}}{t}=\frac{150}{2}=75\,N/mm^2,$$

$$\underline{\tau}_{xy}=\frac{n_{xy}}{t}=\frac{50}{2}=25\,N/mm^2.$$

Now the strains ε_{xx}, ε_{yy} and γ_{xy} can be computed in the following way:

$$\varepsilon_{xx} = \underline{c}_{11} \cdot \underline{\sigma}_{xx} + \underline{c}_{12} \cdot \underline{\sigma}_{yy} = \left(170.4 \cdot 10^{-6}\right) \cdot (150) - \left(25.6 \cdot 10^{-6}\right) \cdot (75) = 0.0236,$$

$$\varepsilon_{yy} = \underline{c}_{12} \cdot \underline{\sigma}_{xx} + \underline{c}_{22} \cdot \underline{\sigma}_{yy} = \left(-25.6 \cdot 10^{-6}\right) \cdot (150) + \left(170.4 \cdot 10^{-6}\right) \cdot (75) = 0.0089,$$

$$\gamma_{xy} = \underline{c}_{33} \cdot \underline{\tau}_{xy} = \left(680.8 \cdot 10^{-6}\right) \cdot (25) = 0.017.$$

Seventh, I have computed the strains of each lamina using the relations (2.55):

- <u>For laminae 1 and 3:</u>

$$\varepsilon_{II\,1,3} = 0.0236 \cdot \cos^2 0° + 0.0089 \cdot \sin^2 0° - \frac{1}{2} \cdot 0.017 \cdot \sin 0° = 0.0236,$$

$$\varepsilon_{\perp 1,3} = 0.0236 \cdot \sin^2 0° + 0.0089 \cdot \cos^2 0° + \frac{1}{2} \cdot 0.017 \cdot \sin 0° = 0.0089,$$

$$\gamma_{II\,\perp 1,3} = (0.0236 - 0.0089) \cdot \sin 0° + 0.017 \cdot \cos 0° = 0.017.$$

- <u>For laminae 2 and 4:</u>

$$\varepsilon_{II\,2,4} = 0.0236 \cdot \cos^2 90° + 0.0089 \cdot \sin^2 90° - \frac{1}{2} \cdot 0.017 \cdot \sin 180° = 0.0089,$$

$$\varepsilon_{\perp 2,4} = 0.0236 \cdot \sin^2 90° + 0.0089 \cdot \cos^2 90° + \frac{1}{2} \cdot 0.017 \cdot \sin 180° = 0.0236,$$

$$\gamma_{II\perp 2,4}=(0.0236-0.0089)\cdot\sin 180°+0.017\cdot\cos 180°=-0.017.$$

Finally, I have determined the stresses in each lamina using the relations (2.56) – (2.58):

- For laminae 1 and 3:

$$\sigma_{II\,1,3}=\frac{(45300)\cdot 0.0236}{(1-0.29\cdot 0.101)}+\frac{0.29\cdot(15800)\cdot 0.0089}{(1-0.29\cdot 0.101)}=1143.34\,N/mm^2,$$

$$\sigma_{\perp 1,3}=\frac{0.29\cdot(15800)\cdot 0.0236}{(1-0.29\cdot 0.101)}+\frac{(15800)\cdot 0.0089}{(1-0.29\cdot 0.101)}=256.26\,N/mm^2,$$

$$\tau_{II\perp 1,3}=(5873)\cdot 0.017=99.84\,N/mm^2.$$

- For laminae 2 and 4:

$$\sigma_{II\,2,4}=\frac{(45300)\cdot 0.0089}{(1-0.29\cdot 0.101)}+\frac{0.29\cdot(15800)\cdot 0.0236}{(1-0.29\cdot 0.101)}=526.73\,N/mm^2,$$

$$\sigma_{\perp 2,4}=\frac{0.29\cdot(15800)\cdot 0.0089}{(1-0.29\cdot 0.101)}+\frac{(15800)\cdot 0.0236}{(1-0.29\cdot 0.101)}=426.14\,N/mm^2,$$

$$\tau_{II\perp 2,4}=(5873)\cdot(-0.017)=-99.84\,N/mm^2.$$

Case of a unidirectional [30] epoxy/carbon fibers-reinforced lamina

A unidirectional [30] epoxy/carbon fibers-reinforced lamina being in a stress plane state is considered. The fibers volume fraction is 45% and the fibers'

disposal angle against the x-axis is 30˚. The aim is to compute the lamina's transformed compliances knowing the variation of fibers disposal angle between -45˚ and 45˚. Following input data have been used:

- $E_{F\parallel}$ = 520 GPa;
- $E_{F\perp}$ = 24 GPa;
- υ_F = 0.32;
- E_M = 4.05 GPa;
- υ_M = 034.

The results are presented in Table 2.15.

Table 2.15. Transformed compliances of a unidirectional [30] epoxy/carbon fibers-reinforced lamina. Results in (10^{-3} GPa^{-1})

	- 45°	**- 30°**	**- 15°**	**0°**	**15°**	**30°**	**45°**
$\mathbf{c_{11}}$	82	50.6	18	4.2	18	50.6	82
$\mathbf{c_{22}}$	82	100	104	104	104	100	82
$\mathbf{c_{33}}$	111.3	139.9	197.1	225.7	197.1	139.9	111.3
$\mathbf{c_{12}}$	- 30	- 22.8	- 8.5	- 1.4	- 8.5	- 22.8	- 30
$\mathbf{c_{13}}$	- 49.4	- 67.9	- 49.5	0	49.5	67.9	49.4
$\mathbf{c_{23}}$	- 49.8	- 18.5	- 0.009	0	0.009	18.5	49.8

Case of a unidirectional [30] polyester/glass fibers-reinforced lamina

A unidirectional [30] polyester/glass fibers-reinforced lamina being in a stress plane state is considered. The fibers volume fraction is 35% and the fibers' disposal angle against the x-axis is 30˚. The aim is to compute the lamina's transformed rigidities knowing the variation of fibers disposal angle between - 30˚ and 30˚. Following input data have been used:

- E_F = 73 GPa;

- $\upsilon_F = 0.2$;
- $E_M = 1.5$ GPa;
- $\upsilon_M = 0.35$.

The results are presented in Table 2.16.

Table 2.16. Transformed rigidities of a unidirectional [30] polyester/glass fibers-reinforced lamina. Results in (GPa)

	- 30°	**- 15°**	**0°**	**15°**	**30°**
$\mathbf{r_{11}}$	16.5	23.75	26.79	23.75	16.5
$\mathbf{r_{22}}$	4.76	3.32	3.21	3.32	4.76
$\mathbf{r_{33}}$	5.58	2.7	1.26	2.7	5.58
$\mathbf{r_{12}}$	5.27	2.39	0.95	2.39	5.27
$\mathbf{r_{13}}$	7.6	5.44	0	- 5.44	- 7.6
$\mathbf{r_{23}}$	- 7.6	- 5.44	0	5.44	7.6

Case of a unidirectional [α] glass fibers-reinforced lamina

A unidirectional [α] glass fibers-reinforced lamina with angle α disposed against the x-axis is considered. The fibers volume fraction is 58% and lamina's thickness is 0.5 mm. The aim is to compute the stresses on the material's main directions in case of following fibers disposal angles: α = 0°, 30°, 60° and 90° knowing that the lamina is subjected to normal load $n_{xx} = 250$ N/mm and a shear load $n_{xy} = 25$ N/mm that acts in x-y plane. Following input data have been used:

- $E_F = 73$ GPa;
- $\upsilon_F = 0.25$;
- $G_F = 28.5$ GPa;
- $E_M = 3.65$ GPa;
- $\upsilon_M = 0.35$;

- G_M = 1.27 GPa.

The results are presented in Table 2.17.

Table 2.17. Stresses in a unidirectional [α] glass fibers-reinforced lamina subjected to normal load n_{xx} = 250 N/mm and a shear load n_{xy} = 25 N/mm. Results in (MPa)

	0°	30°	60°	90°
$\sigma_{\parallel}$	480	329	90.4	0.4
$\sigma_{\perp}$	3	168	412	497
$\tau_{\parallel\perp}$	49.7	131	33.5	- 49.7

Case of a [0/45/-45/90]$_S$ glass fibers-reinforced composite laminate subjected to a biaxial field of normal and shear loads

A symmetric [/0/45/-45/90]$_S$ glass fibers-reinforced composite laminate is considered. Each lamina present 43% fibers volume fraction. The overall laminate's thickness is 3.5 mm and each lamina presents 0.43 mm thickness. The aim is to compute the stresses in each lamina of the composite laminate knowing the fact that this is subjected to a biaxial field of normal loads n_{xx} = 330 N/mm, n_{yy} = 250 N/mm and a shear load n_{xy} = 55 N/mm that acts in x-y plane. The fibers and matrix features are:

- E_F = 73 GPa;
- υ_F =0.23;
- E_M = 4.2 GPa;
- υ_M =0.34.

The results are presented in Table 2.18.

Table 2.18. Stresses in each lamina of a symmetric $[/0/45/-45/90]_S$ glass fibers-reinforced composite laminate subjected to a biaxial field of normal and shear loads. Results in (GPa)

	Ply 1 and 8	Ply 2 and 7	Ply 3 and 6	Ply 4 and 5
$\sigma_{\parallel}$	1.6	0.84	1.82	1.06
$\sigma_{\perp}$	0.43	0.61	0.37	0.56
$\tau_{\parallel\perp}$	0.13	0.072	- 0.072	- 0.13

Case of a [(0)$_8$] carbon fibers-reinforced composite laminate subjected to a biaxial field of normal loads

A $[(0)_8]$ carbon fibers-reinforced composite laminate is considered. The laminae present following fibers volume fractions: $\varphi_{1,3,5,7} = 39\%$ and $\varphi_{2,4,6,8} = 60\%$. The overall laminate's thickness is 2 mm, the laminae present following thicknesses: $t_{1,8} = 0.5$ mm; $t_{2,7} = 0.25$ mm and $t_{3,4,5,6} = 0.125$ mm. The aim is to compute the stresses in each lamina of the composite laminate knowing that this is subjected to a biaxial field of normal loads $n_{xx} = 165$ N/mm and $n_{yy} = 85$ N/mm. The fibers and matrix features are:

- $E_{F\parallel} = 527000$ MPa;
- $E_{F\perp} = 21500$ MPa;
- $\upsilon_F = 0.3$;
- $E_M = 3825$ MPa;
- $\upsilon_M = 0.37$.

The results are visualized in Table 2.19.

Table 2.19. Stresses in in each lamina of a [$(0)_8$] carbon fibers-reinforced composite laminate subjected to a biaxial field of normal loads. Results in (GPa)

	Plies 1, 3, 5, 7	**Plies 2, 4, 6, 8**
$\sigma_{\parallel}$	0.54	0.83
$\sigma_{\perp}$	0.27	0.44

Chapter 3

Contributions to the thermo-mechanical behavior of fibers-reinforced laminates subjected to temperature and humidity variations

3.1. Introduction

Personal simulations regarding thermo-mechanical behavior of various unidirectional fibers-reinforced laminae subjected to temperature and humidity variations have been published in 2006, 2008 and 2010 in different proceedings [50], [63] and [76]. Following composite laminae have been considered: [-45] and [45] glass/epoxy, [30] glass/epoxy and [55] carbon/epoxy. Process related loadings variations from curing to environment temperature as well as some percentage humidity variation of these composites have been taken into account to compute the coefficients of thermal and humidity expansions. Distributions of these coefficients as well as respective strains have been computed versus fibers volume fraction variation of each composite. Thermal conductivities on axial and transverse directions of various unidirectional carbon Fibers-reinforced resins with possible applications in heating radiant systems have been computed using the ESHCON software developed by Clyne and Withers [7]. Thermal response of a sandwich structure with thin nonwoven polyester mat as core and dissimilar skins is presented. Thermal expansion, coefficient of thermal expansion and the alpha feature have been also experimentally determined only for the structure's upper skin [50].

3.2. Scientific context

Both fibers and matrix material, present extreme different deformations at temperature and humidity variations. These variations can cause internal stresses in a laminate structure, both at micro and macro mechanical level. This paper takes only the macro mechanical internal stresses into account, stresses that appear, for example, at cooling from the curing temperature to the environment temperature of a laminate structure. These internal stresses, due to temperature variations, are very dangerous and can lead to the damage of the structure even in the absence of an external mechanical loading [33]. This fact is more striking in case of carbon fibers-reinforced composite structures, fibers that present extreme different coefficients of linear thermal expansion along and perpendicular to their direction. Exposing a composite laminate structure to humidity, inside of it appears an internal stress state caused by the matrix volume increase, due to its swelling. Glass and carbon fibers do not absorb humidity but aramid fibers are strongly influenced by it.

According to Schneider, the coefficients of linear thermal expansion along and perpendicular to fibers direction of a unidirectional fibers-reinforced lamina, are [34]:

$$\alpha_{II} = \alpha_{FII} + \frac{\alpha_M - \alpha_{FII}}{\frac{\varphi}{1-\varphi} \cdot \frac{E_{FII}}{E_M} + 1}, \tag{3.1}$$

$$\alpha_{\perp} = \alpha_M - (\alpha_M - \alpha_{F\perp}) \left[\frac{2\left(\upsilon_M^3 + \upsilon_M^2 - \upsilon_M - 1\right) \cdot 1{,}1\varphi}{1{,}1\varphi \cdot \left(2\upsilon_M^2 + \upsilon_M - 1\right) - \left(1 + \upsilon_M\right)} - \frac{\upsilon_M \cdot \frac{E_{F\perp}}{E_M}}{\frac{E_{F\perp}}{E_M} + \frac{(1 - 1{,}1\varphi)}{1{,}1\varphi}} \right], \tag{3.2}$$

where: $\alpha_{F\parallel}$ is the coefficient of linear thermal expansion for fiber in the longitudinal direction; $\alpha_{F\perp}$ is the coefficient of linear thermal expansion for fiber in

the radial direction; α_M represents the coefficient of linear thermal expansion for matrix; $E_{F\parallel}$ is the fiber longitudinal modulus; $E_{F\perp}$ represents the fiber radial modulus; E_M is the matrix Young's modulus; υ_M represents the matrix Poisson's ratio and φ is the fibers volume fraction. Equations (3.1), (3.2) show that these coefficients of linear thermal expansion can be calculated as a function of the properties of composite material components and fibers volume fraction. If the fibers are disposed at an angle θ with the x-axis direction, the coefficients of thermal expansion in the x and y directions can be determined using $\alpha_\parallel$ and $\alpha_\perp$ [36]:

$$\alpha_{xx} = \alpha_{II} \cos^2\theta + \alpha_\perp \sin^2\theta, \tag{3.3}$$

$$\alpha_{yy} = \alpha_{II} \sin^2\theta + \alpha_\perp \cos^2\theta, \tag{3.4}$$

$$\alpha_{xy} = (2\sin\theta\cos\theta)(\alpha_{II} - \alpha_\perp), \tag{3.5}$$

where α_{xx} and α_{yy} are coefficients of linear thermal expansion and α_{xy} is the coefficient of shear thermal expansion. According to Tsai and Hahn, in case of a unidirectional fibers-reinforced lamina, the coefficients of expansion due to the humidity can be computed from the following equations [78]:

$$\beta_{II} = \frac{\beta_M \cdot E_M}{\varphi \cdot E_{FII} + (1-\varphi)\cdot E_M} \cdot \frac{\rho_{composite}}{\rho_M}, \tag{3.6}$$

$$\beta_\perp = \frac{(1-\upsilon_M)\cdot \beta_M \cdot \rho_{composite}}{\rho_M} - \left[\varphi \cdot \upsilon_F + (1-\varphi)\cdot \upsilon_M\right]\cdot \beta_{II}, \tag{3.7}$$

where: $\beta_\parallel$ is the coefficient of expansion due to humidity, in longitudinal (0°) direction; $\beta_\perp$ represents the coefficient of expansion due to humidity, in transverse (90°) direction; β_M is the coefficient of expansion due to humidity, for matrix and $\rho_{composite}$ represents the composite material's density.

3.3. Simulations of thermo-mechanical behavior of fibers-reinforced laminates subjected to temperature and humidity variations

The coefficients of expansion in *x* and *y* directions, due to humidity, if the fibers are disposed at an angle θ with the *x*-axis direction, can be computed in the following way:

$$\beta_{xx} = \beta_{II} \cos^2 \theta + \beta_{\perp} \sin^2 \theta, \tag{3.8}$$

$$\beta_{yy} = \beta_{II} \sin^2 \theta + \beta_{\perp} \cos^2 \theta, \tag{3.9}$$

$$\beta_{xy} = (2 \sin\theta \cos\theta)(\beta_{II} - \beta_{\perp}), \tag{3.10}$$

where β_{xx} and β_{yy} are coefficients of linear expansion and β_{xy} is the coefficient of shear expansion due to humidity. The strains of a fibers-reinforced composite lamina $\varepsilon_{xx\ t\text{-}h}$, $\varepsilon_{yy\ t\text{-}h}$ and $\gamma_{xy\ t\text{-}h}$ due to a ΔT temperature and ΔH humidity variation, without a mechanical loading, can be computed in the following manner:

$$\varepsilon_{xx\ t-h} = \alpha_{xx} \cdot \Delta T + \beta_{xx} \cdot \Delta H, \tag{3.11}$$

$$\varepsilon_{yy\ t-h} = \alpha_{yy} \cdot \Delta T + \beta_{yy} \cdot \Delta H, \tag{3.12}$$

$$\gamma_{xy\ t-h} = \alpha_{xy} \cdot \Delta T + \beta_{xy} \cdot \Delta H, \tag{3.13}$$

where: $\varepsilon_{xx\ t\text{-}h}$ is the strain of lamina in *x*-axis direction, due to a combined loading of ΔT temperature and ΔH humidity variation; $\varepsilon_{yy\ t\text{-}h}$ represents the strain of lamina in *y*-axis direction due to a combined loading of ΔT temperature and ΔH humidity variation; $\gamma_{xy\ t\text{-}h}$ is the shear strain of lamina due to a combined loading of ΔT temperature and ΔH humidity variation. The index *t-h* denotes the combined action

of a temperature variation ΔT and a humidity variation ΔH. Some applications are presented in following sections.

Coefficients of thermal expansion in case of [30] glass/epoxy lamina

A unidirectional glass fibers-reinforced lamina with 30° fibers disposal angle in an epoxy matrix is considered. The fibers volume fraction is 60%. Coefficients of thermal expansions in x and y-axis directions have been computed. The distribution of these coefficients versus fibers volume fraction variation is presented in Fig. 3.1. Following input data regarding the fibers, matrix and composite material have been considered:

- $E_M = 3000$ MPa; $\upsilon_M = 0.35$; $\alpha_M = 65 \cdot 10^{-6}\ K^{-1}$; $\theta = 30°$;
- $E_{F\parallel} = E_{F\perp} = 73000$ MPa; $\alpha_{F\parallel} = \alpha_{F\perp} = 4.8 \cdot 10^{-6}\ K^{-1}$.

For 60% fibers volume fraction, the coefficients of thermal expansion along and transverse to the fibers direction can be computed with relations (3.1) – (3.2):

$$\alpha_{II} = \left(4.8\cdot10^{-6}\right) + \frac{\left(65\cdot10^{-6}\right)-\left(4.8\cdot10^{-6}\right)}{\frac{0.6}{(1-0.6)}\cdot\frac{(73000)}{(3000)}+1} = 6.4\cdot10^{-6}\,K^{-1},$$

$$\alpha_{\perp} = \left(65\cdot10^{-6}\right) - \left[\left(65\cdot10^{-6}\right)-\left(4.8\cdot10^{-6}\right)\right]\cdot$$

$$\cdot\left\{\frac{2\left(0.35^3+0.35^2-0.35-1\right)\cdot1.1\cdot0.6}{1.1\cdot0.6\cdot\left(2\cdot0.35^2+0.35-1\right)-(1+0.35)} - \frac{0.35\cdot\frac{73000}{3000}}{\frac{73000}{3000}+\frac{(1-1.1\cdot0.6)}{1.1\cdot0.6}}\right\} = 27\cdot10^{-6}\,K^{-1}.$$

According to equations (3.3) – (3.5), the coefficients of thermal expansions on x and y-axis directions can be determined in the following way:

$$\alpha_{xx} = \left(6.4 \cdot 10^{-6}\right) \cdot \cos^2 30° + \left(27 \cdot 10^{-6}\right) \cdot \sin^2 30° = 11.5 \cdot 10^{-6} K^{-1},$$

$$\alpha_{yy} = \left(6.4 \cdot 10^{-6}\right) \cdot \sin^2 30° + \left(27 \cdot 10^{-6}\right) \cdot \cos^2 30° = 21.8 \cdot 10^{-6} K^{-1},$$

$$\alpha_{xy} = (2 \cdot \sin 30° \cdot \cos 30°) \cdot \left[\left(64 \cdot 10^{-6}\right) - \left(27 \cdot 10^{-6}\right)\right] = -17.8 \cdot 10^{-6} K^{-1}.$$

The variation of coefficients of thermal expansion $\alpha_{\parallel}$, $\alpha_{\perp}$, α_{xx}, α_{yy} and α_{xy} versus fibers volume fraction is presented in Fig. 3.1.

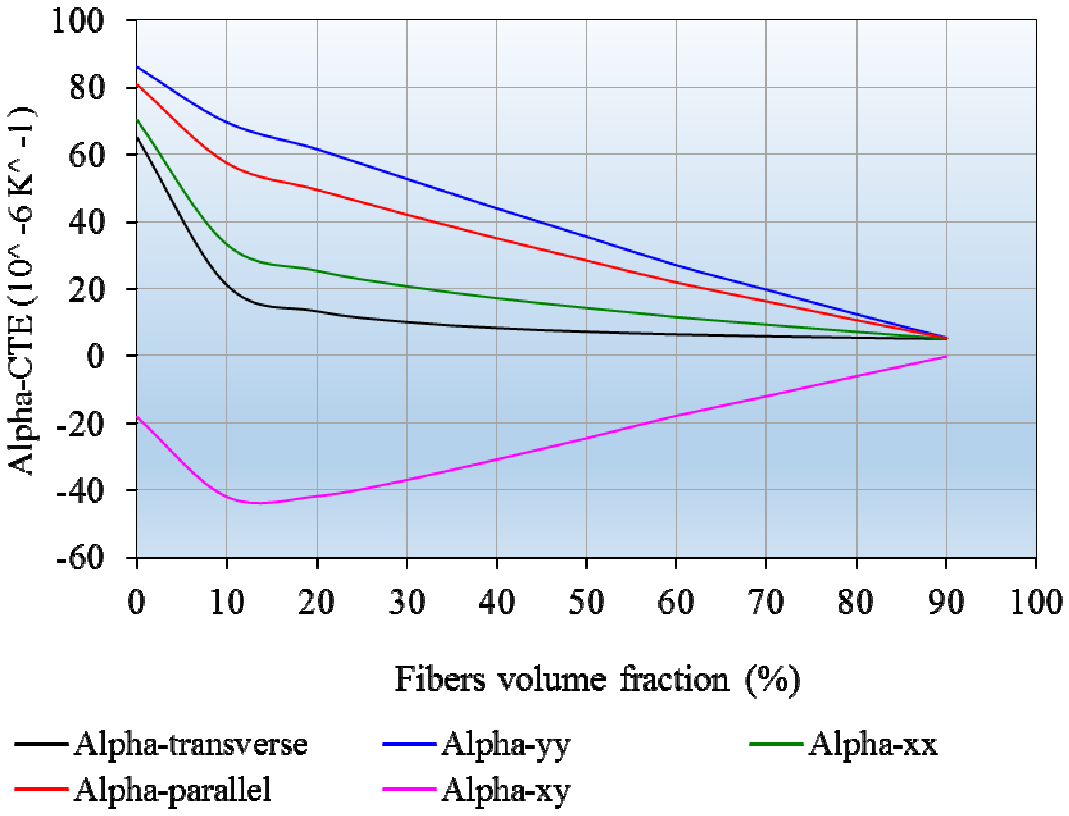

Fig. 3.1. Coefficients of thermal expansion in case of a unidirectional [30] glass/epoxy lamina

Coefficients of humidity expansion in case of [30] glass/epoxy lamina

A unidirectional glass fibers-reinforced lamina with 30° fibers disposal angle in an epoxy matrix is considered. The fibers volume fraction is 60%. Coefficients of humidity expansions in x and y-axis directions have been computed. The distribution of these coefficients versus fibers volume fraction variation is presented in Fig. 3.2. Following input data regarding the fibers, matrix and composite material have been considered:

- $\rho_{composite} = 1950$ kg/m^3;
- $\rho_M = 1200$ kg/m^3;
- $E_M = 3000$ MPa; $\upsilon_M = 0.35$; $\beta_M = 0.18$; $\upsilon_F = 0.25$;
- $E_{F\parallel} = 73000$ MPa; $\theta = 30°$.

According to equations (3.6) – (3.7), the coefficients of humidity expansion along and transverse to the fibers direction can be determined in the following way:

$$\beta_{II} = \frac{0.18 \cdot 3000}{0.6 \cdot 73000 + (1-0.6) \cdot 3000} \cdot \frac{1.95}{1.2} = 0.0195,$$

$$\beta_{\perp} = \frac{(1-0.35) \cdot 0.18 \cdot 1.95}{1.2} - [0.6 \cdot 0.25 + (1-0.6) \cdot 0.35] \cdot 0.0195 = 0.1844.$$

According to equations (3.8) – (3.10), the coefficients of humidity expansions on x and y-axis directions can be computed in the following way:

$$\beta_{xx} = 0.0195 \cdot \cos^2 30° + 0.1844 \cdot \sin^2 30° = 0.0607,$$

$$\beta_{yy} = 0.0195 \cdot \sin^2 30° + 0.1844 \cdot \cos^2 30° = 0.1431,$$

$$\beta_{xy} = (2\sin 30° \cdot \cos 30°) \cdot (0.0195 - 0.1844) = -0.1428.$$

The distribution of coefficients of humidity expansion $\beta_{\parallel}$, $\beta_{\perp}$, β_{xx}, β_{yy} and β_{xy} is visualized in Fig. 3.2.

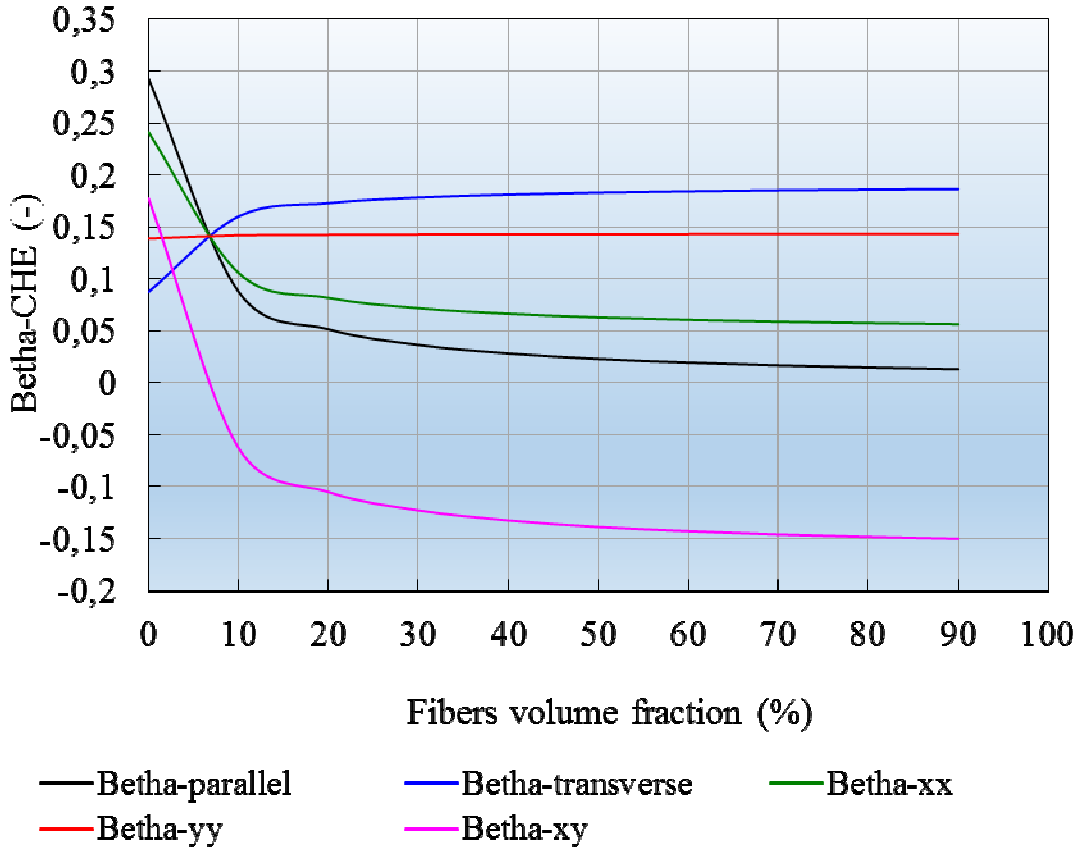

Fig. 3.2. Coefficients of humidity expansion in case of a unidirectional [30] glass/epoxy lamina

Application in case of [-45] glass/epoxy lamina subjected to a ΔT = - 100 K temperature variation

A unidirectional glass fibers-reinforced lamina with – 45° fibers disposal angle in an epoxy matrix is considered. The fibers volume fraction is 60%. In case in which the lamina is subjected only to a ΔT = - 100 K temperature variation due to its cooling from cure to environment temperature, the $\varepsilon_{xx\,t}$, $\varepsilon_{yy\,t}$ and $\gamma_{xy\,t}$ strains in

x and y-axis directions have been computed. In Fig. 3.3, a schematic representation of these strains acting on [-45] glass/epoxy lamina is shown.

Following input data regarding the fibers and matrix material have been considered:

- $E_M = 3500$ MPa;
- $\upsilon_M = 0.35$;
- $\alpha_M = 65 \cdot 10^{-6}\ K^{-1}$;
- $\theta = -45°$;
- $E_{F\parallel} = E_{F\perp} = 73000$ MPa;
- $\alpha_{F\parallel} = \alpha_{F\perp} = 4.8 \cdot 10^{-6}\ K^{-1}$.

For 60% fibers volume fraction, the coefficients of thermal expansion along and transverse to the fibers direction can be computed with relations (3.1) – (3.2):

$$\alpha_{II} = \left(4.8\cdot10^{-6}\right) + \frac{\left(65\cdot10^{-6}\right)-\left(4.8\cdot10^{-6}\right)}{\frac{0.6}{(1-0.6)}\cdot\frac{(73000)}{(3500)}+1} = 6.66\cdot10^{-6}\,K^{-1},$$

$$\alpha_{\perp} = \left(65\cdot10^{-6}\right) - \left[\left(65\cdot10^{-6}\right)\cdot\left(4.8\cdot10^{-6}\right)\right]\cdot$$

$$\cdot\left\{\frac{2\left(0.,35^3+0.35^2-0.35-1\right)\cdot1.1\cdot0.6}{1.1\cdot0.6\cdot\left(2\cdot0.35^2+0.35-1\right)-(1+0.35)} - \frac{0.35\cdot\frac{73000}{3500}}{\frac{73000}{3500}+\frac{(1-1.1\cdot0.6)}{1.1\cdot0.6}}\right\} = 27.35\cdot10^{-6}\,K^{-1}.$$

According to equations (3.3) – (3.5), the coefficients of thermal expansions on x and y-axis directions can be determined as following:

$$\alpha_{xx} = \left(6.66\cdot10^{-6}\right)\cdot\cos^2(-45°) + \left(27.35\cdot10^{-6}\right)\cdot\sin^2(-45°) = 17\cdot10^{-6}\,K^{-1},$$

$$\alpha_{yy} = \left(6.66\cdot10^{-6}\right)\cdot\sin^2(-45°) + \left(27.35\cdot10^{-6}\right)\cdot\cos^2(-45°) = 17\cdot10^{-6}\,K^{-1},$$

$$\alpha_{xy} = [2 \cdot \sin(-45°) \cdot \cos(-45°)] \cdot \left[\left(6.66 \cdot 10^{-6} \right) - \left(27.35 \cdot 10^{-6} \right) \right] = 20.69 \cdot 10^{-6} K^{-1}.$$

The strains $\varepsilon_{xx\,t}$, $\varepsilon_{yy\,t}$ and $\gamma_{xy\,t}$ on x and y-axis directions in case of this lamina subjected only to a ΔT temperature variation can be determined using the relations (3.11) – (3.13):

$$\varepsilon_{xx\,t} = \alpha_{xx} \cdot \Delta T = \left(17 \cdot 10^{-6} \right) \cdot (-100) = -17 \cdot 10^{-4},$$

$$\varepsilon_{yy\,t} = \alpha_{yy} \cdot \Delta T = \left(17 \cdot 10^{-6} \right) \cdot (-100) = -17 \cdot 10^{-4},$$

$$\gamma_{xy\,t} = \alpha_{xy} \cdot \Delta T = \left(20.69 \cdot 10^{-6} \right) \cdot (-100) = -20.69 \cdot 10^{-4}.$$

In Fig. 3.3, the specific shrinkages of a [-45] glass/epoxy lamina subjected to a variation temperature of $\Delta T = -100\ K$ from curing to environment temperature.

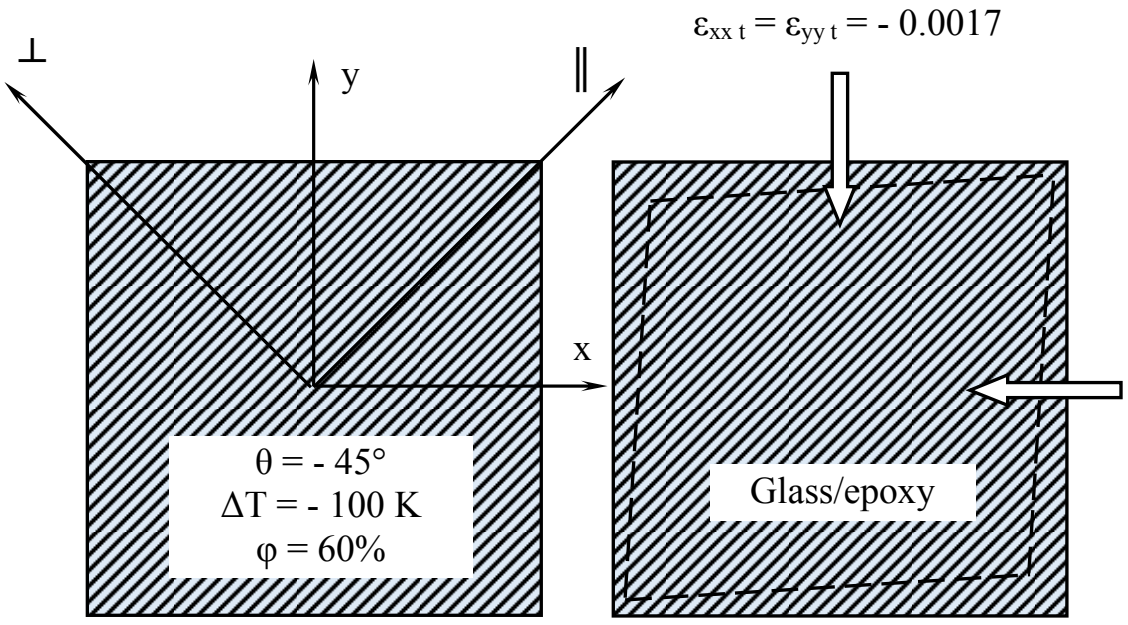

Fig. 3.3. Specific shrinkages of [-45] glass/epoxy lamina from curing to environment temperature

Application in case of [45] glass/epoxy lamina subjected to ΔU = 1% humidity variation

A unidirectional glass fibers-reinforced lamina with 45° fibers disposal angle in an epoxy matrix is considered. The fibers volume fraction is 40%. In case in which the lamina is subjected only to ΔU = 1% humidity variation, the $\varepsilon_{xx\,h}$, $\varepsilon_{yy\,h}$ and $\gamma_{xy\,h}$ strains in x and y-axis directions have been computed.

In Fig. 3.4, a schematic representation of these strains acting on a [45] glass/epoxy lamina subjected to ΔU = 1% humidity variation can be visualized. Following input data regarding the fibers, matrix and composite material have been considered:

- $\rho_{composite} = 1900$ kg/m^3;
- $\rho_M = 1100$ kg/m^3;
- $E_M = 3450$ MPa;
- $\upsilon_M = 0.35$;
- $\beta_M = 0.18$;
- $\upsilon_F = 0.25$;
- $E_{F\parallel} = 73000$ MPa;
- $\theta = 45°$.

The coefficients of expansion due to humidity along and transverse to the fibers direction can be computed according to the relations (3.6) – (3.7):

$$\beta_{II} = \frac{0.18 \cdot 3450}{0.4 \cdot 73000 + (1-0.4) \cdot 3450} \cdot \frac{1900}{1100} = 0.0343,$$

$$\beta_{\perp} = \frac{(1-0.35) \cdot 0.18 \cdot 1900}{1100} - [0.4 \cdot 0.25 + (1-0.4) \cdot 0.35] \cdot 0.0343 = 0.1914.$$

The coefficients of expansion due to humidity on x and y-axis directions have been determined according to equations (3.8) – (3.10):

$$\beta_{xx} = 0.0343 \cdot \cos^2 45° + 0.1914 \cdot \sin^2 45° = 0.1128 ,$$

$$\beta_{yy} = 0.0343 \cdot \sin^2 45° + 0.1914 \cdot \cos^2 45° = 0.1128 ,$$

$$\beta_{xy} = (2 \sin 45° \cdot \cos 45°) \cdot (0.0343 - 0.1914) = -0.0785.$$

The strains $\varepsilon_{xx\,h}$, $\varepsilon_{yy\,h}$ and $\gamma_{xy\,h}$ on x respective y-axis directions in case of this kind of lamina subjected only to $\Delta U = 1\%$ humidity variation have been computed using the relations (3.11) – (3.13):

$$\varepsilon_{xx\,h} = \beta_{xx} \cdot \Delta U = (0.1128) \cdot (0.01) = 11.28 \cdot 10^{-4},$$

$$\varepsilon_{yy\,h} = \beta_{yy} \cdot \Delta U = (0.1128) \cdot (0.01) = 11.28 \cdot 10^{-4},$$

$$\gamma_{xy\,h} = \beta_{xy} \cdot \Delta U = (-0.0785) \cdot (0.01) = -7.85 \cdot 10^{-4}.$$

The strains of a [45] epoxy/glass fibers unidirectional reinforced lamina subjected to a humidity variation of 1% are presented in Fig. 3.4.

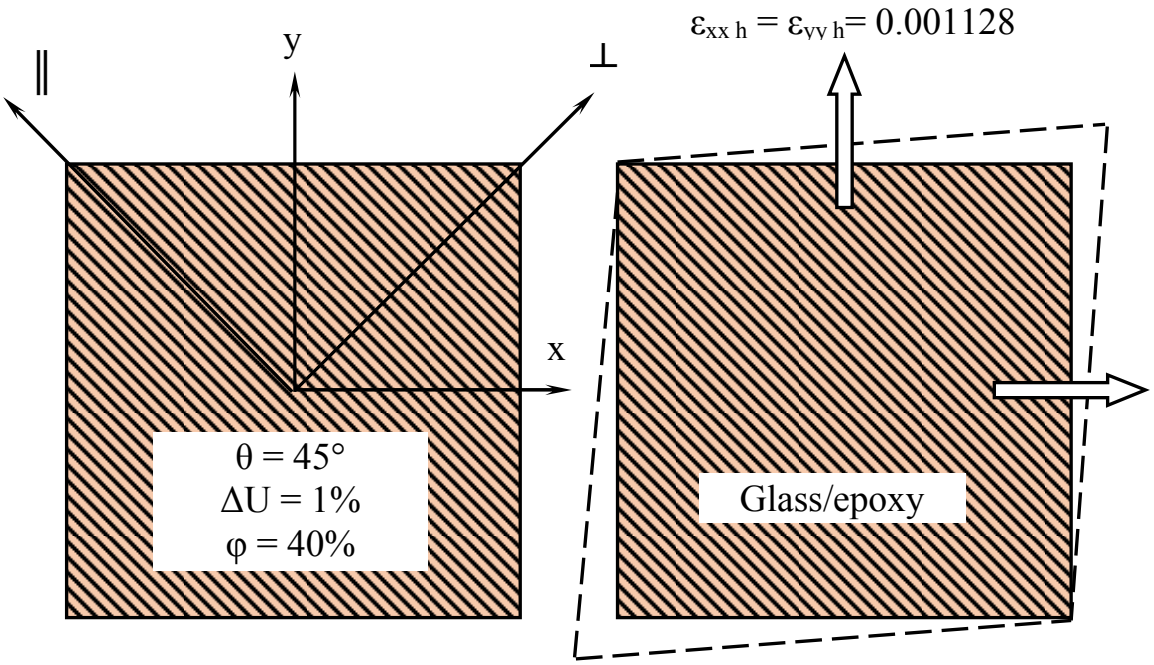

Fig. 3.4. Strains of a [45] glass/epoxy lamina subjected to ΔU = 1% humidity variation

Application in case of [55] carbon/epoxy lamina subjected to a ΔT = - 40 K temperature and ΔU = 1.5% humidity variation

A unidirectional carbon fibers-reinforced lamina with 55° fibers disposal angle in an epoxy matrix is considered. The fibers volume fraction is 60%. In case in which the lamina is subjected to a combined loading of ΔT = - 40 K temperature variation due to its cooling from cure to environment temperature and ΔU = 1.5% humidity variation, the $\varepsilon_{xx\ t\text{-}h}$, $\varepsilon_{yy\ t\text{-}h}$ and $\gamma_{xy\ t\text{-}h}$ strains in x and y-axis directions have been computed.

Following input data regarding the fibers, matrix and composite material have been considered:

- $E_M = 3.9$ GPa;
- $\upsilon_M = 0.35$;
- $\alpha_M = 65 \cdot 10^{-6}\ K^{-1}$;
- $\theta = 55°$;

- $\varphi = 60\%$;
- $E_{F\parallel} = 540$ GPa;
- $E_{F\perp} = 27$ GPa;
- $\alpha_{F\parallel} = -0.5 \cdot 10^{-6}\ K^{-1}$;
- $\upsilon_F = 0.2$;
- $\alpha_{F\perp} = 30 \cdot 10^{-6}\ K^{-1}$;
- $\rho_{composite} = 2100\ kg/m^3$;
- $\rho_M = 1250\ kg/m^3$;
- $\beta_M = 0.18$.

First I have computed the coefficients of thermal expansion along and transverse to the fibers direction:

$$\alpha_{II} = \left(-0.5\cdot 10^{-6}\right) + \frac{\left(65\cdot 10^{-6}\right) - \left(-0.5\cdot 10^{-6}\right)}{\frac{0.6}{(1-0.6)}\cdot\frac{(540)}{(3.9)}+1} = -0.18\cdot 10^{-6}K^{-1},$$

$$\alpha_{\perp} = \left(65\cdot 10^{-6}\right) - \left[\left(65\cdot 10^{-6}\right)\cdot\left(30\cdot 10^{-6}\right)\right]\cdot$$

$$\cdot\left\{\frac{2\left(0.35^3+0.35^2-0.35-1\right)\cdot 1.1\cdot 0.6}{1.1\cdot 0.6\cdot\left(2\cdot 0.35^2+0.35-1\right)-(1+0.35)} - \frac{0.35\cdot\frac{27}{3.9}}{\frac{27}{3.9}+\frac{(1-1.1\cdot 0.6)}{1.1\cdot 0.6}}\right\} = 45.76\cdot 10^{-6}K^{-1},$$

The coefficients of thermal expansions on x and y-axis directions will be:

$$\alpha_{xx} = \left(-0.18\cdot 10^{-6}\right)\cdot\cos^2 55° + \left(45.76\cdot 10^{-6}\right)\cdot\sin^2 55° = 30.64\cdot 10^{-6}K^{-1},$$

$$\alpha_{yy} = \left(-0.18\cdot 10^{-6}\right)\cdot\sin^2 55° + \left(45.76\cdot 10^{-6}\right)\cdot\cos^2 55° = 14.93\cdot 10^{-6}K^{-1},$$

$$\alpha_{xy} = (2\cdot\sin 55°\cdot\cos 55°)\cdot\left[\left(-0.18\cdot 10^{-6}\right) - \left(45.76\cdot 10^{-6}\right)\right] = -43.16\cdot 10^{-6}K^{-1}.$$

Second, I have determined the coefficients of expansion due to humidity along and transverse to the fibers direction:

$$\beta_{II} = \frac{0.18 \cdot 3.9}{0.6 \cdot 540 + (1-0.6) \cdot 3.9} \cdot \frac{2.1}{1.25} = 0.0036,$$

$$\beta_{\perp} = \frac{(1-0.35) \cdot 0.18 \cdot 2.1}{1.25} - [0.6 \cdot 0.2 + (1-0.6) \cdot 0.35] \cdot 0.0036 = 0.1956,$$

Then I have computed the coefficients of expansion due to humidity on x and y-axis directions:

$$\beta_{xx} = 0.0036 \cdot \cos^2 55° + 0.1956 \cdot \sin^2 55° = 0.1324,$$

$$\beta_{yy} = 0.0036 \cdot \sin^2 55° + 0.1956 \cdot \cos^2 55° = 0.0667,$$

$$\beta_{xy} = (2 \cdot \sin 55° \cdot \cos 55°) \cdot (0.0036 - 0.1956) = -0.1804.$$

Third, I have determined the strains $\varepsilon_{xx\ t\text{-}h}$, $\varepsilon_{yy\ t\text{-}h}$ on x respective y-axis directions due to the combined action of temperature and humidity variation:

$$\varepsilon_{xx\,t-h} = \alpha_{xx} \cdot \Delta T + \beta_{xx} \cdot \Delta U = \left(30 \cdot 10^{-6}\right) \cdot (-40) + (0.1324) \cdot (0.015) = 7.86 \cdot 10^{-4},$$

$$\varepsilon_{yy\,t-h} = \alpha_{yy} \cdot \Delta T + \beta_{yy} \cdot \Delta U = \left(14.93 \cdot 10^{-6}\right) \cdot (-40) + (0.0667) \cdot (0.015) = 4.03 \cdot 10^{-4},$$

$$\gamma_{xy\,t-h} = \alpha_{xy} \cdot \Delta T + \beta_{xy} \cdot \Delta U = \left(-43.16 \cdot 10^{-6}\right) \cdot (-40) + (-0.1804) \cdot (0.015) = -9.79 \cdot 10^{-4}.$$

In Fig. 3.5, a schematic representation of these strains acting on a [55] carbon/epoxy lamina subjected to a combined loading of ΔT = - 40 K temperature and ΔU = 1.5% humidity variation is presented.

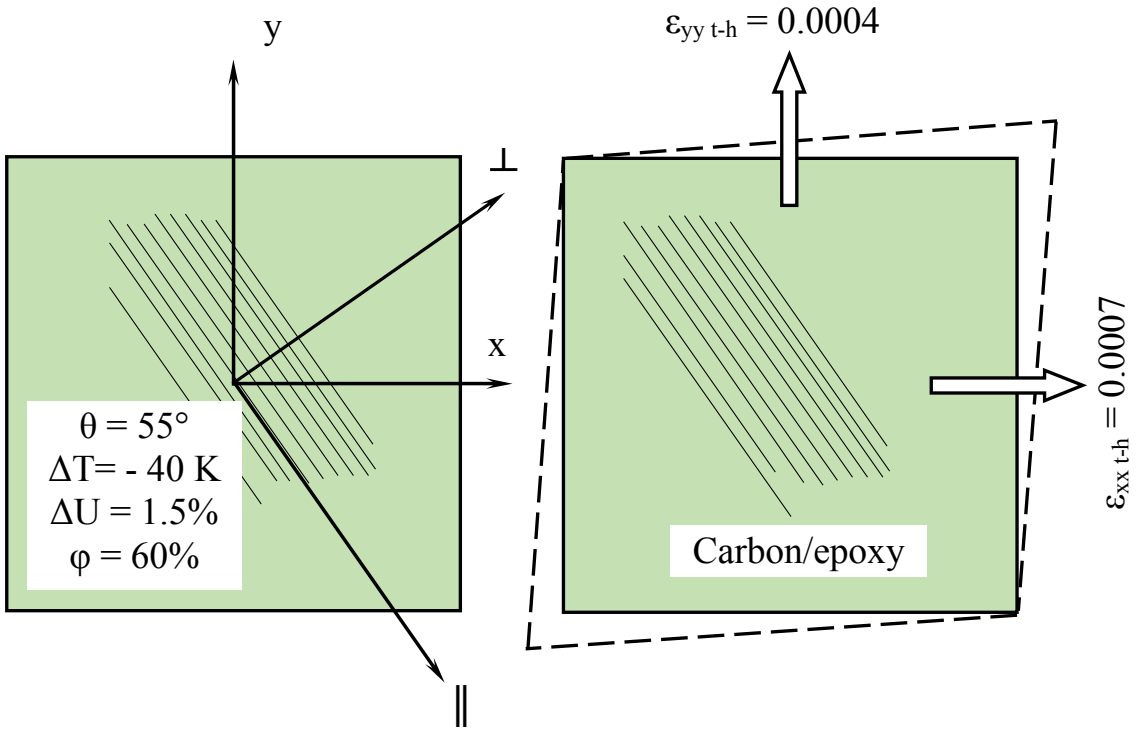

Fig. 3.5. Strains of a [55] carbon/epoxy lamina subjected to a combined loading of ΔT = - 40 K temperature and ΔU = 1.5% humidity variation

Application in case of a unidirectional [α] glass fibers-reinforced lamina subjected to a temperature variation of ΔT = - 35 K

A unidirectional [α] glass fibers-reinforced lamina with the fibers disposal angle α against x-axis direction is considered. This lamina presents 39% fibers volume fraction and is subjected only due to a temperature variation of ΔT = - 35 K that appears due to its cooling from the cure to the environment temperature. The aim is to compute the strains $\varepsilon_{xx\ t}$, $\varepsilon_{yy\ t}$ and $\gamma_{xy\ t}$ with respect to the fibers disposal angle α = 15°, 30°, 45°, 60°, 75° and 90°. Following input date have been used:

- $\alpha_{F\parallel} = \alpha_{F\perp} = 4.8 \cdot 10^{-6}\ K^{-1}$;

- $\alpha_M = 65 \cdot 10^{-6}\ K^{-1}$
- $E_{F\parallel} = E_{F\perp} = 73000$ MPa;
- $E_M = 4120$ MPa;
- $\upsilon_M = 0.38$.

The results are presented in Table 3.1.

Table 3.1. Strains in a unidirectional [α] glass fibers-reinforced lamina subjected only due to a temperature variation of ΔT = - 35 K. Results multiplied with 10^{-6}

	15°	30°	45°	60°	75°	90°
$\varepsilon_{xx\ t}$	- 410.9	- 607.9	- 877.4	- 1146.6	- 1343.6	- 1416.1
$\varepsilon_{yy\ t}$	- 1343.6	- 1146.6	- 877.4	- 607.9	- 410.9	- 338.8
$\gamma_{xy\ t}$	538.6	932.7	1077.3	932.7	538.6	0

Application in case of a unidirectional [α] carbon fibers-reinforced lamina subjected to a humidity variation of ΔU = 3.5%

A unidirectional [α] carbon fibers-reinforced lamina with the fibers disposal angle α against x-axis direction is considered. This lamina presents 62% fibers volume fraction and is subjected only due to a humidity variation of ΔU = 3.5%. The aim is to compute the strains $\varepsilon_{xx\ h}$, $\varepsilon_{yy\ h}$ and $\gamma_{xy\ h}$ with respect to the fibers disposal angle α = 15°, 30°, 45°, 60°, 75° and 90°. Following input date have been used:

- $\rho_{composite} = 1450\ kg/m^3$;
- $\rho_M = 1150\ kg/m^3$;
- $E_M = 4120$ MPa;
- $\upsilon_M = 0.35$;
- $\beta_M = 0.18$;

- $\upsilon_F = 0.3$;
- $E_{F\parallel} = 537000$ MPa.

The results are shown in Table 3.2.

Table 3.2. Strains in a unidirectional [α] carbon fibers-reinforced lamina subjected only due to a humidity variation of ΔU = 3.5%.

	15°	30°	45°	60°	75°	90°
$\varepsilon_{xx\ h}$	0.00042	0.0013	0.0025	0.0038	0.0047	0.0051
$\varepsilon_{yy\ h}$	0.0047	0.0038	0.0025	0.0013	0.00042	0.00009
$\gamma_{xy\ h}$	- 0.0024	- 0.0043	- 0.005	- 0.0043	- 0.0024	0

Application in case of a symmetric [0/90/45/-45]$_S$ carbon fibers-reinforced laminate subjected to complex loadings

A symmetric $[0/90/45/-45]_S$ carbon fibers-reinforced composite laminate is considered. The fibers volume fraction of each lamina is 57% and the thickness of each lamina is 0.25 mm. The aim is to compute the strains in each lamina knowing that the laminate is subjected to:

- A temperature variation of $\Delta T = -100$ K that appears due to its cooling from the cure to environment temperature;
- A humidity variation of $\Delta U = 2.3\%$;
- A biaxial field of normal loads $n_{xx} = 215$ N/mm and $n_{yy} = 185$ N/mm as well as a shear load $n_{xy} = 75$ N/mm that acts in x-y plane.

Following input date have been used:

- $\alpha_{F\parallel} = -0.45 \cdot 10^{-6}\ K^{-1}$;
- $\alpha_{F\perp} = 29 \cdot 10^{-6}\ K^{-1}$;
- $\alpha_M = 65 \cdot 10^{-6}\ K^{-1}$;
- $\rho_{composite} = 1700\ kg/m^3$;

- $\rho_M = 1100$ kg/m^3;
- $\beta_M = 0.18$
- $E_{F\parallel} = 528$ GPa;
- $E_{F\perp} = 21$ GPa;
- $\upsilon_F = 0.3$;
- $E_M = 3.84$ GPa;
- $\upsilon_M = 0.37$.

The results are presented in Table 3.3.

Table 3.3. Stresses and strains in a symmetric $[0/90/45/-45]_S$ carbon fibers-reinforced composite laminate subjected to complex loadings. Stresses are given in GPa.

	Plies 1 and 8	**Plies 2 and 7**	**Plies 3 and 6**	**Plies 4 and 5**
$\varepsilon_\parallel$	0.036184	0.028602	0.012785	0.052
$\varepsilon_\perp$	0.028602	0.036184	0.052	0.012785
$\gamma_{\parallel\perp}$	0.039216	- 0.039216	0.007582	- 0.007582
$\sigma_\parallel$	11.11	8.83	4.09	15.85
$\sigma_\perp$	0.49	0.55	0.68	0.36
$\tau_{\parallel\perp}$	0.22	- 0.22	0.043	- 0.043

Conclusions

At 10% fibers volume fraction, the coefficients of thermal expansion in x and y-axis directions in case of a unidirectional [30] glass/epoxy lamina present the widest range of values. With the increase of fibers volume fraction, these coefficients present closer values (Fig. 3.1). In case of a unidirectional glass fibers-reinforced lamina with 30° fibers disposal angle in an epoxy matrix, the distributions of coefficients of humidity expansion in x and y-axis directions

present very small variations at fibers volume fractions greater than 20% (Fig. 3.2). This phenomenon is due to outstanding stability at humidity variations of glass fibers.

Subjecting a unidirectional [-45] glass/epoxy lamina (60% fibers volume fraction) only to a $\Delta T = -100$ K temperature variation due to its cooling process from cure to environment temperature, the specific shrinkages exhibit the same values in x and y-axis directions (Fig. 3.3).

The unidirectional glass fibers-reinforced lamina with 45° fibers disposal angle in an epoxy matrix subjected only to a $\Delta U = 1\%$ humidity variation shows equal strains in lamina's x and y-axis directions (Fig. 3.4). Both strains presented in Figs. 3 and 4 present equal values in x and y-axis directions due to the fact that both the trigonometric functions at 45° and – 45°, given in equations (3.3) to (3.5) and (3.8) to (3.10), present equal values. In case of a unidirectional [55] carbon/epoxy lamina subjected to a combined loading of $\Delta T = -40$ K temperature variation due to its cooling process from cure to environment temperature and $\Delta U = 1.5\%$ humidity variation, the strains exhibit different values mainly due to strong anisotropy of carbon fibers that present extreme different coefficients of linear thermal expansion along and transverse to their direction (Fig. 3.5). The different values of trigonometric functions at 55° fibers disposal angle play also a significant role.

3.4. Simulations of axial and transverse thermal conductivity of unidirectional carbon fibers-reinforced laminates

Simulations of axial and transverse thermal conductivity of various unidirectional carbon fibers-reinforced laminates with potential applications in heating radiant systems have been carried out using the ESHCON software developed by Clyne and Withers [7]. Twelve composite laminates have been taken into consideration in these simulations due to their thermal and electrical properties:

- Matrix : Polyurethane resin type RE-12551 ; Fibers : carbon type T300/PAN 1373K ;
- Matrix : Polyurethane resin type RE-12551 ; Fibers : carbon type T300/PAN 2673K ;
- Matrix : Polyurethane resin type RE-12551 ; Fibers : carbon type P55/PITCH 1373K ;
- Matrix : Polyurethane resin type RE-12551 ; Fibers : carbon type P55/PITCH 2673K ;
- Matrix : Pitch-matrix 1373K ; Fibers : T300/PAN 1373K ;
- Matrix : Pitch-matrix 1373K ; Fibers : T300/PAN 2673K ;
- Matrix : Pitch-matrix 1373K ; Fibers : P55/PITCH 1373K ;
- Matrix : Pitch-matrix 1373K ; Fibers : P55/PITCH 2673K ;
- Matrix : Pitch-matrix 2673K ; Fibers : T300/PAN 1373K ;
- Matrix : Pitch-matrix 2673K ; Fibers : T300/PAN 2673K ;
- Matrix : Pitch-matrix 2673K ; Fibers : P55/PITCH 1373K ;
- Matrix : Pitch-matrix 2673K ; Fibers : P55/PITCH 2673K.

Following input data have been used:

- Fibers volume fraction: 50%;
- Fibers aspect ratio: 10•E+5;

- Thermal conductivity of the non-reinforced matrix type RE-12551: 0.73 $Wm^{-1}K^{-1}$;
- Thermal conductivity of the non-reinforced Pitch-matrix type 1373K: 6.2 $Wm^{-1}K^{-1}$;
- Thermal conductivity of the non-reinforced Pitch-matrix type 2673K: 257 $Wm^{-1}K^{-1}$;
- Thermal conductivity of the reinforcement type T300/PAN 1373K: 8.5 $Wm^{-1}K^{-1}$;
- Thermal conductivity of the reinforcement type T300/PAN 2673K: 76 $Wm^{-1}K^{-1}$;
- Thermal conductivity of the reinforcement type P55/PITCH 1373K: 113 $Wm^{-1}K^{-1}$;
- Thermal conductivity of the reinforcement type P55/PITCH 2673K: 196 $Wm^{-1}K^{-1}$.

Thermal conductivity distributions versus fibers volume fraction has been determined both in axial and transverse direction of the composite laminate. The results are presented in Figs. 3.6 – 3.11.

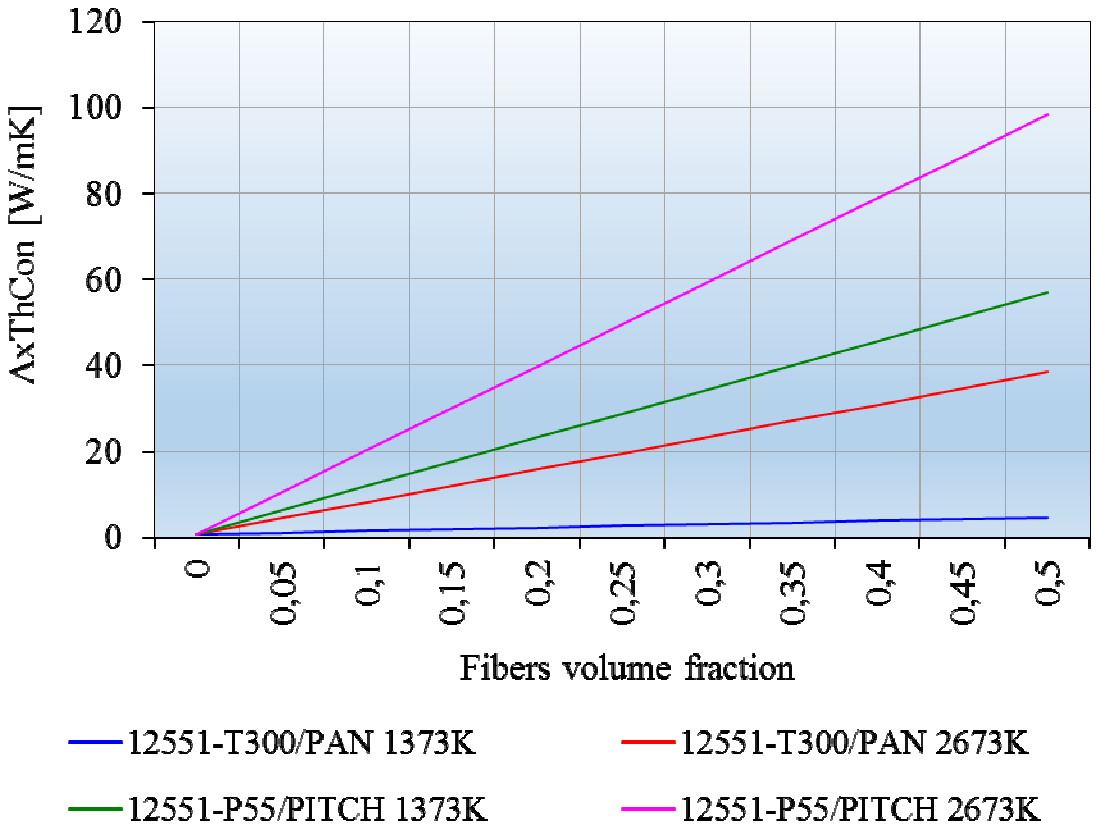

Fig. 3.6. Thermal conductivities on axial direction of various carbon fibers-reinforced polyurethane resin

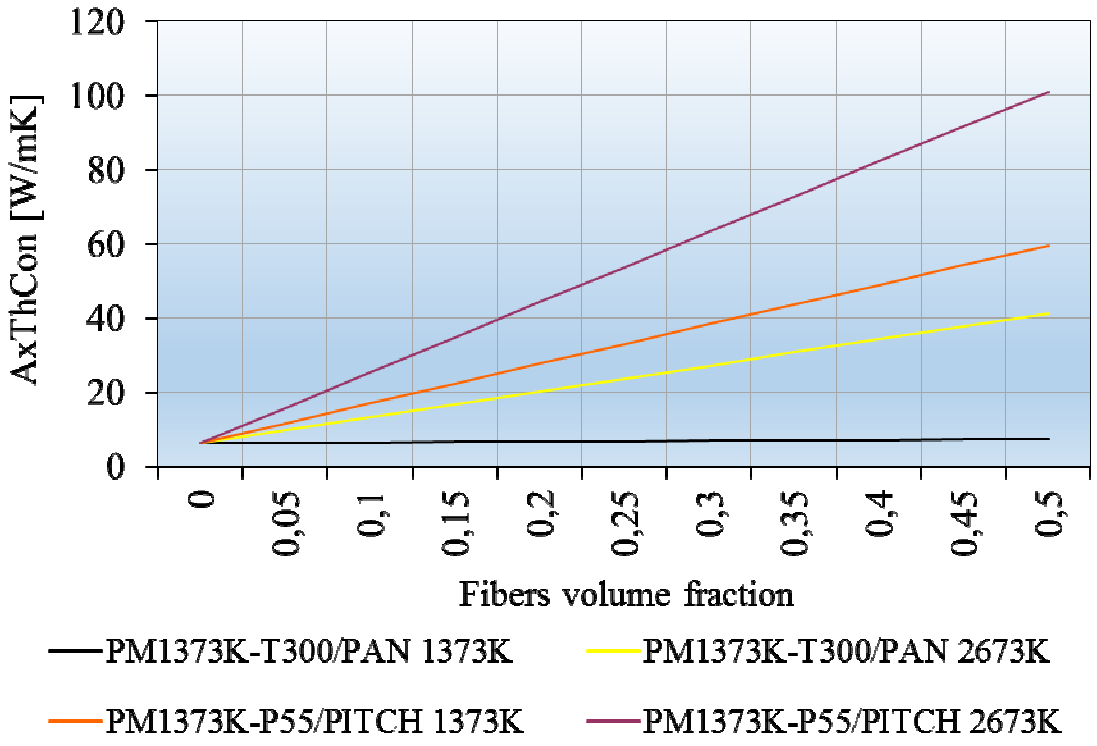

Fig. 3.7. Thermal conductivities on axial direction of various carbon fibers-reinforced PM1373K resin

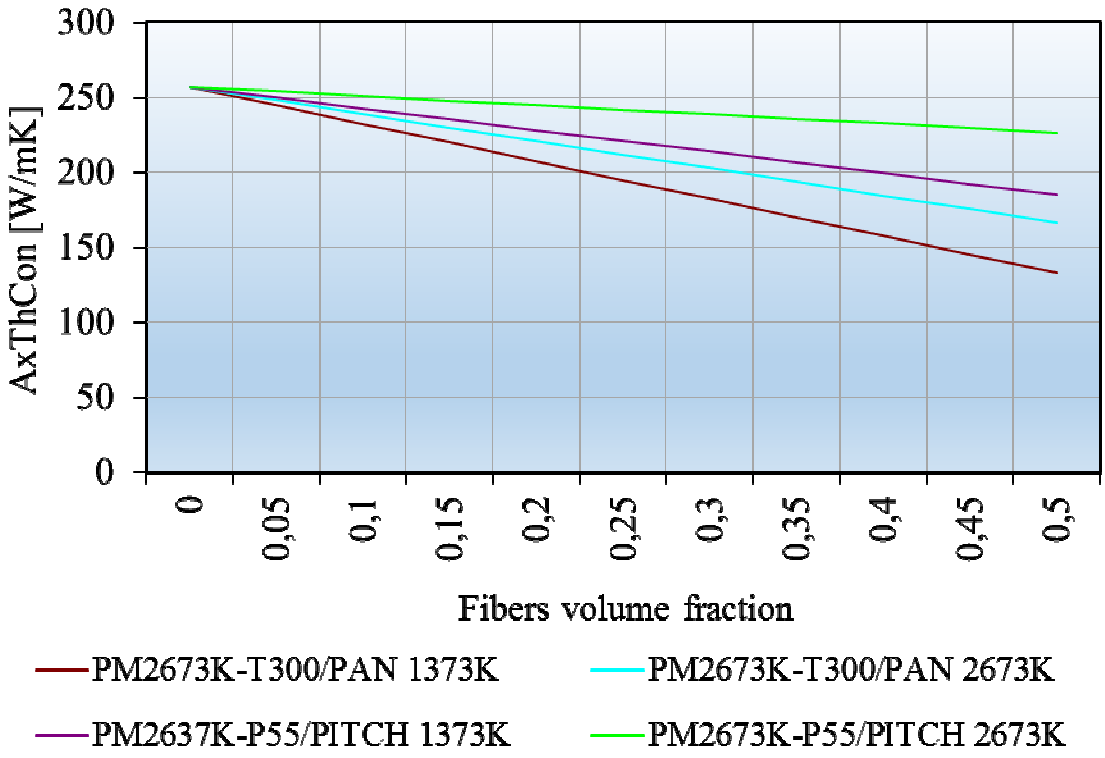

Fig. 3.8. Thermal conductivities on axial direction of various carbon fibers-reinforced Pitch-matrix type PM2673K resin

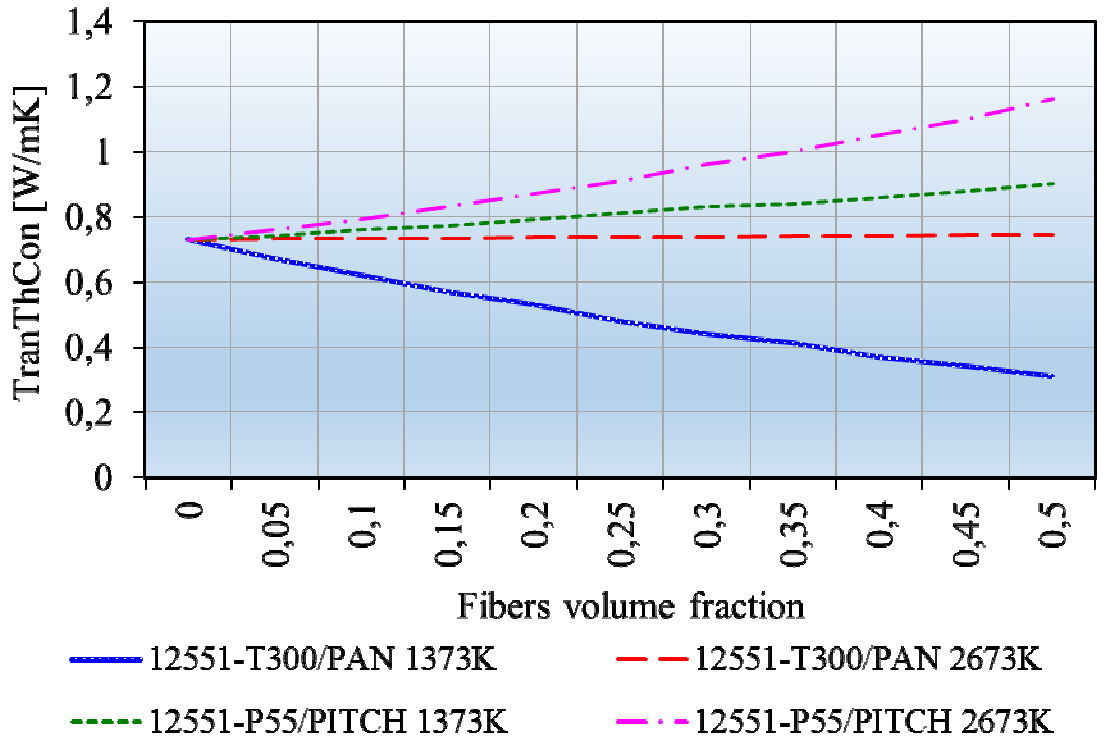

Fig. 3.9. Thermal conductivities on transverse direction of various carbon fibers-reinforced polyurethane resin

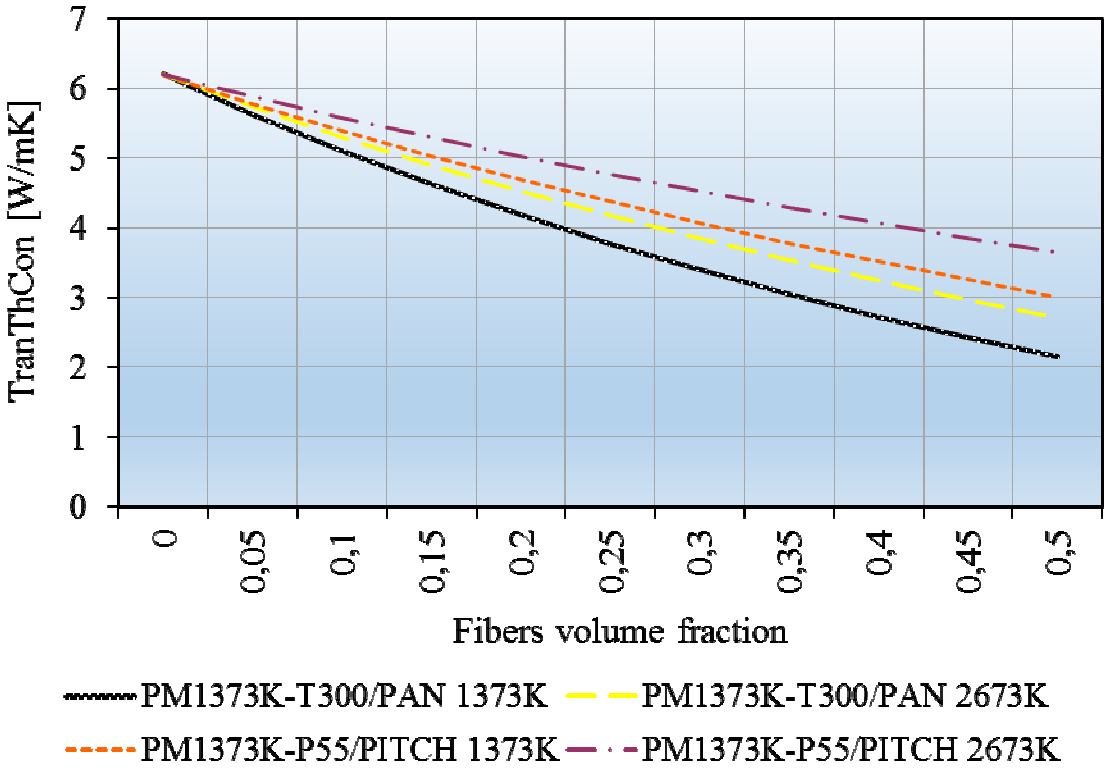

Fig. 3.10. Thermal conductivities on transverse direction of various carbon fibers-reinforced Pitch-matrix type PM1373K resin

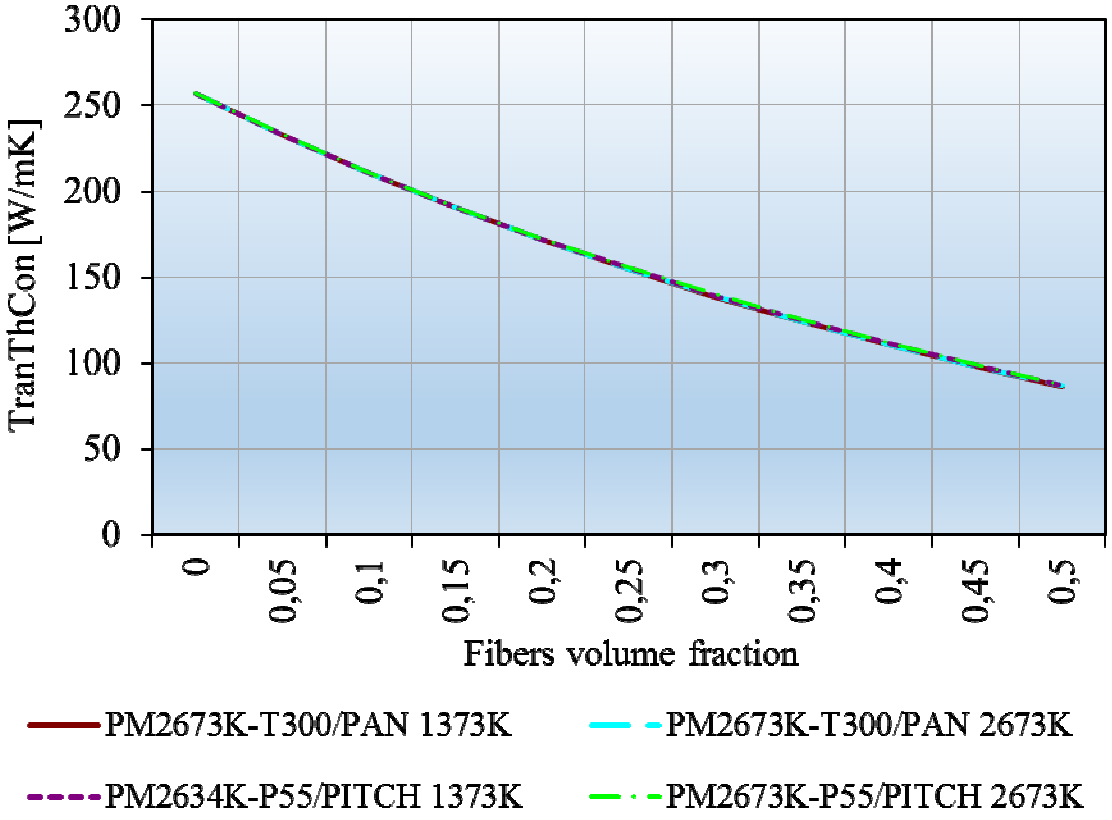

Fig. 3.11. Thermal conductivities on transverse direction of various carbon fibers-reinforced Pitch-matrix type PM2673K resin

Conclusions

While the thermal conductivities on axial direction of composites based on polyurethane and PM1373K resins are very similar and present an increased distribution, the PM2673K based ones exhibit scattered values and have a decreased distribution. While the thermal conductivities on transverse direction of composites based on polyurethane and PM1373K resins present an increased distribution and exhibit scattered values, the PM2673K based ones present very close values.

3.5. Thermal response of a thin sandwich composite structure

Thermal response of a sandwich structure with thin nonwoven polyester mat as core has been experimentally determined. The structure presents dissimilar skins from which one is a glass fabric reinforced polyester. Following layers has been used:

- 1 layer RT500 glass roving fabric;
- 2 layers RT800 glass roving fabric;
- 1 layer CSM450 chopped strand mat;
- 1 layer 4 mm thick nonwoven polyester mat as core;
- 1 layer CSM450 chopped strand mat;
- A usually used gelcoat layer.

The thermal expansions have been measured using a DIL 420 PC dilatometer from NETZSCH GmbH, on both glass fabric reinforced polyester skin and for the whole structure. The coefficients of thermal expansion have been experimentally determined only for the structure's upper skin. For each sample, two successive heating stages, in order to size the influence of the thermal cycling and temperature interval from 20^0C to 250^0C at a heating rate of 1 K/min, have been used. To eliminate the system errors, the dilatometer has been calibrated by measuring a standard SiO_2 specimen under identical conditions.

Distributions of thermal expansion and coefficients of thermal expansion (also known as technical alpha) have been presented in Figs. 3.12 – 3.15.

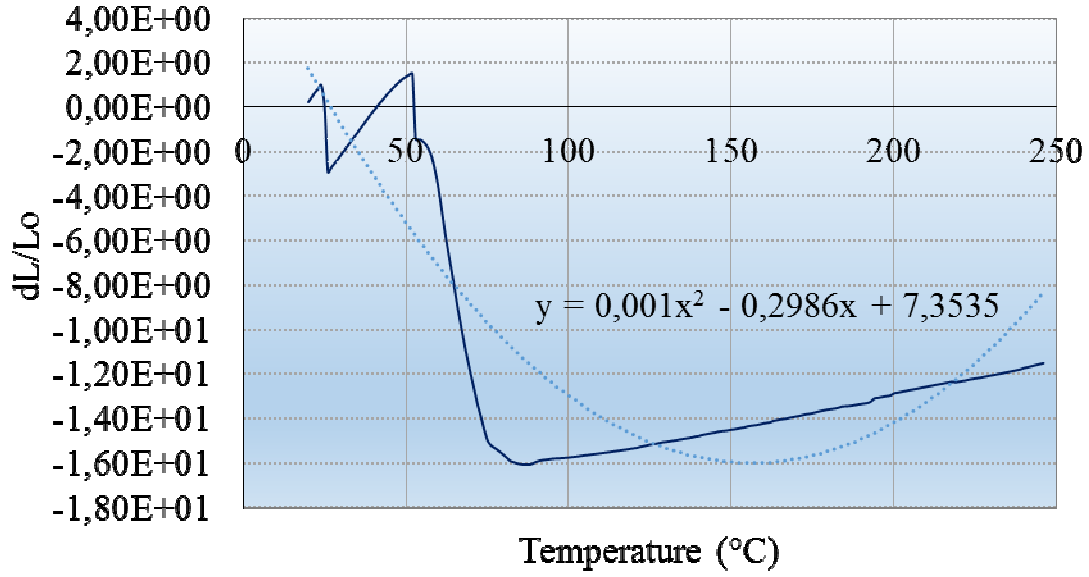

Fig. 3.12. Distribution of upper skin's thermal expansion

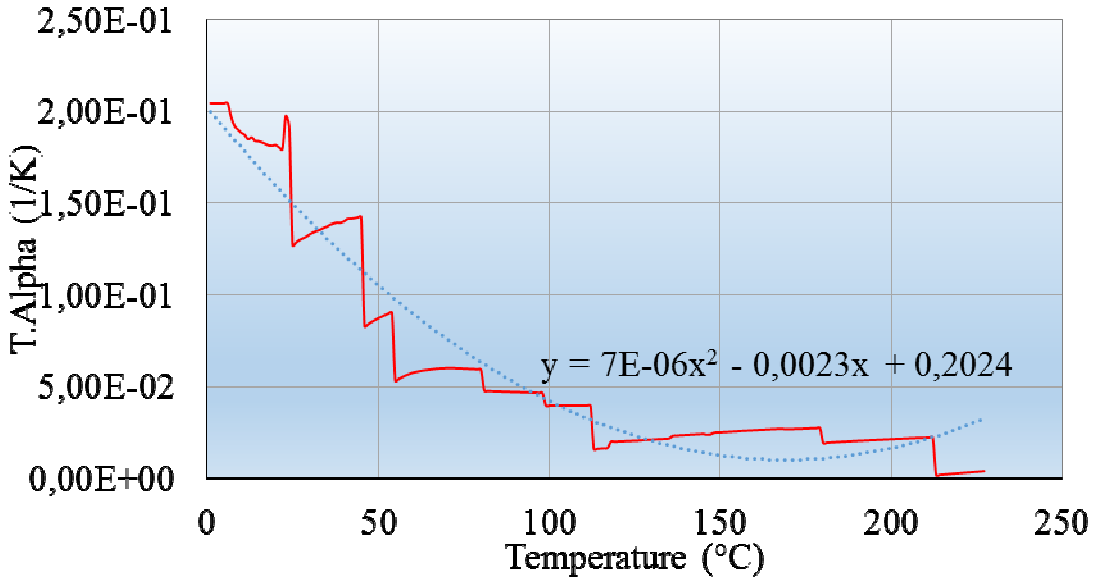

Fig. 3.13. Distribution of upper skin's coefficient of thermal expansion (technical alpha)

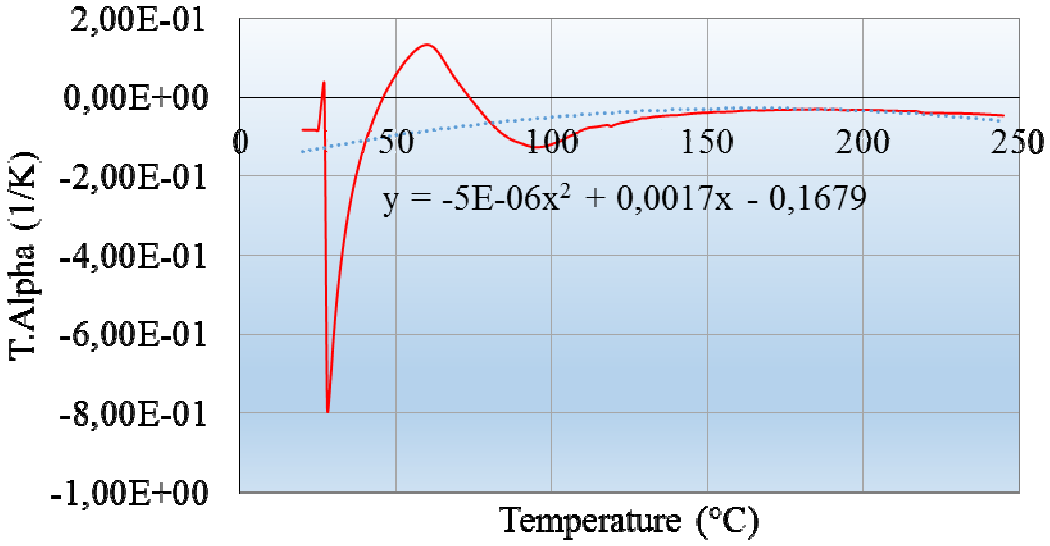

Fig. 3.14. Distribution of sandwich structure's coefficient of thermal expansion in the first heating stage

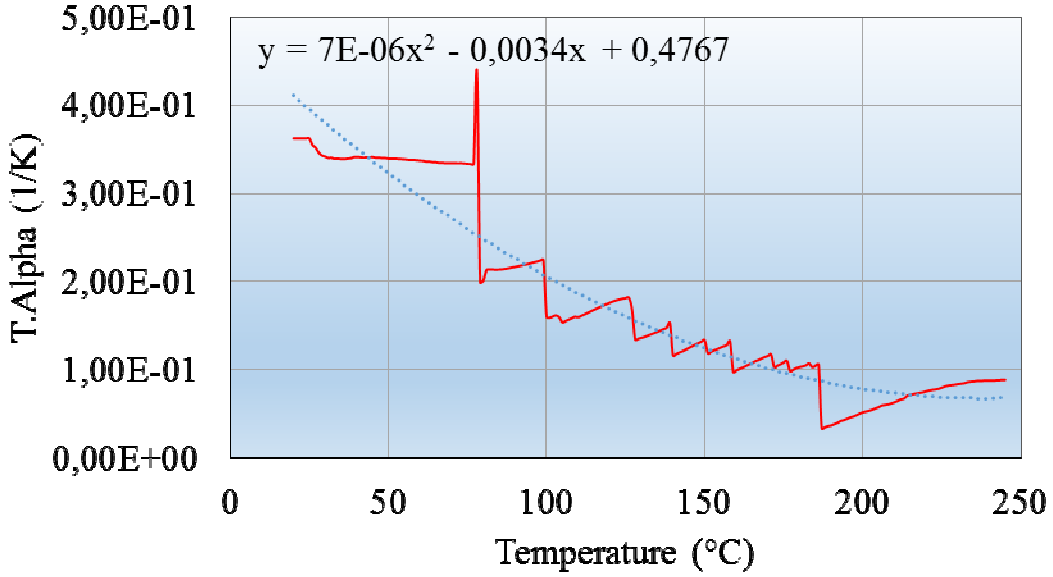

Fig. 3.15. Distribution of sandwich structure's coefficient of thermal expansion in the second heating stage

Conclusions

In Fig. 3.12, the negative thermal expansion in the first heating stage is due to the beginning of curing in the upper skin's structure. Regarding Fig. 3.15, in the

second heating stage, the significant peak is due to the high shrinkage that took place in the sandwich structure. An application of this kind of structure is an underground large spherical cap shelter and formed by twelve curved shells bonded together. To withstand the soil weight, the wall structure present a variable thickness. This kind of structure can be used in outdoor applications also. For each distribution, a polynomial tendency curve of rank two has been generated. Their equation is:

- For upper skin's thermal expansion:

$$y = 0.001x^2 - 0.2986x + 7.3535. \quad (3.14)$$

- For upper skin's coefficient of thermal expansion:

$$y = 7 \cdot 10^{-6}x^2 - 0.0023x + 0.2024. \quad (3.15)$$

- For the sandwich structure's coefficient of thermal expansion in the first heating stage:

$$y = -5 \cdot 10^{-6}x^2 + 0.0017x - 0.1679. \quad (3.16)$$

- For the sandwich structure's coefficient of thermal expansion in the second heating stage:

$$y = 7 \cdot 10^{-6}x^2 - 0.0034x + 0.4767. \quad (3.17)$$

Chapter 4

Contributions to the damping's analysis of a twill weave carbon/epoxy fabric

4.1. Introduction

The most important damping's features in case of a twill weave carbon/epoxy fabric have been computed and published in references [53], [68], [75], [77]. At the damping's analysis of fibers-reinforced composite materials, a so called concept of complex moduli will be used in which the elastic constants will be replaced through their viscoelastic correspondences. The mechanical modeling is based on the correspondence principle of linear viscoelastic theory [8], [14], [85].

Dampings, rigidities and compliances of this kind of fabric have been also computed using an equivalence model of the twill weave carbon/epoxy fabric. In general technique, damping is usually defined as the decrease of oscillations, in which the mechanical energy contained in the system is converted into heat. In materials science, this dissipation process which occurs at the interior of materials is called material's damping.

4.2. Scientific context

When a composite material is subjected to a sinusoidal varying stress in which the strain is also sinusoidal, the angular frequency is retarded in phase by an angle δ, retardation which takes place due to viscoelastic behavior of the matrix.

The introduction of material's damping in the conditions of elastic deformations, occurs under the assumption of harmonic stresses and strains. If the abscissa is chosen as time axis where the strain reaches its maximum, the strain and stress can be written as a function of time [26]:

$$\varepsilon = \varepsilon_0 \cos \omega t, \tag{4.1}$$

$$\sigma = \sigma_0 \cos(\omega t + \delta). \tag{4.2}$$

In the analysis of harmonic systems is more convenient to write the stress function as a complex quantity σ^* which presents a real and an imaginary part [26]:

$$\sigma^* = \sigma_0' \cos \omega t + i\sigma_0'' \sin \omega t, \tag{4.3}$$

where σ_0' and σ_0'' can be expressed as following [26]:

$$\sigma_0' = \sigma_0 \cos \delta, \tag{4.4}$$

$$\sigma_0'' = \sigma_0 \cos \delta. \tag{4.5}$$

Representing the ratios of stresses σ_0' and σ_0'' to ε_0, a dynamic or "storage" Young's modulus and a "loss" modulus can be defined [26]:

$$E' = \frac{\sigma_0'}{\varepsilon_0}, \tag{4.6}$$

$$E'' = \frac{\sigma_0''}{\varepsilon_0}. \tag{4.7}$$

According to equations (4.4) and (4.5), the ratio between the loss Young's modulus and the dynamic modulus defines the material's damping [26]:

$$\frac{E''}{E'} = \frac{\sigma_0''}{\sigma_0'} = \tan\delta = d. \tag{4.8}$$

It is also convenient to express the harmonic stress and strain in the form of an exponential function [26]:

$$\sigma^* = \sigma_0^* \cdot e^{i\omega t}, \tag{4.9}$$

$$\varepsilon^* = \varepsilon_0^* \cdot e^{i\omega t}. \tag{4.10}$$

Now, the complex Young modulus can be written as following [26]:

$$E^* = \frac{\sigma^*}{\varepsilon^*}. \tag{4.11}$$

Taking into account the assumptions of linear viscoelasticity theory, the following material's law can be defined [26]:

$$\sigma^* = E^* \cdot \varepsilon^* = (E' + i \cdot E'') \cdot \varepsilon^* = E'(1 + i \cdot d) \cdot \varepsilon^*. \tag{4.12}$$

For the equation (4.12), Niederstadt has presented a special resonance method suitable for small amplitudes, where the specimen has been subjected at bending respective torsion oscillations [26].

According to the resonance diagram of a glass fiber reinforced lamina, the first three eigenfrequencies at bending, $f_{n,b}$, and first eigenfrequency at torsion, $f_{1,t}$, have been determined. To determine the dynamic Young's modulus, E', and the dynamic shear modulus, G', the motion equations for bending, *w (x,t)*, and torsion,

θ (x,t) have been analyzed. In the case of a rectangular cross section specimen with one side fixed connection, the following equations for bending are [26]:

$$E'(1+i\cdot d_b)\cdot I_y\frac{\partial^4 w(x,t)}{\partial x^4}+\rho\cdot h\cdot\frac{\partial^2 w(x,t)}{\partial t^2}=0, \tag{4.13}$$

$$E'=\frac{48\pi^2}{(\beta_n^2)^2}\cdot\frac{l^4}{h^2}\cdot\rho\cdot f_n^2, \tag{4.14}$$

$$d_b=\frac{\Delta f_b}{f_{nb}}, \tag{4.15}$$

with the eigenvalue equation [26]:

$$1+\cosh\beta_n\cdot\cos\beta_n=0. \tag{4.16}$$

For torsion [26]:

$$G'(1+i\cdot d_T)\cdot I_t\frac{\partial^2\theta(x,t)}{\partial x^2}+r\cdot b\cdot h\frac{b^2+h^2}{12}\cdot\frac{\partial^2\theta(x,t)}{\partial t^2}=0, \tag{4.17}$$

$$G'=\frac{4}{3\cdot(2n-1)^2}\cdot\frac{1+\left(\frac{b}{h}\right)^2}{x_1\frac{b}{h}}\cdot l^2\cdot r\cdot f_n^2, \tag{4.18}$$

$$d_T=\frac{\Delta f_T}{f_{nT}}. \tag{4.19}$$

The dampings d_b and d_T can be determined from the halve value domains Δf of the resonance peaks. For the analysis of micromechanical lamina behavior, the prism model described by Tsai has been used [78]. So, the dynamic modulus along the fibers direction can be computed from the mixture rule as following [78]:

$$E'_{\parallel}=E'_{F\parallel}\cdot\varphi+E'_M(1-\varphi). \tag{4.20}$$

Perpendicular to fibers direction, the dynamic modulus presented by Niederstadt, as a function of fibers and matrix dynamic moduli as well as the fibers and matrix dampings, can be used [26]:

$$E'_{\perp} = -\frac{E'_{F\perp}E'_{M}\{d^2_{F\perp}E'_{F\perp}(\varphi-1)-[d^2_{M}E'_{M}\varphi+E'_{M}\varphi-E'_{F\perp}(\varphi-1)]\}}{d^2_{F\perp}E'^2_{F\perp}(\varphi-1)^2-2d_{F\perp}d_{M}E'_{F\perp}E'_{M}\varphi(\varphi-1)+d^2_{M}E'^2_{M}\varphi^2+\cdots}$$

$$-\frac{E'_{F\perp}E'_{M}\{d^2_{F\perp}E'_{F\perp}(\varphi-1)-[d^2_{M}E'_{M}\varphi+E'_{M}\varphi-E'_{F\perp}(\varphi-1)]\}}{\ldots+E'^2_{F\perp}(\varphi-1)^2-2E'_{F\perp}E'_{M}\varphi(\varphi-1)+E'^2_{M}\varphi^2} \qquad (4.21)$$

For the damping of unidirectional reinforced lamina, the computing relations given by Saravanos and Chamis can be used, starting from the cylinder model presented by Tsai [21], [31], [78]:

$$d_{\parallel} = \frac{d_{F\parallel}E'_{F\parallel}\varphi+d_{M}E'_{M}(1-\varphi)}{E'_{\parallel}}, \qquad (4.22)$$

$$d_{\perp} = d_{F\perp}\sqrt{\varphi}\,\frac{E'_{\perp}}{E'_{F\perp}} + d_{M}(1-\sqrt{\varphi})\,\frac{E'_{\perp}}{E'_{M}}, \qquad (4.23)$$

$$d_{\#} = d_{F\#}\sqrt{\varphi}\,\frac{G'_{\#}}{G'_{F\#}} + d_{M}(1-\sqrt{\varphi})\,\frac{G'_{\#}}{G'_{M}}. \qquad (4.24)$$

The index F describes the fibers, index M is used for matrix, φ represents the fibers volume fraction and υ_M is the Poisson ratio for matrix.

4.3. Damping's simulation of twill weave carbon/epoxy fabric

The carbon-fibers fabric used in this simulation is a high rigidity one, that presents a so-called twill weave with 0.3 kg/m^3 specific weight. The main feature of this weave is that the warp and the weft threads are crossed in a programmed order and frequency, to obtain a flat appearance (Fig. 4.1). In order to accomplish the damping analysis, an equivalence model of the twill weave fabric is presented in Fig. 4.2.

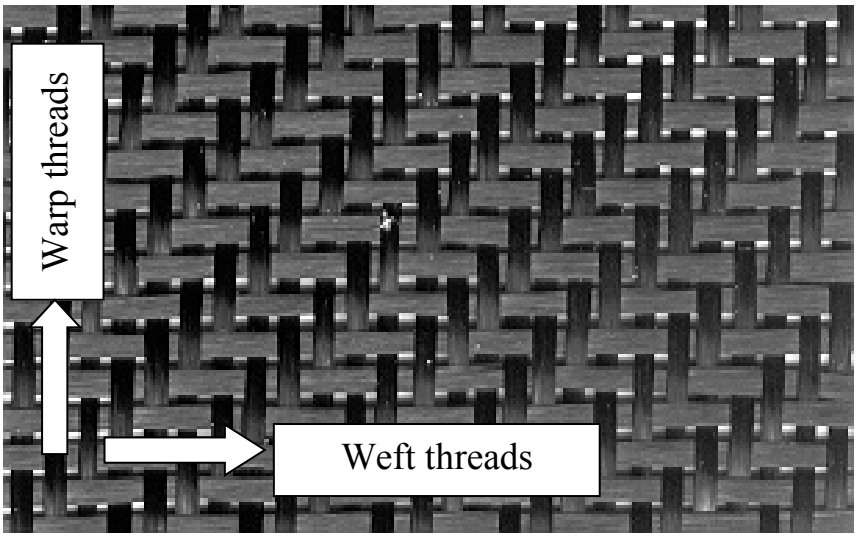

Fig. 4.1. The architecture of carbon/epoxy twill weave fabric

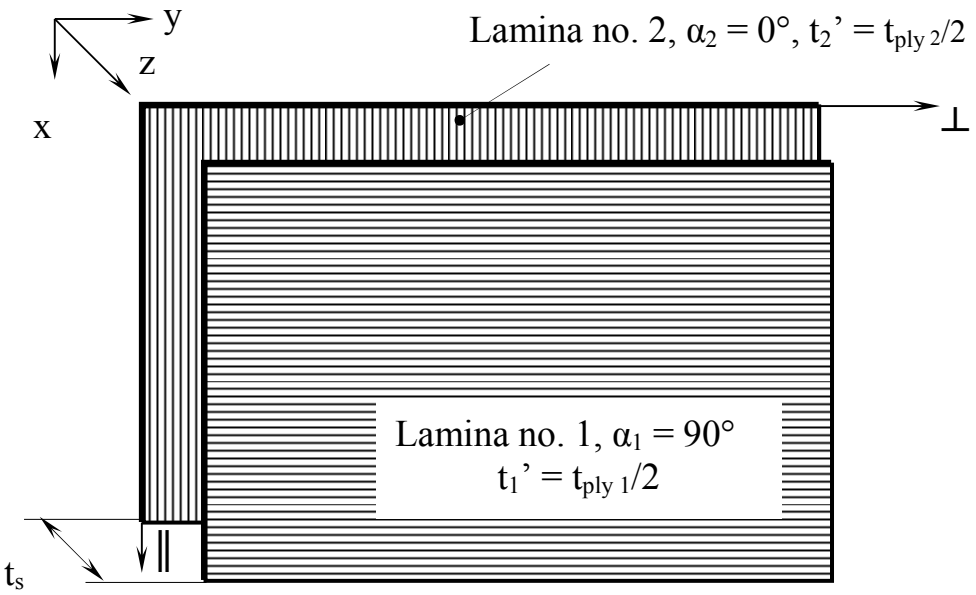

Fig. 4.2. The carbon/epoxy twill weave fabric equivalence model

The data regarding the architecture of the twill weave carbon/epoxy fabric are: thickness of each lamina: $t'_{1...2}$ = 0.175 mm; fibers disposal angle of each lamina: $\alpha_1 = 90°$, $\alpha_2 = 0°$; fibers volume fraction of each lamina: $\varphi = 56\%$. The data regarding the structure features: reinforcement: HM carbon fibers; fabric type: twill weave; fibers specific weight: 0.3 kg/m^2; matrix type: epoxy resin; fibers Young's modulus in longitudinal direction: $E_{F\parallel}$ = 540 GPa; fibers Young's modulus in transverse direction: $E_{F\perp}$ = 27 GPa; fibers Poisson's ratio: $\upsilon_F = 0.3$; fibers shear modulus: G_F = 10.38 GPa; matrix Young's modulus: E_M = 3.5 GPa; matrix Poisson's ratio: $\upsilon_M = 0.34$; matrix shear modulus: G_M= 1.42 GPa.

In the followings, we will consider exclusive linear damping mechanisms, linear elastic behavior of the reinforcement and marked linear viscoelasticity of the matrix [1], [32], [86].

The viscoelastic material's law according to the concept of complex moduli, for an orthotropic lamina, can be written as following:

$$\begin{bmatrix} \varepsilon_{\parallel}^* \\ \varepsilon_{\perp}^* \\ \gamma_{\#}^* \end{bmatrix} = \begin{bmatrix} C_{\parallel}^* & C_{\parallel\perp}^* & 0 \\ C_{\perp\parallel}^* & C_{\perp}^* & 0 \\ 0 & 0 & C_{\#}^* \end{bmatrix} \cdot \begin{bmatrix} \sigma_{\parallel}^* \\ \sigma_{\perp}^* \\ \tau_{\#}^* \end{bmatrix} = \begin{bmatrix} \frac{1}{E_{\parallel}^*} & \frac{-\upsilon_{\parallel\perp}}{E_{\perp}^*} & 0 \\ \frac{-\upsilon_{\perp\parallel}}{E_{\parallel}^*} & \frac{1}{E_{\perp}^*} & 0 \\ 0 & 0 & \frac{1}{G_{\#}^*} \end{bmatrix} \cdot \begin{bmatrix} \sigma_{\parallel}^* \\ \sigma_{\perp}^* \\ \tau_{\#}^* \end{bmatrix}. \tag{4.25}$$

Expressing the complex stresses as a function of complex strains, it can be obtained:

$$\begin{bmatrix} \sigma_{\parallel}^* \\ \sigma_{\perp}^* \\ \tau_{\#}^* \end{bmatrix} = \begin{bmatrix} \Gamma_{\parallel}^* & \Gamma_{\parallel\perp}^* & 0 \\ \Gamma_{\perp\parallel}^* & \Gamma_{\perp}^* & 0 \\ 0 & 0 & \Gamma_{\#}^* \end{bmatrix} \cdot \begin{bmatrix} \varepsilon_{\parallel}^* \\ \varepsilon_{\perp}^* \\ \gamma_{\#}^* \end{bmatrix} = \begin{bmatrix} \frac{E_{\parallel}^*}{1-\upsilon_{\parallel\perp}^2 \frac{E_{\perp}^*}{E_{\parallel}^*}} & \frac{\upsilon_{\parallel\perp} E_{\perp}^*}{1-\upsilon_{\parallel\perp}^2 \frac{E_{\perp}^*}{E_{\parallel}^*}} & 0 \\ \frac{\upsilon_{\parallel\perp} E_{\perp}^*}{1-\upsilon_{\parallel\perp}^2 \frac{E_{\perp}^*}{E_{\parallel}^*}} & \frac{E_{\perp}^*}{1-\upsilon_{\parallel\perp}^2 \frac{E_{\perp}^*}{E_{\parallel}^*}} & 0 \\ 0 & 0 & G_{\#}^* \end{bmatrix} \cdot \begin{bmatrix} \varepsilon_{\parallel}^* \\ \varepsilon_{\perp}^* \\ \gamma_{\#}^* \end{bmatrix}. \tag{4.26}$$

For fibers-reinforced polymer matrix composites, assuming that the dampings $d^2 << 1$, the complex compliances and rigidities for a unidirectional reinforced lamina are:

$$c_{ij}^{*} = c_{ij}' + i \cdot c_{ij}'' = c_{ij}'(1 + i \cdot d_{c_{ij}}), \tag{4.27}$$

$$r_{ij}^{*} = r_{ij}' + i \cdot r_{ij}'' = r_{ij}'(1 + i \cdot d_{r_{ij}}). \tag{4.28}$$

For $d^2 << 1$, according to equations (4.27) and (4.28), the dynamic compliances can be written in the form:

$$[C'] = \begin{bmatrix} c_{\parallel}' & c_{\parallel\perp}' & 0 \\ c_{\perp\parallel}' & c_{\perp}' & 0 \\ 0 & 0 & c_{\#}' \end{bmatrix} = \begin{bmatrix} \frac{1}{E_{\parallel}'} & \frac{-v_{\parallel\perp}}{E_{\perp}'} & 0 \\ \frac{-v_{\perp\parallel}}{E_{\parallel}'} & \frac{1}{E_{\perp}'} & 0 \\ 0 & 0 & \frac{1}{G_{\#}'} \end{bmatrix} \tag{4.29}$$

and the dynamic rigidities can be written under the following form:

$$[R'] = \begin{bmatrix} r_{\parallel}' & r_{\parallel\perp}' & 0 \\ r_{\perp\parallel}' & r_{\perp}' & 0 \\ 0 & 0 & r_{\#}' \end{bmatrix} = \begin{bmatrix} \frac{E_{\parallel}'}{1-v_{\parallel\perp}^2 \frac{E_{\perp}'}{E_{\parallel}'}} & \frac{v_{\parallel\perp} E_{\perp}'}{1-v_{\parallel\perp}^2 \frac{E_{\perp}'}{E_{\parallel}'}} & 0 \\ \frac{v_{\parallel\perp} E_{\perp}'}{1-v_{\parallel\perp}^2 \frac{E_{\perp}'}{E_{\parallel}'}} & \frac{E_{\perp}'}{1-v_{\parallel\perp}^2 \frac{E_{\perp}'}{E_{\parallel}'}} & 0 \\ 0 & 0 & G_{\#}' \end{bmatrix}. \tag{4.30}$$

Results

Following input data have been taken into consideration in the damping analysis of the twill weave carbon/epoxy fabric (Table 4.1). The results of computational micromechanics of the lamina's damping is presented in Table 4.2 and the twill weave carbon/epoxy fabric's dynamic compliances, rigidities and

dampings are shown in Table 4.3. The analysis has been carried out using the twill weave carbon/epoxy fabric's equivalence model presented in Fig. 4.2.

Table 4.1. Input data

$E_M^{'}$ (GPa)	2.6
υ_M (-)	0.34
d_M (%)	1.4
$E_{F\,II}^{'}$ (GPa)	226
$E_{F\perp}^{'}$ (GPa)	16
$G_{F\#}^{'}$ (GPa)	43
$d_{F\,II}$ (%)	0.13

Table 4.2. Results of the computational micromechanics of lamina's damping

$E_{II}^{'}$ (GPa)	127.7
$E^{'}{}_{\perp}$ (GPa)	5.89
d_{II} (%)	0.141
$d_{\perp}$ (%)	0.833
$d_{\#}$ (%)	1.929
$G_M^{'}$ (GPa)	0.97

Table 4.3. Twill weave carbon/epoxy fabric's dynamic compliances, rigidities and dampings

c'_{II} (GPa^{-1})	0.00783
$c'_{II\perp}$ (GPa^{-1})	- 0.04923
$c'_{\perp}$ (GPa^{-1})	0.16977
$c_{\#}$ (GPa^{-1})	0.18939
d_{cII} (%)	0.141
$d_{cII\perp}$ (%)	- 0.833
$d_{c\#}$ (%)	- 1.929
r'_{II} (GPa)	128.19
$r'_{II\perp}$ (GPa)	1.71
$r'_{\perp}$ (GPa)	5.91
$r'_{\#}$ (GPa)	5.28
d_{rII} (%)	0.143
$d_{rII\perp}$ (%)	0.835
$d_{r\#}$ (%)	1.929

Conclusions

The dampings of twill weave carbon/epoxy fabric are very different along and transverse to the fibers direction. The maximum value of the damping seems to be at 45° against the fibers direction.

Chapter 5

Contributions to the hysteresis effect in a three-phase polymer matrix composite subjected to static cyclic loadings

5.1. Introduction

Experimental researches regarding hysteresis behaviors of three-phase polymer matrix composite material (Chopped Strand Mat-Al_2O_3 ceramic particles-reinforced polyester resin) subjected to static cyclic tension-compression loadings have been carried out and published in two issues of *Optoelectronics and Advanced Materials-Rapid Communications (OPTOELECTRON ADV MAT)* in 2011 [47], [83]. Various cyclic tests with different test speeds, load limits and number of cycles have been accomplished on a Lloyd Instruments LS100Plus materials testing machine using a STGA/50/50 E85454 extensometer and Nexygen software. The experiments have been carried out at Department of Mechanical Engineering within Transilvania University of Brasov. Among over forty-five mechanical properties determined in extended experimental researches, maximum hysteresis data as well as stiffness distributions of specimens that exhibit maximum hysteresis have been presented. The difference between first and last cycle extension in every single test has been computed to determine maximum hysteresis effect reported to be at 10 mm/min test speed with a decreasing tendency once test speed is increased.

5.2. Scientific context

Static cyclically tension-compression tests are for a significant importance to put into evidence time dependent structural changes inside a material [10], [24]. One of the most important problems in a static cyclic tension-compression test of any composite material and especially in thin polymer matrix composite laminates is the gripping of the specimen without introducing unacceptable stress concentrations in its structure [5], [79]. For instance, grips are clamped into the specimen ends, transferring the applied cyclic tension-compression loads at the specimen's surface into tensile-compression stresses within the specimen and therefore the clamping forces are significant [3], [20], [38]. To avoid high clamping forces it is necessary to manufacture specimens as thin as practically possible or to ensure longer grip lengths so that the clamping forces can be distributed over a larger area [80].

Setiadi *et al.*, have been accomplished tensile and fatigue tests on both polyester and polyurethane-based fiber-reinforced polymer matrix composites as well as studies concerning the damage development in randomly disposed E-glass fiber-reinforced polymers under fatigue loadings up to 105 cycles [35]. To estimate the failure and cyclic life, Tan and Dharan have determined cyclic hysteresis experimental data, for instance, on notched [0/90] E-glass/epoxy laminates [39]. In general, a randomly disposed chopped strand mat presents 25.4 mm or 50 mm glass fibers lengths. This type of reinforcement is manufactured from E-glass continuous fibers, bound with powder binder, compatible with synthetic resins and used in a wide range of applications. It is usually used for the hand lay-up technique and for parts that do not require high strength.

5.3. Materials and experimental procedure

The composite material used in static cyclic tension-compression loadings is a three-phase one based on following compounds:

- Chopped strand mat CSM 600 (up to 60% E-glass fibers volume fraction);
- Al2O3 ceramic particles (up to 10% volume fraction);
- Polyester resin.

A 5 mm thick composite plate has been manufactured from which specimens (dimensions: 5 x 15 x 150 mm) have been cut. The composite specimens have been subjected to different static tension-compression cyclic loadings at various test speeds and cycle limits on a Lloyd Instruments LS100Plus (up to 100 kN force range) materials testing machine with a STGA/50/50 E85454 extensometer (Epsilon Technology Corp.). All experimental data have been processed using the Nexygen Plus materials testing software. Specimens and tests features are presented in Table 5.1.

Table 5.1. Test speeds, cycle limits, number of cycles and specimens features used in cyclic tests

Gauge length [mm]	50	50	50	50	50	50
Test speed [mm/min]	1	10	20	40	60	60
Specimens' width [mm]	15	15	15	15	15	15
Specimens' thickness [mm]	4.86	4.86	4.86	4.86	4.86	4.86
Cycle limit 1 [kN]	3	3	3	3	3.5	3.5
Cycle limit 2 [kN]	0.3	0.3	0.3	-2	-3.5	-3.5
Number of cycles	10	10	10	10	10	100

5.4. Experimental results and conclusions

Following mechanical properties have been determined: stiffness, Young's modulus, load at maximum load, stress at maximum load, machine extension at maximum load, extension at maximum load, strain at maximum load, percentage strain at maximum load, work to maximum load, load at maximum extension, stress at maximum extension, machine extension at maximum extension, extension at maximum extension, strain at maximum extension, percentage strain at maximum extension, work to maximum extension, load at minimum load, stress at minimum load, machine extension at minimum load, extension at minimum load, strain at minimum load, percentage strain at minimum load, work to minimum load, load at minimum extension, stress at minimum extension, machine extension at minimum extension, extension at minimum extension, strain at minimum extension, percentage strain at minimum extension, work to minimum extension, load at first cycle, stress at first cycle, machine extension at first cycle, extension at first cycle, strain at first cycle, percentage strain at first cycle, first cycle work, load at last cycle, stress at last cycle, machine extension at last cycle, extension at last cycle, strain at last cycle, percentage strain at last cycle, last cycle work, load at break, stress at break, machine extension at break, extension at break, strain at break, percentage strain at break and work to break.

Distributions of tension-compression cycles determined on specimens that exhibit maximum hysteresis, at various test speeds and cycle limits are presented in Figs. 5.1 – 5.5. Maximum hysteresis at different test speeds and cycle limits are presented in Fig. 5.6. The maximum hysteresis values have been determined as a difference between maximum extension at first cycle and maximum extension at last cycle.

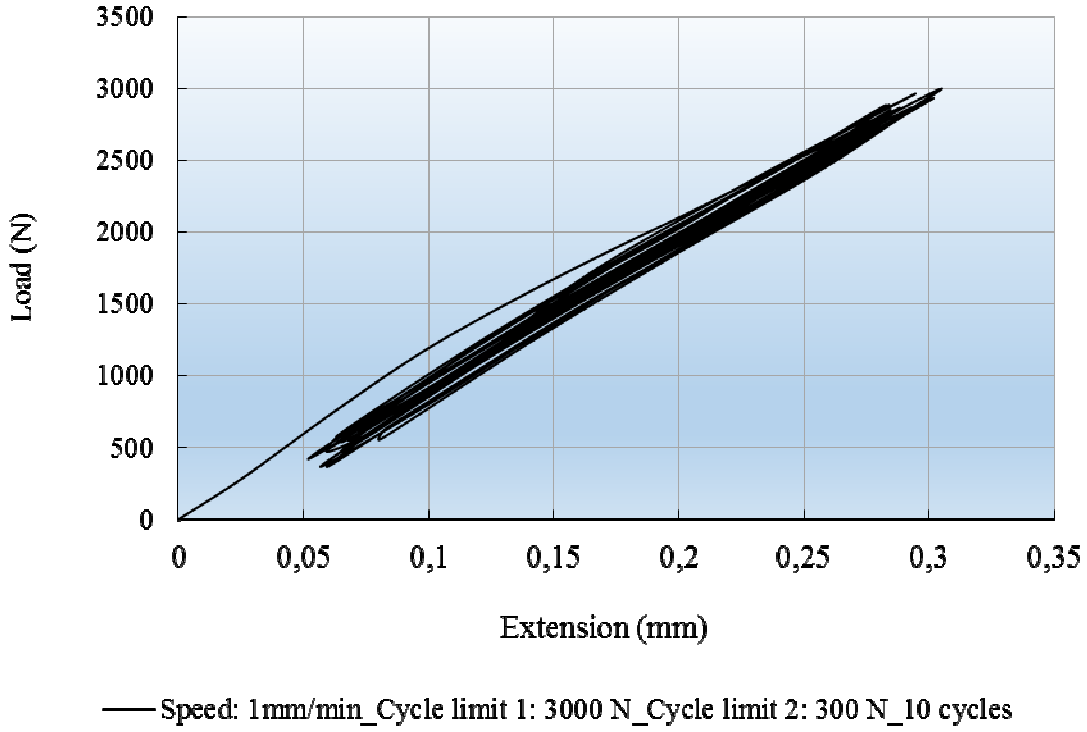

Fig. 5.1. Tension-compression loadings (1 mm/min test speed, 10 cycles). Maximum hysteresis specimen

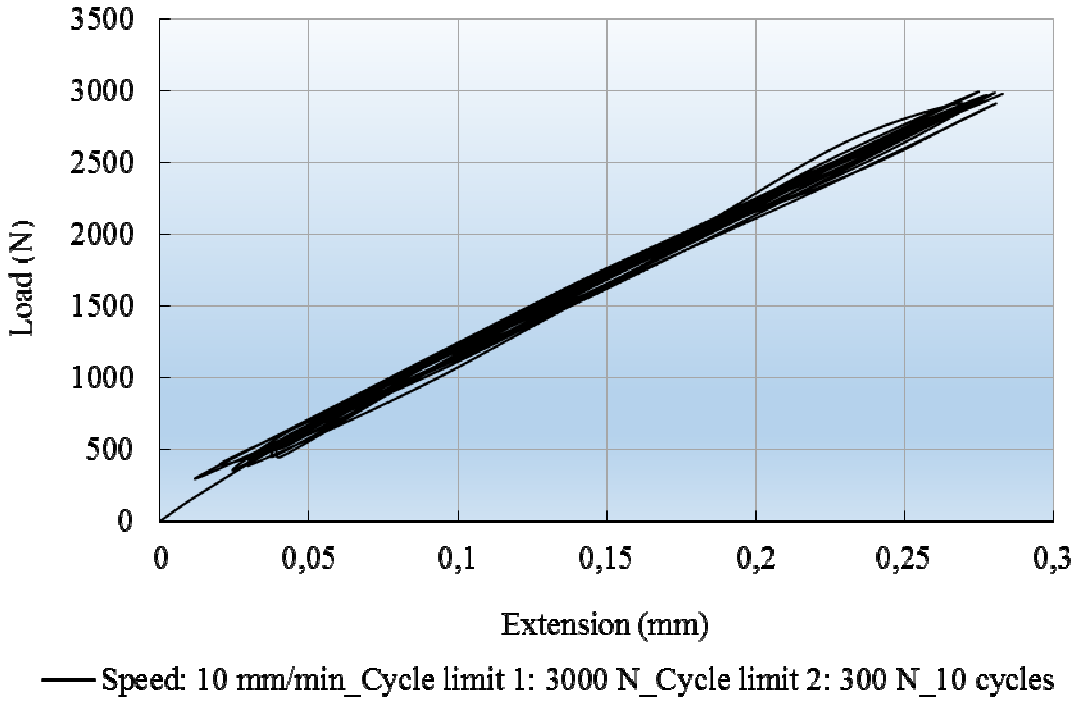

Fig. 5.2. Tension-compression loadings (10 mm/min test speed, 10 cycles). Maximum hysteresis specimen

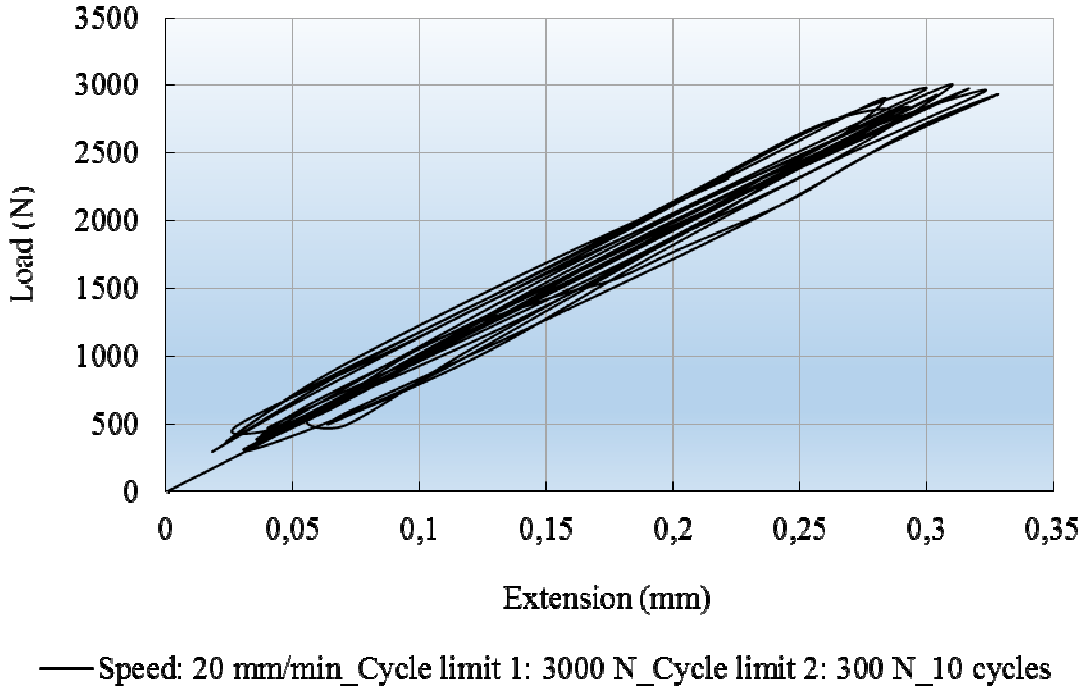

Fig. 5.3. Tension-compression loadings (20 mm/min test speed, 10 cycles). Maximum hysteresis specimen

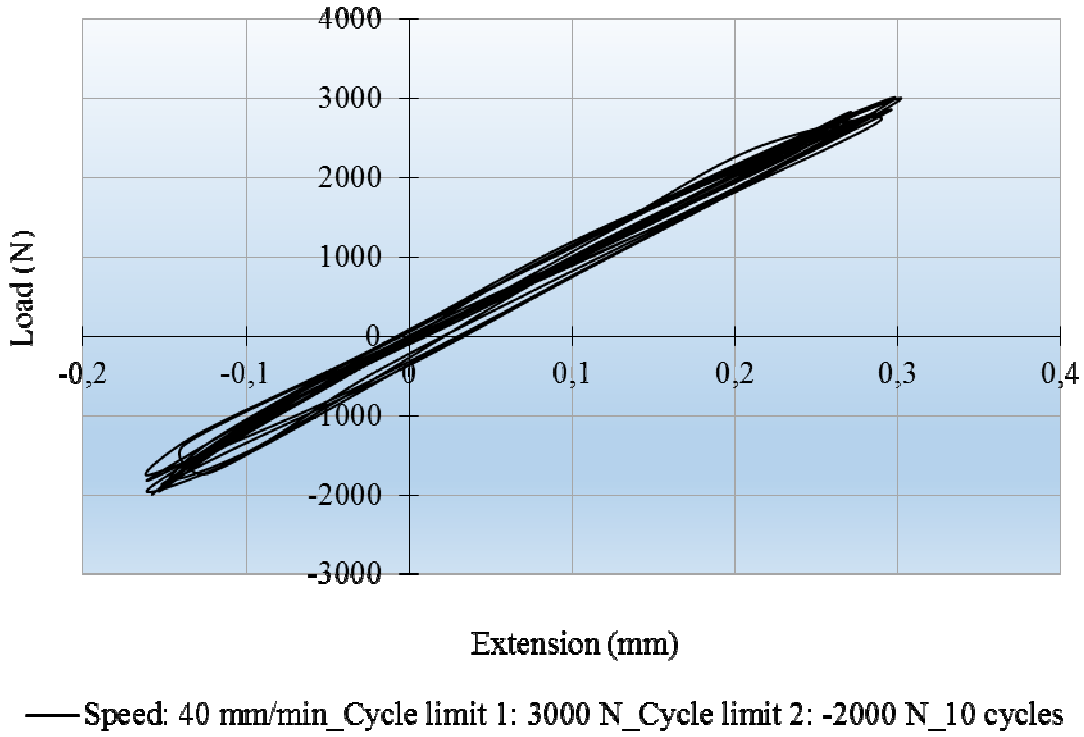

Fig. 5.4. Tension-compression loadings (40 mm/min test speed, 10 cycles). Maximum hysteresis specimen

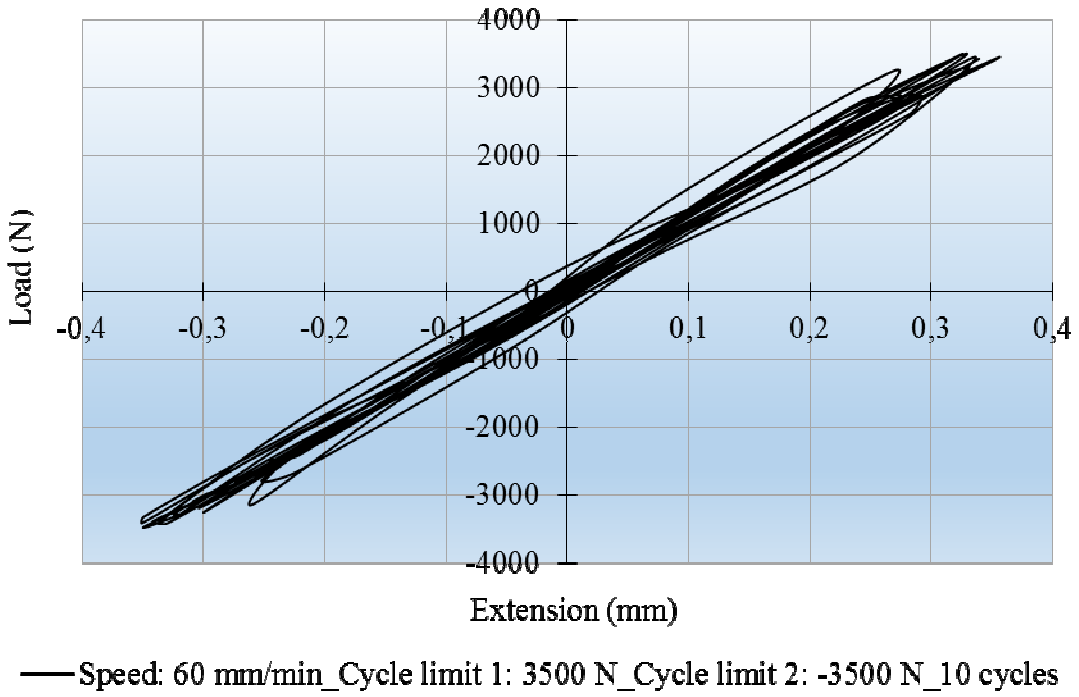

Fig. 5.5. Tension-compression loadings (60 mm/min test speed, 10 cycles). Maximum hysteresis specimen

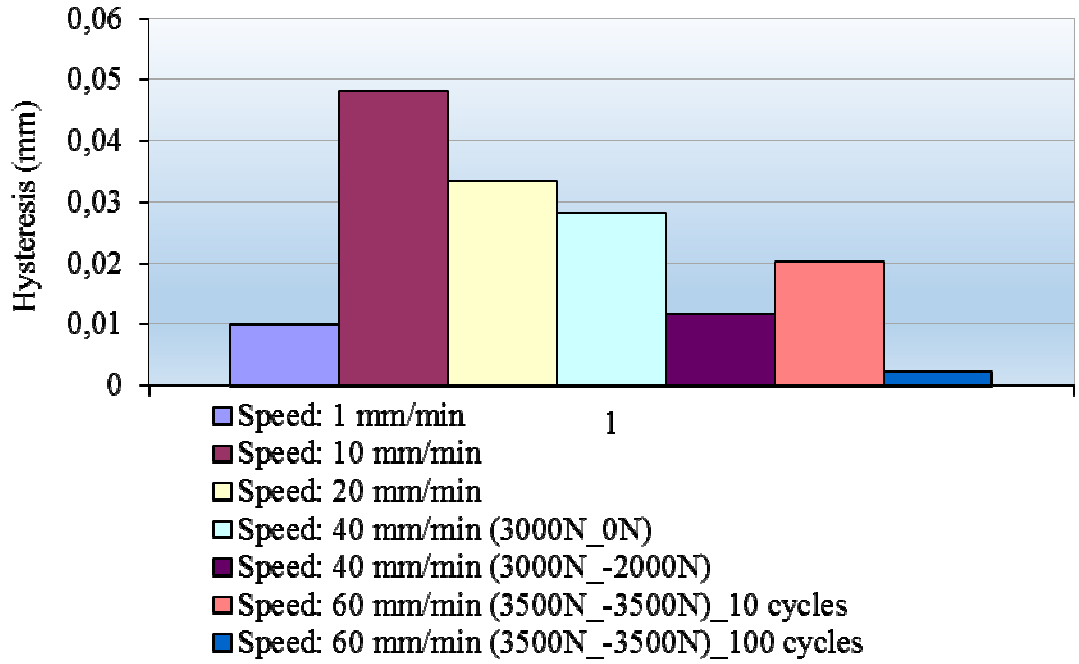

Fig. 5.6. Maximum hysteresis at different test speeds and cycle limits

More results regarding stiffness, loads at maximum load and extensions at maximum load are shown in Tables 5.2 – 5.5.

Table 5.2. Ten cycles loadings on five specimens. Results at 1 mm/min test speed

Stiffness [N/m]	Load at Maximum Load [kN]	Extension at Maximum Load [mm]
13475942.4	3.00377393	0.30719793
15132051.5	3.00759271	0.32767069
16549676.8	3.002124	0.29343876
16095991.2	3.00837308	0.30559519
33332739.9	3.00593337	0.25764742

Table 5.3. Ten cycles loadings on five specimens. Results at 10 mm/min test speed

Stiffness [N/m]	Load at Maximum Load [kN]	Extension at Maximum Load [mm]
13967680.9	3.00937169	0.28241922
16661178.1	3.00540243	0.28349737
135859632	3.00931013	0.30639223
73525334.1	3.01062039	0.20652689
60387410.8	3.00700736	0.33509265

At 1 mm/min test speed the composite material presents a 0.29 mm extension at maximum load while at 10 mm/min test speed, the extension at maximum load exhibits 0.28 mm. The decreasing tendency maintains until 40 mm/min test speed when the extension at maximum load presents the median value of 0.26 mm.

With the test speed of 60 mm/min, this extension at maximum load increases quickly at a median value of 0.31 mm. Unlike the decreasing tendency of this

extension, the load at maximum load presents an increasing tendency once the test speed is increased (from 3.005 kN median value at 1 mm/min test speed to 3.542 kN median value at 60 mm/min test speed). The stiffness of the composite material presents an increased tendency with the increase of test speed. This increase is up to 10 times at 60 mm/min test speed.

Table 5.4. Ten cycles loadings on five specimens. Results at 20 mm/min test speed

Stiffness [N/m]	Load at Maximum Load [kN]	Extension at Maximum Load [mm]
17827375	3.00943709	0.28685673
13379229.6	3.01802144	0.31033918
15775800.3	3.01335963	0.25577515
13231534.5	3.01604018	0.2722434
14079242	3.015046	0.2523938

Table 5.5. Ten cycles loadings on five specimens. Results at 40 mm/min test speed

Stiffness [N/m]	Load at Maximum Load [kN]	Extension at Maximum Load [mm]
23242274	3.03827211	0.2401018
19543018.2	3.0141013	0.26273534
15370866.1	3.0401521	0.28077099
13525374.8	3.02023364	0.28549097
15314877.1	3.03328912	0.2537304

Between 300 N and 3000 N cycle limits, the load at first cycle presents an increased distribution from a median value of 0.308 kN at 1 mm/min test speed to 0.33 kN at 20 mm/min test speed. The extension at last cycle distribution presents a decreased tendency while the load at last cycle presents an increasing tendency.

Conclusions

It can be noticed that with the test speed increase, non-linear behavior at unloading phase is more significant. Maximum hysteresis value has been determined at 10 mm/min test speed with a decreasing tendency once the test speed increases. Maximum stiffness has been determined at 60 mm/min tests speed, the general tendency is the increase of this stiffness. With the increase of cycle limits, the maximum hysteresis presents a decreasing tendency while the stiffness distribution increases. The same specimens have been subjected to increased loading conditions; this means increased cycle limits, test speeds and number of cycles. The break detector reported breaking of the composite material after 115 static cyclic tension-compression loadings. All the experimental data have been processed statistically. For instance, some statistics for maximum hysteresis results are presented below:

- Stiffness coefficient of variance: 74.19%;
- Young's modulus coefficient of variance: 72.14%;
- Load at maximum load coefficient of variance: 0.06%;
- Extension at maximum load coefficient of variance: 15.09%;
- Work to maximum load coefficient of variance: 18.61%;
- Load at maximum extension coefficient of variance: 0.29%;
- Extension at maximum extension coefficient of variance: 7.87%;
- Work to maximum extension coefficient of variance: 16.16%;
- Load at first cycle coefficient of variance: 2.47%;
- Extension at first cycle coefficient of variance: 36.72%;
- Load at last cycle coefficient of variance: 2.37%;
- Extension at last cycle coefficient of variance: 126.82%.

Chapter 6

Contributions to the experimental characterization of polyester and epoxy/glass fibers-reinforced laminates

6.1. Introduction

Seven types of composite laminates have been developed at Compozite Ltd., Brasov, based on polyester and epoxy resins reinforced with chopped strand mats (CSM) and glass fabrics of various specific weights and then subjected to three and four-point bend tests both on warp and weft direction to determine their mechanical properties. One type of Polylite 440-M888/RT300 glass fabric composite laminate has been developed and subjected to tensile loads until break. These experimental researches, have been published in four issues of *Optoelectronics and Advanced Materials-Rapid Communications (OPTOELECTRON ADV MAT)* [25], [36], [45], [81] and one issue of *Journal of Optoelectronics and Advanced Materials (J OPTOELECTRON ADV M)* [82]. The tests have been carried out on two Lloyd Instruments materials testing machines from Department of Mechanical Engineering within Transilvania University of Brasov using the Nexygen materials testing software. Some specimens have been used to determine strain distributions inserting strain gages between specimens' layers and connecting them in SPIDER8 data acquisition system. The resistive strain analysis has been accomplished using the CATMAN software. My previous researches regarding the mechanical behavior of chopped strand mats and roving fabrics subjected to tensile tests have been published in 2007 in references [72], [73], [74].

6.2. Scientific context

Polyester and epoxy reinforced composite laminates are usually used in a wide range of composite structures. As reinforcement, glass fibers in form of chopped strand mats and roving fabrics of various specific weights are commonly used. To choose a material for a specific application is quite a challenging task. The user should consult the supplier for detailed mechanical property data on current materials, together with wider databases required for other property data (e.g. electrical, thermal, fire properties, surface finish, etc.), process information (e.g. gel time, working life, curing temperature, cure time, mold release temperature, etc.), as well as material or process costs. For composite applications, most design procedures, whether simple or sophisticated, will be based initially on stiffness data and will often relate to strain or deflection limits design. Consequently, Young's modulus values are normally required for the main in-plane directions of a composite laminate using orthogonal axes. Young's modulus is an important feature of any kind of material since represents its stiffness [9]. In addition, many applications of composites are based on thin-walled structures (e.g. thin pultruded profiles, skins of sandwich structures, etc.). The Young's modulus is also important in controlling the ultimate load for the commonly observed buckling failures. For a two phase composite material (e.g. matrix and fibers), Young's modulus as well as shear modulus can be determined using the well-known rule of mixture. For multiphase composite materials, formed basically from matrix, fibers and filler, to predict their elastic properties, some homogenization methods can be used. Such approaches can be accomplished on prepregs like Sheet Molding Compounds, Bulk Molding Compounds and Dough Molding Compounds.

6.3. Materials and experimental procedure

There is a wide range of fiber formats that together with the process used, provide a useful information of different classes of composite materials. The fibers lengths can vary from discontinuous fibers (milled, short and long) to continuous fibers in swirled mats, fabrics, non-crimped fabrics and so on. The major use of glass fibers is still represented by chopped strand mats (CSM). In general, a composite structure is manufactured of various plies of discontinuous or unidirectional fibers with different orientations, stacked together to form so called laminates. Following polyester and epoxy/glass fibers composite laminates have been manufactured at Compozite Ltd., Brasov and cured in specific dimensional panels from which specimens have been cut using a diamond mill and water as cooling agent to avoid introduce internal stresses in composite:

1. Four layers Epoxy/Chopped Strand Mat CSM450 (450 g/m^2 specific weight), 3.2 – 3.6 mm thick laminate;
2. Four layers Epoxy/RT800 glass fabric (800 g/m^2 specific weight), 3.2 – 3.6 mm thick laminate, from which specimens have been cut on warp direction;
3. Four layers Epoxy/RT800 glass fabric (800 g/m^2 specific weight), 3.2 – 3.6 mm thick laminate, from which specimens have been cut on weft direction;
4. Combination of two layers Epoxy/CSM600 (600 g/m^2 specific weight), 2 – 2.6 mm thick – four layers Epoxy/RT800 on warp (3.2 – 3.6 mm thick) – two layers Epoxy/CSM450 (1.6 – 2 mm thick);
5. Combination of two layers Epoxy/CSM600 (600 g/m^2 specific weight), 2 – 2.6 mm thick – four layers Epoxy/RT800 on weft (3.2 – 3.6 mm thick) – two layers Epoxy/CSM450 (1.6 – 2 mm thick);
6. Twelve layers of Polylite 440-M888/RT300 glass fabric on weft (300 g/m^2 specific weight), 4 mm thick laminate;
7. Five layers of Heliopol 9431ATYX_LSE/Stratimat300 glass fabric (300 g/m^2 specific weight), 6 mm thick laminate.

Between the layers of some types of composite laminates, strain gages have been applied and connected to a SPIDER8 device suitable for resistive stress analysis (Fig. 6.1). All specimens designed for resistive stress analysis have been subjected up to 1000 N load, using the four-point bend test. The distributions of load versus time as well as specific deformations versus time have been experimentally determined using the CATMAN software.

Fig. 6.1. Specimen connected to SPIDER8 device and subjected to four-point bend test

For instance, the four layers Epoxy/CSM450 specimens with three strain gages and three compensation strain gages applied between these layers, have been connected to the SPIDER8 device and subjected to four-point bend test using a special device designed especially for this purpose (Fig. 6.2).

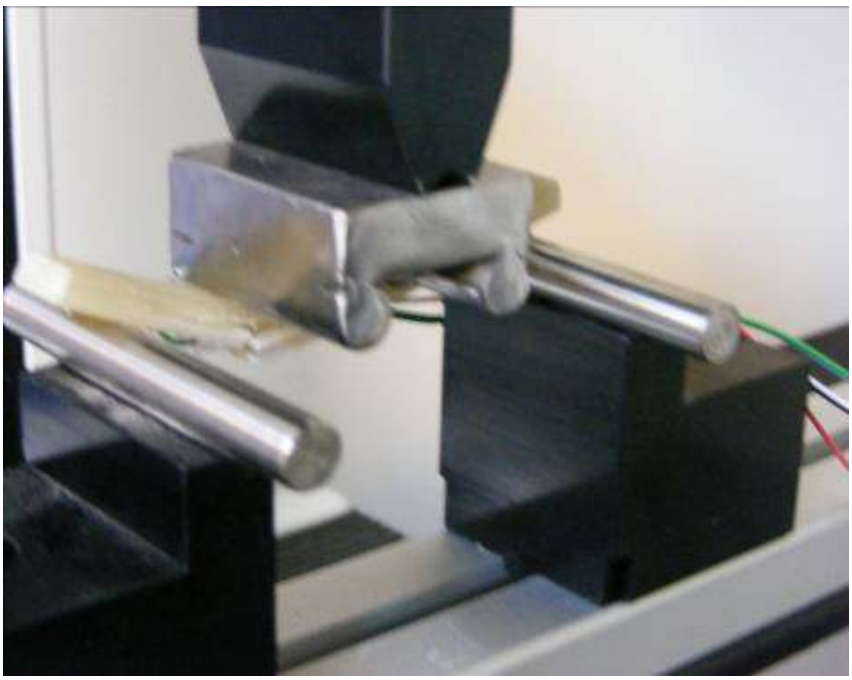

Fig. 6.2. Epoxy/CSM450 specimen with strain gages inserted between layers subjected to four-point bend test

The composite laminate used in tensile tests is a thermoset polymer (i.e. unsaturated polyester resin of type Polylite 440-M888) reinforced with twelve plies of glass fabric of type RT300 (300 g/m2 specific weight). In general, the RT fabrics are manufactured from roving with cut margins and strengthened with Dreher threads. From a cured plate, fifteen specimens have been cut on weft direction using a diamond powder mill with added water to avoid introduce internal stresses and especially thermal stresses that can appear in the cutting process (Fig. 6.3). The specimens have been tempered for 24 hours at a temperature of 20°C and then subjected to tensile loads until break according to SR EN 527-1: „Determination of tensile properties of fiber reinforced composite materials". A "LS100 Plus" Lloyd Instruments materials testing machine have been used without extensometer to perform the tensile tests.

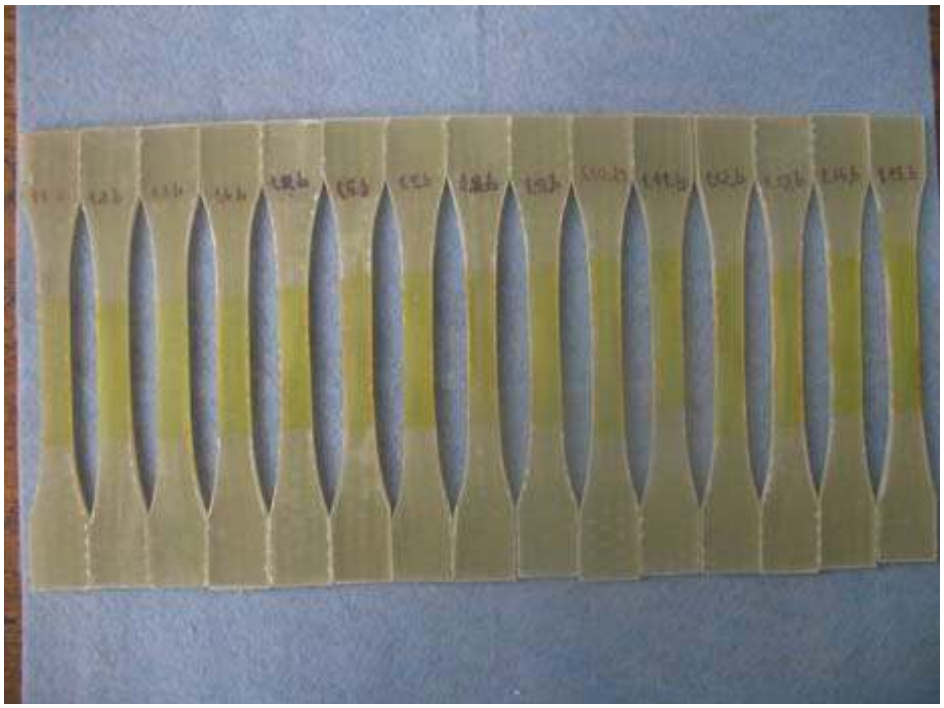

Fig. 6.3. RT300 glass fabric-reinforced Polylite 440-M888 polyester resin specimens cut on weft direction

The seventh type of composite laminate presents following compounds:

- Resin: HELIOPOL 9431ATYX_LSE;
- Hardener: BUTANOX M50;
- Glass fibers: STRATIMAT300 with 300 g/m^2 specific weight.

From cured plate, nine specimens have been cut using a diamond powder mill and a suitable cooling system to avoid introduce internal stresses in the composite laminate.

The specimens have been subjected to three-point bend tests until break on a LR5Kplus Lloyd Instruments' materials testing machine with maximum 5kN load cell.

6.4. Experimental results and conclusions

Load-deflection distributions for every type of composite specimen have been experimentally determined on an LR5Kplus Lloyd Instruments materials testing machine and presented in Figs. 6.4 – 6.8. On epoxy/CSM450 composite, equations of linear tendency for every four-point bend tests load-deflection distributions have been computed and presented on diagram (Fig. 6.6). Young's modulus of bending distributions of all epoxy/glass fibers composite laminates taken into consideration in this experimental analysis have been presented in Fig. 6.9. There are no significant differences between load-deflection distributions of Epoxy/RT800 specimens cut on warp or weft directions (Figs. 6.4 – 6.5).

Using chopped strand mats of type CSM450 as reinforcement, the Epoxy/CSM450 laminates present maximum load at about half value of those manufactured from Epoxy/RT800 glass fabric (Fig. 6.6). In case of combination of Epoxy/CSM450-CSM600_RT800 laminates, the maximum load has been reached between those determined on Epoxy/RT800 glass fabric and Epoxy/CSM450 laminates, showing that hybrid reinforcement does not generally improve the overall mechanical properties of a laminate (Figs. 6.7 – 6.8). Anyway, best mechanical properties can be reached using glass fabrics as reinforcement in common composite laminates.

Fig. 6.10 presents the Young's modulus distribution of eight RT300 glass fabric-reinforced Polylite 440-M888 specimens cut on weft direction and subjected to tensile loads.

Following distributions have been experimentally determined on five layers of Heliopol 9431ATYX_LSE/Stratimat300 glass fabric specimens using data recorded by the materials testing machine:

- Load (N)-deflection (mm) plotted in Fig. 6.11;
- Stiffness (N/m) of each specimen, presented in Fig. 6.12;

- Young's Modulus of Bending (MPa) of each specimen, shown in Fig. 6.13;
- Flexural Rigidity (Nm^2) according to each specimen, plotted in Fig. 6.14;
- Maximum Bending Stress at Maximum Load (MPa)-Maximum Bending Strain at Maximum Load (Fig. 6.15);
- Work to Maximum Load (Nmm) of each specimen, presented in Fig. 6.16;
- Load at Break (kN)-Deflection at Break (mm), shown in Fig. 6.17;
- Maximum Bending Stress at Break (MPa)- Maximum Bending Strain at Break (Fig. 6.18);
- Work to Break (Nmm) of each specimen, presented in Fig. 6.19.

Regarding the load-deflection distribution of nine Heliopol/Stratimat300 specimens subjected to three-point bend tests, maximum load of 942.12 N has been reached at specimen number eight and a maximum deflection of 18.8 mm presents specimens number three (Fig. 6.11). Specimen number eight presents also maximum stiffness of 100911 N/m and specimens number four exhibits minimum stiffness of 54009.42 N/m (Fig. 6.12).

Young's modulus of bending distribution is situated between a maximum value of 6.29 GPa at specimen number one and a minimum one of 4.43 GPa at specimen number five (Fig. 6.13). The maximum value of Young's modulus of bending represents an outstanding value for this kind of composite laminate subjected to three-point bend tests. The flexural rigidity distribution follows the stiffness distribution and exhibits a maximum flexural rigidity of 1.07 Nm^2 in case of specimen number eight and a minimum value of 0.57 Nm^2 reached by specimen number four (Fig. 6.14). Maximum bending stress at maximum load of 327.99 MPa has been obtained at specimen number one and maximum bending strain at maximum load of 0.08 presents specimen number four (Fig. 6.15).

Regarding the work to maximum load distribution of nine Heliopol/Stratimat300 specimens subjected to three-point bend tests, maximum value of 7121.64 Nmm exhibits specimen number four and a minimum value of 3264.84 Nmm has been experimentally determined at specimen number six (Fig.

6.16). Specimen number four exhibits the greatest load at break of 0.74 kN and the greatest deflection at break of 19.15 mm has been reached by specimen number three (Fig. 6.17). Maximum bending stress at break follows the same distribution as the load at break distribution, the maximum value of 316.27 MPa being noted at specimen number four and the maximum bending strain at break of 0.098 exhibits specimen number three (Fig. 6.18). The work to break distribution of nine Heliopol/Stratimat300 specimens subjected to three-point bend tests present a maximum value of 8541.08 Nmm in case of specimen number eight and a minimum value of 3660.39 Nmm has been reached by specimen number six (Fig. 6.19).

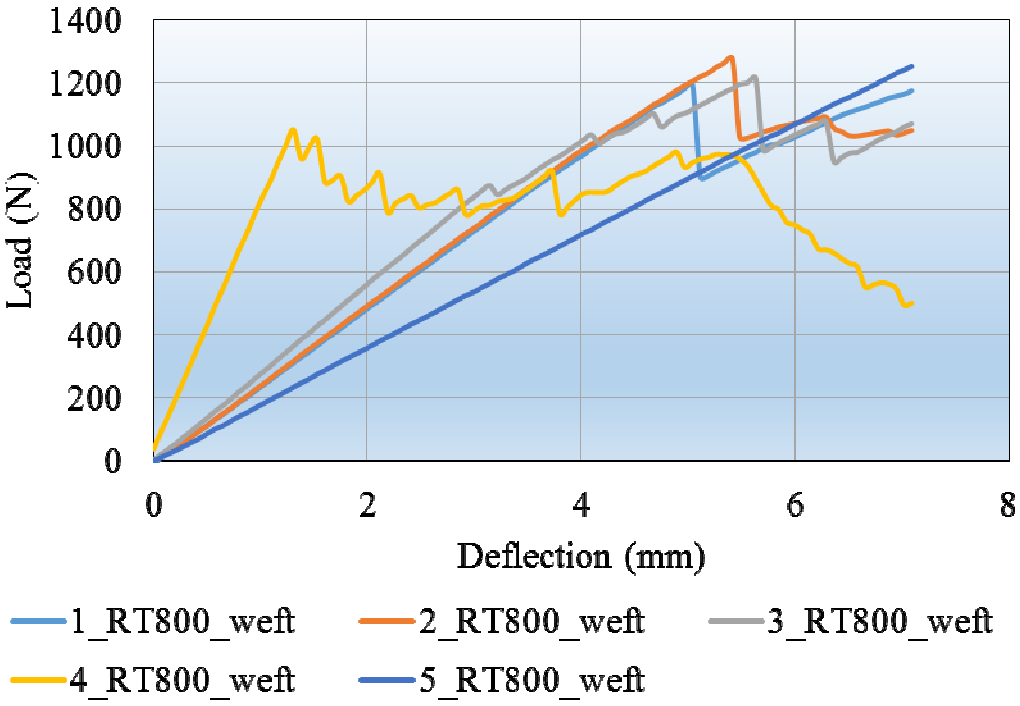

Fig. 6.4. Load-deflection distributions of five Epoxy/RT800 glass fabric specimens cut on weft direction (four-point bend tests)

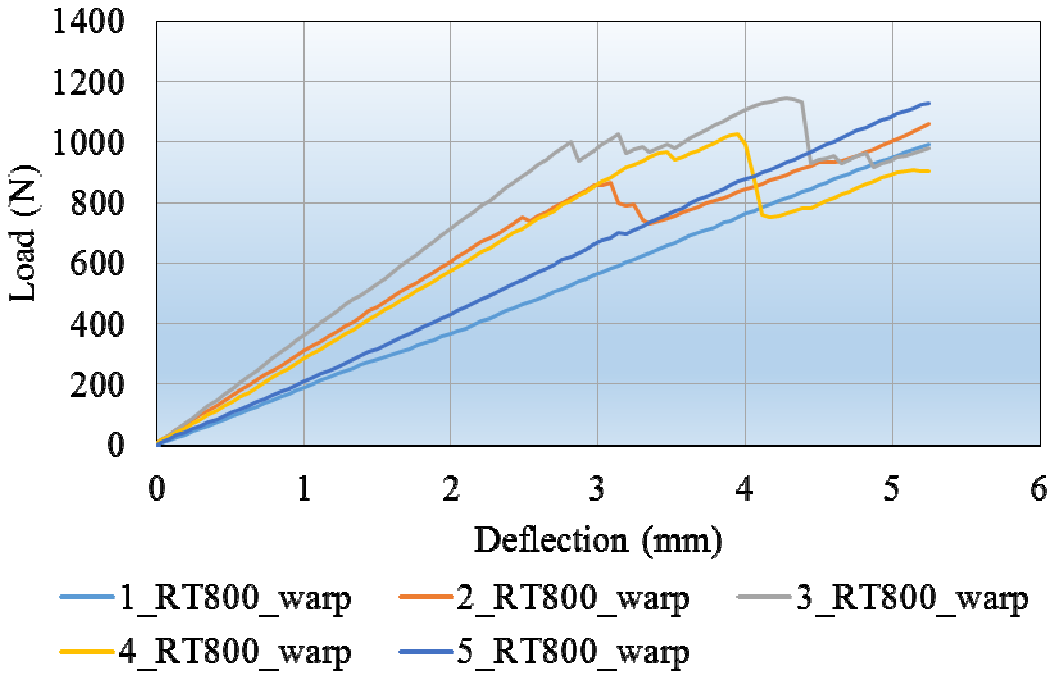

Fig. 6.5. Load-deflection distributions of five Epoxy/RT800 glass fabric specimens cut on warp direction (four-point bend tests)

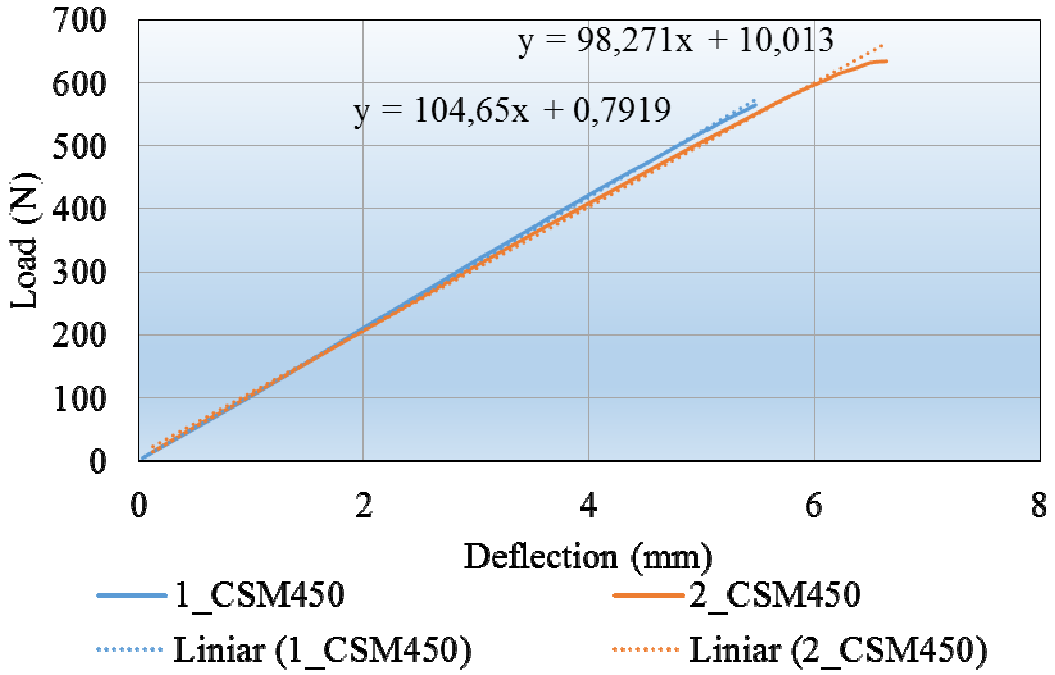

Fig. 6.6. Load-deflection distributions of two Epoxy/CSM450 specimens (four-point bend tests)

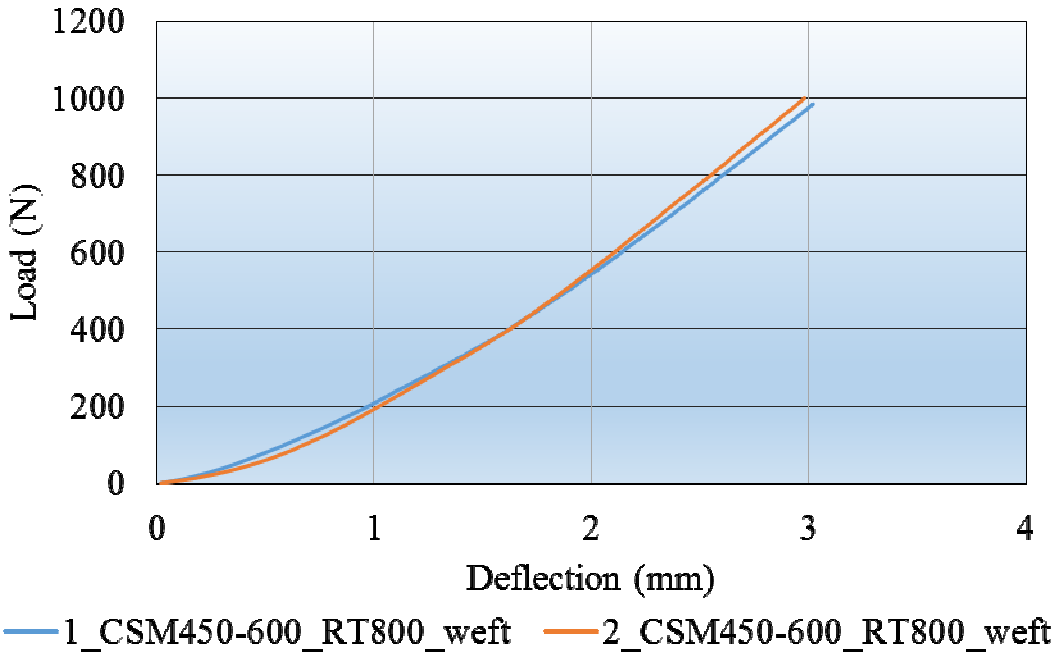

Fig. 6.7. Load-deflection distributions of two Epoxy/CSM450-CSM600_RT800 specimens on weft direction (four-point bend tests)

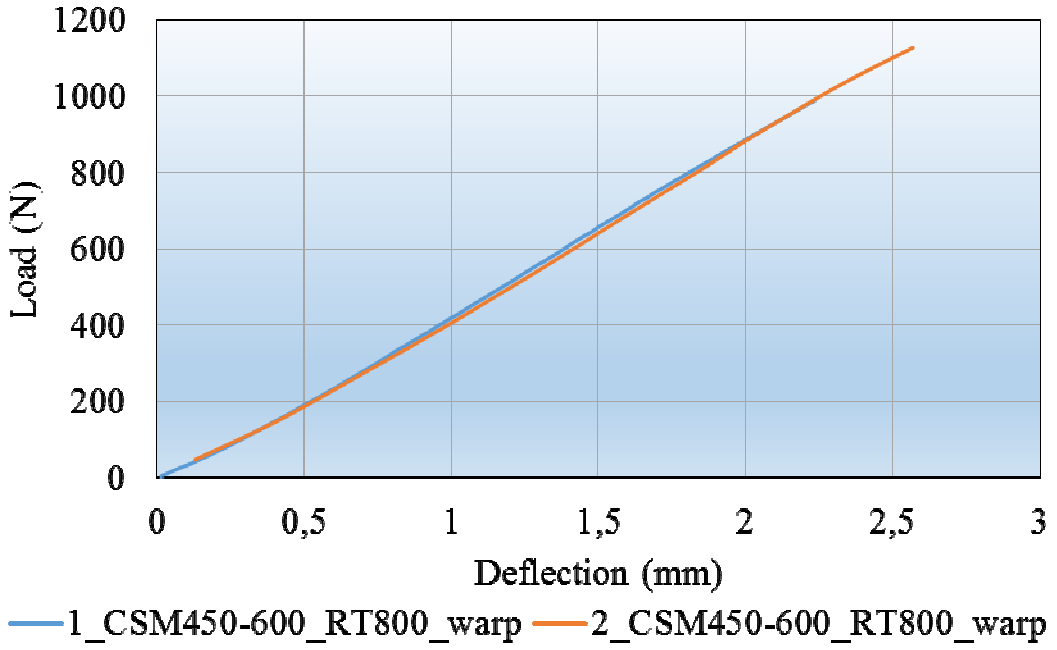

Fig. 6.8. Load-deflection distributions of two Epoxy/CSM450-CSM600_RT800 specimens on warp direction (four-point bend tests)

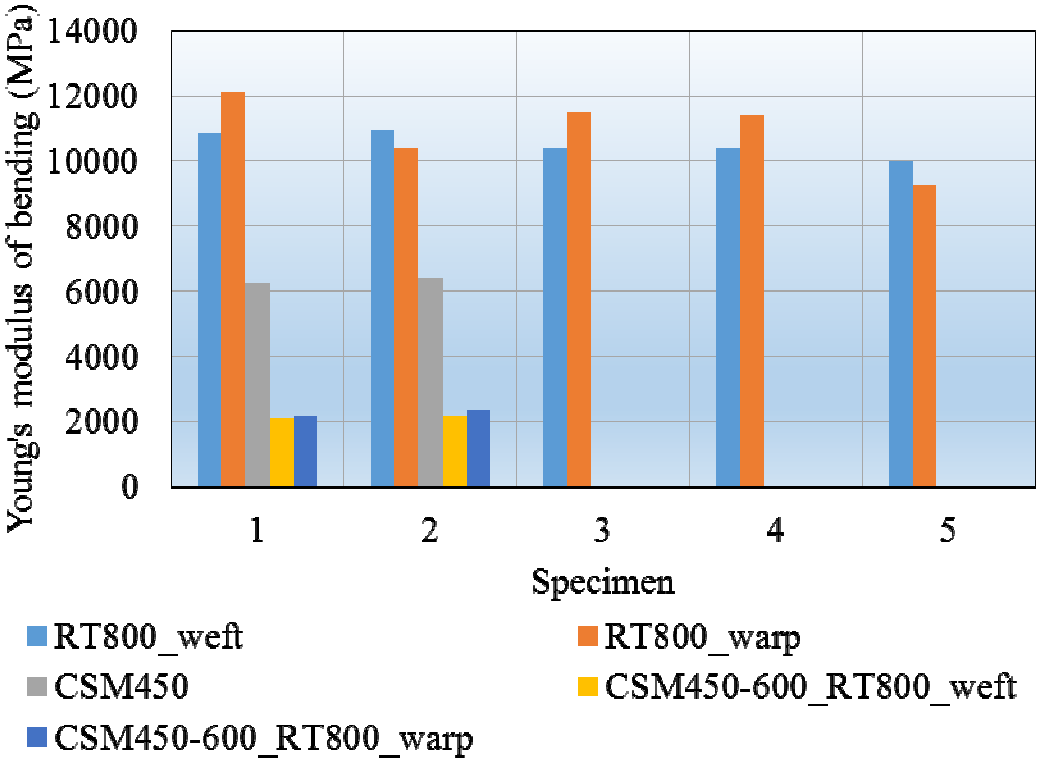

Fig. 6.9. Young's modulus of bending distributions of epoxy/glass fibers composite laminates subjected to four-point bend tests

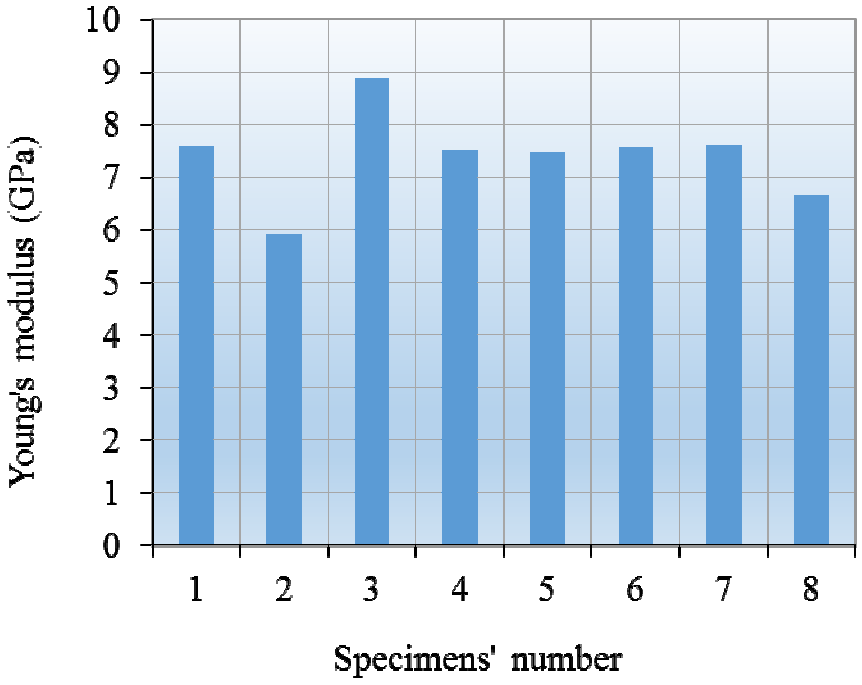

Fig. 6.10. Young's modulus distribution of eight RT300 glass fabric-reinforced Polylite 440-M888 specimens subjected to tensile tests

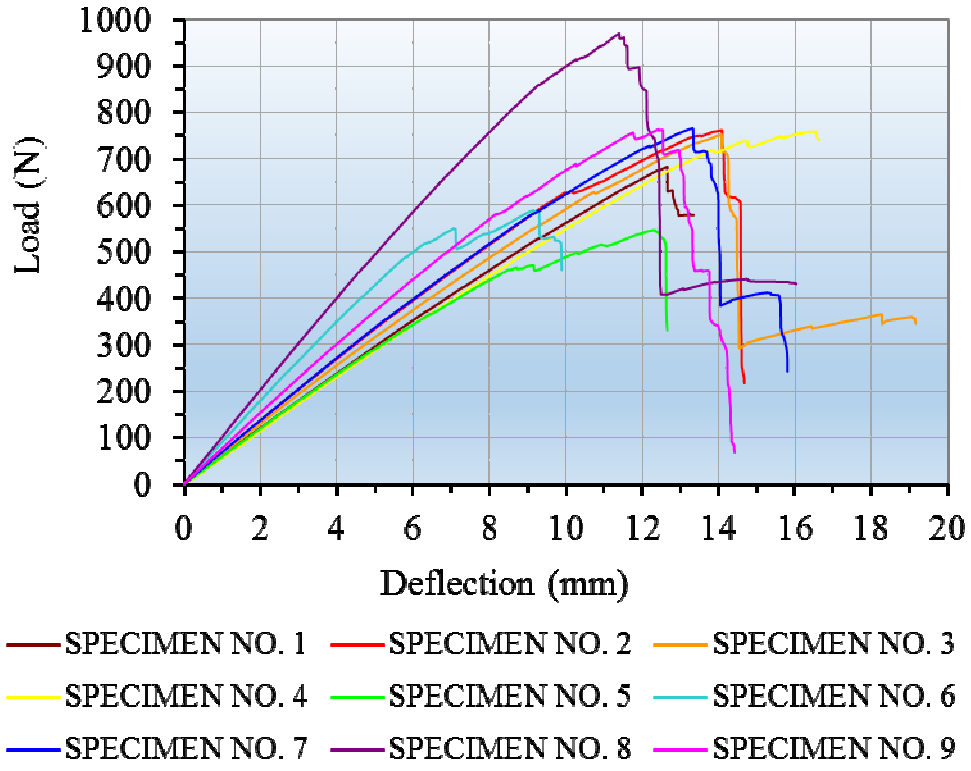

Fig. 6.11. Load-Deflection distribution of five layers Heliopol/Stratimat300 composite laminate

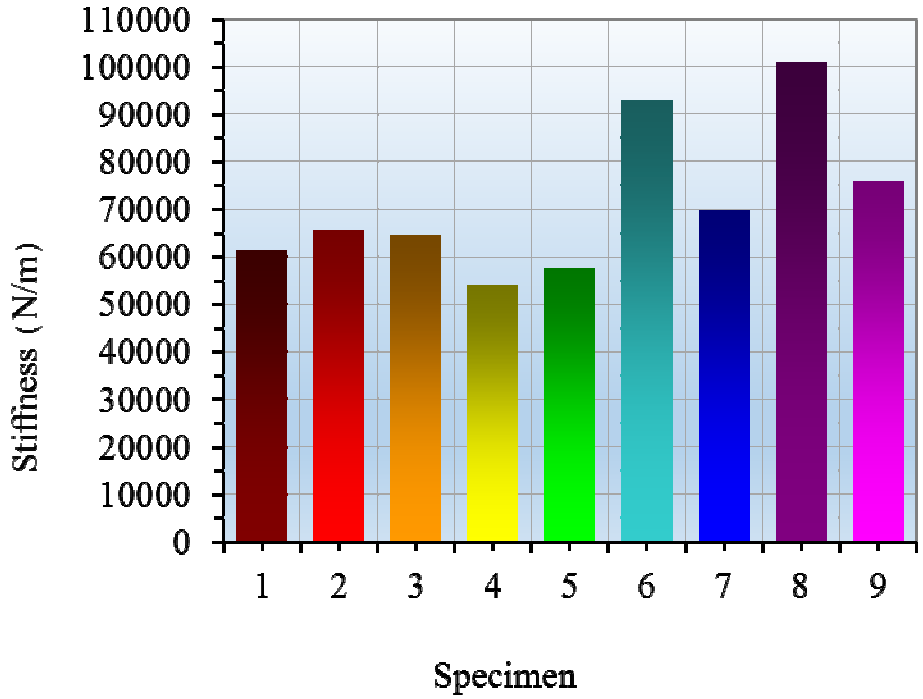

Fig. 6.12. Stiffness distribution of five layers Heliopol/Stratimat300 composite laminate

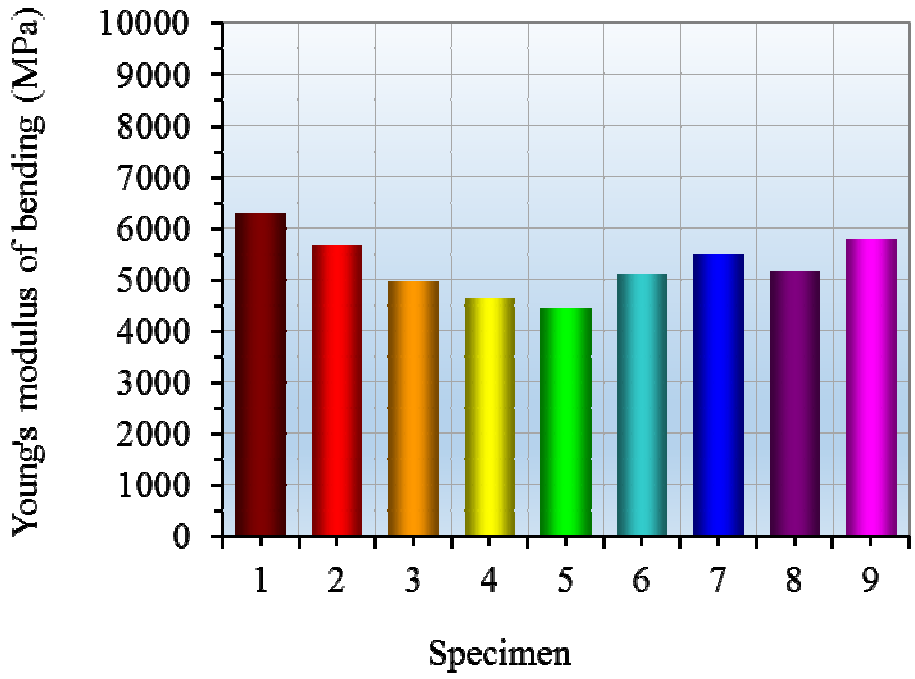

Fig. 6.13. Young's modulus of bending distribution of five layers Heliopol/Stratimat300 composite laminate

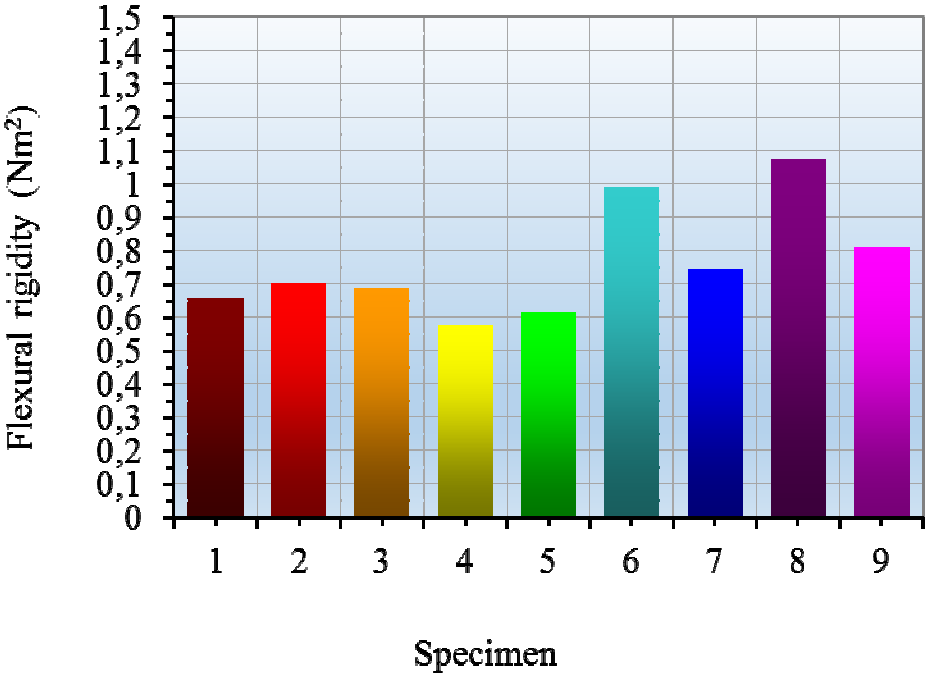

Fig. 6.14. Flexural rigidity distribution of five layers Heliopol/Stratimat300 composite laminate

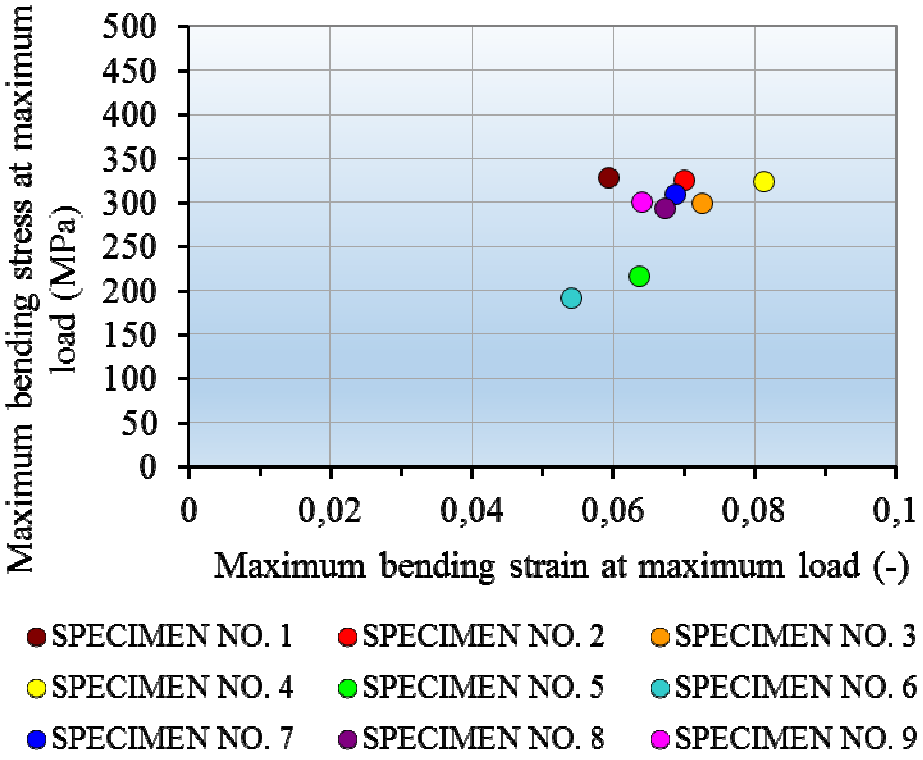

Fig. 6.15. Maximum bending stress at maximum load distribution of five layers Heliopol/Stratimat300

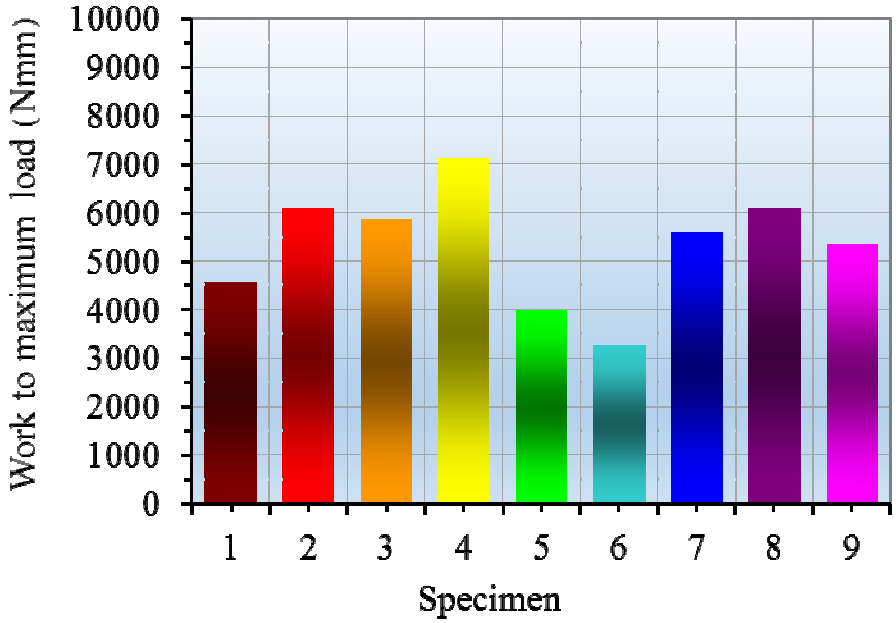

Fig. 6.16. Work to maximum load distribution of five layers Heliopol/Stratimat300 composite laminate

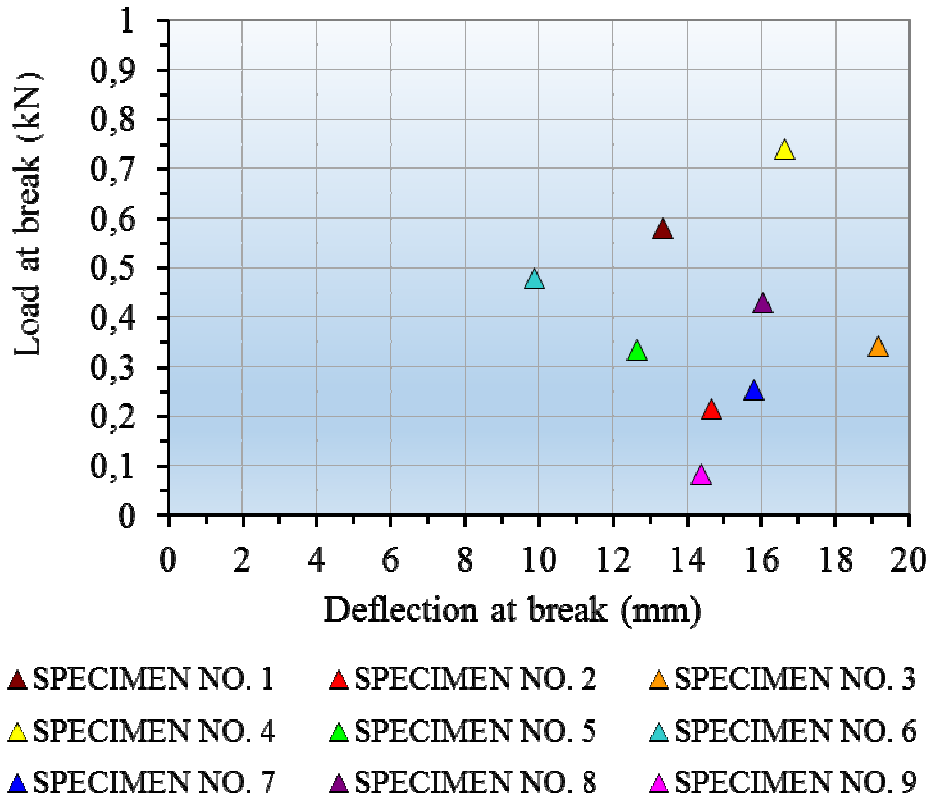

Fig. 6.17. . Load-deflection at break distribution of five layers Heliopol/Stratimat300 composite laminate

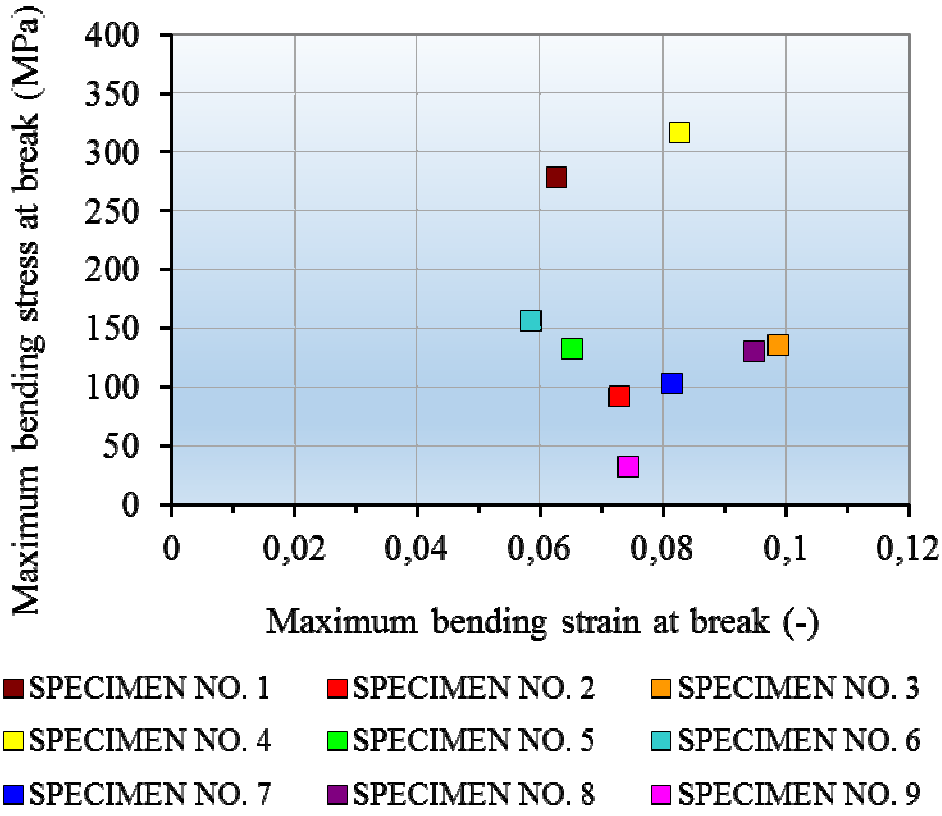

Fig. 6.18. Maximum bending stress at break distribution of five layers Heliopol/Stratimat300

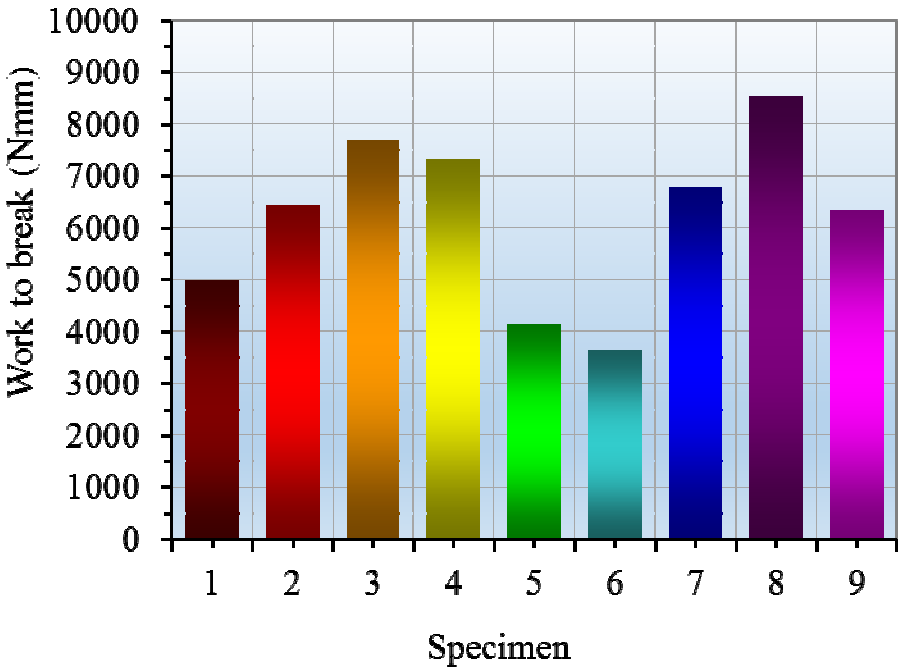

Fig. 6.19. Work to break distribution of five layers Heliopol/Stratimat300 composite laminate

Chapter 7

Contributions to the experimental characterization of a new advanced sandwich composite with twill weave carbon and EPS

7.1. Introduction

Following researches present the most important mechanical properties that I have determined in a simple tensile test on a 0.4 mm thickness 2/2 carbon twill weave fabric impregnated with epoxy resin, used as skins for an advanced ultralight sandwich composite structure with expanded polystyrene (EPS) as core. The sandwich panel developed at Compozite Ltd., Brasov, has been subjected to flexural load-unload tests. This kind of fabric presents very good drapeability and is suitable to reinforce a quite large range of epoxy resins. The aim of using this fabric is to obtain thin structures with complex shapes and high stiffness for the automotive industry. A comparison with a sandwich structure with EWR-300 glass fabric/epoxy resin skins has been accomplished. Due to its high stiffness, the twill weave carbon fabric is used as skins in large sandwich structures even with low stiffness cores. The flexural load-unload tests show an outstanding stiffness of the whole sandwich panel. Various specimens' thickness have been used. Latest researches have been published in one issue of *Journal of Optoelectronics and Advanced Materials (J OPTOELECTRON ADV M)* in 2013 [41]. Previous researches in this field have been published between 2006 – 2010 in references [13], [30], [61].

7.2. Scientific context

Carbon fibers-reinforced epoxy resins are used extensively to build composite structures with an outstanding specific weight/strength ratio. Such structures, usually called laminates, present a relative poor tensile stiffness and the flexural stiffness remains at a low level due to low sensitivity at flexural loads of the carbon fibers, especially of the unidirectional reinforced ones [10], [24], [79]. A method to increase a little bit this flexural stiffness is the use of a large variety of fabrics as reinforcing material. A common fabric is a so called twill weave. The main feature of this weave is that the warp and the weft threads are crossed in a programmed order and frequency, to obtain a flat appearance with a distinct diagonal line. A twill weave fabric needs at least three threads. More threads can be used for fabrics with high specific weight depending on their complexity [5], [20], [38]. After the plain weave, the twill is the second most common weave. It is often denoted as a fraction, for instance three twill weaves can be designated, in the following way:

- 2/1 in which two threads are raised and one is lowered when a weft thread is inserted;
- 2/2 in which two threads are raised and two are lowered when a weft thread is inserted;
- 3/1 in which three threads are raised and one is lowered when a weft thread is inserted.

The characteristic structure of the twill weave fabric makes it to present a very good dreapability. In general, composite laminates are manufactured from thin layers called laminae. These laminates present a quite low stiffness and flexural rigidity.

A solution to increase their stiffness could be the use of stiffening ribs [3], [80]. Not all constructive situations require built-in ribs. A solution could be the

increase of the layers but this leads to the disadvantage of increasing the overall weight as well as the resin and reinforcement consumption. A better solution to increase the overall stiffness of a composite laminate is to use a thin nonwoven polyester mat as core material embedded in the structure [28]. This core of non-continuous and nonwoven mat presents the advantage to absorb the excessive resin. A composite laminate with this kind of embedded core material presents following main advantages: weight saving, stiffness increase, quick build of the structure's thickness, saving of resin and reinforcement as well as an increased possibility to obtain a better surface finish when it is applied against the "gelcoat". This mat when is impregnated with resin presents high drapeability being suitable for complex shapes and for hand lay-up and spray-up processes.

Unidirectional carbon fibers-reinforced composite laminates have been experimentally characterized subjecting them to tensile loads. These latest results are presented in reference [15].

7.3. Materials and experimental procedure

The sandwich presents two carbon/epoxy skins reinforced with 300 g/mm^2 twill weave carbon fabric and an expanded polystyrene (EPS) 9 mm thick core with a density of 30 kg/m^3 (Fig. 7.1). The final thickness of the structure is 10 mm. Other input data are [30]:

- structure's thickness: 10 mm;
- skins' plies number: two;
- thickness of each ply: 0.175 mm;
- skins thickness: 0.35 mm;
- core thickness: 9 mm;
- fibers' disposal angle of each ply: 90° and 0°;

- fibers' volume fraction of each ply: 56%.

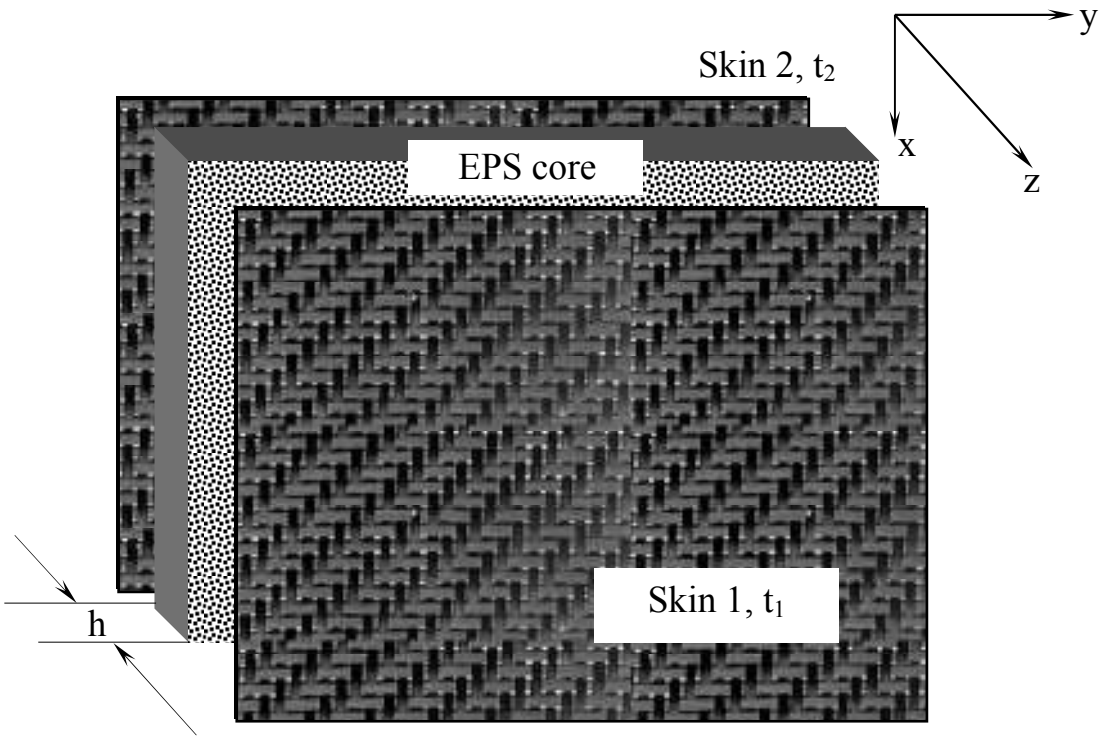

Fig. 7.1. The architecture of sandwich structure

The data regarding the structure's features are presented below:

- skins reinforcement: HM carbon fibers;
- fabric type: twill weave;
- fibers' specific weight: 0.3 kg/m^2;
- matrix type: epoxy resin;
- core's type: expanded polystyrene.

Other useful data are:

- core density: 30 kg/m^3;
- core Young's modulus: 30 MPa;
- core Poisson's ratio: 0.35;
- core shear modulus: 11 MPa;
- fibers' Young's modulus in longitudinal direction: 540 GPa;
- fibers' Young's modulus in transverse direction: 27 GPa;
- fibers' Poisson's ratio: 0.3; fibers' shear modulus: 10.38 GPa;

- matrix Young's modulus: 3.5 GPa; matrix Poisson's ratio: 0.34;
- matrix shear modulus: 1.42 GPa.

During the flexural tests of the sandwich panel, following experimental determinations have been accomplished:

- Two flexural load-unload tests of the sandwich panel clamped on contour (Fig. 7.2);
- One simple three-point bend test (load-unload) of the sandwich panel supported linearly on two opposite edges (Fig. 7.3).

Fig. 7.2. Flexural load-unload test detail. Sandwich panel clamped on contour

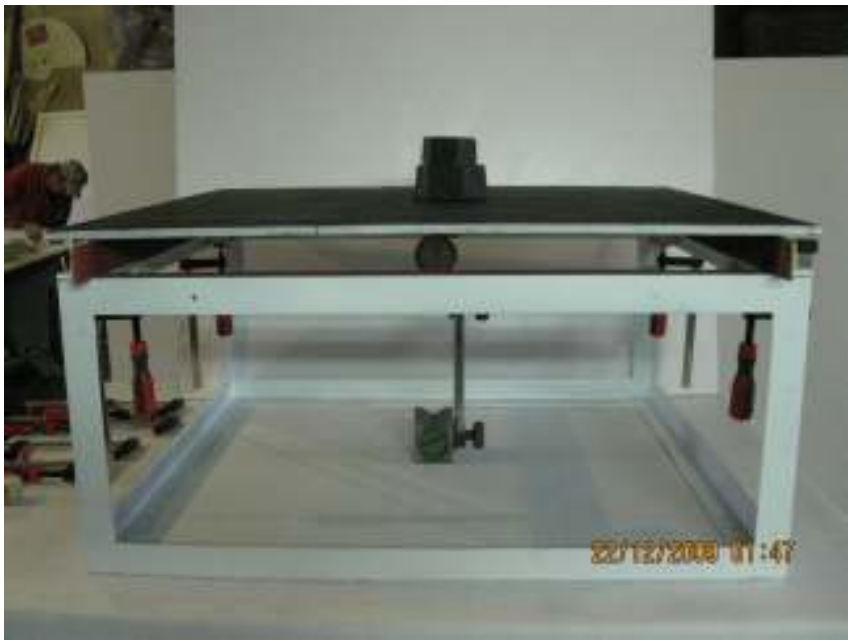

Fig. 7.3. Three-point bend load-unload test detail. Sandwich panel supported linearly on two opposite edges

The loads are applied in the middle of the panel and a displacements' measuring device has been placed under panel at its center. The tensile test on one layer 2/2 twill weave carbon fabric impregnated with epoxy resin has been accomplished on a "LR5K Plus" materials testing machine produced by Lloyd Instruments (Fig. 7.4). The testing machine presents the following characteristics:

- Force range: 5 kN;
- Speed accuracy: <0.2%;
- Load resolution: <0.01% from the load cell used;
- Analysis software: NEXYGEN Plus.

The features of the 2/2 twill weave carbon fabric is presented below:

- Fabric type: twill weave;
- Fibres type: HM carbon;
- Fabric specific weight: 300 g/m^2;
- Type of resin impregnation: epoxy resin;
- Impregnation process: vacuum bag molding;
- Impregnation resin: epoxy;

- Fabric thickness: 0.4 mm.

Fig. 7.4. Tensile test detail on an epoxy impregnated 2/2 twill weave carbon fabric

7.4. Experimental results and conclusions

The specimen has been subjected to a test speed of 1 mm/min and the length between extensometer's lamellae is 50 mm. The tensile test results on an epoxy impregnated 2/2 twill weave carbon fabric are presented in Table 7.1. Following main features have been determined: Stiffness; Young's modulus; Load at Maximum Load; Stress at Maximum Load; Extension from preload at Maximum Load; Strain at Maximum Load; Load at Maximum Extension; Stress at Maximum Extension; Extension from preload at Maximum Extension; Strain at Maximum Extension; Load at Minimum Load; Stress at Minimum Load; Extension from preload at Minimum Load; Strain at Minimum Load; Load at Minimum Extension; Stress at Minimum Extension; Extension from preload at Minimum Extension; Strain at Minimum Extension; Tensile Strength; Extension at Maximum Load;

Extension at Maximum Extension; Extension at Minimum Load; Extension at Minimum Extension; Load at Break; Stress at Break.

Force-deflection distributions of various loading-unloading cycles are presented in Figs. 7.5 – 7.7. Various specimens with different thickness (10, 20, 30 and 40 mm) have been manufactured and subjected to three-point bend tests until break occurs. Force-deflection distributions of these specimens are presented in Figs. 7.8 – 7.11.

Table 7.1. Tensile test results on an epoxy impregnated 2/2 twill weave carbon fabric

Characteristics	Value
Length between extensometer's lamellae (mm)	50
Preload stress (kN)	0.0056
Preload speed (mm/min)	21
Test speed (mm/min)	1
Fabric width (mm)	18.5
Fabric thickness (mm)	0.4
Stiffness as ratio between load and extension (N/m)	5785656.99
Young's modulus (Mpa)	31273.82
Load at maximum load (kN)	1.92
Stress at maximum load (MPa)	207.61
Strain at maximum load (-)	0.009
Strain at maximum extension (-)	0.344
Strain at minimum load (-)	0.087
Load at break (kN)	1.919
Stress at break (MPa)	207.55
Strain at break (-)	0.009
Tensile strength (MPa)	207.61

Due to the non-linear behavior of the carbon fibers subjected to tensile loads, the stress-strain as well as the load-extension distributions of an epoxy impregnated 2/2 twill weave carbon fabric subjected to tensile loads follows the same non-linear behavior. Due to its high stiffness and good dreapeability the epoxy impregnated 2/2 twill weave carbon fabric can be used as skins in large sandwich panels even with low stiffness cores, with applications in the automotive industry.

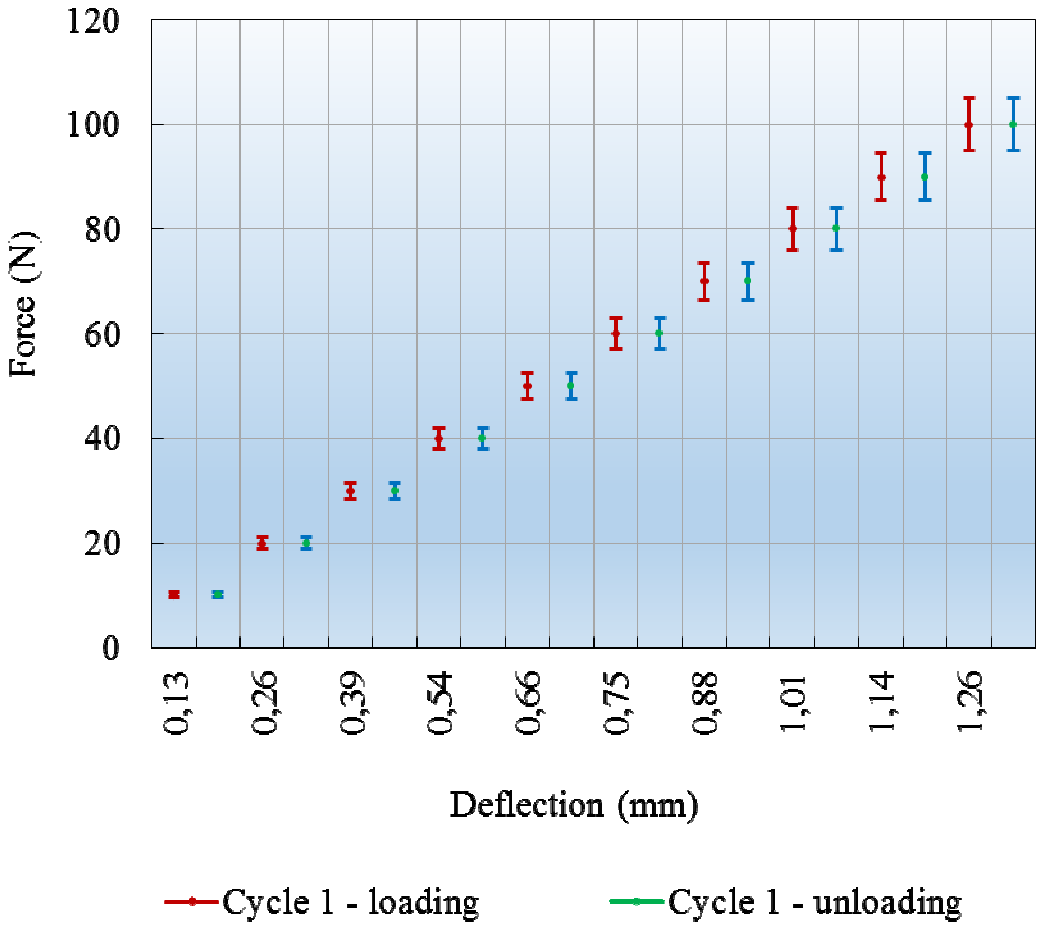

Fig. 7.5. Flexural test of the sandwich panel clamped on contour. Cycle 1 loading-unloading

Carbon fibers are suitable to fit special structures and devices for the future car due to their excellent thermal and electric conductivity. The comparison between the flexural rigidity of the structure obtained experimentally and that

obtained through the theoretical approach shows a good agreement between the experimental data and the theoretical approach.

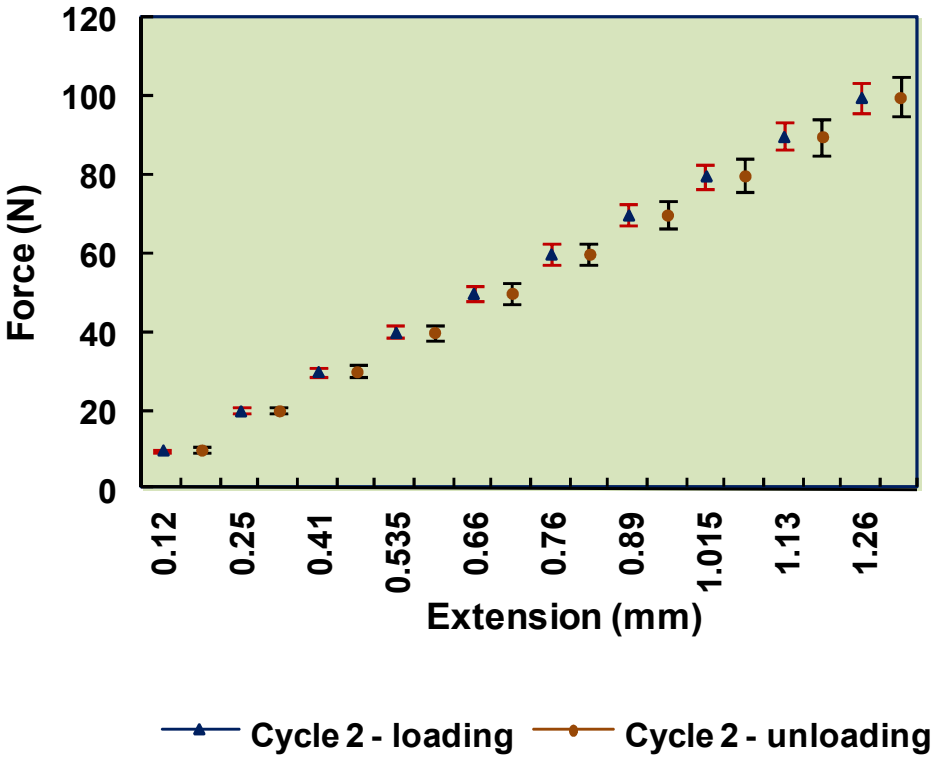

Fig. 7.6. Flexural test of the sandwich panel clamped on contour. Cycle 2 loading-unloading

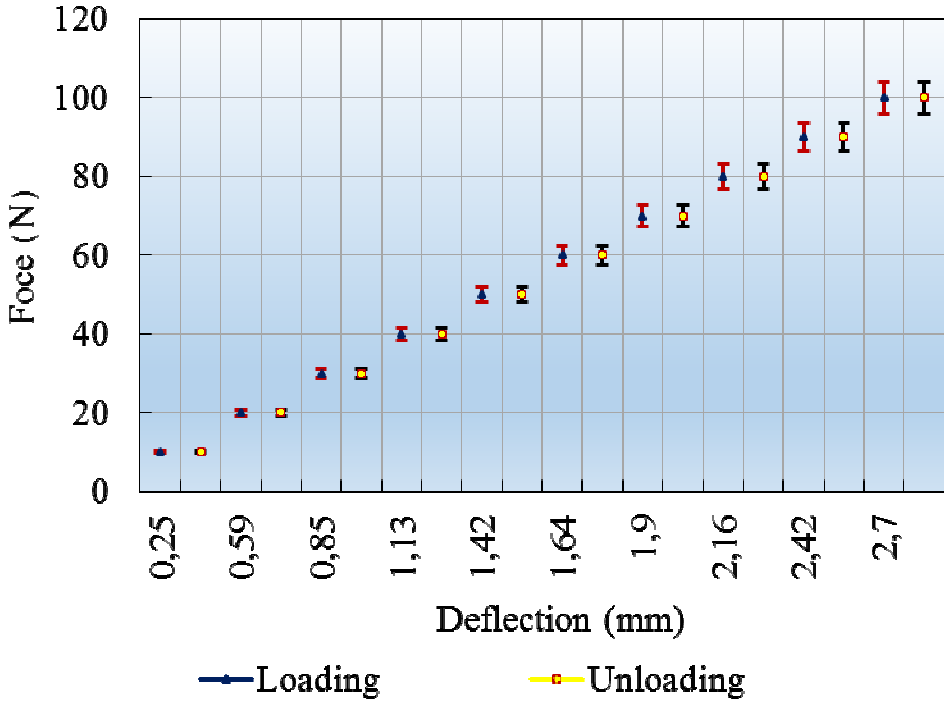

Fig. 7.7. Three-point bend test of the sandwich panel supported linearly on two opposite edges

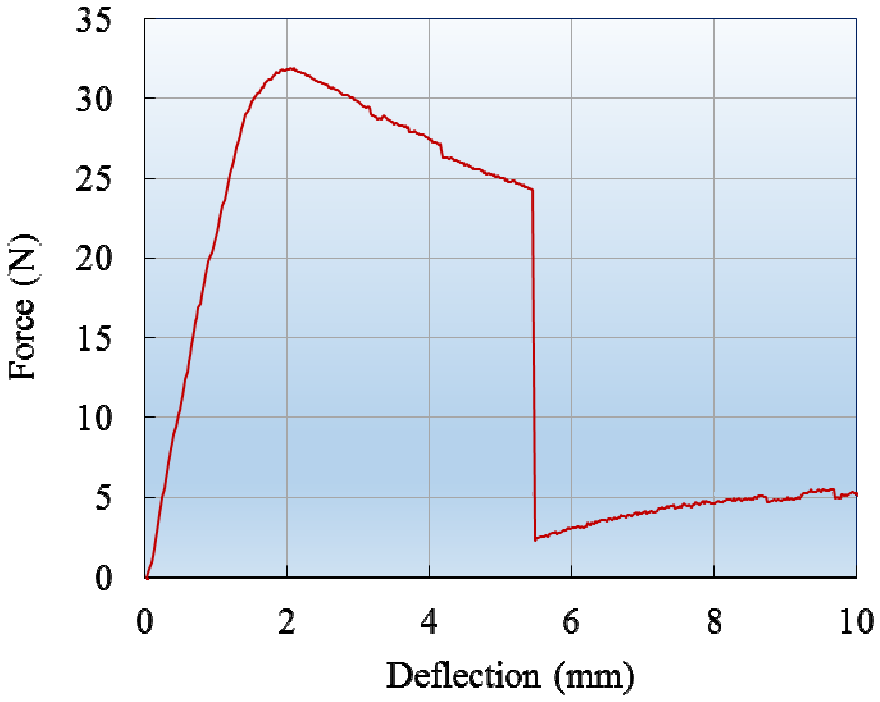

Fig. 7.8. Force-deflection distribution on 10 mm thickness specimen subjected to three-point bend test

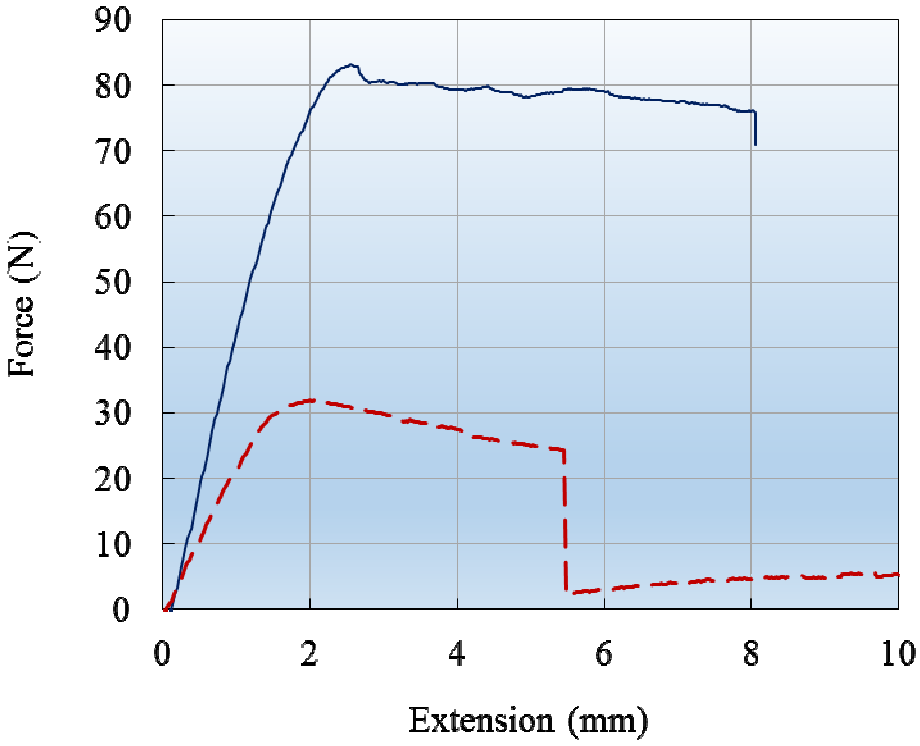

Fig. 7.9. Force-deflection distribution on 20 mm thickness specimen subjected to three-point bend test

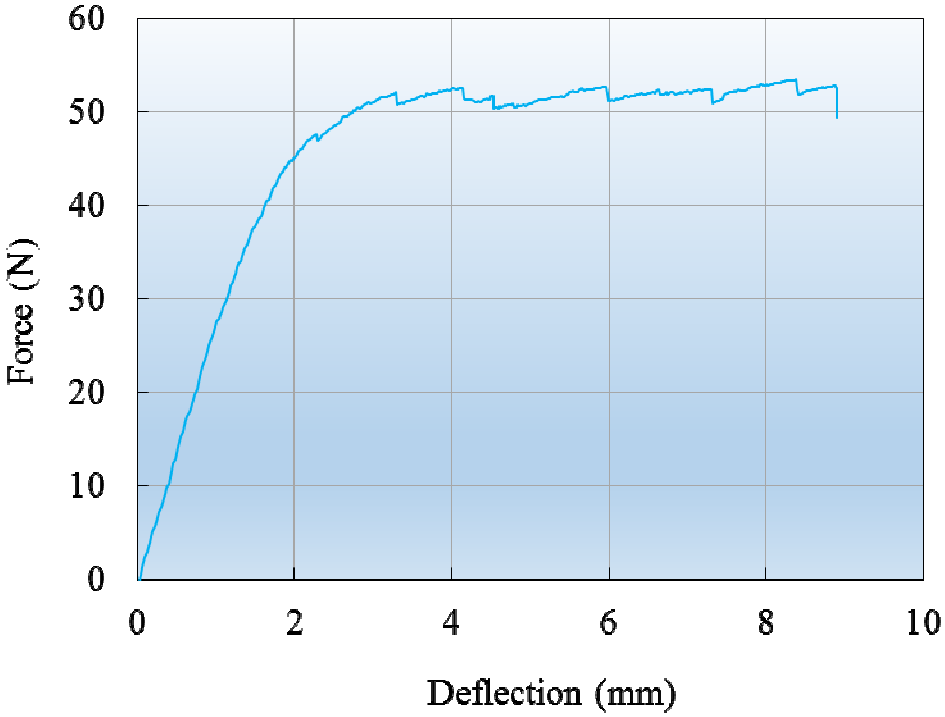

Fig. 7.10. Force-deflection distribution on 30 mm thickness specimen subjected to three-point bend test

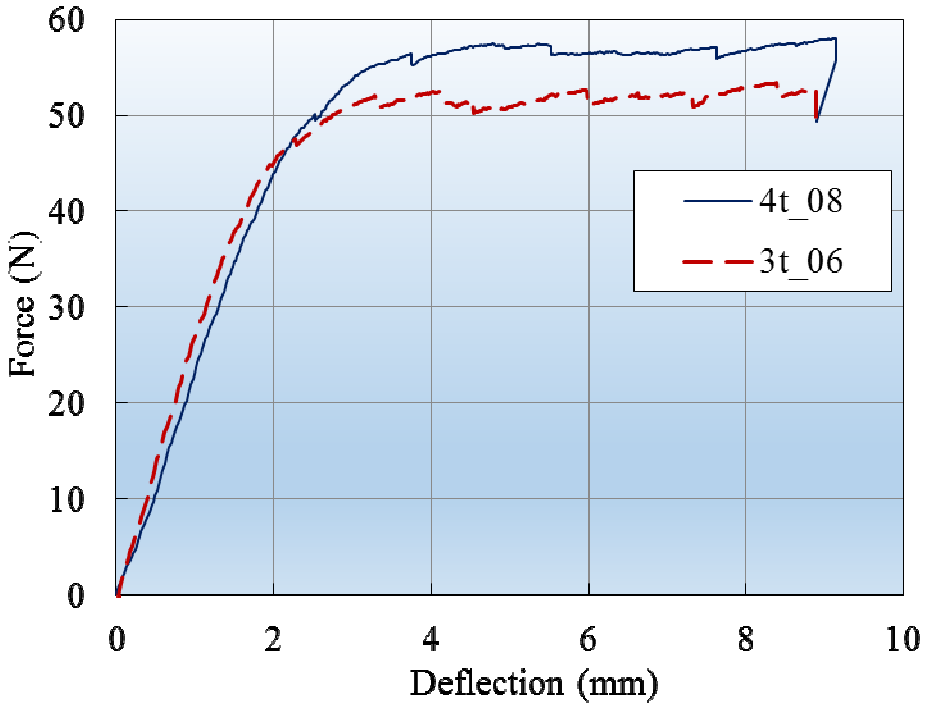

Fig. 7.11. Comparison between force-deflection distributions on 30/40 mm thickness specimens subjected to three-point bend tests

Conclusions

- The sandwich structure with two carbon/epoxy skins reinforced with a 300 g/m^2 twill weave fabric and an expanded polystyrene (EPS) 9 mm thick core with a density of 30 kg/m^3, fulfils following special requirements:
  - Panel dimensions: 10 × 2350 × 4070 mm;
  - Overall weight: maximum 10 kg.
- The sandwich structure's strains with skins based on twill weave carbon fabric reinforced epoxy resin are comparable with those of the structure with skins based on EWR-300 glass fabric/epoxy resin;
- Stresses in fibers direction in case of the sandwich structure with carbon fabric/epoxy resin reinforced skins, are up to six times higher than those existent in EWR-300 glass fabric/epoxy resin skins;
- Stresses transverse to the fibers direction in case of the sandwich structure with carbon fabric/epoxy resin reinforced skins are 20% lower than those existent in EWR-300 glass fabric/epoxy resin skins;
- The shear stresses in carbon fabric/epoxy resin reinforced skins' plies are almost identical with those existent in EWR-300 glass fabric/epoxy resin skins' plies;
- The core stresses are almost zero, so the loading is taken over exclusively by skins;
- Using a 9 mm thick expanded polystyrene core (EPS) the stiffness of the sandwich structure with carbon fibers reinforced epoxy resin skins is more than ten times higher than the skins' plies stiffness.

Chapter 8

Professional and academic achievements

In 1985 I graduated from Transilvania University of Brasov, Faculty of Technology of Machine Construction.

In 2001 I was granted the title of Ph.D. in Sciences, field of Mechanical Engineering, after defending the thesis: "Contributions to the increase of loading capability of fibers-reinforced polymer matrix composite tubes by introducing supplementary internal stresses", during the May 5th 2001 meeting at Mechanical Engineering Faculty, Department of Strength of Materials and Vibrations, Transilvania University of Brasov.

I began my professional career at IMASA Sf. Gheorghe plant in 1985. Between 1987 and 2000 I was Main Technologist Engineer 3rd rank at the research institute ICDEM Bucharest. Between 2000 and 2002 I worked as Design Manager at SC METALOPLAST SA Brasov. At COMPOZITE Ltd., Brasov I followed my activity as Quality Manager between 2002 and 2005.

I began my academic career as Assistant Professor in Department of Mechanics, Faculty of Mechanical Engineering within Transilvania University of Brasov. Currently, I am Associate Professor and also hold the position of Secretary of Scientific Committee of the Senate of Transilvania University of Brasov. Since 2007 I am member of Romanian Strain Gages Measurements Association (ARTENS) and member of Romanian Cracking Mechanics Association (ARMR).

Regarding the teaching activities, currently I am the course coordinator of Experimental Methods in Mechanical Engineering at the Department of Mechanical Engineering (Licence studies in Romanian), the seminar coordinator of Theoretical Mechanics (Kinematics and Dynamics) at the Department of Automotive and Transport within Faculty of Mechanical Engineering (Licence

studies in English), as well as the course coordinator of Advanced Notions of Dynamic Systems (Master of Science studies, in Romanian).

I am the coordinator of Materials Testing Laboratory from the Department of Mechanical Engineering where usually there are practical seminars for students both at Licence and Master of Science studies as well for PhD students.

As first author I have published two books: *Basics and Mechanics of Polymer Matrix Composite Materials*, Transilvania University of Brasov Publishing House, 2007, ISBN 978-635-878-4 (178 pgs.) and *Mechanics of Composite Materials*, Transilvania University of Brasov Publishing House, 2013, ISBN 978-606-19-0300-9 (252 pgs.) and 41 articles at international level: 4 articles published in ISI indexed journals with impact factor, 16 articles in ISI indexed proceedings, 2 articles in BDI indexed journals, 4 articles in BDI indexed proceedings, 19 articles published in proceedings issued for symposiums and conferences.

Regarding my research activity, I have been involved in 22 research projects in the field of polymer matrix composite materials, with following positions:

- Execution in 1 international research project by competition, on behalf Compozite Ltd., Brasov for Competitive and Sustainable Growth Programme/CRAF-1999-71564, Contract No. G5ST-CT-2002-50329.
- Project manager in 2 national research projects by competition, on behalf Compozite Ltd., Brasov, for program INVENT, project STAR2 (contract 171/10.2004) and on behalf SC INAR SA Brasov for program POSCCE, priority axis 2, operation 2.1.1, project no. 1132/code SMIS: 35420 (contract 379/16.01.2012).
- Project responsible in 3 national research projects by competition on behalf Transilvania University of Brasov, program CEEX, project SICOMSUV (contract 129/2006) and program INOVARE, projects SISCOMP (contract 218/2008) and MARECICLA (contract 267/2008).
- Project responsible in 1 national research project by competition on behalf Compozite Ltd., Brasov for program CEEX, project ROBOSIS (contract

41/2005).

- Researcher in 6 national research projects by competition on behalf Transilvania University of Brasov for program CEEX, projects: COMPMEF (contract 42/2005), CAMCOM (contract 23/2006), MECPMC (contract 35/2006), IMAGID (contract 212/2006), ADEL (contract 61/2006), PROECO (contract 220/2006).
- Execution in 9 national research projects by competition on behalf Compozite Ltd., Brasov for program RELANSIN, project SIRTEM (contract 1795/17.09.2003), program CEEX, projects: DITEH (contract 191/2006), CAFICMEIS (contract 240/2006), MOSCOM (contract 202/2006), program CEEX-AMTRANS, project COMPAS (contract X1C05/2005), program CNMP-P4, projects: MAVIAT (contract 71-125/2007), NANOAERO (contract 71-027/2007), SISUAR (contract 81-020/2007), SUPERSOLID (contract 71 – 001/2007).

Between 2002 and 2008 I have participated at following specializations and qualifications:

- Specialization firm WOLFANGEL GmbH Germany, 2002, in the field of technology of polymer matrix composite materials.
- Specialization firm GOM GmbH Germany, 2007, in the field of optical measurement techniques.
- Participation at "Computational and Experimental Mechanics of Advanced Materials" course, CISM, Udine, Italy, 2008.

As coauthor I have two patents abstracts published in the Official Bulletin of Industrial Property as well as at international level:

- Patent title: "Carbon-hemp hybrid composite material and its process for the application in the automotive and engineering" (CBI_A_00297_11.04.13_Rez_BOPI_4_2014__Espacenet14_SCUTARU_ML_sa.pdf; http://worldwide.espacenet.com/publicationDetails/biblio?DB=worldwide.es

pacenet.com&II=3&ND=3&adjacent=true&locale=en_EP&FT=D&date=20140430&CC=RO&NR=129354A0&KC=A0)

- Patent title: "Composite material based on COREMAT used in the construction of underground shelters and auto parts" (CBI_A_00401_24.05.13__Rez_BOPI_8_2014__Espacenet14_PurcareaR_sa.pdf; http://worldwide.espacenet.com/publicationDetails/biblio?DB=worldwide.espacenet.com&II=1&ND=3&adjacent=true&locale=en_EP&FT=D&date=20140829&CC=RO&NR=129712A0&KC=A0)

I hold the Inovator Certificate No. 454 / 04.11.1988 released by Romanian Defense Department. The innovation was registered at 04.11.1988 at UM 02550 S, Bucharest.

Regarding the activity for editorial and/or scientific boards representing publications and scientific conferences, I will mention the following:

- Member in organizing committee of following conferences: 7th WSEAS International Conference on Non-Linear Analysis, Non-Linear Systems and Chaos (NOLASC'08) Corfu Island, Greece, October 26-28, 2008; 2nd Int. Conf. "Advanced Composite Materials Engineering" COMAT 2008, 9-11 October 2008, Transilvania University of Brasov, Romania; 3rd International Conference "Computational Mechanics and Virtual Engineering" COMEC 2009, Transilvania University of Brasov, Romania, 29-30 October, 2009; 3rd Int. Conf. "Advanced Composite Materials Engineering" COMAT 2010, 27-29 October 2010, Transilvania University of Brasov, Romania; 4th Int. Conf. "Computational Mechanics and Virtual Engineering" COMEC 2011, Transilvania University of Brasov, Romania, 20-22 October, 2011; 5th Int. Conf. "Computational Mechanics and Virtual Engineering" COMEC 2013, Transilvania University of Brasov, Romania, 24-25 October, 2013; 5th International Conference "Advanced Composite Materials Engineering" COMAT 2014, Transilvania University of Brasov, Romania, 16-17 October, 2014.

Total number of citations: 18 – from which:

- 5 citations as first author in references:
  - [45] (1 citation in: Scutaru, M.L., Baba, M., Investigation of the mechanical properties of hybrid carbon-hemp laminated composites used as thermal insulation for different industrial applications, *Advances In Mechanical Engineering*, article number 829426, published: 2014, http://dx.doi.org/10.1155/2014/829426),
  - [46] and [47] (4 citations in: Niculita, C., Mechanical behavior of epoxy 1050_GBX300L-1250 glass fabric laminates subjected to three-point bend tests, *Optoelectronics And Advanced Materials-Rapid Communications*, Vol. 6, Issue3-4, p. 487-490, published: MAR-APR 2012,

http://oam-rc.inoe.ro/index.php?option=magazine&op=view&idu=1860&catid=71; Niculita, C., Mechanical behavior of carbon fibre-reinforced epoxy/plain200 prepregs subjected to three-point bend tests, *Optoelectronics And Advanced Materials-Rapid Communications*, Vol. 6, Issue3-4, p. 504-507, published: MAR-APR 2012,

http://oam-rc.inoe.ro/index.php?option=magazine&op=view&idu=1864&catid=71).

- 13 citations as coauthor in references:
  - [15] (1 citation in: Scutaru, M.L., Toward the use of irradiation for the composite materials properties improvement, *Journal Of Optoelectronics And Advanced Materials*, Vol. 16, Issue 9-10, p. 1165-1169, published: SEP-OCT 2014,

http://joam.inoe.ro/index.php?option=magazine&op=view&idu=3568&catid=86),

  - [25] (3 citations in: Scutaru, M.L., Toward the use of irradiation for the composite materials properties improvement, *Journal Of Optoelectronics And Advanced Materials*, Vol. 16, Issue 9-10, p. 1165-1169, published: SEP-OCT 2014,

http://joam.inoe.ro/index.php?option=magazine&op=view&idu=3568&catid=86;

Scutaru, M.L., Baba, M., Baritz, M.I., Irradiation influence on a new hybrid hemp bio-composite, *Journal Of Optoelectronics And Advanced Materials*, Vol. 16, Issue 7-8, p. 887-891, published: JUL-AUG 2014, http://joam.inoe.ro/index.php?option=magazine&op=view&idu=3524&catid=85;

Wang Baogang, Wang Xu, Zhou, Jixue, et. al., Modification effects of as cast Mg-Al-Si magnesium alloy with strontium, *Optoelectronics And Advanced Materials-Rapid Communications*, Vol. 8, Issue 1-2, p. 63-67, published: JAN-FEB 2014, http://oam-rc.inoe.ro/index.php?option=magazine&op=view&idu=2240&catid=82),

- [81] (2 citations in: Scutaru, M.L., Toward the use of irradiation for the composite materials properties improvement, *Journal Of Optoelectronics And Advanced Materials*, Vol. 16, Issue 9-10, p. 1165-1169, published: SEP-OCT 2014, http://joam.inoe.ro/index.php?option=magazine&op=view&idu=3568&catid=86;

Scutaru, M.L., Baba, M., Baritz, M.I., Irradiation influence on a new hybrid hemp bio-composite, *Journal Of Optoelectronics And Advanced Materials*, Vol. 16, Issue 7-8, p. 887-891, published: JUL-AUG 2014, http://joam.inoe.ro/index.php?option=magazine&op=view&idu=3524&catid=85),

- [83] (5 citations in: Scutaru, M.L., Toward the use of irradiation for the composite materials properties improvement, *Journal Of Optoelectronics And Advanced Materials*, Vol. 16, Issue 9-10, p. 1165-1169, published: SEP-OCT 2014, http://joam.inoe.ro/index.php?option=magazine&op=view&idu=3568&catid=86;

Scutaru, M.L., Baba, M., Baritz, M.I., Irradiation influence on a new hybrid hemp bio-composite, *Journal Of Optoelectronics And Advanced Materials*, Vol. 16, Issue 7-8, p. 887-891, published: JUL-AUG 2014,

http://joam.inoe.ro/index.php?option=magazine&op=view&idu=3524&catid=85; Scutaru, M.L., Baba, M., Investigation of the mechanical properties of hybrid carbon-hemp laminated composites used as thermal insulation for different industrial applications, *Advances In Mechanical Engineering*, article number 829426, published: 2014, http://dx.doi.org/10.1155/2014/829426; Niculita, C., Mechanical behavior of epoxy 1050_GBX300L-1250 glass fabric laminates subjected to three-point bend tests, *Optoelectronics And Advanced Materials-Rapid Communications*, Vol. 6, Issue3-4, p. 487-490, published: MAR-APR 2012, http://oam-rc.inoe.ro/index.php?option=magazine&op=view&idu=1860&catid=71; Niculita, C., Mechanical behavior of carbon fibre-reinforced epoxy/plain200 prepregs subjected to three-point bend tests, *Optoelectronics And Advanced Materials-Rapid Communications*, Vol. 6, Issue3-4, p. 504-507, published: MAR-APR 2012, http://oam-rc.inoe.ro/index.php?option=magazine&op=view&idu=1864&catid=71),

- [84] (2 citations in: Niculita, C., Mechanical behavior of epoxy 1050_GBX300L-1250 glass fabric laminates subjected to three-point bend tests, *Optoelectronics And Advanced Materials-Rapid Communications*, Vol. 6, Issue3-4, p. 487-490, published: MAR-APR 2012, http://oam-rc.inoe.ro/index.php?option=magazine&op=view&idu=1860&catid=71; Niculita, C., Mechanical behavior of carbon fibre-reinforced epoxy/plain200 prepregs subjected to three-point bend tests, *Optoelectronics And Advanced Materials-Rapid Communications*, Vol. 6, Issue3-4, p. 504-507, published: MAR-APR 2012, http://oam-rc.inoe.ro/index.php?option=magazine&op=view&idu=1864&catid=71).

Part (B-ii)

The evolution and development plans for career development

Directions of scientific research

As previous shown, my research activity belongs to the field of mechanics of fibers-reinforced polymer matrix composites, focused mainly both on theoretical and experimental approaches. These approaches cover following issues:

Theoretical approaches

1. Tensile behavior and prediction of elastic properties of pre-impregnated composite materials;
2. Simulations of elastic properties of fibers-reinforced laminates under off-axis loading system;
3. Thermo-mechanical behavior of fibers-reinforced laminates subjected to temperature and humidity variations;
4. Damping's analysis of a twill weave carbon/epoxy fabric;

Experimental approaches

1. Hysteresis effect in a three-phase polymer matrix composite subjected to static cyclic loadings;
2. Experimental characterization of polyester and epoxy/glass fibers-reinforced laminates;
3. Experimental characterization of a new advanced sandwich composite with twill weave carbon and EPS.

Regarding the theoretical approaches focused on tensile behavior and prediction of elastic properties of pre-impregnated composite materials, following directions of scientific research will be carried out:

- Determination of replacement matrix' Young's modulus in case of fibers-reinforced polymer matrix composites with more than three compounds, using various averaging methods and rules of mixture.
- Development of computing models regarding the longitudinal tensile behavior of multiphase composite materials with various fibers lengths.

- Predictions of elastic properties of pre-impregnated composite materials with various periodicity cells or representative volume elements (RVEs) in connection with fibers volume fractions.
- Determination of upper and lower limits of the homogenized coefficients for various prepregs and fibers volume fractions using various averaging methods.

Regarding the elastic properties of fibers-reinforced laminates under off-axis loading system and subjected to complex loadings, I have in mind to cover following research issues:

- Development of a data base that include various fibers-reinforced laminates and the prediction of their elastic properties simulating the action of some complex loadings on their mechanical behavior.
- Determination of matrix strain increase factor for various unidirectional fibers-reinforced laminae subjected to transverse tensile loadings and with various shapes of disposed fibers.
- Determination of some mathematical expressions to simulate basic experimental tests (tensile and bending) on various fibers-reinforced composite laminates.

Regarding the thermo-mechanical behavior of fibers-reinforced laminates I will focus on:

- Determination of mathematical expressions to simulate the temperature distributions versus time of various fibers-reinforced polymer matrix composites.

Regarding the experimental approaches, future researches will be focused on following issues:

- Determination of glass transition temperature for various types of resins and fibers as well as for fibers-reinforced polymer matrix composite laminates using the Differential Scanning Calorimetry (DSC) method. Development of a data base.

- Experimental characterization (tensile, three and four-point bend tests) of bio-composites reinforced with various natural fibers. Development of a data base.
- Stiffness evaluation of ultralight composite structures including sandwich structures with various types of cores and skins. Development of a data base.
- Three and four-point bend tests on thermoplastic honeycomb structures with various cell sizes and thickness. Development of a data base.
- Compression tests of ultralight sandwich structures and cores as well as the determination of some patterns regarding the cores' failure modes. Development of a data base.
- Determination of hysteresis effect in various fibers-reinforced polymer matrix composite laminates subjected to static tensile-compression cyclic loadings at various test speeds and cycle limits. Development of a data base.
- Determination of hysteresis effect in various fibers-reinforced polymer matrix composite laminates subjected to static three and four-point bending cyclic loadings at various test speeds and cycle limits. Development of a data base.
- Development of new composite structures with a wide range of applications in cooperation with Compozite Ltd., Brasov and their mechanical characterization.
- Development of new devices for the existing materials testing machines within Department of Mechanical Engineering used for mechanical characterization of fabrics and yarns.
- Development of new devices to be used for static three and four-point bending cyclic tests of various fibers-reinforced polymer matrix composite laminates.
- Development of new devices for the existing materials testing machines within Department of Mechanical Engineering used for mechanical

characterization of composite structures subjected to combined tensile/compression and torsion loadings.

- Determination of mechanical properties of composite tubes with and without liner for various applications subjected to compression loadings as well as their failure modes. Development of a data base.
- Stiffness, Young's modulus of bending and flexural rigidity evaluation of composite rings with and without liner subjected to three-point bending loads. Development of a data base.
- Development of new testing techniques for mechanical characterization of thin unidirectional fibers-reinforced composite laminae and ultrathin fabric-reinforced composite laminates.
- Determination of mechanical properties of thin unidirectional fibers-reinforced composite laminae and ultrathin fabric-reinforced composite laminates. Development of a data base.

Plans for the evolution and development in the professional and academic career

My activity tends to a continue progress of teaching centered on student to respond to the requirements of a true education, a perfect agreement to the quality standards governed at the university level and by the institutions of quality assurance in higher education, allowing our Mechanical Engineering graduates to acquire the necessary competences for the professional recognition and insertion into the economic environment.

In this sense I will follow the activities presented below:

- Implementation of modern technologies and methods of teaching and learning based on information technology to provide a comprehensive

training especially in practical applications in the Laboratory For Materials Testing within Department of Mechanical Engineering.

- Updating the laboratory facilities with new devices designed by PhD students that prepare their thesis in the field of mechanics of fibers-reinforced composite materials.
- Support and stimulation of students' research activity.
- Affiliation of young PhD students in research teams with experienced researchers to materialize their ideas.
- Promotion of a national and international recognized multidisciplinary research activity with solid theoretical and experimental background materialized in publication of scientific papers in journals with impact factor.
- Development of partnership agreements with firms, laboratories and universities to facilitate PhD students to participate at these research infrastructures.
- Participation at national and international conferences to sustain the research results of PhD students in the field of mechanics of composite materials.

Regarding the doctoral supervision I intend to do following activities:

- Affiliation to the Doctoral School of the Faculty of Mechanical Engineering within Transilvania University of Brasov.
- As a doctoral supervisor I will coordinate research topics in the field of mechanics of polymer matrix composites with applications in various industries focused on the scientific trend in this field.

The future development of academic career will be focused to fulfill the criteria of promotion to the rank of professor.

Being the beneficiary of a Christian education I am committed to a comprehensive education including both transmitting the necessary information and formation of moral skills in our students that help them throughout life. The

character of a man is all that matters. In my teaching activities I am guided by the following educational and moral principles:

- True education is based on simplicity. No evidence is as strong as the success based on simplicity.
- True education relies on the value of scientific knowledge but above information it values power; above power, goodness; above intellectual achievements it values a character. The economic environment does not so much need individuals of great intellect as of a great character. The labor market needs young men and women whose talents are controlled by consistent moral principles.
- True education means more than following a particular high school. Means more than a preparation for a specific task in a particular firm. It has to do with the whole being and the whole period in which is possible a man to live. It has to do with the harmonious development of the physical, mental and spiritual powers. It prepares the student for the joy of service in this world and for the higher joy of wider service in the world to come.

Part (B-iii)

References

References

1. J.D. Achenbach, *A Theory of Elasticity with Microstructure for Directionally Reinforced Composites*, Springer, (1975).
2. G. Allaire, *Shape Optimization by the Homogenization Method*, Springer, (2001).
3. B.F. Backman, *Composite Structures, Design, Safety and Innovation*, Elsevier Science, (2005).
4. N. Bakhvalov, G. Panasenko, *Homogenization. Averaging Processes in Periodic Media: Mathematical Problems in the Mechanics of Composite Materials*, Kluwer Academic Publishers, (1989).
5. L.C. Bank, *Composites for Construction: Structural Design with FRP Materials*, Wiley, (2006).
6. T.J. Barth, T. Chan, R. Haimes, *Multiscale and Multiresolution Methods: Theory and Applications*, Springer, (2001).
7. T.W. Clyne, P.J. Withers, *An Introduction to Metal Matrix Composites,* CUP (1993), pp. 280 – 282.
8. R.M. Christensen, *Theory of Viscoelasticity*, Dover Publications, (1990).
9. N.D. Cristescu, E.M. Craciun, E. Soos, *Mechanics of Elastic Composites*, Chapman & Hall/CRC, (2003).
10. I.M. Daniel, O. Ishai, *Engineering of Composite Materials*, Oxford University Press, 2nd ed., (2005).
11. G.W. Ehrenstein, *Techologie der Faserverbund-Kunststoffe*, Umdruck zur Vorlesung, Lehrstuhl für Kunststofftechnik, Universität Erlangen-Nürnberg, (1993).
12. H.I. Ene, G.I. Pasa, *The Homogenization Method. Applications at Composite Materials Theory*, Romanian Academy Publishing House, Bucharest, 1987 (in Romanian).
13. I. Goia, D. Rosu, S. Vlase, H. Teodorescu-Draghicescu, *Tensile and bending tests of an advanced ultra-lightweight sandwich composite structure*, Proc. of the 1st Int. Conf. "Advanced Composite Materials Engineering" COMAT 2006, 19 – 22 October (2006), Transilvania University of Brasov, ISBN 973-635-821-8, ISBN 978-973-635-821-0, pp. 195 – 201.
14. Y.M. Haddad, *Viscoelasticity of Engineering Materials*, Chapman and Hall, (1994).
15. T. Heitz, H. Teodorescu-Draghicescu, S. Lache, A. Chiru, M.R. Calin, *Advanced T700/XB3585 UD carbon fibers-reinforced composite*, Journal of Optoelectronics and Advanced Materials (J OPTOELECTRON ADV M), Vol. 16, Issue 5-6, (2014), INOE Publishing House, ISSN: 1454-4164, pp. 568 – 573.
http://joam.inoe.ro/index.php?option=magazine&op=view&idu=3474&catid=84
16. M. Hori, S. Nemat-Naser, *On Two Micromechanics Theories For Determining Micro-Macro Relations In Heterogeneous Solids*, Mechanics of Materials, 31, (1999), pp. 667 – 682.
17. D. Hull, T.W. Clyne, *An Introduction to Composite Materials*, CUP (1996).

18. V.V. Jikov, S.M. Kozlov, O.A. Oleynik, *Homogenization of Differential Operators and Integral Functions*, Springer, (1994).
19. H.G. Kia, *Sheet Molding Compounds. Science and Technology*, Hanser, (1993).
20. D.G. Lee, N.P. Suh, *Axiomatic Design and Fabrication of Composite Structures: Applications in Robots, Machine Tools and Automobiles*, Oxford University Press, (2005).
21. P.K. Mallick, *Fibre Reinforced Composite Materials. Manufacturing and Design*, Third Edition, CRC Press, Taylor & Francis Group, LLC, (2008).
22. C. Miehe, J. Schröder, M. Becker, *Computational Homogenization Analysis In Finite Elasticity: Material And Structural Instabilities On The Micro- And Macro-Scales Of Periodic Composites And Their Interaction*, Comput. Methods Appl. Mech. Eng. 191, (2002), pp. 4971 – 5005.
23. G. Milton, *The Theory of Composites*, Cambridge University Press, (2002).
24. D.B. Miracle, R.L. Donaldson, *ASM Handbook*, Vol. 21: Composites, ASM International, (2001).
25. A. Modrea, S. Vlase, H. Teodorescu-Draghicescu, M. Mihalcica, M.R. Calin, C. Astalos, *Properties of Advanced New Materials Used in Automotive Engineering*, Optoelectronics And Advanced Materials – Rapid Communications (OPTOELECTRON ADV MAT), Vol. 7, Issue 5-6, (2013), INOE Publishing House, ISSN: 1454-4164, pp. 452 – 455.
http://oam-rc.inoe.ro/index.php?option=magazine&op=view&idu=2107&catid=78
26. G. Niederstadt, *Ökonomischer und ökologischer Leichtbau mit Faserverstärkten Polymeren: Gestaltung, Berechnung und Qualifizierungen*, Renningen-Malmsheim, Expert Verlag, (1997).
27. A. Pavliotis, A. Stuart, *Multiscale Methods: Averaging and Homogenization*, Springer, (2008).
28. I. Pirna, Teodorescu-Draghicescu, S. Vlase, I. Candea, M.L. Scutaru, D.L. Motoc, A. Chiru, *Flexural rigidity evaluation of a new sandwich structure with nonwoven polyester mat*, Proc. of the 11th WSEAS Int. Conf. on Automatic Control, Modelling and Simulation (ACMOS'09), Istanbul Turkey, May 30 – June 1, (2009), Demiralp, M., Baykara, N.A., Mastorakis, N.E. (editors), ISBN: 978-960-474-082-6, ISSN: 1790-5117, WSEAS Press, pp. 234 – 239.
29. I. Pirna, H. Teodorescu-Draghicescu, S. Vlase, I. Candea, M.L. Scutaru, I. Enescu, I. Burca, *Elasticity evaluation of carbon and aramid fibre-reinforced laminates*, Proc. of the 11th WSEAS Int. Conf. on Automatic Control, Modelling and Simulation (ACMOS'09), Istanbul Turkey, May 30 – June 1, (2009), Demiralp, M., Baykara, N.A., Mastorakis, N.E. (editors), ISBN: 978-960-474-082-6, ISSN: 1790-5117, WSEAS Press, pp. 240 – 243.
30. D. Rosu, O. Pop, I. Goia, H. Teodorescu-Draghicescu, *Stiffness Evaluation of an Advanced Sandwich Composite Panel*, 3rd Int. Conf. Advanced Composite Materials Engineering COMAT 2010, 27-29 October (2010), Transilvania University of Brasov, Romania, Vol. 2, Eds. D. Bigoni, S. Vlase, A. Chiru, ISSN: 1844-9336, pp. 211 – 216.
31. D.A. Saravanos, C.C. Chamis, *Unified Micromechanics of Damping for Composite Plies*, Journal of Composite Technology and Research, 89-1191-CP, (1989).

32. A.B. Schultz, S.W. Tsai, *Measurement of Complex Dynamic Moduli for Laminated Fiber-Reinforced Composites*, Springer, (1975).

33. H. Schürmann, *Konstruiren mit Faser-Kunststoff-Verbunden*, Springer, (2007).

34. W. Schneider, *Wärmeausdehnungskoeffizienten und Wärmespannungen von Glasfaser/Kunststoff-Verbunden Aus Unidirektionalen Schichten,* Kunststoffe, Bd. 61, (1971), pp. 273 – 277.

35. Y. Setiadi, P.–Y.B. Jar, T. Kuboki, J.- J.R. Cheng, *Comparison of Damage Development in Random Fiber-Reinforced Polymers (FRPs) under Cyclic Loading*, J. of Comp. Mat., **40**, 1, (2006).

36. R.A. Shapery, *Thermal Expansion Coefficients of Composite Materials Based on Energy Principles*, Journal of Composite Materials, 2:280, (1968).

37. A. Stanciu, H. Teodorescu-Draghicescu, S. Vlase, M.L. Scutaru, M.R. Calin, *Mechanical Behavior of CSM450 and RT800 Laminates Subjected to Four-Point Bend Tests*, Optoelectronics and Advanced Materials – Rapid Communications (OPTOELECTRON ADV MAT), Vol. 6, Issue 3-4, (2012), INOE Publishing House, ISSN: 1842-6573, pp. 495 – 497.
http://oam-rc.inoe.ro/index.php?option=magazine&op=list&revid=71

38. A.B. Strong, *Fundamentals of Composites Manufacturing: Materials, Methods and Applications*, Society of manufacturing Engineers, 2nd ed., (2007).

39. T.F. Tan, C.K.H. Dharan, *Cyclic Hysteresis Evolution as a Damage Parameter for Notched Composite Laminates*, J. of Comp. Mat., **44**, 16, (2010).

40. F. Teodorescu, *Contributions Regarding the Modeling of Fiber Reinforced Composite Structures*, PHD thesis, Transilvania University of Brasov, (2001) (in Romanian).

41. H. Teodorescu-Draghicescu, M.L. Scutaru, D. Rosu, M.R. Calin, P. Grigore, *New Advanced Sandwich Composite with twill weave carbon and EPS*, Journal of Optoelectronics and Advanced Materials (J OPTOELECTRON ADV M), Vol. 15, Issue 3-4, (2013), INOE Publishing House, ISSN: 1454 - 4164, pp. 199 – 203.
http://joam.inoe.ro/index.php?option=magazine&op=view&idu=3177&catid=76

42. H. Teodorescu-Draghicescu, A. Modrea, *Mechanics of Composite Materials*, Transilvania University Publishing House, (2013), ISBN: 978-606-19-0300-9, (in Romanian).

43. H. Teodorescu-Draghicescu, S. Vlase, *Prediction Of Elastic Properties Of Some Sheet Molding Compounds*, 5th Int. Conf. "Computational Mechanics and Virtual Engineering" COMEC 2013, Transilvania University of Brasov, Romania, 24-25 October, (2013), pp. 448 – 454.

44. H. Teodorescu-Draghicescu, S. Vlase, *Stresses In Various Composite Laminates For General Set Of Applied In-Plane Loads*, 5th Int. Conf. "Computational Mechanics and Virtual Engineering" COMEC 2013, Transilvania University of Brasov, Romania, 24-25 October, (2013), pp. 148 – 153.

45. H. Teodorescu-Draghicescu, S. Vlase, *Homogenization and Averaging Methods to Predict Elastic Properties of Pre-Impregnated Composite Materials*, Computational Materials Science (COMP MATER SCI), Vol. 50, Issue 4, (2011), ISSN: 0927-0256, Elsevier, pp. 1310 – 1314.
http://www.sciencedirect.com/science/article/pii/S0927025610002533

46. H. Teodorescu-Draghicescu, A. Stanciu, S. Vlase, L. Scutaru, M.R. Călin, L. Serbina, *Finite Element Method Analysis Of Some Fibre-Reinforced Composite Laminates*,

Optoelectronics and Advanced Materials – Rapid Communications (OPTOELECTRON ADV MAT), Vol. 5, Issue 7, (2011), INOE Publishing House, ISSN: 1842-6573, pp. 782 – 785.
http://oam-rc.inoe.ro/index.php?option=magazine&op=view&idu=1628&catid=64

47. H. Teodorescu-Draghicescu, S. Vlase, L. Scutaru, L. Serbina, M.R. Calin, *Hysteresis Effect in a Three-Phase Polymer Matrix Composite Subjected to Static Cyclic Loadings*, Optoelectronics and Advanced Materials – Rapid Communications (OPTOELECTRON ADV MAT), Vol. 5, Issue 3-4, (2011), ISSN: 1842-6573, INOE Publishing House, pp. 273 – 277.
http://oam-rc.inoe.ro/index.php?option=magazine&op=list&revid=60

48. H. Teodorescu-Draghicescu, S. Vlase, I. Goia, F. Teodorescu, D. Scărlătescu, *Compliances and Stiffness Matrices of a Glass Fibre-Reinforced Composite Lamina Subjected to Biaxial Loadings*, The 4th Int. Conf. "Computational Mechanics and Virtual Engineering COMEC 2011", 20-22 October, (2011), Transilvania University of Brasov, Romania, Vol. 2, pp. 477-480.

49. H. Teodorescu-Draghicescu, S. Vlase, A. Chiru, D. Rosu, M.L. Scutaru, E. Secara, *Simulation of Elastic Properties of Sheet Molding Compounds*, Recent Advances in Applied Mathematics. Proceedings of the American Conference on Applied Mathematics (AMERICAN-MATH'10), Harvard University, Cambridge, USA, January 27-29, (2010), Stephen Lagakos, Leonid Perlovsky, Manoj Jha, Brindusa Covaci, Azami Zaharim, Nikos Mastorakis (Eds.), WSEAS Press, ISBN: 978-960-474-150-2, ISSN: 1790-2768, pp. 642 – 646.

50. H. Teodorescu-Draghicescu, S. Vlase, D.L. Motoc, A. Chiru, *Thermomechanical Response of a Thin Sandwich Composite Structure,* Engineering Letters, Vol. 18, Issue 3, Sept. (2010), Publisher: Newswood Limited (for the International Association of Engineers), Hong Kong, ISSN: 1816-093X (print version); ISSN: 1816-0948 (online version), pp. 273-278.

51. H. Teodorescu-Draghicescu, S. Vlase, *Prediction of Elastic Properties of Multiphase Prepregs With Multiple Applications*, 3rd Int. Conf. Advanced Composite Materials Engineering COMAT 2010, 27-29 October, (2010), Transilvania University of Brasov, Romania, Vol. 1, Eds. D. Bigoni, S. Vlase, A. Chiru, ISSN: 1844-9336, pp. 248 – 253.

52. H. Teodorescu-Draghicescu, S. Vlase, A. Chiru, M.L. Scutaru, D.L. Motoc, A *Homogenization Method for Pre-Impregnated Composite Materials*, Lecture Notes in Engineering and Computer Science, WCE 2009 - World Congress on Engineering 2009, Imperial College London, London, UK, 1-3 July, (2009), Vol. II, S.I. Ao, L. Gelman, D.W.L. Hukins, A. Hunter, A.M. Korsunsky (Eds.), International Association of Engineers IAENG, ISBN: 978-988-18210-1-0, pp. 1563 – 1568.

53. H. Teodorescu-Draghicescu, S. Vlase, D. Rosu, R. Purcarea, V. Munteanu, *Damping Analysis of a New Sandwich Structure*, Lecture Notes in Engineering and Computer Science, WCE 2009 - World Congress on Engineering 2009, Imperial College London, London, UK, 1-3 July, (2009), Vol. II, S.I. Ao, L. Gelman, D.W.L. Hukins, A. Hunter, A.M. Korsunsky (Eds.), International Association of Engineers IAENG, ISBN: 978-988-18210-1-0, pp. 1797-1802.

54. H. Teodorescu-Draghicescu, S. Vlase, A. Chiru, M.L. Scutaru, D.L. Motoc, *On the Elastic Constants of a Fibre-Reinforced Composite Laminate*, Proc. of the 2nd WSEAS Int. Conf. on Engineering Mechanics, Structures And Engineering Geology (EMESEG'09), N. Mastorakis, O. Martin, Xiaojing Zheng (Eds.), Rodos, Greece, 22-24 July, (2009), WSEAS Press, ISBN: 978-960-474-101-4, ISSN: 1790-2769, pp. 155-158.

55. H. Teodorescu-Draghicescu, S. Vlase, A. Chiru, R. Purcarea, I. Popa, *Averaging Methods In The Micromechanics Of Pre-Impregnated Composite Materials*, Proceedings of the 13th Int. Conf. On Modern Technologies, Quality and Innovation ModTech 2009, Iasi & Chisinau, 21-23 May, (2009), Politehnium Publishing House of Technical University "Gheorghe Asachi" Iasi, Romania, ISSN: 2066-3919, pp. 643 – 646.

56. H. Teodorescu-Draghicescu, S. Vlase, M.L. Scutaru, D.L. Motoc, V. Guiman, *Some advanced symmetric composite laminates subjected to off-axis loading systems. A stiffness evaluation*, Proc. of the 13th Int. Conf. on Modern Technologies, Quality and Innovation MODTECH 2009, Iasi & Chisinau, 21-23 May (2009), Politehnium Publishing House of Technical University "Gheorghe Asachi" Iasi, Romania, ISSN: 2066-3919, pp. 647 – 650.

57. H. Teodorescu-Draghicescu, S. Vlase, A. Chiru, R. Purcarea, V. Munteanu, *Theoretical and Experimental Approaches Regarding the Stiffness Increase of Fibre-Reinforced Composite Structures*, Proc. of the 1st Int. Conf. on Manufacturing Engineering, Quality and Production Systems (MEQAPS'09), Vol. II, D. Lepadatescu, N. Mastorakis (Eds.), Transilvania University of Brasov, Romania, 24-26 September, (2009), WSEAS Press, ISBN: 978-960-474-122-9, ISSN: 1790-2769, pp. 449-452.

58. H. Teodorescu-Draghicescu, S. Vlase, A. Chiru, M.L. Scutaru, I. Popa, A. Stanciu *Stiffness Evaluation Of Some Quasi-Isotropic Fibre-Reinforced Composite Laminates*, The 3rd Int. Conf. "Computational Mechanics and Virtual Engineering" COMEC 2009, Transilvania University of Braşov, Romania, 29-30 October, (2009), ISBN 978-973-598-572-1, pp. 783-788.

59. H. Teodorescu, S. Vlase, L. Scutaru, *Modeling The Tensile Behavior Of Pre-Impregnated Composite Materials*, Proceedings of the 3rd IASME/WSEAS Int. Conf. On Continuum Mechanics (CM'08), University of Cambridge, Cambridge, UK, February 23-25, (2008), ISBN: 978-960-6766-38-1, ISSN: 1790-2769, pp. 89 – 92.

60. H. Teodorescu-Draghicescu, S. Vlase, L. Scutaru, F. Teodorescu, *An Original Approach Of Tensile Behavior And Elastic Properties Of Multiphase Pre-Impregnated Composite Materials*, WSEAS Transactions on Applied and Theoretical Mechanics, Issue 2, Vol. 3, February (2008), ISSN: 1991-8747, pp. 53 – 62.

61. H. Teodorescu, S. Vlase, D.L. Motoc, I. Popa, D. Rosu, F. Teodorescu, *Mechanical behavior of an advanced sandwich composite structure*, WSEAS Int. Conf. on Engineering Mechanics, Structures, Engineering Geology (EMESEG '08), Heraklion, Greece, July 22-24, (2008), ISBN 978-960-6766-88-6, ISSN 1790-2769, pp. 280 – 285.

62. H. Teodorescu, S. Vlase, I. Candea, D.L. Motoc, *Some Averaging Methods In The Micromechanics Of Composite Materials With Periodic Structure*, Proceedings of the 10th WSEAS Int. Conf. On Automatic Control, Modelling & Simulation (ACMOS'08), Istanbul, Turkey, May 27-30, (2008), ISBN: 978-960-6766-63-3, ISSN: 1790-5117, pp. 210 – 214.

63. H. Teodorescu-Draghicescu, S. Vlase, V. Mihalcica, M. Vasii, *Modeling some composite laminates subjected to temperature and humidity variations,* Proc. of the 10th WSEAS Int. Conf. "Automatic Control, Modelling & Simulation" ACMOS'08, Istanbul, Turkey, May 27-30, (2008), ISBN 978-960-6766-63-3, ISSN 1790-5117, pp. 215 – 220.

64. H. Teodorescu-Draghicescu, S. Vlase, L.D. Motoc, M.L. Scutaru, R. Purcarea, *On the Elastic Properties of Some Advanced Composite Laminates Subjected to Off-axis Loading Systems*, Proc. of the 1st WSEAS Int. Conf. on Materials Science (MATERIALS'08), Bucharest, Romania, 7-9 November, (2008), ISBN: 978-960-474-024-6, ISSN: 1790-2769, pp. 40 – 43.

65. H. Teodorescu-Draghicescu, S. Vlase, M.L. Scutaru, A. Stanciu, L. Serbina, *Stiffness Evaluation Of Some Advanced Composite Laminates Un der Off-Axis Loading System*, 2nd Int. Conf. "Advanced Composite Materials Engineering" COMAT 2008, Transilvania University of Brasov, Romania, 9-11 October (2008), Vol. 1A, ISSN 1844-9336, pp. 213 – 218.

66. H. Teodorescu, *Basics and Mechanics of Polymer Matrix Composite Materials*, Transilvania University Publishing House, (2007), ISBN: 978-635-878-4, (in Romanian).

67. H. Teodorescu, S. Vlase, D. Cotoros, V. Munteanu, V. Guiman, *Modelling Of Tensile Behaviour Of Sheet Moulding Compounds*, The 2007 Int. Conf. Of Mechanical Engineering ICME'07, World Congress On Engineering 2007, Imperial College London, 2 – 4 July, (2007), Lecture Notes In Engineering And Computer Science, ISBN (Vol. I): 978-988-98671-5-7, ISBN (Vol. II): 978-988-98671-2-6, pp. 1407 – 1410.

68. H. Teodorescu-Draghicescu, S. Vlase, *Dynamic Analysis Of An Ultra-Lightweight Sandwich Structure For Multiple Applications*, 3rd WSEAS Int. Conf. on Dynamical Systems and Control, Arcachon, France, 13 – 15 Oct. (2007), ISBN 978-960-6766-08-4, ISSN 1790-5117, pp. 229 – 234.

69. H. Teodorescu, V. Munteanu, A. Stanciu, et. at., *On Upper And Lower Limits Of Elastic Coefficients Of SMC Composite Materials*, 7th WSEAS Int. Conf. On Simulation, Modelling And Optimization (SMO'07), September 15-17, (2007), Beijing, China, pp. 191 – 196.

70. H. Teodorescu, S. Vlase, I. Candea, *On Tensile Behaviour Of Sheet Moulding Compounds*, 7th WSEAS Int. Conf. On Simulation, Modelling And Optimization (SMO'07), September 15-17, (2007), Beijing, China, pp. 197 – 200.

71. H. Teodorescu-Draghicescu, S. Vlase, I. Candea, L. Scutaru, *Estimation Of Homogenized Elastic Coefficients Of Pre-Impregnated Composite Materials*, Studies In Mechanics, Environment And Geoscience. Proc. of the 2nd IASME/WSEAS Int. Conf. On Continuum Mechanics, Portorose, Slovenia, (2007), ISSN: 1790-5095, ISBN: 978-960-8457-70-6, pp. 134 – 139.

72. H.Teodorescu, S. Vlase, I. Goia, L. Scutaru, A. Stanciu, M. Vasii, *Tensile Behaviour of Composite Specimens Made From Chopped Strand Mat Reinforced Polyester Resin*, 24th Danubia – Adria Symposium on Developments in Experimental Mechanics, 19 – 22 Sept. (2007), Sibiu, Publishing House of Lucian Blaga University, Sibiu, ISBN 978-973-739-456-9, pp. 255 – 256.

73. H.Teodorescu, S. Vlase, M. Vasii, D. Rosu, *Tensile tests on "RT300" roving fabric reinforced polymer matrix composites*, The 2nd Int. Conf. "Computational Mechanics and Virtual Engineering" COMEC 2007, 11 – 13 Oct. (2007), Transilvania University of Brasov, Romania, ISBN 978-973-598-117-4, pp. 399 – 402.

74. H.Teodorescu, S. Vlase, V. Munteanu, V. Guiman, *Tensile tests on randomly reinforced polymer matrix composites*, The 2nd Int. Conf. "Computational Mechanics and Virtual Engineering" COMEC 2007, 11 – 13 Oct. (2007), Transilvania University of Brasov, Romania, ISBN 978-973-598-117-4, pp. 187 – 190.

75. H. Teodorescu-Draghicescu, S. Vlase, D. Cotoros, D. Rosu, *Damping Analysis Of An Advanced Sandwich Composite Structure*, WSEAS Transactions On Applied And Theoretical Mechanics, Issue 2, Vol. 1, Dec. 2006, ISSN: 1991-8747, 2nd WSEAS Int. Conf. on Applied and Theoretical Mechanics, MECHANICS'06, 20-22 Nov. (2006), Venice, Italy, pp. 147-152.

76. H. Teodorescu-Draghicescu, F. Teodorescu, *Analysis of [0/45-45/90]$_S$ composite laminate subjected to mechanical loading and temperature-humidity variation*, Proc. of the 1st Int. Conf. "Advanced Composite Materials Engineering" COMAT 2006, 19 – 22 October, (2006), Transilvania University of Brasov, ISBN 973-635-821-8, ISBN 978-973-635-821-0, pp. 58 – 64.

77. H. Teodorescu-Draghicescu, S. Vlase, L. Scutaru, *Dynamic Analysis Of An Ultra-Lightweight Sandwich Composite Structure*, Proc. of the 1st Int. Conf. "Advanced Composite Materials Engineering" COMAT 2006, 19 – 22 Oct. (2006), Transilvania University of Brasov, ISBN 973-635-821-8, ISBN 978-973-635-821-0, pp. 51 – 57.

78. S.W. Tsai, H.T. Hahn, *Introduction to Composite Materials*, Technomic, (1980).

79. J.R. Vinson, *Plate and Panel Structures of Isotropic, Composite and Piezoelectric Materials, Including Sandwich Construction*, Springer, 1st ed., (2005).

80. J.R. Vinson, R.L. Sierakovski, *The Behavior of Structures Composed of Composite Materials*, Springer, (2008).

81. S. Vlase, R. Purcarea, H. Teodorescu-Draghicescu, M.R. Calin, I. Szava, M. Mihalcica, *Behavior of a new Heliopol/Stratimat300 composite laminate*, Optoelectronics And Advanced Materials – Rapid Communications (OPTOELECTRON ADV MAT), Vol. 7, Issue 7-8, (2013), INOE Publishing House, ISSN: 1454-4164, pp. 569 – 572.
http://oam-rc.inoe.ro/index.php?option=magazine&op=view&idu=2132&catid=79

82. S. Vlase, H. Teodorescu-Draghicescu, M.R. Calin, M.L. Scutaru, *Advanced Polylite composite laminate material behavior to tensile stress on weft direction*, Journal of Optoelectronics and Advanced Materials (J OPTOELECTRON ADV M), Vol. 14, Issue 7-8, (2012), ISSN: 1454-4164, INOE Publishing House, pp. 658 – 663.
http://joam.inoe.ro/index.php?option=magazine&op=view&idu=3073&catid=72

83. S. Vlase, H. Teodorescu-Draghicescu, M.R. Calin, L. Serbina, *Simulation of the Elastic Properties of Some Fibre-Reinforced Composite Laminates Under Off-Axis Loading System,* Optoelectronics and Advanced Materials – Rapid Communications (OPTOELECTRON ADV MAT), Vol. 5, Issue 3-4, (2011), ISSN: 1842-6573, INOE Publishing House, pp. 424 – 429.
http://oam-rc.inoe.ro/index.php?option=magazine&op=view&idu=1528&catid=61

84. S. Vlase, H. Teodorescu-Draghicescu, D.L. Motoc, M.L. Scutaru, L. Serbina, M.R. Calin, *Behavior of Multiphase Fiber-Reinforced Polymers Under Short Time Cyclic Loading*, Optoelectronics and Advanced Materials – Rapid Communications (OPTOELECTRON ADV MAT), Vol. 5, Issue 3-4, (2011), ISSN: 1842-6573, INOE Publishing House, pp. 419 – 423.
http://oam-rc.inoe.ro/index.php?option=magazine&op=view&idu=1528&catid=61

85. I.M. Ward, J. Sweeney, *An Introduction to the Mechanical Properties of Solid Polymers*, Wiley, (2004).

86. J.M. Whitney, R.L. McCullough, *Delaware Composite Design Encyclopedia: Micromechanical Materials Modelling*, Vol. 2, University of Delaware, L.A., (1990).

87. J.M. Whitney, B.W. Rosen, *Structural Analysis of Laminated Anisotropic Plates*, Technomic, (1987).

88. T.I. Zohdi, P. Wriggers, *Introduction to Computational Micromechanics*, Springer, (2005).